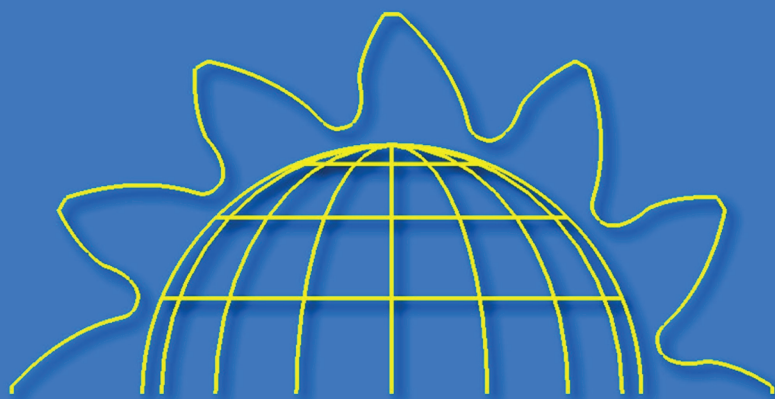


# DIRECT GEAR DESIGN



ALEXANDER L. KAPELEVICH



CRC Press  
Taylor & Francis Group

**DIRECT**

**GEAR**

**DESIGN**



# DIRECT GEAR DESIGN

ALEXANDER L. KAPELEVICH



CRC Press

Taylor & Francis Group

Boca Raton London New York

---

CRC Press is an imprint of the  
Taylor & Francis Group, an **informa** business

CRC Press  
Taylor & Francis Group  
6000 Broken Sound Parkway NW, Suite 300  
Boca Raton, FL 33487-2742

© 2013 by Taylor & Francis Group, LLC  
CRC Press is an imprint of Taylor & Francis Group, an Informa business

No claim to original U.S. Government works  
Version Date: 20130204

International Standard Book Number-13: 978-1-4398-7619-0 (eBook - PDF)

This book contains information obtained from authentic and highly regarded sources. Reasonable efforts have been made to publish reliable data and information, but the author and publisher cannot assume responsibility for the validity of all materials or the consequences of their use. The authors and publishers have attempted to trace the copyright holders of all material reproduced in this publication and apologize to copyright holders if permission to publish in this form has not been obtained. If any copyright material has not been acknowledged please write and let us know so we may rectify in any future reprint.

Except as permitted under U.S. Copyright Law, no part of this book may be reprinted, reproduced, transmitted, or utilized in any form by any electronic, mechanical, or other means, now known or hereafter invented, including photocopying, microfilming, and recording, or in any information storage or retrieval system, without written permission from the publishers.

For permission to photocopy or use material electronically from this work, please access [www.copyright.com](http://www.copyright.com) (<http://www.copyright.com/>) or contact the Copyright Clearance Center, Inc. (CCC), 222 Rosewood Drive, Danvers, MA 01923, 978-750-8400. CCC is a not-for-profit organization that provides licenses and registration for a variety of users. For organizations that have been granted a photocopy license by the CCC, a separate system of payment has been arranged.

**Trademark Notice:** Product or corporate names may be trademarks or registered trademarks, and are used only for identification and explanation without intent to infringe.

Visit the Taylor & Francis Web site at  
<http://www.taylorandfrancis.com>

and the CRC Press Web site at  
<http://www.crcpress.com>

*Dedicated to the memory of Prof. Edgar B. Vulgakov*



---

# Contents

---

<b>Preface</b> .....	xi
<b>Acknowledgments</b> .....	xiii
<b>About the Author</b> .....	xv
<b>1 Historical Overview</b> .....	1
1.1 Direct Gear Design® Origin.....	1
1.2 Gear Design Based on Rack Generating Technology.....	2
1.3 Gear Design without Rack Generation.....	8
1.4 Gears with Asymmetric Teeth.....	10
<b>2 Macrogeometry of Involute Gears</b> .....	17
2.1 Involute Tooth Parameters.....	17
2.1.1 Symmetric Gear Teeth.....	17
2.1.2 Asymmetric Gear Teeth.....	22
2.2 Gear Mesh Characteristics.....	28
2.2.1 Symmetric Gearing.....	28
2.2.2 Asymmetric Gearing.....	40
2.2.3 Contact Ratio for Helical Gears.....	47
2.3 Pitch Factor Analysis.....	49
2.4 Application of Direct Gear Design for Different Types of Involute Gears.....	55
<b>3 Area of Existence of Involute Gears</b> .....	59
3.1 Area of Existence of Symmetric Gears.....	59
3.1.1 Pressure Angle Isograms.....	61
3.1.2 Transverse Contact Ratio Isograms.....	63
3.1.3 Interference Isograms.....	67
3.1.4 Pitch Point Location Isograms.....	68
3.1.5 Performance Parameters' Isograms.....	71
3.1.6 Area of Existence and Gear Tooth Profiles.....	81
3.1.7 Areas of Existence for Gear Pairs with Different Relative Tooth Tip Thicknesses.....	83
3.1.8 Areas of Existence for Gear Pairs with Different Numbers of Teeth.....	86
3.2 Area of Existence of Asymmetric Gears.....	88
3.2.1 Area of Existence and Gear Tooth Profiles.....	88
3.2.2 Areas of Existence for Gear Pairs with Different Asymmetry Factors.....	91
3.3 Area of Existence and Pitch Factors.....	93
3.4 Application of Area of Existence.....	99



<b>4</b>	<b>Involute Gearing Limits</b> .....	101
4.1	Number of Teeth .....	101
4.1.1	Symmetric Gearing.....	102
4.1.2	Asymmetric Gearing.....	107
4.2	Pressure Angle .....	109
4.3	Contact Ratio.....	114
4.4	Practical Range of Involute Gear Parameters .....	117
<b>5</b>	<b>Tooth Geometry Optimization</b> .....	123
5.1	Involute Profile Optimization .....	123
5.1.1	Gear Pair Size Reduction .....	124
5.1.2	Asymmetry Factor Selection .....	125
5.1.3	Mesh Efficiency Maximization .....	134
5.2	Tooth Modeling and Bending Stress Calculation .....	135
5.3	Root Fillet Optimization .....	135
5.3.1	Root Fillet Optimization Method .....	139
5.3.2	Fillet Optimization Analysis.....	143
5.3.3	Benefits of Fillet Optimization.....	145
5.4	Bending Strength Balance .....	149
5.5	Final Stress Definition .....	150
<b>6</b>	<b>Gear Design Details</b> .....	155
6.1	Gear Transmission Density Maximization .....	155
6.1.1	Introduction of Volume Function.....	155
6.1.2	Volume Functions for Two-Stage Gear Drives .....	160
6.1.3	Internal Gear Ratio Optimization .....	163
6.2	High Gear Ratio Planetary Drives.....	166
6.2.1	One-Stage Arrangements .....	166
6.2.2	Two-Stage Arrangements .....	173
6.3	Self-Locking Gears.....	180
6.3.1	Self-Locking Conditions .....	181
6.3.2	Self-Locking Gear Design.....	184
6.4	Plastic Gear Design Specifics .....	187
6.4.1	Polymer Benefits and Limitations .....	188
6.4.2	Direct Gear Design of Polymer Gears.....	188
6.4.3	Metal-to-Plastic Conversion .....	189
6.5	Gear Tooth Profile Modeling.....	189
<b>7</b>	<b>Tolerancing and Tolerance Analysis</b> .....	195
7.1	Gear Specification .....	195
7.2	Accuracy Selection.....	196
7.3	Tolerance Analysis .....	198

<b>8 Gear Fabrication Technologies and Tooling .....</b>	<b>215</b>
8.1 Gear Machining .....	215
8.1.1 Form Machining .....	215
8.1.2 Generating Machining .....	220
8.1.3 Contour Machining .....	224
8.2 Gear Forming.....	226
<b>9 Gear Measurement .....</b>	<b>231</b>
9.1 Measurement over (between) Balls or Pins.....	231
9.1.1 Spur Gears .....	231
9.1.2 Helical Gears .....	236
9.2 Span Measurement .....	239
9.3 Composite Gear Inspection .....	241
9.4 Elemental Gear Inspection .....	242
<b>10 Comparison of Traditional and Direct Gear Design®.....</b>	<b>245</b>
10.1 Comparable Geometry and Stress Analysis .....	245
10.2 Gear Testing Results Comparison .....	246
10.2.1 Test Specimen Design and Analysis .....	249
10.2.2 Test Specimen Manufacturing.....	249
10.2.3 Test Arrangement and Procedure .....	251
10.2.4 Test Results .....	254
10.2.5 Results Analysis .....	255
10.2.6 Testing Results Conclusion.....	257
10.3 Design Method Selection.....	258
<b>11 Implementation Examples .....</b>	<b>261</b>
11.1 Speed Boat Gearbox.....	261
11.1.1 Gear Design .....	261
11.1.2 Gear Fabrication .....	262
11.1.3 Gearbox Performance Testing.....	264
11.2 Turboprop Engine Gearbox.....	264
11.3 Seed Planter Gearboxes.....	273
<b>References .....</b>	<b>281</b>



---

# Preface

---

Gears and gear drives have been known and used for millennia as critical components of mechanisms and machines. Over the last several decades the development of gearing has mostly focused in the following fields: the improving of material, manufacturing technology and tooling, thermal treatment, tooth surface engineering and coatings, tribology and lubricants, testing technology and diagnostics. Constant demand for high-performance gear transmissions has resulted in significant progress in gear tooth microgeometry, which defines deviation from the nominal involute surface to achieve the optimal tooth contact localization for higher load capacity and lower transmission error. However, the development of gear macrogeometry (the defining of the tooth shape and dimensional proportions) and gear design methods is traditionally based on the preselected instrumental generating rack and has remained frozen in time. The vast majority of gears are designed with the standard  $20^\circ$  pressure angle tooth proportions. For some demanding applications, like aerospace and automotive industries, the standard tooth proportions are altered to provide a higher transmission load capacity. Nevertheless, even for these applications the gear design methodology has not evolved for many years.

This book introduces an alternate gear design approach called Direct Gear Design<sup>®</sup>. Developed over the past thirty years, it has been implemented in custom gear applications to maximize gear drive performance. Some segments of this book were published in technical magazines and presented at gear conferences. The successful implementations of this method, and the positive responses generated by the magazine publications and gear conference presentations, motivated me to write this book and share this knowledge and experience with the gear engineering community. In this book the Direct Gear Design method is presented as another engineering tool that can be beneficial for many gear drives. I tried to avoid general conclusions and recommendations, realizing that in custom gearing one solution can be beneficial for certain types of applications but could be completely unacceptable for others. For practical purposes and to facilitate the understanding of the Direct Gear Design method for gear engineers, I used the same established standard gear nomenclature and specification as much as possible.

This book is written by an engineer, for engineers to show a beneficial alternative to the traditional way of gear design. I hope that it will expand the readers' perspective on the opportunity for further gear transmission improvements and inspire them to be open-minded in solving their practical gear design tasks.



---

# Acknowledgments

---

This book would not have been possible were it not for the collaboration, inspiration, and support from my colleagues and family. I express deep gratitude to

- My wife Svetlana, who provided me unending moral support, and my sons George and Andy, for their inspiration and assistance in seeing this publication to completion
- Dr. Yuriy V. Shekhtman for his assistance in the Direct Gear Design<sup>®</sup> software development and many years of friendship
- Roderick E. Kleiss (Kleiss Gears, Inc.) for having the opportunity to work with and learn from his unique skills in plastic gear design and manufacturing
- Prof. Faydor L. Litvin, who provided guidance in the publication of my first technical papers in the United States; it has been an honor to be his acquaintance
- Robert L. Errichello (Geartech) for his support and encouragement in the writing of this book
- My former colleagues and coauthors in Russia: Prof. Veniamin I. Goldfarb (Izhevsk State Technical University), Dr. Viacheslav M. Ananiev (CIAM), and Prof. Vladislav L. Dorofeev (CIAM) for sharing their expertise and friendship
- Thomas M. McNamara (Thermotech Co.) for his polymer material expertise contribution in mutually written articles
- Dmitry Karfagenskiy, Yefim I. Safris, and Alexander A. Shumskiy for their help in graphic work for this book
- Charles E. Long for the opportunity to use his gear analysis software to construct some of this book's charts
- Kenneth A. Frankel (Three Sigma Mfg, Inc.), Sergo N. Lomovtsev (Klimov Co.), Alexander G. Paikin (Chernyshev Enterprise), and Michael E. Friestad (John Deere Co.) for their help with the Direct Gear Design implementation examples for this book
- Jack McGuinn (*Gear Technology* magazine) for editing assistance
- The CRC Press team that prepared this book for publication: Jonathan Plant, Amy Rodriguez, Marc Gutierrez, and Laurie Schlags
- My fellow colleagues, gear engineers, and gear scientists in Russia and the United States for the privilege to work together and learn from their expertise

- All clients of AKGears, LLC for the opportunity to apply the Direct Gear Design technique in their gear drive development projects
- American Gear Manufacturers Association (AGMA) and specifically to my colleagues from its Aerospace and Plastic Gearing committees for the opportunity to work together on the AGMA gear standards
- The gear experts from across the world that I had the pleasure of meeting over the course of numerous international conferences; it was an honor to share and exchange ideas in the field of gear transmissions

**Alexander L. Kapelevich**

---

## *About the Author*

---

**Dr. Alexander L. Kapelevich** is a gear design consultant at AKGears, LLC. He holds a master's degree in mechanical engineering at Moscow Aviation Institute and a PhD degree in mechanical engineering at Moscow State Technical University. Dr. Kapelevich has more than 30 years of custom gear transmission research and design experience. He began his career working in the Russian Aviation Industry, where he was involved in R&D, software development, testing, and failure investigation for aerospace gear transmissions. Living in the United States since 1994, he developed the Direct Gear Design® methodology for custom gear transmissions that have been implemented in various fields, such as aerospace, automotive, agriculture, defense, robotics, racing, and many others. His specialties are the gear drive architecture, planetary systems, gear tooth macrogeometry optimization, gears with asymmetric teeth, and gear transmission performance maximization. Dr. Kapelevich is a member of American Gear Manufacturers Association.





# 1

---

## *Historical Overview*

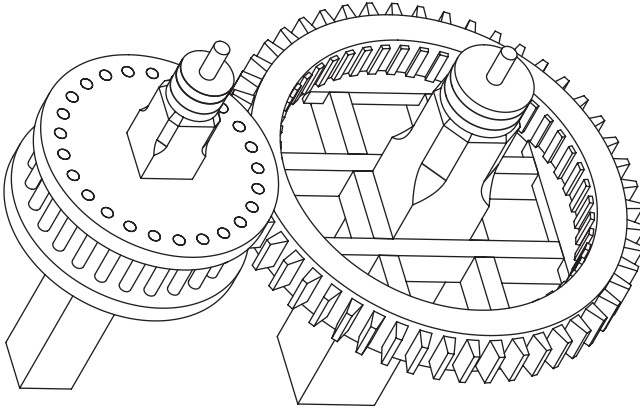
---

### 1.1 Direct Gear Design® Origin

Gears were invented many centuries ago and have been widely used since that time [1]. Historically, the development of gear design dovetailed with the development and design of other mechanisms and mechanical components. This applied design approach could also be called direct design because a shape (geometry) of a part was directly defined only by its function and performance requirements. Ancient engineers were designing custom gears (Figure 1.1) for particular applications based on the knowledge of desired performance (input and output parameters) and available power sources, such as gravity, water current, wind, spring force, human or animal muscular power, etc. This knowledge allowed them to define gear arrangement and geometry, including a number of stages, location and rotation directions of input and output shafts, shape and size of the gear wheels, profile and number of teeth, and other parameters. Gear design also included material selection, which should provide the required strength and durability of every component in the gear drive.

When the gear design was complete, the next stage of gear drive development was fabrication of parts and assembly; this stage included technological process selection and tool design. Ancient engineers were familiar with the two most common ways to produce gears—*cutting* (or carving) and *forming* (gear die cast, for example). In some cases gear wheels and teeth (cogs or pegs) were made separately and then assembled. All of these technologies define the tool shape and process parameters using already known gear design data. Such a development sequence—design data are primary, and technology and tooling parameters are secondary—was typical for practically any mechanical component. It was also essential for gear drives.

Even with the earliest known use of gear mechanisms people knew that gear performance greatly depends on a gear tooth shape. The evolution of gear tooth geometry reflects a growing demand to maximize gear drive performance, i.e., increase load capacity, RPM, and life; reduce vibrations and noise, etc. Simple rectangular or cylindrical tooth profiles were replaced with more sophisticated cycloid profiles. In fact, these types of gear tooth profiles are still used today in watch and clock mechanisms.

**FIGURE 1.1**

Ancient gear drive. (Redrawn from Willis, R., *Principles of Mechanism*, London: John W. Parker, 1841, p. 43.)

## 1.2 Gear Design Based on Rack Generating Technology

In the mid-eighteenth century, Swiss scientist Leonard Euler introduced the gear tooth flank profiles formed by the circle involute curve. An important feature of the involute gear profiles is producing the theoretically constant rotational velocities' ratio. The involute tooth profiles could be used for the external and internal gearings—as well as for the rack and pinion mesh. A gear rack is a gear wheel with an infinite number of teeth; the involute gear rack tooth flank profile becomes a straight line. Another important feature of the involute gear tooth profile is an ability of one gear to generate its mate in conjugate motion. In other words, if one of the mating gears presents a tool, such generating motion can be used for both the forming (gear rolling) and cutting (with the shaper cutter) gear fabrication processes. Similarly, a gear rack can present a cutting (or forming) edge of the tool if its linear velocity is aligned with the rotational velocity of the mating gear blank (Figure 1.2).

Application of a tooling rack for gear manufacturing led to the invention of gear hobbing machines in the nineteenth century. Their invention was motivated by a huge demand for gears to be used in all kinds of mechanisms and machines driven by steam and, later, electric and gasoline engines during the industrial revolution of that same century. Coincidentally, it was also the beginning of industrial standardization, which greatly accelerated progress in gear development and manufacturing.

A basic gear rack is an impression of the tooling rack (Figure 1.3). Its size and proportion parameters became a subject of standardization. The main parameter of the basic gear rack is its scale factor; i.e., the module  $m$  (in millimeters) in the metric system or the diametral pitch DP (in 1/in.) in the English system. The module  $m$  is a gear rack axial pitch divided by  $\pi$ , or the

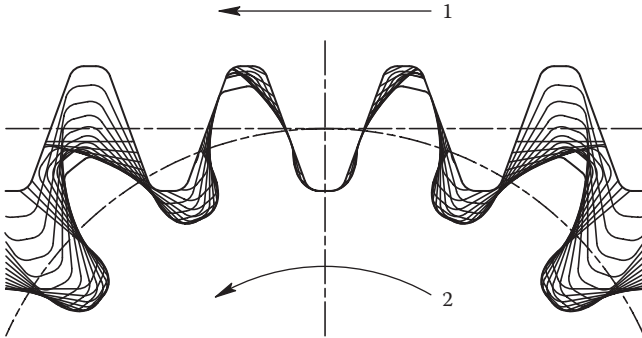


**FIGURE 1.2**  
Rack gear generating: 1 - tooling (generating) rack; 2 - gear blank.

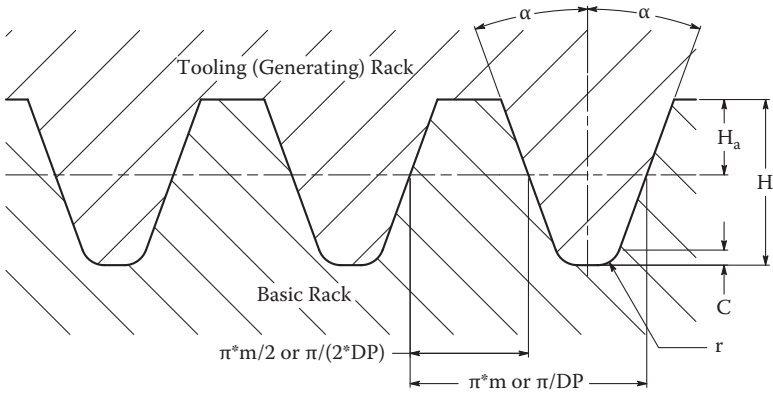


**FIGURE 1.3**  
Basic gear rack as impression of tooling rack.  $\alpha$  - pressure angle;  $H_a$  - addendum;  $H$  - whole depth;  $C$  - radial clearance;  $r$  - root radius.

gear pitch diameter divided by its number of teeth. The diametrical pitch  $DP$  is the number  $\pi$  divided by the gear rack axial pitch, or a number of gear teeth divided by its pitch diameter. The conversion formula for these scale factors is  $m \times DP = 25.4$ . The basic gear rack tooth flank profile angle  $\alpha$  is called a pressure angle. For the gear, a pressure angle  $\alpha$  is at the standard pitch diameter. The height of the gear tooth—from the pitch diameter to the tooth tip diameter—is called an addendum. An addendum—divided by a module or multiplied by a diametral pitch—is a dimensionless addendum coefficient. The height of the gear tooth—from the pitch diameter to the tooth root diameter—is called a dedendum. A dedendum—divided by a module or multiplied by a diametral pitch—is a dimensionless dedendum coefficient. The difference between addendum and dedendum is a radial clearance. The sum of addendum and dedendum is a whole depth. A root radius of the basic gear rack and the radial clearance divided by a module or multiplied by a

diametral pitch are, accordingly, the dimensionless root radius and the radial clearance coefficients. All of these gear rack tooth parameters were standardized. There is a certain set of module or diametral pitch values covering all gear tooth sizes—from tiny microgears for miniature drives to huge gear transmissions for construction and industrial machinery. Originally, standard gears had a pressure angle of  $14.5^\circ$  because its sinus is equal to  $\frac{1}{4}$ , thus making it convenient to calculate gears without trigonometric tables. Later, the  $20^\circ$  pressure angle became more common for standard gears because it provided a higher load capacity while using gears with fewer teeth and without a tooth root undercut. The addendum coefficient is chosen to be equal to 1.0. The standard radial clearance coefficient varies from 0.2 to 0.35. The standard root radius coefficient is about 0.3 for coarse pitch gears with the module  $m \geq 1.0$  or the diametral pitch  $DP \leq 20$ . For the fine pitch gears ( $m < 1.0$  or  $DP > 20$ ) the root radius is not typically specified. These standard gear tooth sizes and proportion coefficients describe simultaneously basic and tooling (generating) rack geometry and complete the gear profile for the given number of teeth.

Before the invention of the gear generating method and beginning of the standardization of the basic gear rack parameters, definition of tooling parameters belonged to the processing and tooling design stage, i.e., when the gear design was already completed. Now the standard basic gear rack parameters are established and the tooling rack (as an impression of the basic rack) also becomes standard. The parameters of these racks became the input parameters for gear design. This made gear design *indirect*, depending on preselected, standard parameters of the basic or tooling rack. From this point forward, the development of gear geometry and design takes a detour from mainstream development of mechanical components.

This rack generation-based gear design has yielded many benefits. First, gear design was drastically simplified in that a given number of gear teeth and a chosen standard tool virtually defined the gearing geometry and mesh parameters. Stress analysis (gear rating), defining tooth bending strength and tooth surface durability, was also simplified. The predefined form and application coefficients, gear load (torque) and RPM, and the gear geometry parameters defined the bending and contact stress values. This design approach also provided gear interchangeability in that the same gears could be used for different mechanisms and machines. Practically all of those mechanisms and machines were designed to run with standard gears. Another benefit is that a single tool could fabricate gears with different number teeth and these standard gears could work together. This allowed a reduction in tooling inventory.

It was perhaps no accident that the prominent gear scientist Prof. F.L. Litvin titled one of his books *Development of Gear Technology and Theory of Gearing* [2], putting technology ahead of the theory of gearing. In fact, many modern gear analysis studies and design procedures are based on preselected, often

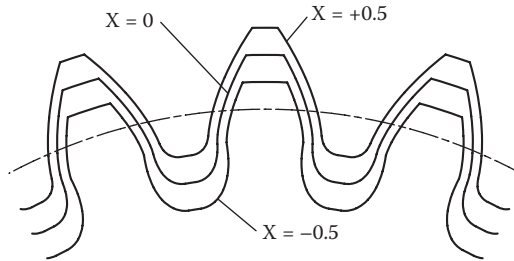


**FIGURE 1.4**  
Gear tooth profiles with different addendum modifications ( $X$ -shifts).

standard, basic gear rack parameters. With this approach gear design begins with the selection or definition of the basic rack parameters.

When a basic rack is chosen the gear designer has only one parameter—the addendum modification or  $X$ -shift [3]—which can be used to change the gear tooth geometry. The  $X$ -shift is a dimensionless factor; it equals the distance between the generating rack pitch line and the standard gear pitch diameter, divided by a module in the metric system or multiplied by a diametral pitch in the English system. In essence, the  $X$ -shift defines the tool position relative to the gear blank during the final cut; it indicates how far the tool is plunged into the blank. Gear tooth profiles with different addendum modifications are shown in Figure 1.4.

When the  $X$ -shift is zero (i.e., the addendum is not modified), the pitch line of the generating rack is tangent to the gear pitch diameter and the gear has standard geometry. If the  $X$ -shift is *less* than zero (negative addendum modification), the gear's outer and root diameters, and the circular tooth thickness at the pitch diameter, are reduced. At the same time, the tooth tip land becomes larger and the load capacity of the gear—with a negative addendum modification—is reduced. For gears with a low number of teeth, this may lead to undercut of the involute profile, resulting in a contact ratio reduction and an additional reduction in tooth strength. If the  $X$ -shift is *greater* than zero (positive addendum modification), the gear's outer and root diameters, and the circular tooth thickness at the pitch diameter, are enlarged. At the same time, the tooth tip land becomes smaller. At a certain value of the positive  $X$ -shift for a gear with a low number of teeth, the tooth has a pointed tooth tip, which is typically unacceptable; load capacity of the gear with a positive addendum modification is increased.

If the  $X$ -shift sum of the mating gear pair is *equal* to zero, the operating pressure angle is the same as the profile angle of the tooling (generating) rack, and the center distance is the same as for the standard gears with zero  $X$ -shifts. This kind of an addendum modification allows a balance (or equalization) of the bending strength of mating gears, or equalizing of the maximum specific sliding velocities of the contacting flanks, thus increasing gear mesh efficiency. The positive sum of the  $X$ -shifts of mating gears increases

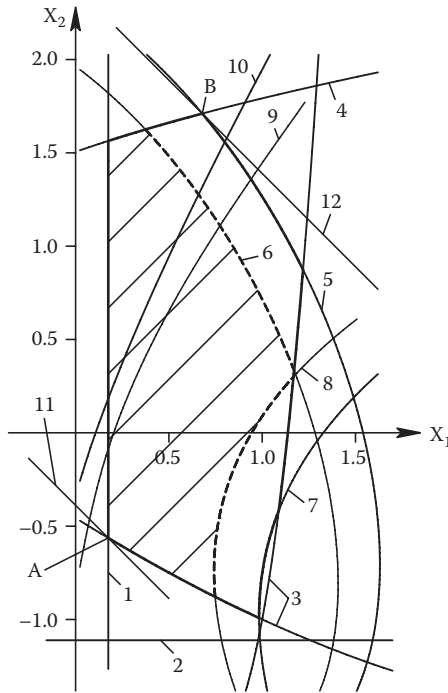


**FIGURE 1.5**  
Blocking contour of gear pair.

operating pressure angle and center distance as compared to a standard gear pair. As a result, the bending and contact (Hertzian) stresses are reduced and tooth flank wear resistance and gear train lifetime are increased. However, the contact ratio becomes lower. The negative sum of the  $X$ -shifts of mating gears reduces the operating pressure angle and center distance, and increases the contact ratio (unless the undercut occurs) and the bending and contact (Hertzian) stresses. Application of addendum modifications also allows a fitting of mating gears to the given center distance—if it is close to, yet different from, the standard one.

The selection of addendum modifications for the mating gear pair is limited by the so-called blocking contour [4]. The blocking contour is constructed for a certain, preselected generating rack and given numbers of teeth for mating pinion and gear. Every point of this contour (Figure 1.5) defines a mating gear pair with certain addendum modifications or  $X$ -shifts in which  $X_1$  is for the pinion and  $X_2$  for the gear. It also contains a number of isograms, presenting a certain tooth geometry or gear mesh conditions. The vertical 1 and horizontal 2 lines show the tooth root undercut conditions for pinion and gear, accordingly. Isograms 3 and 4 indicate the beginning of the tip/root interference near the tooth root of the pinion and the gear. Isogram 5 presents the gear pairs with the minimum allowable transverse

contact ratio; for spur gears it is 1.0. Practical limitation of the spur gear transverse contact ratio to 1.1, for example, as shown by isogram 6; gear pairs with a pointed tooth tip of the pinion are described by isogram 7. Practical limitation of the pinion tooth tip land (isogram 8) must be larger than zero, e.g.,  $0.2m$  or  $0.2/DP$ . The blocking contour may contain many other isograms describing different gear pair properties. For instance, isogram 9 shows gear pairs with equalized bending stresses for both mating gears (the face widths are also considered equal). The maximum mesh efficiency (isogram 10) presents gears with equalized, maximum specific sliding velocities that provide maximum gear mesh efficiency. The gear pair located in point *A* of the blocking contour has a minimum operating pressure angle (isogram 11) and a maximum contact ratio. The gear pair located in point *B* of the blocking contour has a maximum operating pressure angle (isogram 12) and a minimum contact ratio for spur gears of 1.0. Some of the blocking contour border conditions—such as the tip/root interference and the pointed tooth tip isograms—cannot be violated. However, the undercut condition may be acceptable for some (not highly loaded) gear applications if it does not reduce the transverse contact ratio below the permissible level. In some cases helical gears can have the transverse contact ratio below 1.0 by compensating for it with sufficient axial (or face) contact ratio.

This traditional gear design based on the standard basic rack provides satisfactory, universal solutions for the majority of gear applications. However, it is well known that universal solutions do not always work well for custom application and optimized design is required for performance maximization. A search for these optimized solutions led to a creation of different, nonstandard custom generating gear racks. Some of these racks actually became standard for different industries, like, for example, the  $22.5^\circ$  pressure angle rack that is commonly used in the automotive industry. The  $25^\circ$ , and even the  $28^\circ$ , pressure angle racks, and the  $20^\circ$  pressure angle rack with increased addendum (for high transverse contact ratio) are used in aerospace gear transmissions [5]. Other custom generating racks are also used for gear design in order to meet specific application requirements.

The traditional, rack-based gear design has existed for more than 150 years, and its contribution to industrial progress cannot be underestimated. But it becomes clear that, at its core, a rack generating approach imposes its own natural limits on gear performance improvements. And yet, despite a tremendous amount of innovation and development in science, technology, and machinery during the last few decades, it is still commonly used today by gear researchers and engineers. Modern trends for product customization are driven by technical and market performance maximization requirements. This leaves practically no place for universal standard gears. Gears have become more and more custom—and not interchangeable—for different applications. Also, low gear tooling inventory is no longer a priority; critical application gears are made using specifically dedicated cutting, forming, holding, and other tools.



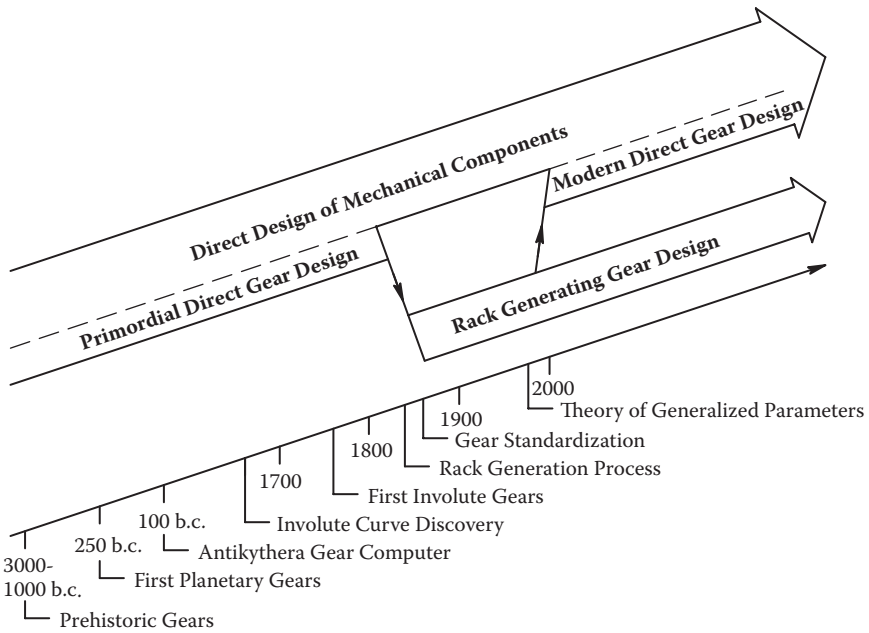


**FIGURE 1.6**  
Evolution of Direct Gear Design.

Of course generating rack machining and forming technologies are not alone in the manufacture of gears. Many gears are fabricated by form cutting and grinding, broaching, powder metal processing, injection molding, precision forging and die casting, etc.—all made without gear generating rack tools. Nevertheless, the gears produced by these methods are designed by the traditional generating rack-based method.

The new reality of gear development and use diminishes virtually all of the benefits of traditional, indirect gear design. Mathematical modeling, finite element analysis (FEA), and computer-aided design (CAD) software open new boundaries in developing the optimized gear macrogeometry for custom transmissions. This technology can get custom gear design back on track—from that previously mentioned detour taken in the mid-nineteenth century—to join the mainstream direct design of other mechanical components (Figure 1.6).

### 1.3 Gear Design without Rack Generation

Modern Direct Gear Design is based on the theory of generalized parameters created by Prof. E.B. Vulgakov [6–8] that separates gear geometry from

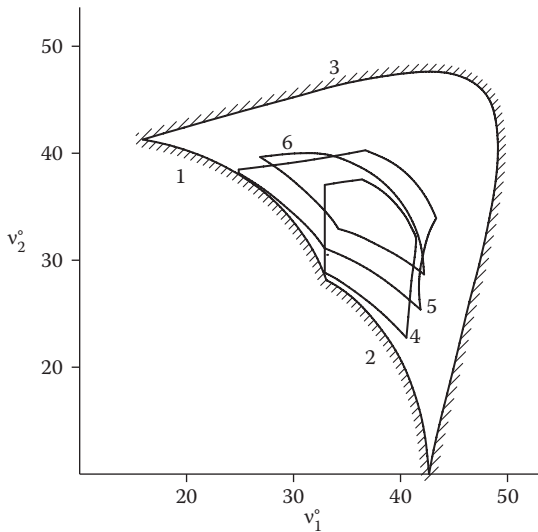


**FIGURE 1.7**

Area of existence of gear pair.  $v_1$  and  $v_2$  - pinion and gear involute intersection profile angles; 1 - pinion root interference isogram; 2 - gear root interference isogram; 3 - isogram of transverse contact ratio equal to 1.0; 4–6 - blocking contour borders of standard 20° and 25°, and custom 28° generating racks constructed in  $v_1$ - $v_2$  coordinates.

fabrication technology and tooling parameters. In this theory he has demonstrated how an involute gear tooth, a gear, and a gear mesh could be defined, analyzed, and optimized without using the basic or generating rack. He defined the gear mesh parameter limits and introduced so-called areas of existence of the gear pair. An area of existence for a particular gear pair is a significantly greater blocking contour of the same gear pair created for a generating rack. In fact, an area of existence covers gear pairs that could be generated by any possible rack (Figure 1.7), including cases when the mating gears are generated by different racks.

Indeed, Professor Vulgakov's theory liberated gear development and design from limitations imposed by a preselected, standard (or custom) generating rack. It significantly expanded the range of possible gear and mesh parameters and returned gear geometry development to its rightful prominence along with other mechanical components designs.

R.E. Kleiss of Kleiss Gears has independently developed his own approach to design of plastic gears without the use of basic or generating rack parameters [9, 10]. With his method, "a basic generating rack is not used to define root and tooth geometry. Here the mating gear in close mesh defines these geometries and produces a gear in its maximum material condition. The tip of one gear forms the root of the other." This allowed the use of involute tooth shapes and proportions—which are not achievable by standard rack generation—for improving the performance of plastic gears. He also

developed his own approach to plastic gear specification, where the base circle diameter is used, rather than the traditional reliance upon module or diametral pitch [11]. The tooth thickness is also defined at the base circle diameter—not at the pitch circle diameter.

---

## 1.4 Gears with Asymmetric Teeth

Flanks of a gear tooth are functionally different for many gear drives. Tooth load on one flank is significantly higher and is applied for longer periods of time than for the opposite one. An asymmetric tooth shape reflects this functional difference (Figure 1.8). A design objective of asymmetric gear teeth is to improve the performance of primary drive profiles at the expense of the performance of opposite coast profiles. The coast flanks are unloaded or lightly loaded during a relatively short work period. Asymmetric tooth profiles make it possible to simultaneously increase the contact ratio and operating pressure angle beyond those limits achievable with conventional symmetric gears. The main advantage of asymmetric gears is contact stress reduction on the drive flanks that results in higher power transmission density (load capacity per gear size). Another important advantage is the possibility of designing the coast tooth flanks independently from the drive tooth flanks, i.e., managing tooth stiffness while keeping a desirable pressure angle and contact ratio of drive flanks. This allows an increase in tooth tip deflection, thus damping tooth mesh impact and resulting in a reduction of gear noise and vibration.

While they have been known for many years, the history of gears with asymmetric teeth (or asymmetric gears) is not sufficiently recorded in modern gear literature. The first asymmetric gears had a buttress tooth

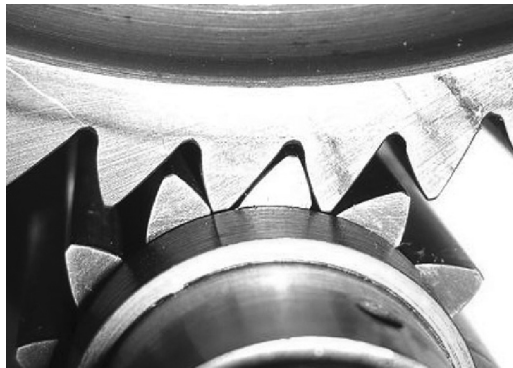


**FIGURE 1.8**  
Gears with asymmetric teeth.

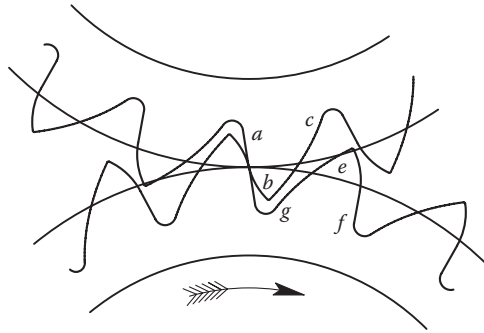


**FIGURE 1.9**

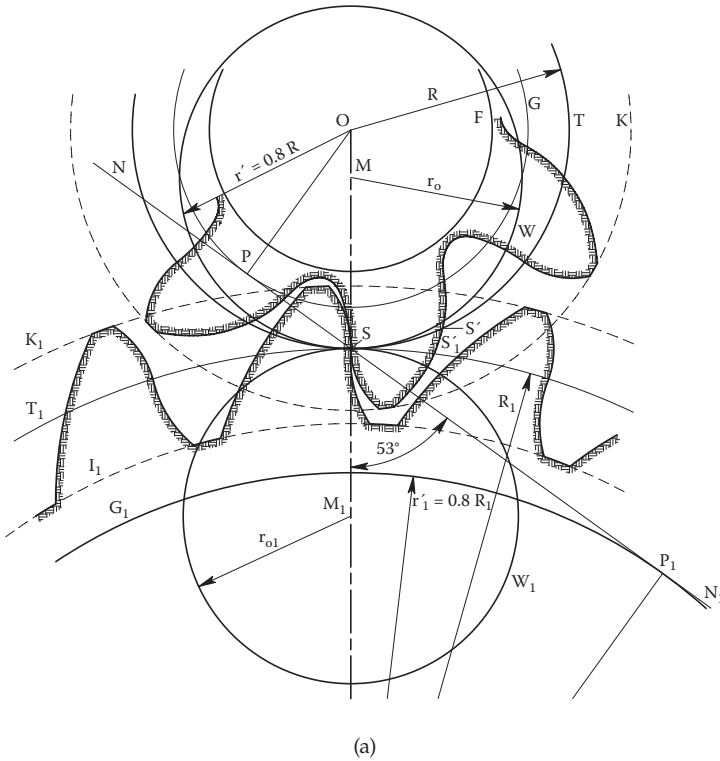
Asymmetric gear mesh. (Redrawn from Willis, R., *Principles of Mechanism*, London: John W. Parker, 1841, p. 138.)

shape with low-pressure angle at the drive tooth flanks, and with supporting coast flanks with high-pressure angle. According to Darle W. Dudley [1], “By 100 BC the gear art included both metal and wooden gears. Triangular teeth, *buttress teeth*, and pin-teeth were all in use.” R.S. Woodbury wrote [12]: “In Leonardo da Vinci we find some drawings of tooth form—one very like a buttress tooth.” R. Willis [13] had shown the asymmetric buttress gear teeth (Figure 1.9) with the following explanation: “If a machine be of such a nature that the wheels are only required to turn in one direction, the strength of the teeth may be doubled by an alteration of form.” He chose the epicycloid profile for the drive tooth flanks and the involute one for the coast flanks.

Later, F. Reuleaux elaborated upon asymmetric tooth shape proportions. He also used the epicycloid drive tooth flanks and the involute coast flanks with the  $53^\circ$  pressure angle. In his book [14] these tooth profiles are called the thumb-shaped teeth (Figure 1.10), and he wrote, “By combining *evolute* and epicycloids—using the two curves for opposite sides of the same tooth—a profile of great strength is obtained. This form is of especial service for heavy-duty driving when motion is constantly in the same direction.”

O.A. Leutwiler [16] applies involute profiles for both drive and coast flanks of the buttress or, as he called them, hook-tooth gears (Figure 1.11). He suggested the  $15^\circ$  pressure angle for drive flanks and the  $35^\circ$  pressure angle for coast flanks.

Much of the research [17–24] has defined asymmetric gear geometry traditionally by the preselected asymmetric generating gear rack parameters (Figure 1.12), which is typically modified from the standard symmetric rack by increasing the pressure angle of one flank. The opposite flank and other rack tooth proportions remain unchanged. There are no standards on gears with asymmetric teeth. They are for custom high-performance gear transmissions, and the modified asymmetric tooling gear racks cannot satisfy demanding applications and requirements of such gear drives.

**FIGURE 1.10**

The Reuleaux's thumb-shaped tooth gears. (a) Mesh schematics. (Redrawn from Reuleaux, F., *The Constructor. A Hand-Book of Machine Design*, Philadelphia: H.H. Suplee, 1894, p. 134.) (b) Gear model from Reuleaux Collection of Kinematic Mechanisms of Cornell University. (From Jon Reis Photography, Q05 thumb shaped gear teeth profiles, Cornell University Library, [http://kmoddl.library.cornell.edu/model\\_metadata.php?m=111](http://kmoddl.library.cornell.edu/model_metadata.php?m=111). Copyright © Jon Reis. With permission.)

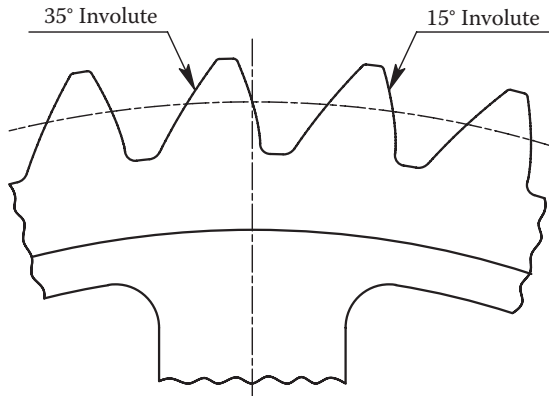


**FIGURE 1.11**

Buttress or hook-tooth gear. (Redrawn from Leutwiler, O.A., *Element of Machine Design*, London: McGraw-Hill Book Company, 1917, p. 134.)

Authors of earlier and some modern publications about asymmetric gear geometry chose the buttress tooth form that has drive flanks with low-pressure angle and the coast supporting flanks with high-pressure angle, because it provides noticeable bending stress reduction in comparison with the standard symmetric tooth form. The high-contact-ratio (HCR) buttress tooth form was considered for noise and vibration reduction in aerospace gear transmissions [25, 26]. However, an increased stiffness of buttress teeth prevented the desired goal.

It is well known that gear transmission load capacity and power density depend mainly upon the tooth flank surface durability, which is defined by the contact stress level and scuffing resistance. From this point, the application of a higher-pressure angle for drive tooth flanks and a lower-pressure angle for coast tooth flanks is more promising. In addition, this tooth form provides lower stiffness and better gear mesh impact dampening.

Prof. E.B. Vulgakov applied his theory of generalized parameters to asymmetric gears [7, 27], defining their geometry without using rack generation parameters. According to his approach, an asymmetric tooth is constructed with two halves of the symmetric teeth with different base circles (Figure 1.13). In order to achieve the maximum operating pressure angle and contact ratio, the drive tooth flank uses one-half of the symmetric tooth, with pointed tip and smaller base circle. Necessary tooth tip land is provided by the coast flank that is one-half of the other symmetric tooth, but with a greater base circle and large tooth tip land.

The maximum transverse contact ratio and pressure angle of such asymmetric gears are the same as for symmetric gears with pointed tooth tips. This limitation does not allow for realization of all asymmetric tooth performance improvement potentials, and this design approach did not find a practical application.

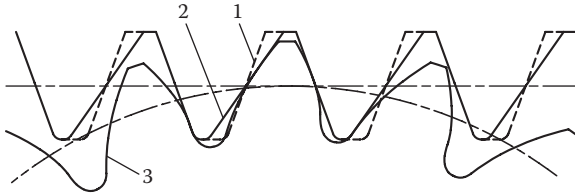


**FIGURE 1.12**

Asymmetric gear rack generation: 1 - standard symmetric generating rack; 2 - modified asymmetric generating rack profile; 3 - gear profile.

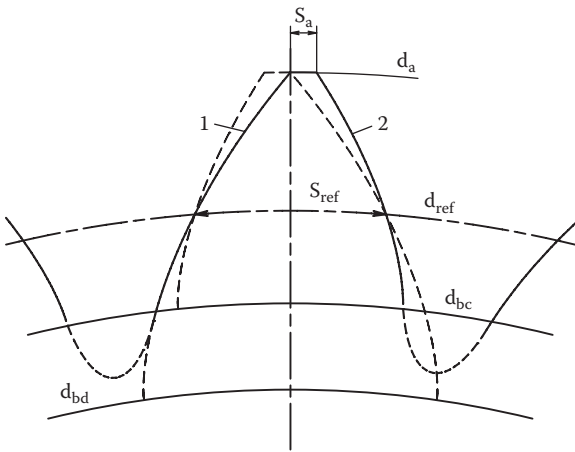


**FIGURE 1.13**

Asymmetric tooth constructed with two halves of the symmetric teeth: 1 - drive flank from base diameter  $d_{bd}$ ; 2 - coast flank from base diameter  $d_{bc}$ ;  $S_{ref}$  - tooth thickness at reference diameter  $d_{ref}$ ;  $S_a$  - thickness at tooth tip diameter  $d_a$ .

Publications [28–31] suggested an asymmetric tooth formed with two involutes of two different base circles. Figure 1.14 shows that the symmetric tooth with identical drive pressure angle and tooth thicknesses at the reference and tip diameters has a much shorter active involute flank than the drive flank of an asymmetric tooth. This simultaneously enables a high-pressure angle and contact ratio in the asymmetric gear mesh. Such an approach addresses all possible asymmetric tooth profiles—from a virtually symmetric tooth shape to a tooth shape with very high asymmetry. Asymmetric gear geometry development and design specifics are described in the following chapters.

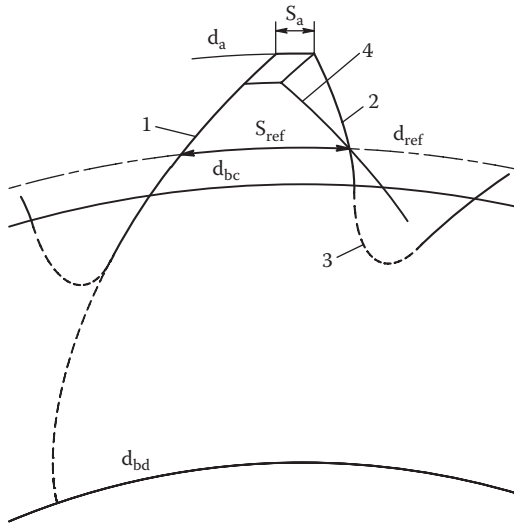


**FIGURE 1.14**

Asymmetric tooth constructed with two involutes: 1 - drive flank from base diameter  $d_{bd}$ ; 2 - coast flank from base diameter  $d_{bc}$ ; 3 - root fillet; 4 - symmetric tooth profile with the same drive flank, and tooth thicknesses  $S_{ref}$  and  $S_a$  at the reference diameter  $d_{ref}$  and the tooth tip diameter  $d_a$ .





# 2

---

## *Macrogeometry of Involute Gears*

---

Flanks of involute gears typically have deviations from a theoretical involute surface. These deviations are partially a result of technological imperfections. However, in many cases, a designer modifies tooth flanks to compensate possible gear teeth dislocations related to an assembly misalignment and operating conditions (thermal expansion, deflections under the load, etc.). A goal of involute flank modification is to provide tooth contact localization (also known as profile and lead crowning), which is a subject of gear microgeometry development [32–34]. Microgeometry of gear flanks is not considered in this book.

The subject of this chapter is a gear macrogeometry—analysis of the gear meshes with true involute profiles. Practically all equations, except those in Sections 2.2.3 and 2.4, are related to the spur gears or the transverse section of the helical gears.

---

### 2.1 Involute Tooth Parameters

An involute curve (or involute) can be presented as a trajectory of the end of a string unwrapped from a base diameter  $d_b$ .

#### 2.1.1 Symmetric Gear Teeth

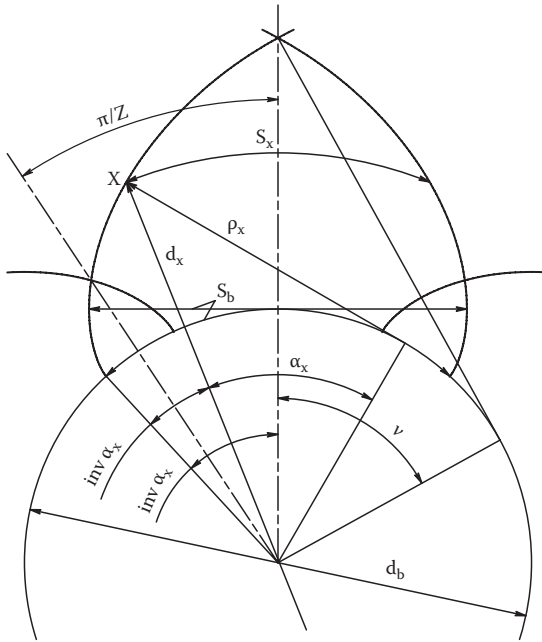
Two involutes unwrapped in opposite (clockwise and counterclockwise) directions are used to form tooth flanks (Figure 2.1). An angle  $\alpha_x$  is the involute profile angle at some tooth flank point  $X$ . Involute function  $\text{inv } \alpha_x = \tan \alpha_x - \alpha_x$  (where  $\alpha_x$  is in radians) presents the angle between radial lines from the center  $O$  to the start point of the involute and to point  $X$ . An angle  $v$  is the involute profile angle at intersection of the tooth flank involutes.

The base tooth thickness of the external tooth is

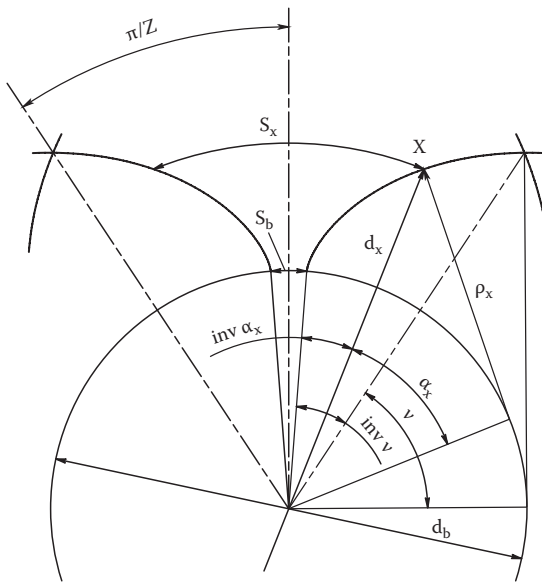
$$S_b = d_b \times \text{inv}(v) . \tag{2.1}$$

The base tooth thickness of the internal tooth is

$$S_b = d_b (\pi / z - \text{inv}(v)) , \tag{2.2}$$



(a)



(b)

**FIGURE 2.1**  
Involute flanks of external (a) and internal (b) gear teeth.

where  $z$  is a number of teeth. If  $inv(v) \geq \pi/z$ , the base tooth thickness of the internal gear tooth is equal to zero or negative.

A diameter at the tooth flank point  $X$  is

$$d_x = d_b / \cos \alpha_x . \quad (2.3)$$

An involute profile curvature radius at point  $X$  is

$$\rho_x = \frac{d_b \tan \alpha_x}{2} . \quad (2.4)$$

A tooth thickness at the diameter  $d_x$  is:

For external gear tooth:

$$S_x = d_x(inv(v) - inv(\alpha_x)) \quad (2.5)$$

or

$$S_x = d_b(inv(v) - inv(\alpha_x)) / \cos \alpha_x . \quad (2.6)$$

For internal gear tooth:

$$S_x = d_x(\pi / z - inv(v) + inv(\alpha_x)) \quad (2.7)$$

or

$$S_x = d_b(\pi / z - inv(v) + inv(\alpha_x)) / \cos \alpha_x . \quad (2.8)$$

A tooth profile must also include the tip land and tip radii or chamfers to exclude the sharp pointed tooth, and the fillet between teeth (see Figures 2.2 and 2.3). A root fillet of the tooth is not in contact with the mating gear tooth. However, it is an important part of the tooth profile because this is an area of the maximum bending stress, which may limit performance and life of a gear drive. The fillet design and optimization are presented in Section 5.3.

The tooth tip diameter  $d_a$  can be defined by Equation (2.3):

$$d_a = d_b / \cos \alpha_a , \quad (2.9)$$

where  $\alpha_a$  is the profile angle at the diameter  $d_a$ . This diameter is also called the outer diameter for the external gears and the minor diameter for the internal gears.

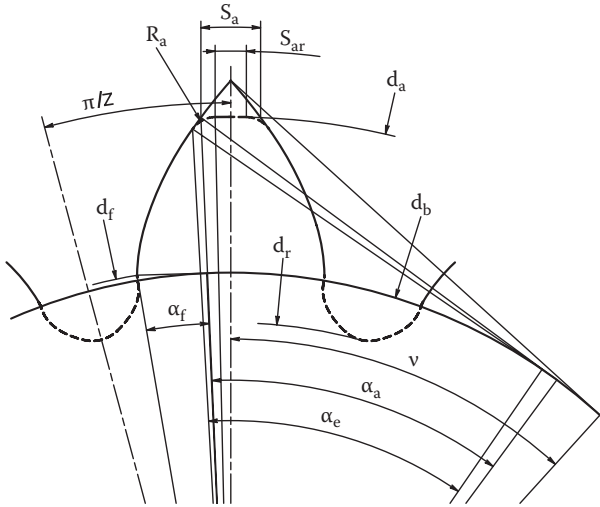


**FIGURE 2.2**  
External gear tooth.

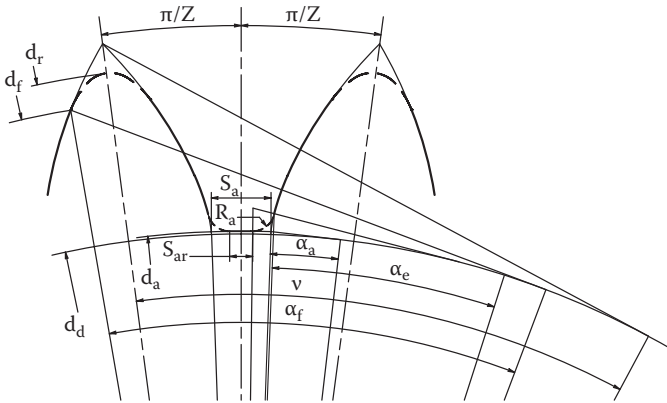


**FIGURE 2.3**  
Internal gear tooth.

The virtual tooth tip land  $S_a$  of an external gear tooth (Figure 2.2) is defined by Equation (2.5) considering tip radius equal to zero:

$$S_a = d_a(\text{inv}(v) - \text{inv}(\alpha_a)) . \tag{2.10}$$

The virtual tooth tip land  $S_a$  of the internal gear tooth (Figure 2.3) is defined from Equation (2.7):

$$S_a = d_a(\pi / z - \text{inv}(v) + \text{inv}(\alpha_a)) . \tag{2.11}$$

The profile angle  $\alpha_e$  is an effective involute angle at the tooth tip. It is defined considering the tooth tip radius  $R_a$  as

$$\alpha_e = \arctan\left(\tan\left(\arccos\left(\frac{d_b}{d_a \mp 2R_a}\right)\right) \pm \frac{2R_a}{d_b}\right), \quad (2.12)$$

where signs  $\mp$  and  $\pm$  are for external gears and internal gears, respectively.

The tooth tip land  $S_{ar}$  is defined considering the tip radius  $R_a$ :

For an external gear tooth:

$$S_{ar} = d_a(\operatorname{inv}(\nu) - \tan \alpha_e + \arctan(\tan \alpha_e - 2R_a / d_b)). \quad (2.13)$$

For an internal gear tooth:

$$S_{ar} = d_a\left(\frac{2\pi}{z} - \operatorname{inv}(\nu) + \tan \alpha_e - \arctan(\tan \alpha_e + \frac{2R_a}{d_b})\right). \quad (2.14)$$

Direct Gear Design<sup>®</sup> defines the form diameter  $d_f$  and related profile angle  $\alpha_f$  considering a mesh with the mating gear (see Section 2.2). The root diameter  $d_r$  is defined as a result of the fillet profile optimization (see Section 5.3).

A gear rack (Figure 2.4) can be considered a gear with an infinite number of teeth. This alters an involute curve to the straight line with a constant profile angle  $\alpha$ . The nominal pitch line equally splits the rack pitch for the tooth thickness and space between teeth. The rack nominal effective tooth addendum  $H_{ae}$  is defined from the nominal pitch line. In the rack and pinion

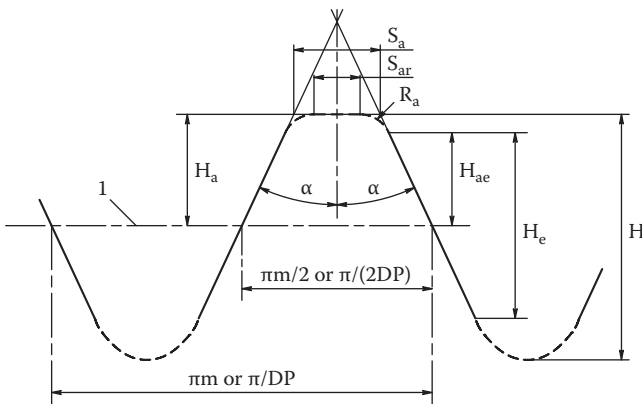


**FIGURE 2.4**

Gear rack tooth. 1 - nominal pitch line;  $\alpha$  - rack profile angle;  $m$  - rack module (metric system);  $DP$  - rack diametral pitch (English system);  $H_a$  - nominal tooth addendum;  $H_{ae}$  - nominal effective tooth addendum;  $H_e$  - effective tooth profile depth;  $H$  - whole tooth depth.

mesh the operating pitch line can be different than the nominal pitch line. This makes the operating pitch line tooth thickness and tooth addendum also different from the nominal ones.

The tooth tip land  $S_{ar}$  of the rack tooth is:

In the metric system:

$$S_{ar} = \frac{\pi m}{2} - 2H_{ae} \tan \alpha - 2R_a \cos \alpha. \quad (2.15)$$

In the English system:

$$S_{ar} = \frac{\pi}{2DP} - 2H_{ae} \tan \alpha - 2R_a \cos \alpha. \quad (2.16)$$

The nominal gear rack tooth addendum  $H_a$  is

$$H_a = H_{ae} + R_a(1 - \sin \alpha). \quad (2.17)$$

The virtual tooth tip land  $S_a$  of the gear rack tooth is:

In the metric system:

$$S_a = \frac{\pi m}{2} - 2H_a \tan \alpha, \text{ or} \quad (2.18)$$

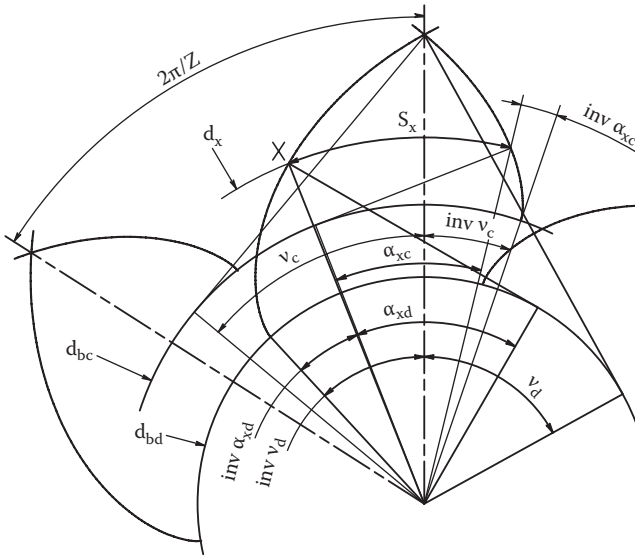
in the English system

$$S_a = \frac{\pi}{2DP} - 2H_a \tan \alpha. \quad (2.19)$$

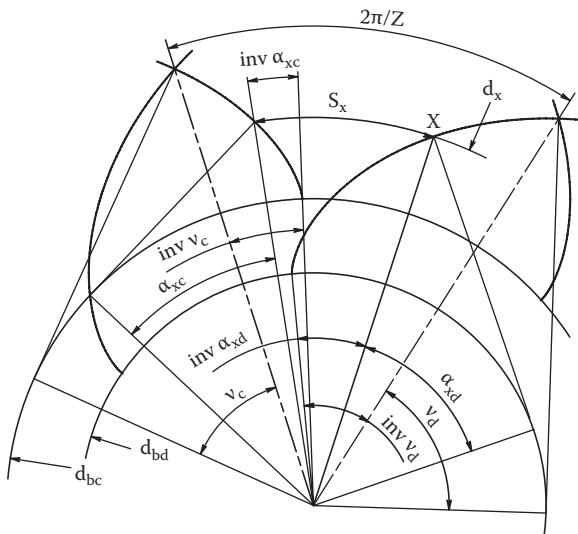
### 2.1.2 Asymmetric Gear Teeth

Application of asymmetric teeth allows improving performance of gear drives, which transmit more load by one tooth flank in comparison to the opposite flank. This type of tooth macrogeometry is practically disregarded by traditional gear design that is based on a standard gear rack with symmetric teeth. Direct Gear Design is naturally suitable for gears with asymmetric teeth because standards for traditional design for such gears do not exist.

Two involute flanks of the asymmetric tooth (see Figure 2.5) are unwound from two different base diameters  $d_{bd}$  and  $d_{bc}$ . The symbol  $d$  is used for



(a)



(b)

**FIGURE 2.5**  
Involute flanks of external (a) and internal (b) asymmetric gear teeth.



drive flank and the symbol  $c$  is used for coast flank of an asymmetric tooth. A diameter  $d_x$  at the drive flank point  $X$  can be defined from (2.3):

$$d_x = d_{bd} / \cos \alpha_{xd} = d_{bc} / \cos \alpha_{xc} . \quad (2.20)$$

Then the tooth asymmetry factor  $K$  is

$$K = d_{bc} / d_{bd} = \cos \alpha_{xc} / \cos \alpha_{xd} . \quad (2.21)$$

For many applications the drive flank profile angle  $\alpha_{xd}$  is greater than the coast flank profile angle  $\alpha_{xc}$ . This means  $d_{bd} < d_{bc}$  and the asymmetry factor  $K > 1.0$ . For symmetric tooth  $K = 1.0$ .

At the coast flank base circle  $d_{bc}$  the coast flank profile angle  $\alpha_{xc} = 0$  and the drive flank profile angle  $\alpha_{xd}$  from (2.21) is

$$\alpha_{xd} = \arccos(1 / K) . \quad (2.22)$$

The base tooth thickness of the asymmetric tooth can be defined only at the coast flank base circle  $d_{bc}$ :

For external tooth:

$$S_b = \frac{d_{bc}}{2} \times (\text{inv}(v_d) + \text{inv}(v_c) - \text{inv}(\arccos(1 / K))) . \quad (2.23)$$

For internal tooth:

$$S_b = \frac{d_{bc}}{2} \times (2\pi / z - \text{inv}(v_d) - \text{inv}(v_c) + \text{inv}(\arccos(1 / K))) . \quad (2.24)$$

The tooth thickness at diameter  $d_x$  is:

For external tooth:

$$S_x = \frac{d_x}{2} \times (\text{inv}(v_d) + \text{inv}(v_c) - \text{inv}(\alpha_{xd}) - \text{inv}(\alpha_{xc})) \quad (2.25)$$

or

$$S_x = \frac{d_{bd}}{2 \cos \alpha_{xd}} \times (\text{inv}(v_d) + \text{inv}(v_c) - \text{inv}(\alpha_{xd}) - \text{inv}(\alpha_{xc})) . \quad (2.26)$$

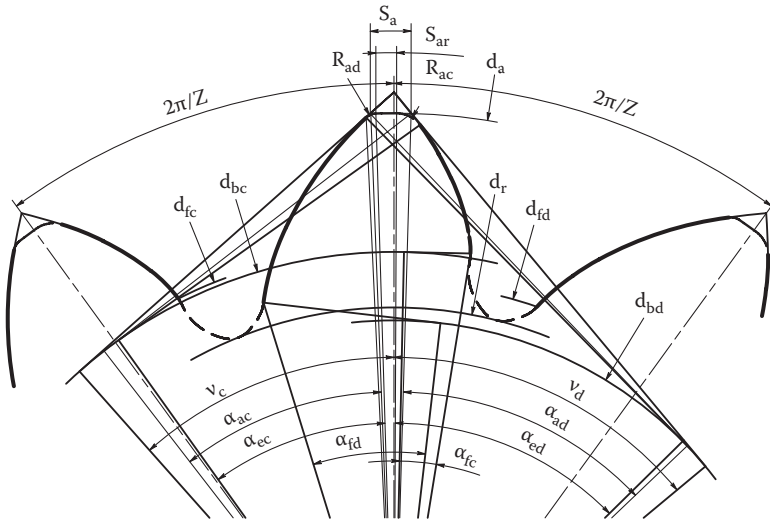


**FIGURE 2.6**  
External asymmetric gear tooth.

For internal tooth:

$$S_x = \frac{d_x}{2} \times \left( \frac{2\pi}{z} - \text{inv}(v_d) - \text{inv}(v_c) + \text{inv}(\alpha_{xd}) + \text{inv}(\alpha_{xc}) \right) \quad (2.27)$$

or

$$S_x = \frac{d_{bd}}{2 \cos \alpha_{ad}} \times \left( \frac{2\pi}{z} - \text{inv}(v_d) - \text{inv}(v_c) + \text{inv}(\alpha_{xd}) + \text{inv}(\alpha_{xc}) \right). \quad (2.28)$$

The same as in a symmetric tooth, an asymmetric tooth profile must include the tip land and tip radii, and the root fillet between teeth (see Figures 2.6 to 2.8). The tooth tip diameter  $d_a$  can be defined from (2.9):

$$d_a = d_{bd} / \cos \alpha_{ad} = d_{bc} / \cos \alpha_{ac}, \quad (2.29)$$

where  $\alpha_{ad}$  and  $\alpha_{ac}$  are the drive and coast profile angles at the diameter  $d_a$ .

The virtual tooth tip land  $S_a$  of the external gear tooth is defined considering tooth tip radii equal to zero from Equation (2.25) or (2.26):

For external tooth (Figure 2.6):

$$S_a = \frac{d_a}{2} \times (\text{inv}(v_d) + \text{inv}(v_c) - \text{inv}(\alpha_{ad}) - \text{inv}(\alpha_{ac})) \quad (2.30)$$

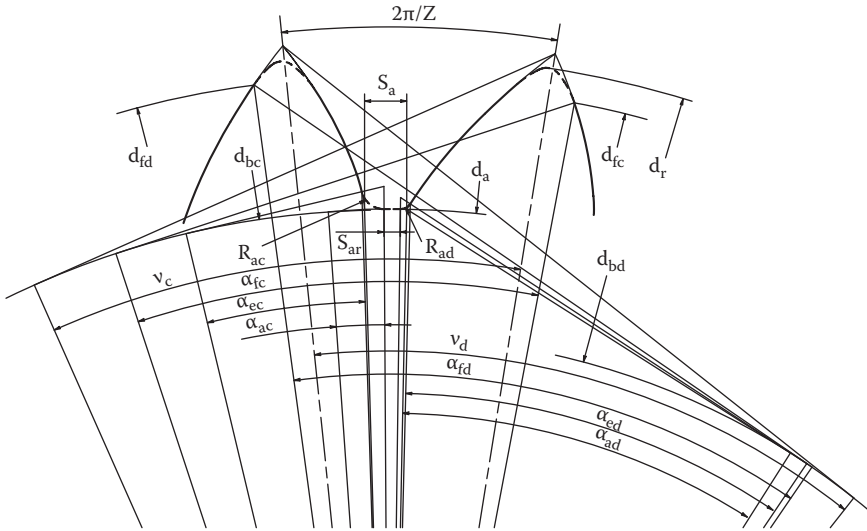


**FIGURE 2.7**  
Internal asymmetric gear tooth.

or

$$S_a = \frac{d_{bd}}{2 \cos \alpha_{ad}} \times (\operatorname{inv}(v_d) + \operatorname{inv}(v_c) - \operatorname{inv}(\alpha_{ad}) - \operatorname{inv}(\alpha_{ac})). \quad (2.31)$$

For internal tooth (Figure 2.7):

$$S_a = \frac{d_a}{2} \times (2\pi / z - \operatorname{inv}(v_d) - \operatorname{inv}(v_c) + \operatorname{inv}(\alpha_{ad}) + \operatorname{inv}(\alpha_{ac})) \quad (2.32)$$

or

$$S_a = \frac{d_{bd}}{2 \cos \alpha_{ad}} \times (2\pi / z - \operatorname{inv}(v_d) - \operatorname{inv}(v_c) + \operatorname{inv}(\alpha_{ad}) + \operatorname{inv}(\alpha_{ac})). \quad (2.33)$$

The profile angles  $\alpha_{ed}$  and  $\alpha_{ec}$  are the effective involute angles at the tooth tip. They are defined considering the tooth tip radii  $R_{ad}$  and  $R_{ac}$  for external gears as:

For drive flanks:

$$\alpha_{ed} = \arctan\left(\tan\left(\arccos\left(\frac{d_{bd}}{d_a \mp 2R_{ad}}\right)\right) \pm \frac{2R_{ad}}{d_{bd}}\right). \quad (2.34)$$

For coast flanks:

$$\alpha_{ec} = \arctan\left(\tan\left(\arccos\left(\frac{d_{bc}}{d_a \mp 2R_{ac}}\right)\right) \pm \frac{2R_{ac}}{d_{bc}}\right). \quad (2.35)$$

In Equations (2.33) and (2.34) signs  $\mp$  and  $\pm$  are the external gears and internal gears, respectively.

The tooth tip land  $S_{ar}$  of an external gear tooth is defined considering the tip radii  $R_{ad}$  and  $R_{ac}$ :

$$\begin{aligned} S_{ar} = & \frac{d_a}{2} \times (inv(v_d) + inv(v_c) - \tan \alpha_{ed} - \tan \alpha_{ec} + \arctan\left(\tan \alpha_{ed} - \frac{2R_{ad}}{d_{bd}}\right) \\ & + \arctan\left(\tan \alpha_{ec} - \frac{2R_{ac}}{d_{bc}}\right)). \end{aligned} \quad (2.36)$$

The tooth tip land  $S_{ar}$  of the internal gear tooth is

$$\begin{aligned} S_{ar} = & \frac{d_a}{2} \times \left(\frac{2\pi}{z} - inv(v_d) - inv(v_c) + \tan \alpha_{ed} + \tan \alpha_{ec} \right. \\ & \left. - \arctan\left(\tan \alpha_{ed} + \frac{2R_{ad}}{d_{bd}}\right) - \arctan\left(\tan \alpha_{ec} + \frac{2R_{ac}}{d_{bc}}\right)\right). \end{aligned} \quad (2.37)$$

The form diameters  $d_{fd}$  and  $d_{fc}$  and related profile angles  $\alpha_{fd}$  and  $\alpha_{fc}$  are defined considering a mesh with the mating gear (see Section 2.2). The root diameter  $d_r$  is defined as a result of the fillet profile optimization (see Section 5.3).

The asymmetric gear rack tooth is shown in Figure 2.8. The tooth tip land  $S_{ar}$  of the rack tooth is:

In the metric system:

$$S_{ar} = \frac{\pi m}{2} - H_{aed} \tan \alpha_d - R_{ad} \cos \alpha_d - H_{aec} \tan \alpha_c - R_{ac} \cos \alpha_c, \text{ or} \quad (2.38)$$

in the English system:

$$S_{ar} = \frac{\pi}{2DP} - H_{aed} \tan \alpha_d - R_{ad} \cos \alpha_d - H_{aec} \tan \alpha_c - R_{ac} \cos \alpha_c. \quad (2.39)$$

The nominal gear rack tooth addendum  $H_a$  is

$$H_a = H_{aed} + R_{ad}(1 - \sin \alpha_d) = H_{aec} + R_{ac}(1 - \sin \alpha_c). \quad (2.40)$$

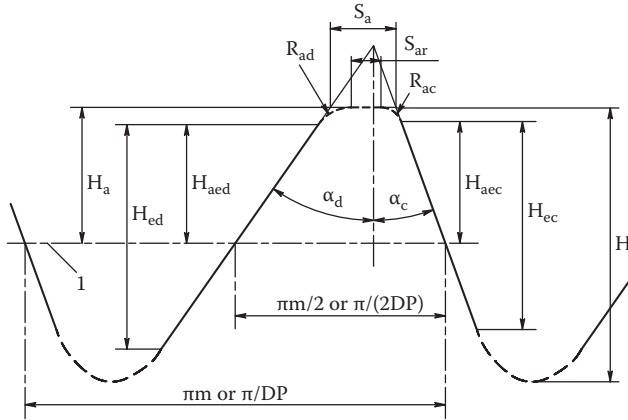


**FIGURE 2.8**

Asymmetric gear rack tooth: 1 - nominal pitch line;  $\alpha_d$  and  $\alpha_c$  - rack profile angles;  $H_a$  - nominal tooth addendum;  $H_{aed}$  and  $H_{aec}$  - nominal effective tooth addendums;  $H_{ed}$  and  $H_{ec}$  - nominal effective tooth profile depths;  $H$  - whole tooth depth.

The virtual tooth tip land  $S_a$  of the gear rack tooth is

In the metric system:

$$S_a = \frac{\pi m}{2} - H_a (\tan \alpha_d + \tan \alpha_c), \quad (2.41)$$

in the English system:

$$S_a = \frac{\pi}{2DP} - H_a (\tan \alpha_d + \tan \alpha_c). \quad (2.42)$$

---

## 2.2 Gear Mesh Characteristics

In this chapter the gear geometry is presented assuming the gear tooth tip radii and the mesh backlash equal to zero. The effect of the tooth tip radii and backlash on the gear mesh is considered in the tolerance analysis (see Chapter 7).

### 2.2.1 Symmetric Gearing

In traditional gear design the module  $m$  in the metric system (or diametral pitch  $DP$  in the English system) is a scale factor defining gear tooth size.

Prof. E.B. Vulgakov [8] proposed to use the gear base circle diameter as a scale factor. R.E. Kleiss also suggested this for the AGMA standard appendix [10]. In Direct Gear Design the nominal operating module  $m_w$  in the metric system (or nominal operating diametral pitch  $DP_w$  in the English system) is used as a gear tooth scale factor to make it easy to understand for engineers who are familiar with the traditional gear design. This also allows defining the nominal operating gear mesh center distance:

$$a_w = \frac{m_w(z_2 \pm z_1)}{2} \text{ or } a_w = \frac{z_2 \pm z_1}{2DP_w}, \quad (2.43)$$

where + is for external gear mesh and – is for internal gear mesh, and indexes 1 and 2 are related to parameters of the pinion with number of teeth  $z_1$  and of the gear with number of teeth  $z_2$ , accordingly. The pinion typically (but not necessarily) has fewer teeth than the gear and is the driving component of the gear pair.

The nominal operating pitch diameters of mating gears are

$$d_{w1,2} = m_w z_{1,2} \text{ or } d_{w1,2} = \frac{z_{1,2}}{DP_w}. \quad (2.44)$$

### 2.2.1.1 Pressure Angle

The external, internal, and rack and pinion gear meshes are shown in Figure 2.9.

The operating circular pitch  $p_w$  is

$$p_w = \frac{\pi \times d_{w1,2}}{z_{1,2}} = \frac{\pi \times d_{b1,2}}{z_{1,2} \times \cos \alpha_w}. \quad (2.45)$$

It can be presented in the metric system:

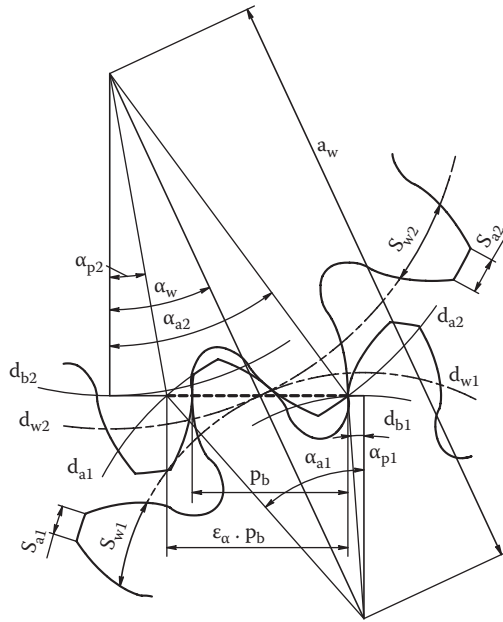
$$p_w = \pi m_w, \quad (2.46)$$

or in the English system:

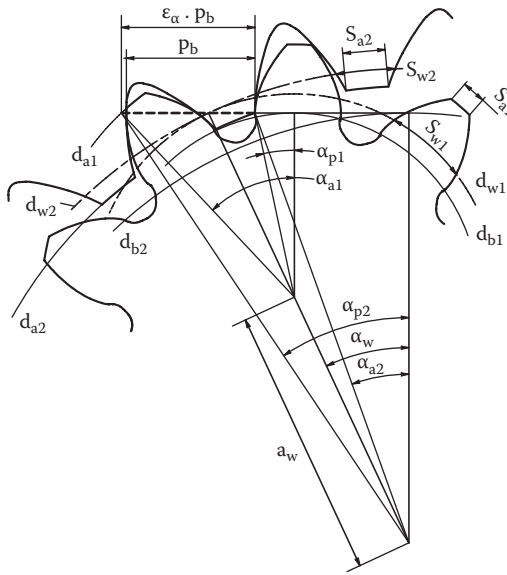
$$p_w = \frac{\pi}{DP_w}. \quad (2.47)$$

It is also

$$p_w = S_{w1} + S_{w2}. \quad (2.48)$$



(a)



(b)

**FIGURE 2.9**  
Symmetric gear mesh: (a) external, (b) internal, (c) rack and pinion.

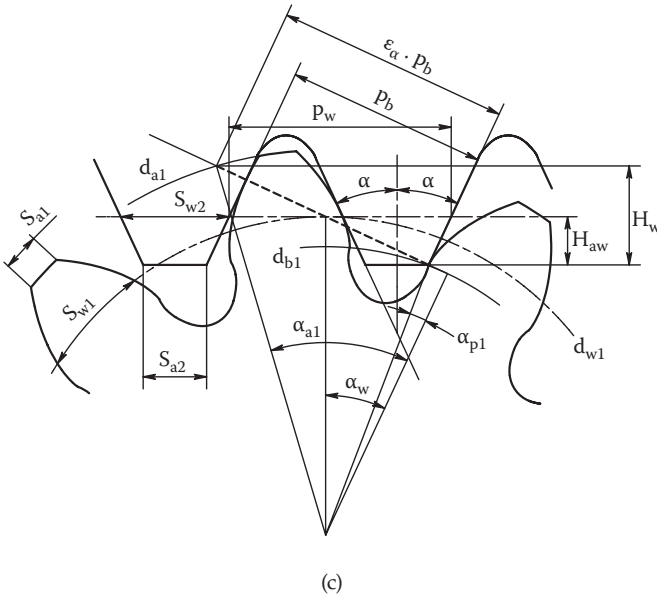


FIGURE 2.9 (continued)

The pinion tooth thicknesses at the nominal operating pitch diameter  $S_{w1}$  are defined from (2.6) as

$$S_{w1} = \frac{d_{b1}}{\cos \alpha_w} (\text{inv}(\nu_1) - \text{inv}(\alpha_w)). \quad (2.49)$$

The mating gear tooth thickness  $S_{w2}$  is:

For external gear mesh:

$$S_{w2} = \frac{d_{b2}}{\cos \alpha_w} (\text{inv}(\nu_2) - \text{inv}(\alpha_w)), \text{ or} \quad (2.50)$$

for internal gear mesh from (2.8):

$$S_{w2} = \frac{d_{b2}}{\cos \alpha_w} \left( \frac{\pi}{z_2} - \text{inv}(\nu_2) + \text{inv}(\alpha_w) \right). \quad (2.51)$$

For rack and pinion mesh the operating module is equal to the rack module  $m_w = m$  in the metric system, or the operating diametral pitch is equal to the rack diametral pitch  $DP_w = DP$  in the English system. The mating gear rack tooth thickness at the operating pitch line  $S_{w2}$  is



$$S_{w2} = \pi m - S_{w1} \quad \text{or} \quad S_{w2} = \frac{\pi}{DP} - S_{w1}. \quad (2.52)$$

Considering Equation (2.49), it is:

In the metric system:

$$S_{w2} = \pi m - \frac{d_{b1}}{\cos \alpha_w} (\text{inv}(v_1) - \text{inv}(\alpha_w)), \quad \text{or} \quad (2.53)$$

in the English system:

$$S_{w2} = \frac{\pi}{DP} - \frac{d_{b1}}{\cos \alpha_w} (\text{inv}(v_1) - \text{inv}(\alpha_w)). \quad (2.54)$$

The rack tooth operating addendum is

$$H_{aw} = \frac{S_{w2} - S_{a2}}{2 \tan \alpha}. \quad (2.55)$$

The nominal operating pressure angle  $\alpha_w$  is defined by substitution of  $S_{w1}$  and  $S_{w2}$  from Equations (2.49) and (2.50) or (2.51) into (2.48) with (2.45):

For external gear mesh [8]:

$$\text{inv}(\alpha_w) = \frac{1}{1+u} (\text{inv}(v_1) + u \times \text{inv}(v_2) - \frac{\pi}{z_1}), \quad \text{or} \quad (2.56)$$

for internal gear mesh:

$$\text{inv}(\alpha_w) = \frac{1}{u-1} (u \times \text{inv}(v_2) - \text{inv}(v_1)), \quad (2.57)$$

where  $u = z_2/z_1$ , the gear ratio.

In the rack and pinion mesh the nominal operating pressure angle  $\alpha_w$  is equal to the rack profile angle  $\alpha$ :

$$\alpha_w = \alpha. \quad (2.58)$$

### 2.2.1.2 Tip/Root Interference

The profile angles at the lowest points of contact near the fillet (see Figure 2.9) are:

For external gear mesh:

$$\alpha_{p1} = \arctan((1 + u) \tan \alpha_w - u \tan \alpha_{a2}), \quad (2.59)$$

$$\alpha_{p2} = \arctan\left(\frac{1 + u}{u} \tan \alpha_w - \frac{1}{u} \tan \alpha_{a1}\right). \quad (2.60)$$

For internal gear mesh:

$$\alpha_{p1} = \arctan(u \tan \alpha_{a2} - (u - 1) \tan \alpha_w), \quad (2.61)$$

$$\alpha_{p2} = \arctan\left(\frac{u - 1}{u} \tan \alpha_w + \frac{1}{u} \tan \alpha_{a1}\right). \quad (2.62)$$

For rack and pinion mesh:

$$\alpha_{p1} = \arctan\left(\tan \alpha - \frac{2H_{aw}}{d_{b1} \sin \alpha}\right), \quad (2.63)$$

$$\alpha_{p2} = \alpha. \quad (2.64)$$

The rack tooth operating depth is

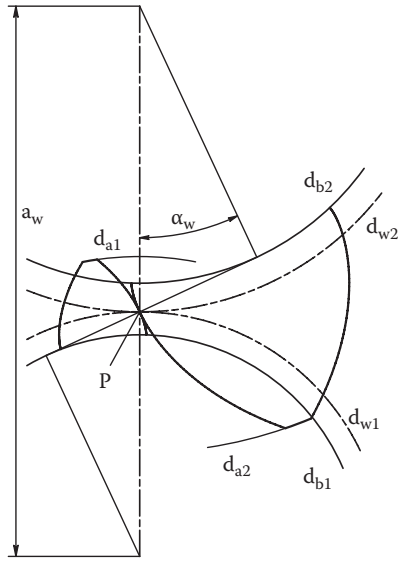
$$H_w = \frac{d_{b1} \sin \alpha}{2} (\tan \alpha_{a1} - \tan \alpha_{p1}). \quad (2.65)$$

If the profile angle  $\alpha_{p1}$  or  $\alpha_{p2}$  in the external mesh or angle  $\alpha_{p1}$  in the internal and rack and pinion meshes is less than zero, then its involute flanks close to the base diameters are interfering with the mating tooth tips. This leads to the involute profile undercut. This type of undercut is different than in the traditional gear design where the gear involute profile near to the tooth root is undercut by the cutter tooth tip.

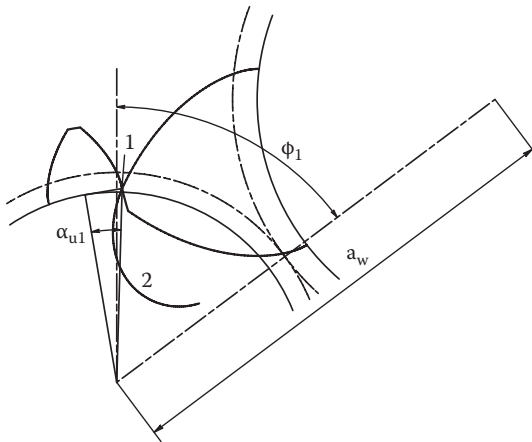
In an external mesh the pinion profile angle  $\alpha_{u1}$  at the undercut point is defined (Figure 2.10) by the equation system

$$\frac{\sin(\text{inv}(\alpha_w) - \text{inv}(\alpha_{u1}))}{\cos \alpha_{u1}} = (1 + u) \frac{\sin \phi_1}{\cos \alpha_w} - \frac{u}{\cos \alpha_{a2}} \sin\left(\phi_1 \left(1 + \frac{1}{u}\right)\right) - \text{inv}(\alpha_{a2}) + \text{inv}(\alpha_w) \quad (2.66)$$

$$\frac{\cos(\text{inv}(\alpha_w) - \text{inv}(\alpha_{u1}))}{\cos \alpha_{u1}} = (1 + u) \frac{\cos \phi_1}{\cos \alpha_w} - \frac{u}{\cos \alpha_{a2}} \cos\left(\phi_1 \left(1 + \frac{1}{u}\right)\right) - \text{inv}(\alpha_{a2}) + \text{inv}(\alpha_w).$$



(a)



(b)

**FIGURE 2.10**

Definition of the undercut profile angle  $\alpha_{u1}$  in external mesh: (a) initial tooth mesh position—gear teeth in contact at the pitch point  $P$ ; (b) undercut position. 1 - undercut profile point; 2 - trajectory of the mating gear tooth tip.

Similarly, in the case of the gear profile undercut, the angle  $\alpha_{u2}$  is defined by the system

$$\frac{u \sin(\text{inv}(\alpha_w) - \text{inv}(\alpha_{u2}))}{\cos \alpha_{u2}} = (1 + u) \frac{\sin \phi_2}{\cos \alpha_w} - \frac{\sin(\phi_2(1 + u) - \text{inv}(\alpha_{a1}) + \text{inv}(\alpha_w))}{\cos \alpha_{a1}} \quad (2.67)$$

$$\frac{u \cos(\text{inv}(\alpha_w) - \text{inv}(\alpha_{u2}))}{\cos \alpha_{u2}} = (1 + u) \frac{\cos \phi_2}{\cos \alpha_w} - \frac{\cos(\phi_2(1 + u) - \text{inv}(\alpha_{a1}) + \text{inv}(\alpha_w))}{\cos \alpha_{a1}}.$$

In an internal mesh the pinion profile angle  $\alpha_{u1}$  at the undercut point is defined (Figure 2.11) by the system

$$\frac{\sin(\text{inv}(\alpha_w) - \text{inv}(\alpha_{u1}))}{\cos \alpha_{u1}} = \frac{u}{\cos \alpha_{a2}} \sin(\phi_1(1 - \frac{1}{u}) - \text{inv}(\alpha_{a2}) + \text{inv}(\alpha_w)) - (u - 1) \frac{\sin \phi_1}{\cos \alpha_w}, \quad (2.68)$$

$$\frac{\cos(\text{inv}(\alpha_w) - \text{inv}(\alpha_{u1}))}{\cos \alpha_{u1}} = \frac{u}{\cos \alpha_{a2}} \cos(\phi_1(1 - \frac{1}{u}) - \text{inv}(\alpha_{a2}) + \text{inv}(\alpha_w)) - (u - 1) \frac{\cos \phi_1}{\cos \alpha_w}.$$

For the gear with internal teeth  $\alpha_{p2}$  is always greater than zero, and this kind of interference with undercut near the gear tooth fillet is impossible.

For a rack and pinion mesh the pinion profile angle  $\alpha_{u1}$  at the undercut point is defined (Figure 2.12) by the equation system

$$\frac{d_{b1}\phi_1}{2 \cos \alpha} - H_a \tan \alpha = \frac{d_{b1}}{2 \cos \alpha_{u1}} \sin(\phi_1 - \text{inv}(\alpha) - \text{inv}(\alpha_{u1})) \quad (2.69)$$

$$\frac{d_{b1}}{2 \cos \alpha} - H_a = \frac{d_{b1}}{2 \cos \alpha_{u1}} \cos(\phi_1 - \text{inv}(\alpha) - \text{inv}(\alpha_{u1})).$$

The rack teeth do not have this kind of interference with undercut near the fillet, because  $\alpha_{p2} = \alpha \geq 0$ .

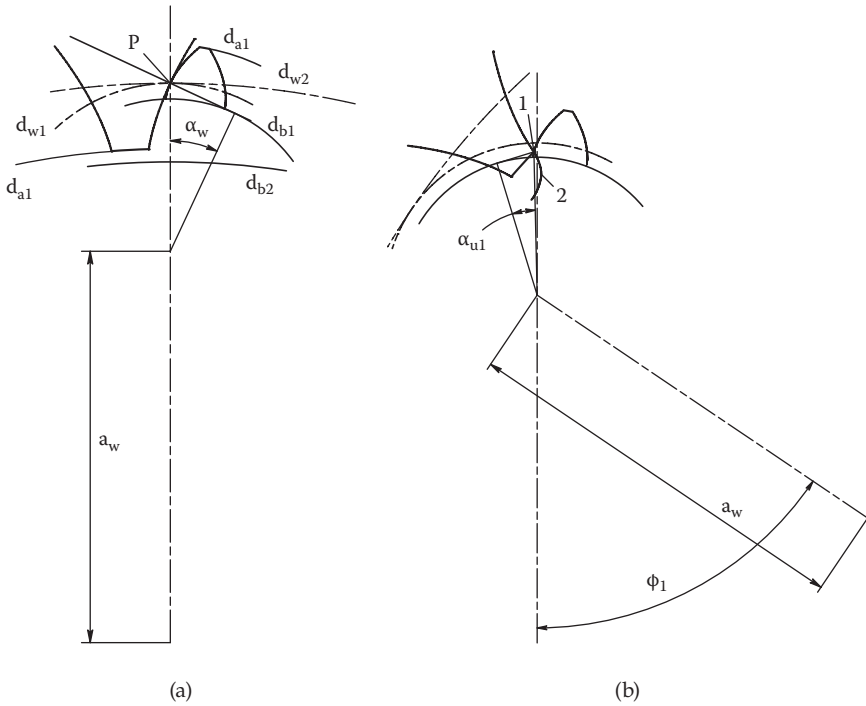


**FIGURE 2.11** Definition of the undercut profile angle  $\alpha_{u1}$  in internal mesh: (a) initial tooth mesh position—gear teeth in contact at the pitch point  $P$ ; (b) undercut position. 1 - undercut profile point; 2 - trajectory of the mating gear tooth tip.

If the undercut occurs, the lowest contact point coincides with the undercut point and the profile angles  $\alpha_{p1,2}$  become equal to profile angles at the undercut point  $\alpha_{u1,2}$ .

**2.2.1.3 Tip/Tip Interference in Internal Gearing**

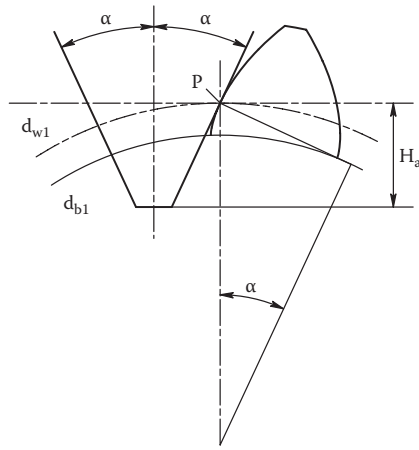
There is another kind of interference, which is typical for internal gearing. At certain gear geometry parameter combinations tips of the mating gears may interfere (Figure 2.13).

The interference condition is

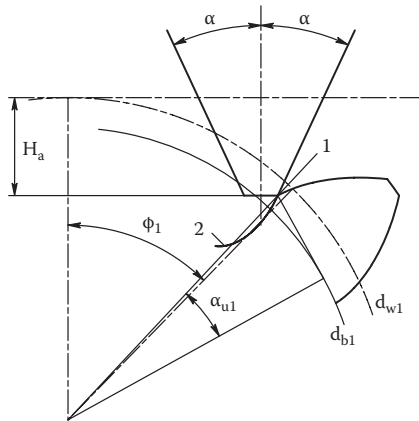
$$\Delta = \lambda_1 - u\lambda_2 \geq 0, \tag{2.70}$$

where

$$\lambda_{1,2} = \gamma_{1,2} + inv(\alpha_{a1,2}) - inv(\alpha_w), \tag{2.71}$$



(a)



(b)

**FIGURE 2.12**

Definition of the undercut profile angle  $\alpha_{u1}$  in rack and pinion mesh: (a) initial tooth mesh position—rack and pinion teeth in contact at the pitch point  $P$ ; (b) undercut position. 1 - undercut profile point; 2 - trajectory of the mating rack tooth tip.

$$\gamma_1 = \pi - \arccos\left(\frac{\frac{d_{a1}^2}{4} + a_w^2 - \frac{d_{a2}^2}{4}}{d_{a1}a_w}\right), \quad (2.72)$$

$$\gamma_2 = \arccos\left(\frac{\frac{d_{a2}^2}{4} + a_w^2 - \frac{d_{a1}^2}{4}}{d_{a2}a_w}\right). \quad (2.73)$$

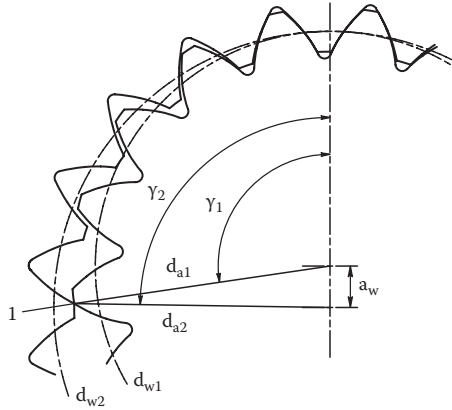


**FIGURE 2.13**

Tip/tip interference in the internal mesh: 1 - the interference point.

This kind of interference is more typical for internal gears with a low tooth number difference  $z_2 - z_1$  and low operating pressure angle  $\alpha_w$ . It can be avoided by increasing the pressure angle and reducing the tooth height.

#### 2.2.1.4 Transverse Contact Ratio

The transverse contact ratio is defined as the contact line length (the dashed line in Figure 2.9) divided by the base pitch  $p_{bt}$  that is,

$$p_b = \frac{\pi d_{b1}}{z_1} = \frac{\pi d_{b2}}{z_2} = p_w \cos \alpha_w. \quad (2.74)$$

Then the transverse contact ratio is [8]:

For external gear mesh:

$$\epsilon_\alpha = \frac{z_1}{2\pi} (\tan \alpha_{a1} + u \tan \alpha_{a2} - (1 + u) \tan \alpha_w). \quad (2.75)$$

For internal gear mesh:

$$\epsilon_\alpha = \frac{z_1}{2\pi} (\tan \alpha_{a1} - u \tan \alpha_{a2} + (u - 1) \tan \alpha_w). \quad (2.76)$$

For rack and pinion mesh:

$$\epsilon_\alpha = \frac{z_1}{2\pi} (\tan \alpha_{a1} - \tan \alpha + \frac{2H_{aw}}{db_1 \sin \alpha}). \quad (2.77)$$

Alternatively, the contact ratio can be defined:

For external gear mesh with Equations (2.59) and (2.60):

$$\varepsilon_{\alpha} = \frac{z_1}{2\pi} ((1 + u) \tan \alpha_w - \tan \alpha_{p1} - u \tan \alpha_{p2}). \quad (2.78)$$

For internal gear mesh with Equations (2.61) and (2.62):

$$\varepsilon_{\alpha} = \frac{z_1}{2\pi} (u \tan \alpha_{p2} - \tan \alpha_{p1} - (u - 1) \tan \alpha_w). \quad (2.79)$$

For rack and pinion mesh with Equation (2.63):

$$\varepsilon_{\alpha} = \frac{z_1}{2\pi} (\tan \alpha - \tan \alpha_{p1} + \frac{2(H_w - H_{aw})}{db_1 \sin \alpha}), \quad (2.80)$$

where  $H_w$  is the effective rack tooth depth.

Common solution of Equations (2.75) and (2.60) or (2.61), (2.76) and (2.62) or (2.63) allows presenting formulas for the transverse contact ratio as

$$\varepsilon_{\alpha} = \frac{z_1}{2\pi} (\tan \alpha_{a1} - \tan \alpha_{p1}), \quad (2.81)$$

$$\varepsilon_{\alpha} = \frac{z_2}{2\pi} (\pm \tan \alpha_{a2} \mp \tan \alpha_{p2}), \quad (2.82)$$

where the symbols  $\pm$  and  $\mp$  are the external gears and internal gears, respectively.

For a rack and pinion mesh the transverse contact ratio can be also defined by solving Equations (2.64), (2.77), and (2.80):

$$\varepsilon_{\alpha} = \frac{H_w}{p_b \sin \alpha} = \frac{2H_w}{p_w \sin 2\alpha}. \quad (2.83)$$

Then the rack and pinion mesh transverse contact ratio is:

In the metric system:

$$\varepsilon_{\alpha} = \frac{2H_w}{\pi m_w \sin 2\alpha}. \quad (2.84)$$

In the English system:

$$\varepsilon_{\alpha} = \frac{2DP \times H_w}{\pi \sin 2\alpha}. \quad (2.85)$$



### 2.2.2 Asymmetric Gearing

Asymmetric external, internal, and rack and pinion gear meshes are shown in Figure 2.14.

In all figures and equations describing gears with asymmetric teeth indexes,  $d$  and  $c$  are for parameters related to the drive and coast tooth flanks, accordingly.

#### 2.2.2.1 Pressure Angles

The pinion and gear tooth thicknesses  $S_{w1}$  and  $S_{w2}$  at the operating pitch diameters  $d_{w1,2}$  are defined by Equations (2.26) and (2.28) as

$$S_{w1} = \frac{d_{bd1}}{2 \cos \alpha_{wd}} (\text{inv}(v_{d1}) + \text{inv}(v_{c1}) - \text{inv}(\alpha_{wd}) - \text{inv}(\alpha_{wc})). \quad (2.86)$$

For external gearing:

$$S_{w2} = \frac{d_{bd2}}{2 \cos \alpha_{wd}} (\text{inv}(v_{d2}) + \text{inv}(v_{c2}) - \text{inv}(\alpha_{wd}) - \text{inv}(\alpha_{wc})). \quad (2.87)$$

For internal gearing:

$$S_{w2} = \frac{d_{bd2}}{2 \cos \alpha_{wd}} \left( \frac{2\pi}{z_2} - \text{inv}(v_{d2}) - \text{inv}(v_{c2}) + \text{inv}(\alpha_{wd}) + \text{inv}(\alpha_{wc}) \right). \quad (2.88)$$

The mating gear rack tooth thickness at the operating pitch line  $S_{w2}$  is from (2.52):

For the metric system:

$$S_{w2} = \pi m - \frac{d_{bd1}}{2 \cos \alpha_d} (\text{inv}(v_{d1}) + \text{inv}(v_{c1}) - \text{inv}(\alpha_d) - \text{inv}(\alpha_c)). \quad (2.89)$$

For the English system:

$$S_{w2} = \frac{\pi}{DP} - \frac{d_{bd1}}{2 \cos \alpha_d} (\text{inv}(v_{d1}) + \text{inv}(v_{c1}) - \text{inv}(\alpha_d) - \text{inv}(\alpha_c)). \quad (2.90)$$

The operating pressure angle for the drive flanks  $\alpha_{wd}$  and the coast flanks  $\alpha_{wc}$  is defined by substitution of  $S_{w1}$  and  $S_{w2}$  from Equations (2.86) and (2.87) or (2.88) into (2.48).

For external gear:

$$\text{inv}(\alpha_{wd}) + \text{inv}(\alpha_{wc}) = \frac{1}{1+u} (\text{inv}(v_{d1}) + \text{inv}(v_{c1}) + u(\text{inv}(v_{d2}) + \text{inv}(v_{c2}))) - \frac{2\pi}{z_1}. \quad (2.91)$$

For internal gear:

$$\text{inv}(\alpha_{wd}) + \text{inv}(\alpha_{wc}) = \frac{1}{u-1} (u(\text{inv}(v_{d2}) + \text{inv}(v_{c2})) - \text{inv}(v_{d1}) - \text{inv}(v_{c1})). \quad (2.92)$$

The relation between pressure angles for the drive flanks  $\alpha_{wd}$  and pressure angles for the coast flanks  $\alpha_{wc}$  is defined from (2.21) as

$$\cos \alpha_{wc} = K \cos \alpha_{wd}. \quad (2.93)$$

In the rack and pinion mesh the operating pressure angles  $\alpha_{wd}$  and  $\alpha_{wc}$  are equal to the pack profile angles  $\alpha_d$  and  $\alpha_c$ :

$$\alpha_{wd} = \alpha_d \text{ and } \alpha_{wc} = \alpha_c. \quad (2.94)$$

### 2.2.2.2 Interference for Asymmetric Gears

The profile angles at the lowest points of contact near the fillet are:

For external gear mesh, drive flanks:

$$\alpha_{pd1} = \arctan((1+u) \tan \alpha_{wd} - u \tan \alpha_{ad2}), \quad (2.95)$$

$$\alpha_{pd2} = \arctan\left(\frac{1+u}{u} \tan \alpha_{wd} - \frac{1}{u} \tan \alpha_{ad1}\right). \quad (2.96)$$

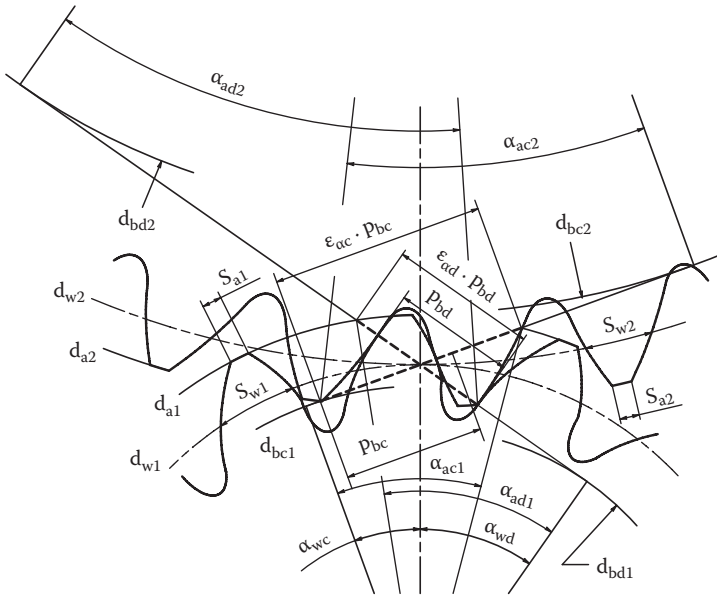
For external gear mesh, coast flanks:

$$\alpha_{pc1} = \arctan((1+u) \tan \alpha_{wc} - u \tan \alpha_{ac2}), \quad (2.97)$$

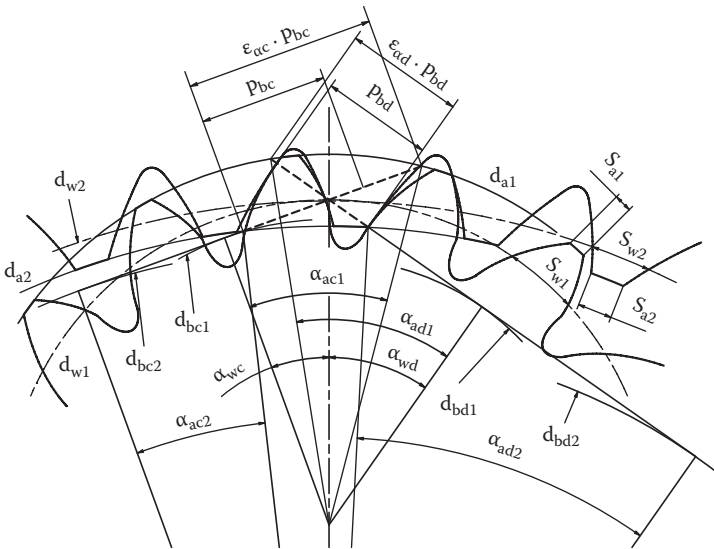
$$\alpha_{pc2} = \arctan\left(\frac{1+u}{u} \tan \alpha_{wc} - \frac{1}{u} \tan \alpha_{ac1}\right). \quad (2.98)$$

For internal gear mesh, drive flanks:

$$\alpha_{pd1} = \arctan(u \tan \alpha_{ad2} - (u-1) \tan \alpha_{wd}), \quad (2.99)$$



(a)



(b)

**FIGURE 2.14**  
Asymmetric gear mesh: (a) external, (b) internal, (c) rack and pinion.

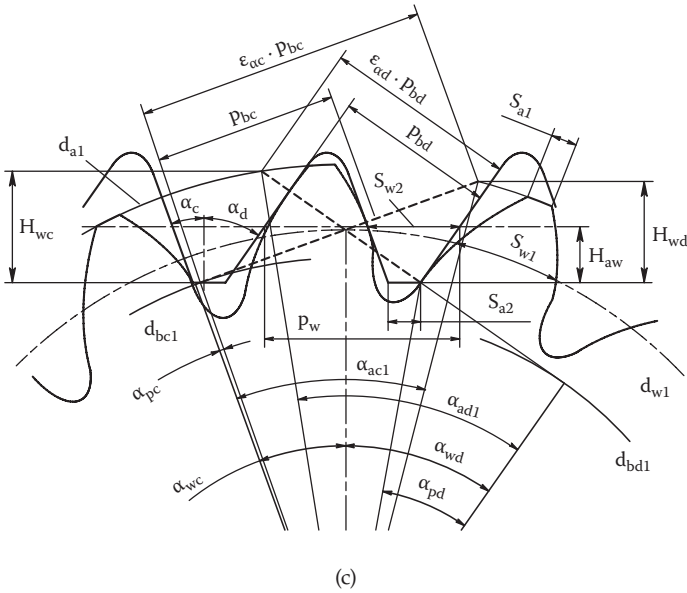


FIGURE 2.14 (continued)

$$\alpha_{pd2} = \arctan\left(\frac{u-1}{u} \tan \alpha_{wd} + \frac{1}{u} \tan \alpha_{ad1}\right). \quad (2.100)$$

For internal gear mesh, coast flanks:

$$\alpha_{pc1} = \arctan(u \tan \alpha_{ac2} - (u-1) \tan \alpha_{wc}), \quad (2.101)$$

$$\alpha_{pc2} = \arctan\left(\frac{u-1}{u} \tan \alpha_{wc} + \frac{1}{u} \tan \alpha_{ac1}\right). \quad (2.102)$$

For rack and pinion mesh, drive flanks:

$$\alpha_{pd1} = \arctan\left(\tan \alpha_d - \frac{2H_a}{d_{bd1} \sin \alpha_d}\right), \quad (2.103)$$

$$\alpha_{pd2} = \alpha_d. \quad (2.104)$$

For rack and pinion mesh, coast flanks:

$$\alpha_{pc1} = \arctan\left(\tan \alpha_c - \frac{2H_a}{d_{bc1} \sin \alpha_c}\right), \quad (2.105)$$

$$\alpha_{pc2} = \alpha_c. \quad (2.106)$$

The rack tooth operating depths are

$$H_{wd} = \frac{d_{bd1} \sin \alpha_d}{2} (\tan \alpha_{ad1} - \tan \alpha_{pd1}), \quad (2.107)$$

$$H_{wc} = \frac{d_{bc1} \sin \alpha_c}{2} (\tan \alpha_{ac1} - \tan \alpha_{pc1}). \quad (2.108)$$

If asymmetry factor  $K > 0$ , interference occurs first for the coast involute flanks. If the profile angle  $\alpha_{pc1}$  or  $\alpha_{pc2}$  in the external mesh or angle  $\alpha_{pc1}$  in the internal and rack and pinion meshes is less than zero, then its involute flanks close to the base diameters are interfering with the mating tooth tips. This leads to the involute profile undercut.

Tooth profile tip/root and tip/tip interference conditions in the asymmetric gearing are exactly the same as in the symmetric one (see Sections 2.2.1.2 and 2.2.1.3). All interference equations of the symmetric gearing are applicable for the asymmetric one.

### 2.2.2.3 Transverse Contact Ratio for Asymmetric Gears

The transverse contact ratios for asymmetric gears are defined exactly the same way as for the symmetric gears (Equations (2.75) to (2.80)), but separately for the drive and coast tooth flanks:

For external gear mesh, drive flanks:

$$\varepsilon_{ad} = \frac{z_1}{2\pi} (\tan \alpha_{ad1} + u \tan \alpha_{ad2} - (1 + u) \tan \alpha_{wd}). \quad (2.109)$$

For external gear mesh, coast flanks:

$$\varepsilon_{ac} = \frac{z_1}{2\pi} (\tan \alpha_{ac1} + u \tan \alpha_{ac2} - (1 + u) \tan \alpha_{wc}). \quad (2.110)$$

For internal gear mesh, drive flanks:

$$\varepsilon_{ad} = \frac{z_1}{2\pi} (\tan \alpha_{ad1} - u \tan \alpha_{ad2} + (u - 1) \tan \alpha_{wd}). \quad (2.111)$$

For internal gear mesh, coast flanks:

$$\varepsilon_{\alpha c} = \frac{z_1}{2\pi} (\tan \alpha_{ac1} - u \tan \alpha_{ac2} + (u - 1) \tan \alpha_{wc}). \quad (2.112)$$

For rack and pinion mesh, drive flanks:

$$\varepsilon_{\alpha d} = \frac{z_1}{2\pi} (\tan \alpha_{ad1} - \tan \alpha_d + \frac{2H_a}{d_{bd1} \sin \alpha_d}). \quad (2.113)$$

For rack and pinion mesh, coast flanks:

$$\varepsilon_{\alpha c} = \frac{z_1}{2\pi} (\tan \alpha_{ac1} - \tan \alpha_c + \frac{2H_a}{d_{bc1} \sin \alpha_c}). \quad (2.114)$$

Alternatively, the contact ratios for external asymmetric gear meshes can be defined with Equations (2.95) to (2.98):

For drive flanks:

$$\varepsilon_{\alpha d} = \frac{z_1}{2\pi} ((1 + u) \tan \alpha_{wd} - \tan \alpha_{pd1} - u \tan \alpha_{pd2}). \quad (2.115)$$

For coast flanks:

$$\varepsilon_{\alpha c} = \frac{z_1}{2\pi} ((1 + u) \tan \alpha_{wc} - \tan \alpha_{pc1} - u \tan \alpha_{pc2}). \quad (2.116)$$

The contact ratios for internal asymmetric gear meshes are defined with Equations (2.99) to (2.102):

For drive flanks:

$$\varepsilon_{\alpha d} = \frac{z_1}{2\pi} (u \tan \alpha_{pd2} - \tan \alpha_{pd1} - (u - 1) \tan \alpha_{wd}). \quad (2.117)$$

For coast flanks:

$$\varepsilon_{\alpha c} = \frac{z_1}{2\pi} (u \tan \alpha_{pc2} - \tan \alpha_{pc1} - (u - 1) \tan \alpha_{wc}). \quad (2.118)$$

The rack and pinion mesh contact ratios are defined with Equations (2.103) and (2.105):

For drive flanks:

$$\epsilon_{\alpha d} = \frac{z_1}{2\pi} (\tan \alpha_d - \tan \alpha_{pd1} + \frac{2(H_{wd} - H_{aw})}{d_{bd1} \sin \alpha_d}). \quad (2.119)$$

For coast flanks:

$$\epsilon_{\alpha c} = \frac{z_1}{2\pi} (\tan \alpha_c - \tan \alpha_{pc1} + \frac{2(H_{wc} - H_{aw})}{d_{bc1} \sin \alpha_c}), \quad (2.120)$$

where  $H_{wd}$  and  $H_{wc}$  are effective rack tooth depths.

Similar to gears with symmetric teeth the transverse contact ratios of gears with asymmetric teeth can be presented using parameters for only one of the mating gears:

For drive flanks:

$$\epsilon_{\alpha d} = \frac{z_1}{2\pi} (\tan \alpha_{ad1} - \tan \alpha_{pd1}), \quad (2.121)$$

$$\epsilon_{\alpha d} = \frac{z_2}{2\pi} (\pm \tan \alpha_{ad2} \mp \tan \alpha_{pd2}). \quad (2.122)$$

For coast flanks:

$$\epsilon_{\alpha c} = \frac{z_1}{2\pi} (\tan \alpha_{ac1} - \tan \alpha_{pc1}), \quad (2.123)$$

$$\epsilon_{\alpha c} = \frac{z_2}{2\pi} (\pm \tan \alpha_{ac2} \mp \tan \alpha_{pc2}), \quad (2.124)$$

where the symbols  $\pm$  and  $\mp$  are the external gears and internal gears, respectively.

For a rack and pinion mesh the transverse contact ratios can be also defined the same way:

For drive flanks:

$$\epsilon_{\alpha d} = \frac{H_{wd}}{p_{bd} \sin \alpha_d} = \frac{2H_{wd}}{p_w \sin 2\alpha_d}. \quad (2.125)$$

For coast flanks:

$$\epsilon_{\alpha c} = \frac{H_{wc}}{p_{bc} \sin \alpha_c} = \frac{2H_{wc}}{p_w \sin 2\alpha_c} . \quad (2.126)$$

In the metric system they are defined as:

For drive flanks:

$$\epsilon_{\alpha d} = \frac{2H_{wd}}{\pi m_w \sin 2\alpha_d} . \quad (2.127)$$

For coast flanks:

$$\epsilon_{\alpha c} = \frac{2H_{wc}}{\pi m_w \sin 2\alpha_c} . \quad (2.128)$$

In the English system they are:

For drive flanks:

$$\epsilon_{\alpha d} = \frac{2DP \times H_{wd}}{\pi \sin 2\alpha_d} . \quad (2.129)$$

For coast flanks:

$$\epsilon_{\alpha c} = \frac{2DP \times H_{wc}}{\pi \sin 2\alpha_c} . \quad (2.130)$$

### 2.2.3 Contact Ratio for Helical Gears

Spur gear mesh has only a transverse contact ratio  $\epsilon_{\alpha}$ . For helical gears there is also axial (or face) contact ratio  $\epsilon_{\beta}$  that in addition to the transverse contact ratio  $\epsilon_{\alpha}$  results with the total gear ratio  $\epsilon_{\gamma}$  which is

$$\epsilon_{\gamma} = \epsilon_{\alpha} + \epsilon_{\beta} . \quad (2.131)$$

The axial contact ratio  $\epsilon_{\beta}$  is defined by the angular shift  $\phi$  of the helical gear sections (see Figure 2.15), which is [35, 36]

$$\phi = \frac{2AC}{d_b} = \frac{2AB}{d_b} . \quad (2.132)$$



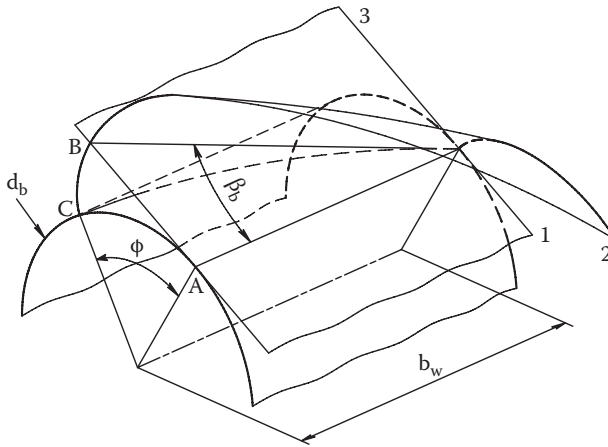


**FIGURE 2.15**

Angular shift  $\phi$  of the helical gear sections: 1 - base cylinder; 2 - helical involute surface; 3 - contact plane tangent to the base cylinder. (From Kapelevich, A.L., et al., *Direct Gear Design for spur and helical gears*, *Gear Technology*, September/October 2002, 29–35. With permission.)

or

$$\phi = \frac{2b_w}{p_b} \tan \beta_b, \quad (2.133)$$

where  $AC$  is arc shift of helical gear sections,  $AB$  is shift of helical gear sections projected on the contact plane tangent to the base cylinder at point  $A$ ,  $b_w$  is contact face width, a distance between helical gear sections in contact, and  $\beta_b$  is helix angle at the base cylinder.

For two mating gears,

$$\phi_1 = u \times \phi_2. \quad (2.134)$$

Axial contact ratio  $\epsilon_\beta$  is defined by Equations (2.74), (2.132), (2.133), and (2.134):

$$\epsilon_\beta = \frac{AB}{p_b} = \frac{z_1}{2\pi} \phi_1 = \frac{z_2}{2\pi} \phi_2 = \frac{b_w}{p_b} \tan \beta_b. \quad (2.135)$$

For asymmetric gears the axial contact ratio is identical for the drive and coast flanks because according to Equation (2.21),

$$p_{bc} = p_{bd} \frac{d_{bc}}{d_{bd}} = p_{bd} \times K \quad (2.136)$$

and

$$\tan \beta_{bc} = \tan \beta_{bd} \frac{d_{bc}}{d_{bd}} = \tan \beta_{bd} \times K . \quad (2.137)$$

This allows presenting Equation (2.135) for asymmetric gears as

$$\epsilon_{\beta} = \epsilon_{\beta d} = \epsilon_{\beta c} = \frac{b_w}{p_{bd}} \tan \beta_{bd} = \frac{b_w}{p_{bc}} \tan \beta_{bc} . \quad (2.138)$$

### 2.3 Pitch Factor Analysis

This section presents an alternative method of involute gear geometry parameters and mesh definition, which is called the pitch factor analysis [28, 29].

The gear mesh operating circular pitch (from Equation (2.45)) is

$$p_w = \frac{\pi \times d_{w1,2}}{z_{1,2}} = S_{w1} + S_{w2} + S_{bl} , \quad (2.139)$$

where  $S_{w1}$  and  $S_{w2}$  are the pinion and gear tooth thicknesses at the operating pitch diameter, and  $S_{bl}$  is the arc backlash.

The tooth thicknesses  $S_{w1}$  and  $S_{w2}$  are (see Figures 2.16 and 2.17)

For symmetric gears:

$$S_{w1,2} = 2S_{1,2} + S_{v1,2} . \quad (2.140)$$

For asymmetric gears:

$$S_{w1,2} = S_{d1,2} + S_{c1,2} + S_{v1,2} , \quad (2.141)$$

where

$$S_{d1,2} = \frac{d_{w1,2}}{2} (\pm \text{inv}(\alpha_{ed1,2}) \mp \text{inv}(\alpha_{wd})) \quad (2.142)$$

are projections of the addendum portion of the drive involute flank on the pitch circle,

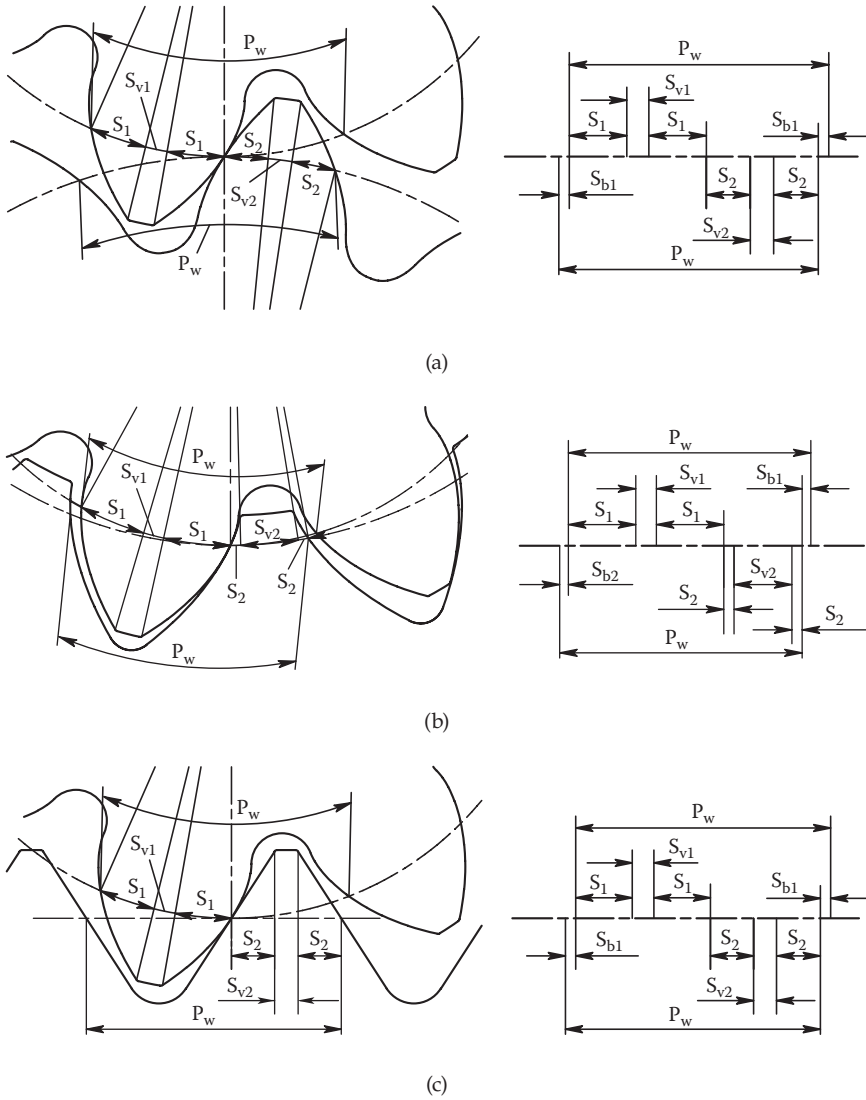


**FIGURE 2.16** Symmetric gear mesh and operating pitch components: (a) external, (b) internal, (c) rack and pinion.

$$S_{c1,2} = \frac{d_{w1,2}}{2} (\pm inv(\alpha_{ec1,2}) \mp inv(\alpha_{vc})) \tag{2.143}$$

are projections of the addendum portion of the coast involute flank on the pitch circle, the symbols  $\mp$  and  $\pm$  are the external gears and internal gears, respectively, and  $S_{v1,2}$  are the pitch circle projections of the tip land and radii.

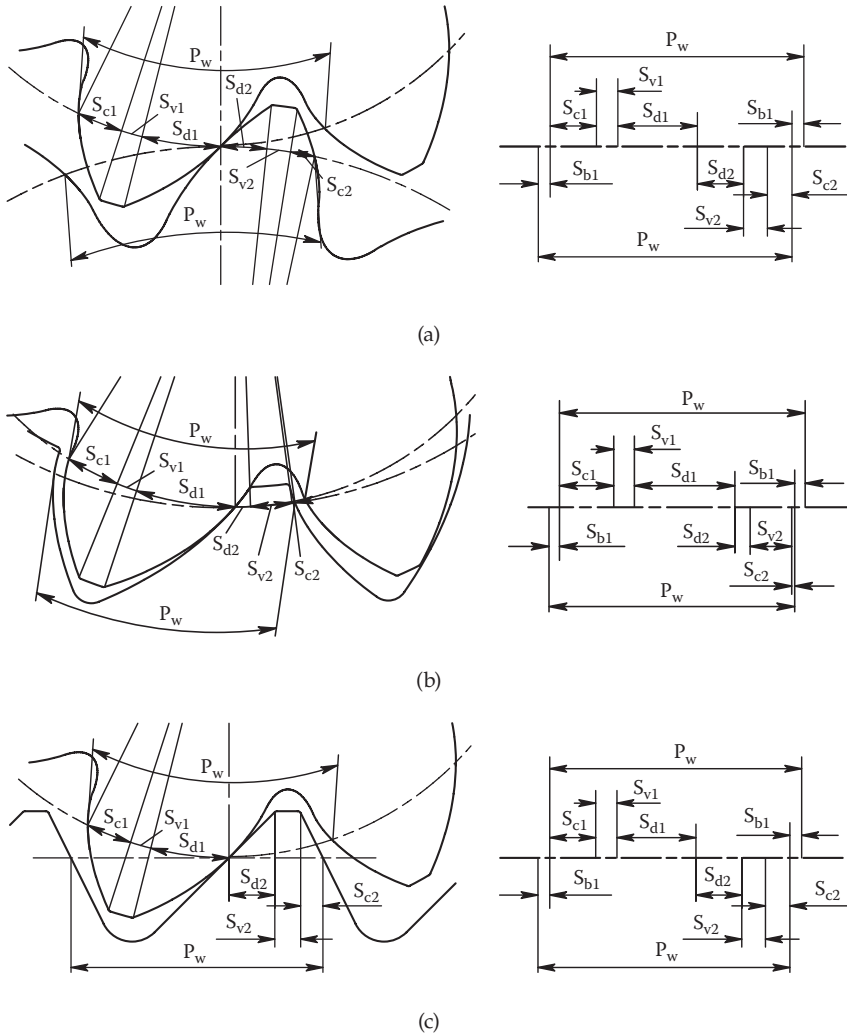


**FIGURE 2.17** Asymmetric gear mesh and operating pitch components: (a) external, (b) internal, (c) rack and pinion.

For rack and pinion gear mesh  $S_{d2}$ ,  $S_{c2}$ , and  $S_{v2}$  are the pitch line projections. In this case a projection of the addendum portion of the drive flank on the pitch line is

$$S_{d2} = H_{aed} \tan \alpha_d . \tag{2.144}$$

A projection of the addendum portion of the coast flank on the pitch line is

$$S_{c2} = H_{aec} \tan \alpha_c . \tag{2.145}$$

Then the gear mesh operating circular pitch from (2.139) is

$$p_w = S_{d1} + S_{d2} + S_{c1} + S_{c2} + S_{v1} + S_{v2} + S_{bl} . \quad (2.146)$$

A pitch factor equation is a result of division of Equation (2.146) by operating circular pitch  $p_w$ :

$$\theta_d + \theta_c + \theta_v = 1 , \quad (2.147)$$

where  $\theta_d$  is the coast pitch factor that is defined as

$$\theta_d = \frac{S_{d1} + S_{d2}}{p_w} , \quad (2.148)$$

$\theta_c$  is the drive pitch factor that is defined as

$$\theta_c = \frac{S_{c1} + S_{c2}}{p_w} , \quad (2.149)$$

and  $\theta_v$  is the noncontact pitch factor that is defined as

$$\theta_v = \frac{S_{v1} + S_{v2} + S_{bl}}{p_w} . \quad (2.150)$$

The drive pitch factor is:

For external gear mesh:

$$\theta_d = \frac{z_1}{2\pi} (inv(\alpha_{ed1}) + uinv(\alpha_{ed2}) - (1 + u)inv(\alpha_{wd})) . \quad (2.151)$$

For internal gear mesh:

$$\theta_d = \frac{z_1}{2\pi} (inv(\alpha_{ed1}) - uinv(\alpha_{ed2}) + (u - 1)inv(\alpha_{wd})) . \quad (2.152)$$

The coast pitch factor is:

For external gear mesh:

$$\theta_c = \frac{z_1}{2\pi} (inv(\alpha_{ec1}) - uinv(\alpha_{ec2}) + (u - 1)inv(\alpha_{wc})) . \quad (2.153)$$

For internal gear mesh:

$$\theta_c = \frac{z_1}{2\pi} (inv(\alpha_{ec1}) + uinv(\alpha_{ec2}) - (1+u)inv(\alpha_{wc})) . \quad (2.154)$$

For rack and pinion gear mesh the drive and coast pitch factors are

$$\theta_d = \frac{z_1}{2\pi} (inv(\alpha_{ed1}) - inv(\alpha_d)) + \frac{H_{acd}}{p_w} \tan \alpha_d \quad (2.155)$$

and

$$\theta_c = \frac{z_1}{2\pi} (inv(\alpha_{ec1}) - inv(\alpha_c)) + \frac{H_{acc}}{p_w} \tan \alpha_c . \quad (2.156)$$

The drive and coast pressure angles are defined by equations:

For external gear mesh:

$$inv(\alpha_{wd}) = \frac{1}{1+u} (inv(\alpha_{ed1}) + uinv(\alpha_{ed2}) - \frac{2\pi\theta_d}{z_1}) , \quad (2.157)$$

$$inv(\alpha_{wc}) = \frac{1}{1+u} (inv(\alpha_{ec1}) + uinv(\alpha_{ec2}) - \frac{2\pi\theta_c}{z_1}) . \quad (2.158)$$

For internal gear mesh:

$$inv(\alpha_{wd}) = \frac{1}{u-1} (\frac{2\pi\theta_d}{z_1} - inv(\alpha_{ed1}) + uinv(\alpha_{ed2})) , \quad (2.159)$$

$$inv(\alpha_{wc}) = \frac{1}{u-1} (\frac{2\pi\theta_c}{z_1} - inv(\alpha_{ec1}) + uinv(\alpha_{ec2})) . \quad (2.160)$$

For rack and pinion gear mesh:

$$\alpha_{wd} = \alpha_d \quad (2.161)$$

and

$$\alpha_{wc} = \alpha_c . \quad (2.162)$$

For gears with symmetric teeth the angles  $\alpha_{e1,2} = \alpha_{ed1,2} = \alpha_{ec1,2}$  and  $\alpha_w = \alpha_{wd} = \alpha_{wc}$ . Then the pitch factor  $\theta = \theta_d = \theta_c$ , that is:

For external gear mesh:

$$\theta = \frac{z_1}{2\pi} (inv(\alpha_{e1}) + uinv(\alpha_{e2}) - (1+u)inv(\alpha_w)). \quad (2.163)$$

For internal gear mesh:

$$\theta = \frac{z_1}{2\pi} (inv(\alpha_{e1}) - uinv(\alpha_{e2}) + (u-1)inv(\alpha_w)). \quad (2.164)$$

For rack and pinion gear mesh:

$$\theta = \frac{z_1}{2\pi} (inv(\alpha_{ed}) - inv(\alpha)) + \frac{H_{ae}}{p_w} \tan \alpha. \quad (2.165)$$

The pressure angle is defined by the following equations:

For external gear mesh:

$$inv(\alpha_w) = \frac{1}{1+u} (inv(\alpha_{e1}) + uinv(\alpha_{e2}) - \frac{2\pi\theta}{z_1}). \quad (2.166)$$

For internal gear mesh:

$$inv(\alpha_w) = \frac{1}{u-1} (\frac{2\pi\theta}{z_1} - inv(\alpha_{e1}) + uinv(\alpha_{e2})). \quad (2.167)$$

For rack and pinion gear mesh:

$$\alpha_w = \alpha. \quad (2.168)$$

For gears with symmetric teeth the pitch factor  $\theta$  from Equation (2.131) is

$$\theta = \theta_d = \theta_c = \frac{1}{2} \times (1 - \theta_v). \quad (2.169)$$

This equation shows that for symmetric gears the pitch factor  $\theta$  always  $\leq 0.5$ . For the standard  $20^\circ$  pressure angle gears  $\theta = 0.25-0.30$ , and for the  $25^\circ$  pressure angle gears  $\theta = 0.30-0.35$ . In custom symmetric gears the pitch  $\theta$  can reach values of  $0.40-0.45$ .

For gears with asymmetric teeth the drive pitch factor  $\theta_d$  from Equation (2.147) is

$$\theta_d = 1 - \theta_c - \theta_v. \quad (2.170)$$

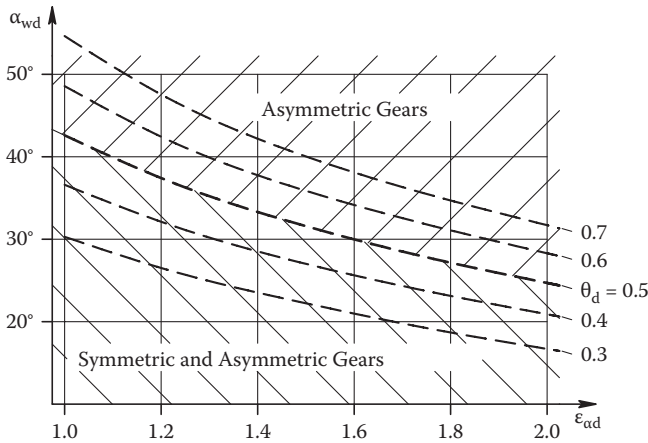


**FIGURE 2.18** A sample of the  $\alpha_{wd} - \epsilon_{ad}$  chart with different values of the drive pitch factor  $\theta_d$  for a gear couple with the pinion number of teeth  $z_1 = 21$  and the gear number of teeth  $z_2 = 37$ .

Reduction of the coast pitch factor  $\theta_c$  and the noncontact pitch factor  $\theta_v$  allows a significant increase in the drive pitch factor  $\theta_d$ . Figure 2.18 presents a sample of the drive pressure angle vs. the drive contact ratio  $\alpha_{wd} - \epsilon_{ad}$  chart at a different value of  $\theta_d$  for a gear couple with the pinion number of teeth  $z_1 = 21$  and the gear number of teeth  $z_2 = 37$ . The chart shows that the symmetric gear solutions lie below the curve  $\theta_d = 0.5$  and the asymmetric gears are located below and above this curve. A simultaneous increase in the drive pressure angle and the drive contact ratio maximizes gear drive performance. It allows reducing the contact and bending stress, increasing load capacity and power transmission density. This indicates potential advantages of the asymmetric gears over the symmetric ones for gear drives that transmit load mostly in one direction.

The pitch factor analysis is the additional Direct Gear Design analytical tool that can be used for comparison of different gear geometry solutions, helping the designer better understand available options and choose the optimal one.

## 2.4 Application of Direct Gear Design for Different Types of Involute Gears

In the previous sections the Direct Gear Design approach was described for spur gears. However, it is applicable to any other type of involute gears: helical, bevel, worm, face gears, etc. Tooth macrogeometry of these gears is



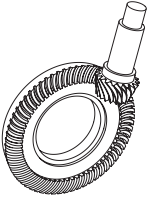
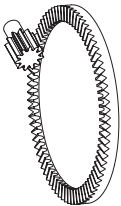
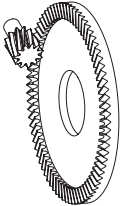
typically defined in a normal plane to the tooth line. This normal plane tooth profile can be considered a tooth profile of the virtual spur gear. Formulas for calculating number of teeth of virtual spur gears that have a tooth profile that is identical to the normal plane tooth profile of different types of involute types of gears are shown in Table 2.1. Virtual numbers of teeth are usually real numbers with the decimal parts. The tooth geometry of virtual spur gears is optimized by means of Direct Gear Design. Then the optimized tooth profiles are considered the normal section tooth profiles of the actual gears.

**TABLE 2.1**  
Virtual Spur Gear Conversion

Type of Gear	Number of Teeth of Virtual Spur Gears
Spur	$Z_{1,2v} = Z_{1,2}$
Helical	$Z_{1,2v} = \frac{Z_{1,2}}{\cos(\beta)^3}$
Crossed helical	$Z_{1,2v} = \frac{Z_{1,2}}{\cos(\beta_{1,2})^3}$
Straight tooth bevel	$Z_{1,2v} = \frac{Z_{1,2}}{\cos(\gamma_{1,2})}$
Spiral and skewed bevel	$Z_{1,2v} = \frac{Z_{1,2}}{\cos(\gamma_{1,2}) \cos(\beta)^3}$

*continued*

**TABLE 2.1 (continued)**  
Virtual Spur Gear Conversion

Type of Gear	Number of Teeth of Virtual Spur Gears
Hypoid	 $Z_{1,2v} = \frac{Z_{1,2}}{\cos(\gamma_{1,2}) \cos(\beta_{1,2})^3}$
Worm	<p data-bbox="712 575 906 601">With involute worm:</p> $Z_{wv} = Z_w / \sin(\beta)^3$ $Z_{wgv} = Z_{wgv} / \cos(\beta)^3$ <p data-bbox="712 760 947 786">With Archimedes' worm:</p> $Z_{wv} = \infty$ $Z_{wgv} = Z_{wgv}$
Face spur	 $Z_{1v} = Z_1$ $Z_{2v} = \infty$
Face helical	 $Z_{1v} = \frac{Z_1}{\cos(\beta)^3}$ $Z_{2v} = \infty$

*Note:*  $Z_{1,2}$  - number of teeth of the real pinion and gear,  $Z_{1,2v}$  - number of teeth of virtual spur pinion and gear,  $Z_w$  and  $Z_{wgv}$  - number of starts of real worm and number of teeth of real worm gear,  $Z_{wv}$  and  $Z_{wgv}$  - number of teeth of virtual spur gears that replace real worm and worm gear,  $\beta$  or  $\beta_{1,2}$  - helix angle of helical or worm gears and spiral angle of spiral bevel gears,  $\gamma_{1,2}$  - pitch angle of bevel gears.

# 3

---

## *Area of Existence of Involute Gears*

---

In traditional gear design the preselected basic or generating rack parameters and addendum modification or X-shift factor define the nominal involute gear geometry. X-shift factor selection for the given pair of gears is limited by the block contour (Figure 1.5). Borders of the block contour include the undercut isograms, the interference isograms, the minimum contact ratio (equal to 1.0 for spur gears) isogram, and the isograms of the minimum tooth tip thickness to exclude the gears with the pointed tooth tips. If a block contour of some generating rack does not contain an optimal gear geometry for a particular gear application, the generating rack parameters (pressure angle, addendum, whole depth proportions, etc.) should be changed. Then the altered rack block contour may include the desired optimal gear geometry.

Direct Gear Design<sup>®</sup> does not use basic or generating rack parameters to define the gear geometry. However, gear pair mesh geometry selection is also limited by an area of existence. This area defines parameter limits for a pair of spur gears. It is also used for any kind of involute gears, by their conversion to the virtual spur gears (see Section 2.4). In this chapter areas of existence are defined and analyzed considering the gear tooth tip radii, mesh backlash, and all tolerances equal to zero.

---

### 3.1 Area of Existence of Symmetric Gears

Prof. E.B. Vulgakov introduced areas of existence of involute gears in his theory of generalized parameters [7]. He suggested using the profile angles  $v_{1,2}$  at the intersection point of the tooth flank involutes as coordinates for an area of existence of two mating gears with number of teeth  $z_1$  and  $z_2$ . Other gear tooth parameters also can be used as coordinates for an area of existence, for example, the tooth tip profile angles  $\alpha_{a1,2}$  or the relative base tooth thicknesses  $m_{b1,2}$  that are,

$$m_{b1,2} = \frac{S_{b1,2}}{d_{b1,2}} = \text{inv}(v_{1,2}), \quad (3.1)$$

where  $S_{b1,2}$  are base tooth thicknesses of the mating gears.

In this book the profile angles  $v_{1,2}$  at the intersection point of the tooth flank involutes are used as coordinates for area of existence.

Unlike traditional design block contours, where the tooth thicknesses at the tip diameters vary depending on the  $X$ -shifts, the area of existence is constructed for selected constant relative tooth tip thicknesses  $m_{a1,2}$ . Prof. Vulgakov defined the relative tooth tip thickness as a ratio of the tip diameter tooth thicknesses to the base circle diameter [7]:

$$m_{a1,2} = \frac{S_{a1,2}}{d_{b1,2}}. \quad (3.2)$$

However, it is more practical to present the relative tooth tip thicknesses as ratios in relation to the operating module  $m_w$  or the operating diametral pitch  $DP_w$ , because  $m_w$  or  $DP_w$  is commonly used to define a range of desirable values for the tooth tip thickness. Then  $m_{a1,2}$  can be described as

$$m_{a1,2} = \frac{S_{a1,2}}{m_w} \text{ or } m_{a1,2} = S_{a1,2} \times DP_w. \quad (3.3)$$

For gears with external teeth the relative tooth tip thickness  $m_{a1,2}$  is

$$m_{a1,2} = \frac{z_{1,2} \cos \alpha_w}{\cos \alpha_{a1,2}} (\operatorname{inv}(v_{1,2}) - \operatorname{inv}(\alpha_{a1,2})). \quad (3.4)$$

For gears with internal teeth the relative tooth tip thickness  $m_{a2}$  is

$$m_{a2} = \frac{z_2 \cos \alpha_w}{\cos \alpha_{a2}} \left( \frac{\pi}{z_2} - \operatorname{inv}(v_2) + \operatorname{inv}(\alpha_{a2}) \right). \quad (3.5)$$

For a gear rack tooth the relative nominal tooth addendum  $h_a$  is a nominal pitch tooth addendum divided by the rack module  $m$  in the metric system,

$$h_a = \frac{H_a}{m}, \quad (3.6)$$

or multiplied by the rack diametral pitch  $DP$  in the English system,

$$h_a = H_a \times DP. \quad (3.7)$$

The gear rack tooth relative tooth tip thickness  $m_{a2}$  is

$$m_{a2} = \frac{\pi}{2} - 2h_a \tan \alpha. \quad (3.8)$$

The gear rack relative operating tooth addendum  $h_{aw}$  is an operating tooth addendum divided by the rack module  $m$  in the metric system,

$$h_{aw} = \frac{H_{aw}}{m} \quad (3.9)$$

or multiplied by the rack diametral pitch  $DP$  in the English system,

$$h_{aw} = H_{aw} \times DP. \quad (3.10)$$

Accordingly, the relative operating tooth depth in the metric system is

$$h_w = \frac{H_w}{m}, \quad (3.11)$$

and in the English system it is

$$h_w = H_w \times DP. \quad (3.12)$$

An area of existence contains a number of isograms, which present the certain constant value of gear mesh parameters or the certain constant mesh condition. The next sections describe construction of these isograms for the following gear pair parameters selected as examples:

Pinion number of teeth  $z_1 = 18$

Mating gear (external or internal) number of teeth  $z_2 = 25$

Mating gear rack number of teeth  $z_2 = \infty$

Pinion relative tooth tip thickness  $m_{a1} = 0.25$

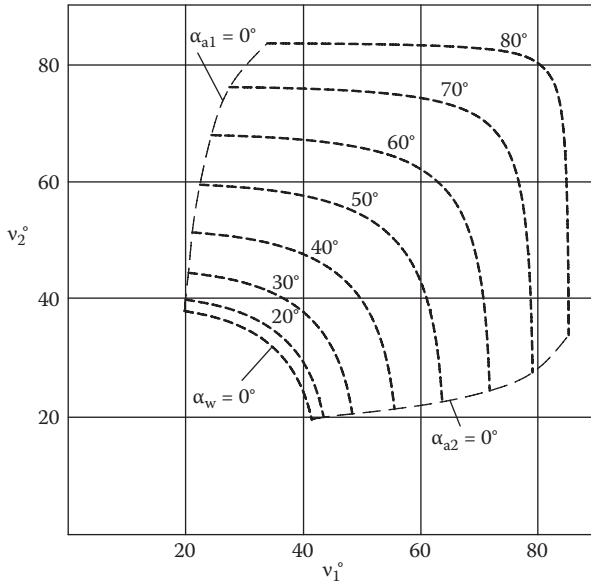
Mating gear or rack relative tooth tip thickness  $m_{a1} = 0.35$

### 3.1.1 Pressure Angle Isograms

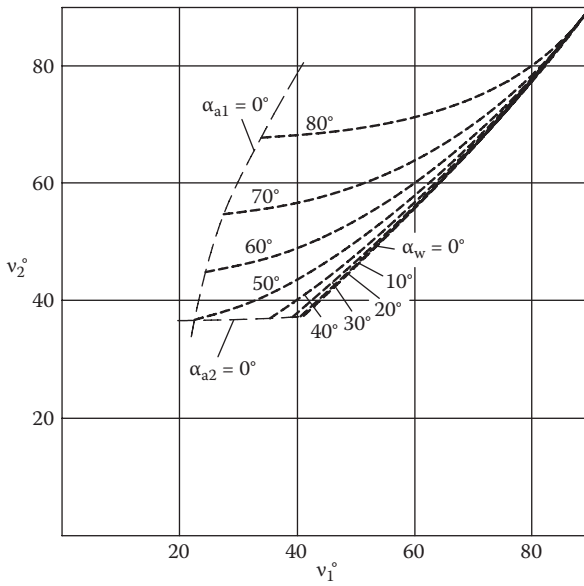
Equations (2.56), (2.57), and (2.58) define the pressure angle  $\alpha_w = \text{const}$  isograms (Figure 3.1). These isograms do not depend on the relative tooth tip thicknesses  $m_{a1,2}$ .

The pressure angle isograms are bordered by isograms of the tooth tip profile angles  $\alpha_{a1} = 0^\circ$  and  $\alpha_{a2} = 0^\circ$  that are defined from Equations (2.56) and (3.4) for the external gears, and (2.57) and (3.5) for the internal gears. In the rack and pinion mesh the rack intersection point profile angle  $\nu_2 = \alpha_w = \alpha$ . Then an equation of the isogram  $\alpha_{a1} = 0^\circ$  is defined from (3.4) as

$$\text{inv}(\nu_1) = \frac{m a_1}{z_1 \times \cos \nu_2}. \quad (3.13)$$



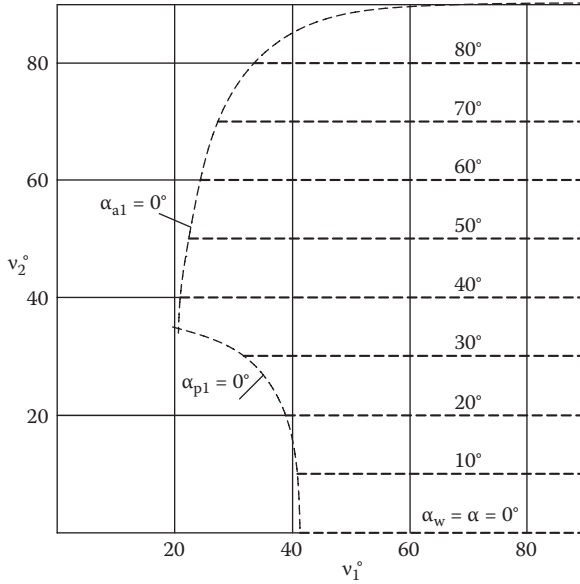
(a)



(b)

**FIGURE 3.1**

Pressure angle  $\alpha_w = \text{const}$  isograms: (a) for external gears, (b) for internal gears, (c) for rack and pinion.



(c)

FIGURE 3.1 (continued)

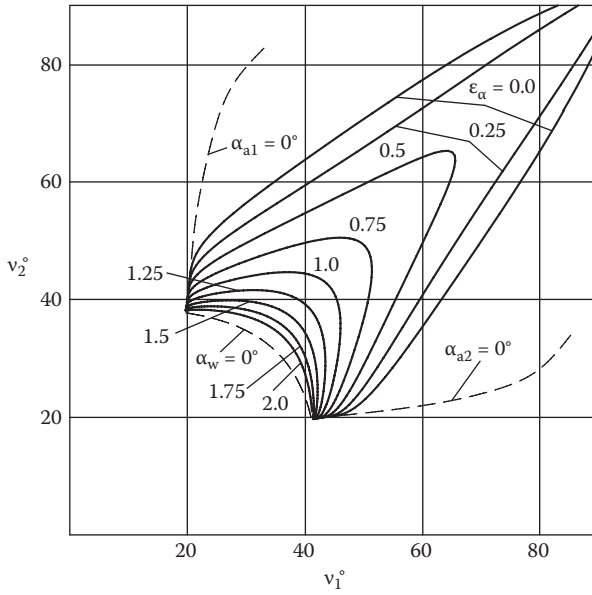
The theoretical limits of the pressure angle are  $0^\circ < \alpha_w < 90^\circ$ . The practical range of the pressure angle varies depending on the type of involute gears and their application. For example, some worm gears with the metal worm and polymer gear have very low ( $5^\circ$  to  $12^\circ$ ) pressure angle. The most common range is  $14.5^\circ$  to  $25^\circ$ . The highly stressed aerospace gears may have pressure angles of  $25^\circ$  to  $30^\circ$ . Spur gears with asymmetric teeth can have pressure angles up to  $45^\circ$  and higher. Helical gears have both transverse and axial contact ratios (see Section 2.2.3). This allows realizing a significantly higher transverse pressure angle level. For example, the self-locking helical gears (Section 6.3) can have transverse operating pressure angles up to  $80^\circ$  and higher.

### 3.1.2 Transverse Contact Ratio Isograms

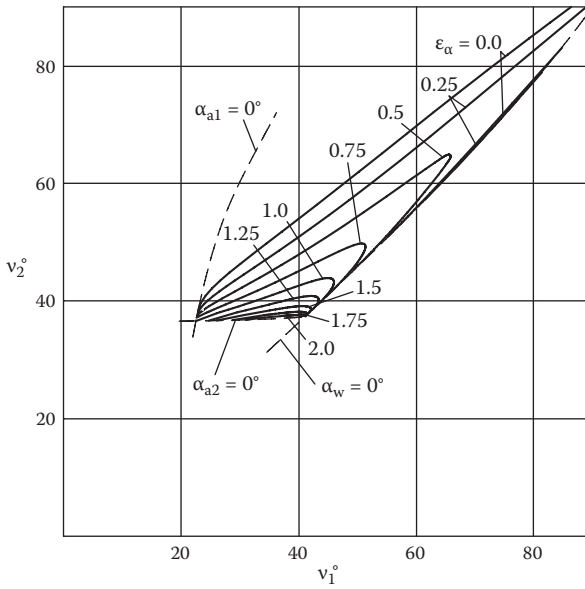
The transverse contact ratio  $\epsilon_\alpha = \text{const}$  isograms for the external gearing are shown in Figure 3.2a. They are described by the system of Equations (3.4) and

$$\begin{aligned}
 (1 + u) \times \text{inv}(\arctan(\frac{1}{1 + u}(\tan \alpha_{a1} + u \times \tan \alpha_{a2} - \frac{2\pi\epsilon_\alpha}{z_1}))) \\
 - \text{inv}(v_1) - u \times \text{inv}(v_2) + \frac{\pi}{z_1} = 0,
 \end{aligned}
 \tag{3.14}$$





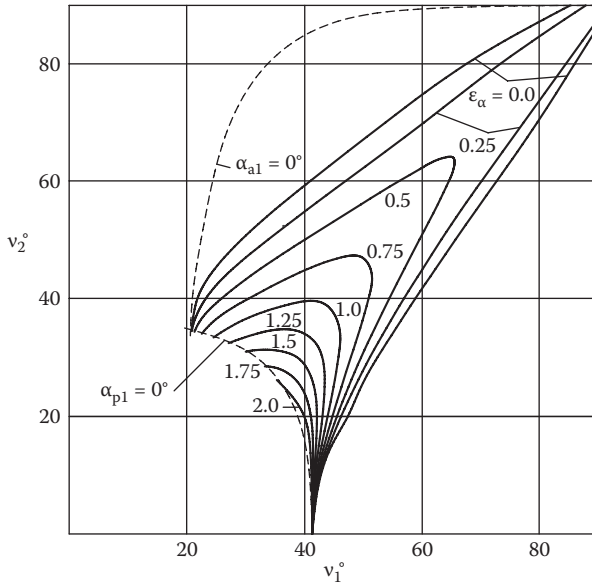
(a)



(b)

**FIGURE 3.2**

Transverse contact ratio  $\epsilon_\alpha = \text{const}$  isograms: (a) for external gears, (b) for internal gears, (c) for rack and pinion.



(c)

FIGURE 3.2 (continued)

which is a result of the combined solution of Equations (2.56) and (2.75).

The  $\epsilon_\alpha = \text{const}$  isograms for internal gearing (Figure 3.2b) are described by the system of Equations (3.4), (3.5), and

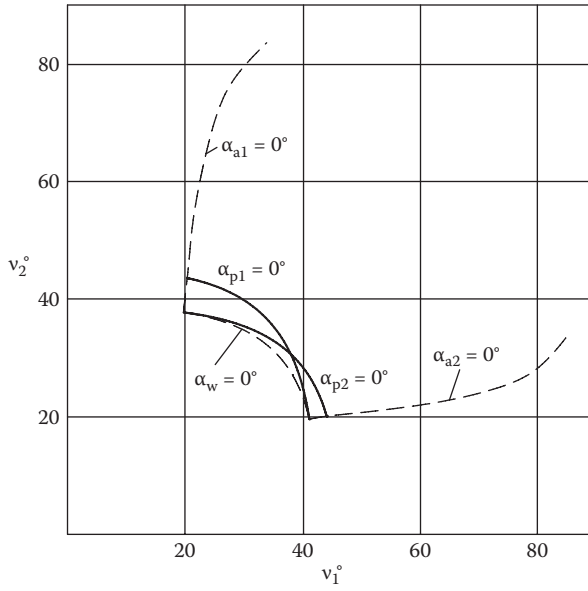
$$(u - 1) \times \text{inv}(\arctan(\frac{1}{u - 1} (u \times \tan \alpha_{a2} - \tan \alpha_{a1} + \frac{2\pi\epsilon_\alpha}{z_1}))) - u \times \text{inv}(v_2) + \text{inv}(v_1) = 0, \tag{3.15}$$

which is a result of the combined solution of Equations (2.57) and (2.76).

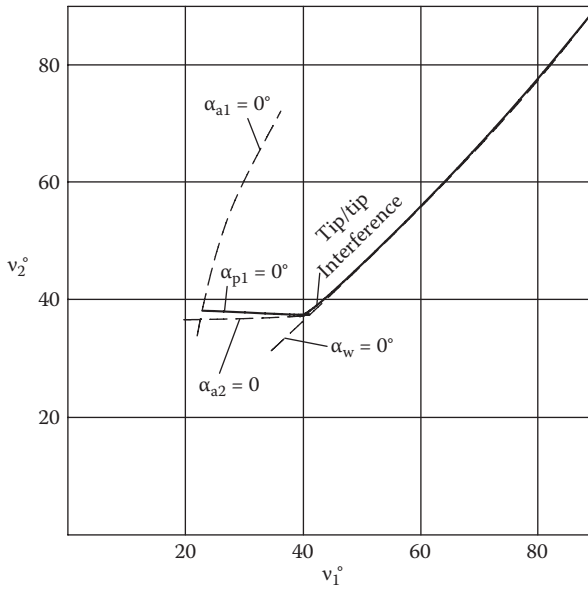
For a gear rack  $v_2 = \alpha$  the  $\epsilon_\alpha = \text{const}$  isograms for the rack and pinion gearing (Figure 3.2c) are described by the solution of Equations (3.4), (3.8), and (3.9):

$$\tan \alpha_{a1} - \tan v_2 - \frac{2\pi\epsilon_\alpha}{z_1} - \frac{4h_{aw}}{z_1 \sin v_2} = 0. \tag{3.16}$$

Spur gears should have the contact ratio  $\epsilon_\alpha \geq 1.0$  to provide a smooth mesh transition from one pair of teeth to the next. Isogram  $\epsilon_\alpha = 1.0$  limits a choice of the spur gear combinations. Helical gears have an additional axial (or face) contact ratio  $\epsilon_\beta$  that allows the transverse contact ratio to be  $\epsilon_\alpha \geq 0$ . The total contact ratio of helical gears must be  $\epsilon_\gamma = \epsilon_\alpha + \epsilon_\beta \geq 1.0$ . Isogram  $\epsilon_\alpha = 0$  limits



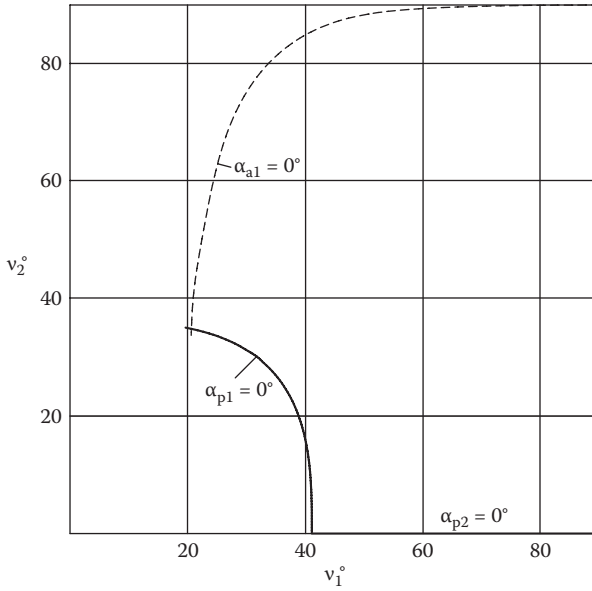
(a)



(b)

FIGURE 3.3

Interference isograms: (a) for external gears, (b) for internal gears, (c) for rack and pinion.



(c)

FIGURE 3.3 (continued)

a choice of the helical gear combinations [37]. However, commonly helical gears have the transverse contact ratio  $\epsilon_\alpha \geq 1.0$ .

### 3.1.3 Interference Isograms

The interference isograms are shown in Figure 3.3. Although the interference isograms present the borders of the area of existence, this does not mean that the gear meshes do not exist beyond these borders. However, those gear combinations have the tooth root undercut in at least one of the mating gears, and they are typically undesirable.

Equations (2.59) to (2.64) define the profile angles  $\alpha_{p1}$  and  $\alpha_{p2}$  at the end-points of the active involute flanks near the tooth root area. In the external gearing (Figure 3.3a)  $\alpha_{p1} = 0^\circ$  and  $\alpha_{p2} = 0^\circ$  describe a beginning of the root area interference (or undercut) for the pinion and the gear accordingly. The  $\alpha_{p1} = 0^\circ$  isogram is described by the system of equations (3.4) and

$$(1 + u) \times \text{inv}(\arctan(\frac{u}{1 + u} \times \tan \alpha_{a2})) - \text{inv}(v_1) - u \times \text{inv}(v_2) + \frac{\pi}{z_1} = 0, \quad (3.17)$$

which is a result of the combined solution of Equations (2.56) and (2.59). The  $\alpha_{p2} = 0^\circ$  isogram is described by the system of Equations (3.4) and

$$(1+u) \times \text{inv}(\arctan(\frac{1}{1+u} \times \tan \alpha_{a1})) - \text{inv}(v_1) - u \times \text{inv}(v_2) + \frac{\pi}{z_1} = 0, \quad (3.18)$$

which is a result of the combined solution of Equations (2.56) and (2.60).

In the internal gearing (Figure 3.3b) the angle  $\alpha_{p2}$  cannot be equal or close to zero, and only  $\alpha_{p1} = 0^\circ$  describes the root area interference (or undercut) condition for the pinion. Its isogram is described by the system of Equations (3.5) and

$$(u-1) \times \text{inv}(\arctan(\frac{u}{u-1} \times \tan \alpha_{a2})) + \text{inv}(v_1) - u \times \text{inv}(v_2) = 0, \quad (3.19)$$

which is a result of the combined solution of Equations (2.57) and (2.61).

The tip/tip interference (Section 2.2.1.3) is possible in the internal gear gearing. Its condition and isogram are defined by Equations (2.70) to (2.73) and (3.5).

For a rack and pinion gearing the angle  $\alpha_{p2} = v_2 = \alpha$ . As a result, isogram  $\alpha_{p2} = 0^\circ$  coincides with the axis  $v_1$  when  $v_2 = \alpha = 0^\circ$ . The equation describing isogram  $\alpha_{p1} = 0^\circ$  (Figure 3.3c) is defined from (3.9) or (3.10), (2.49), (2.58), and (2.63):

$$z_1(\sin v_2)^2 \tan v_2 - (\pi - m_{a2} - z_1(\text{inv}(v_1) - \text{inv}(v_2))) = 0. \quad (3.20)$$

### 3.1.4 Pitch Point Location Isograms

In conventional gearing the operating pitch diameter  $d_{w1}$  or  $d_{w2}$  (or the rack gear tooth operating pitch line) divides the gear tooth height on the addendum and dedendum portions, and the pitch point  $P$  is located on the active part of the contact line  $A_1$ - $A_2$  (Figure 3.4). For external gears this means that the operating pitch diameter is larger than the form diameter and smaller than the tooth tip diameter. For internal gears this means that the operating pitch diameter is smaller than the form diameter and larger than the tooth tip diameter. The gear rack tooth, in this case, has its operating addendum  $0 < H_{aw} < H_w$ . Normally a gear mesh has the approach and recess actions, while the contact point is moving along the contact line. An approach action is when the contact point  $C$  lies between point  $A_2$  and pitch point  $P$  of the contact line, or the driving pinion dedendum is in contact with the driven gear addendum. A recess action is when the contact point  $C$  lies between pitch point  $P$  and point  $A_1$  of the contact line, or the driving pinion addendum is in contact with the driven gear dedendum.

It is also possible to have only the approach action gearing (Figure 3.5) when the driving gear has the tip diameter  $d_{a1} \leq d_{w1}$  or  $\alpha_{a1} \leq \alpha_w$ . In the approach action gearing the driving gear tooth has only the dedendum

without addendum. Accordingly, the driven gear or rack tooth has only the addendum without dedendum. Pitch point  $P$  is located outside the active part of contact line  $A_1-A_2$  (beyond point  $A_1$  on Figure 3.5).

The recess action gearing is shown in Figure 3.6. In the external mesh the driven gear has the tooth tip diameter  $d_{a2} \leq d_{w2}$  or  $\alpha_{a2} \leq \alpha_w$ . In the internal mesh the driven gear has the tooth tip diameter  $d_{a2} \geq d_{w2}$  or  $\alpha_{a2} \geq \alpha_w$ . In the recess action gearing the driving gear tooth has only the addendum without dedendum. Accordingly, the driven gear or rack tooth has only the dedendum without addendum. Pitch point  $P$  is located outside the active part of contact line  $A_1-A_2$  (beyond point  $A_2$  on Figure 3.6).

The isograms of the pitch point location are shown in Figure 3.7. Isogram  $\alpha_{a1} = \alpha_w$  is a border between the conventional and approach action gearing areas. Considering Equations (3.4) and (2.56), this isogram equation is

$$\text{inv}(v_1) - \text{inv}(v_2) + \frac{\pi - m_{a1}(1 + u)}{z_2} = 0. \quad (3.21)$$

For the internal gearing this isogram equation derives from a common solution with (3.4) and (2.57)

$$\text{inv}(v_1) - \text{inv}(v_2) - \frac{m_{a1}(u - 1)}{z_2} = 0. \quad (3.22)$$

For the rack and pinion gearing a gear ratio  $u = \infty$  and isogram  $\alpha_{a1} = \alpha_w = \alpha = v_2$  equation is defined from (3.21) or (3.22):

$$\text{inv}(v_1) - \text{inv}(v_2) - \frac{m_{a2}}{z_1} = 0. \quad (3.23)$$

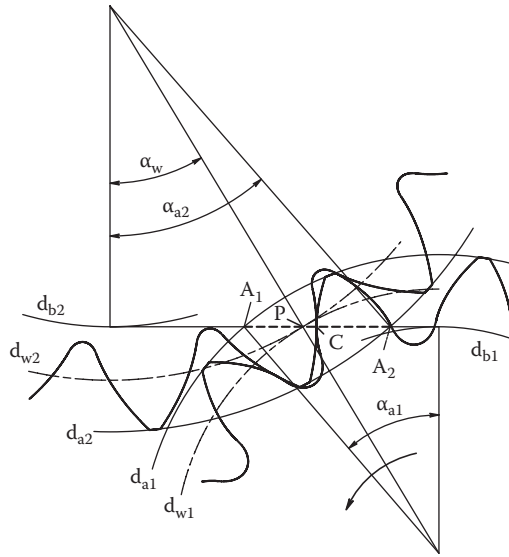
Isogram  $\alpha_{a2} = \alpha_w$  is a border between the conventional and recess action gearing areas. For external gearing it is a solution of a system of Equations (3.4) and (2.56):

$$\text{inv}(v_1) - \text{inv}(v_2) + \frac{m_{a2}(1 + u) - \pi u}{z_2} = 0. \quad (3.24)$$

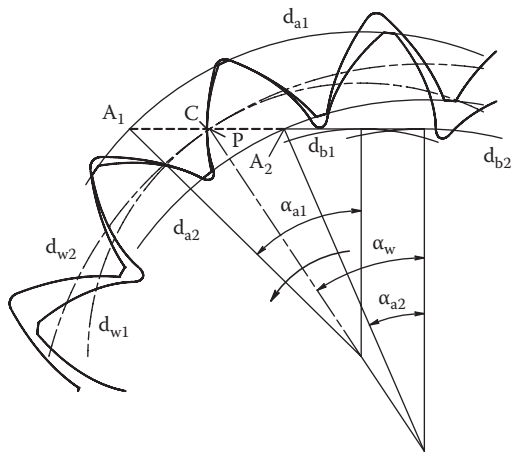
For the internal gearing it is a solution of a system of Equations (3.5) and (2.57):

$$\text{inv}(v_1) - \text{inv}(v_2) - \frac{m_{a2}(u - 1)}{z_2} = 0. \quad (3.25)$$

For the rack and pinion gearing a border between the conventional and recess action gearing areas is presented by the isogram presenting the rack



(a)



(b)

**FIGURE 3.4**

Conventional action gearing: (a) external gears, (b) internal gears, (c) rack and pinion.

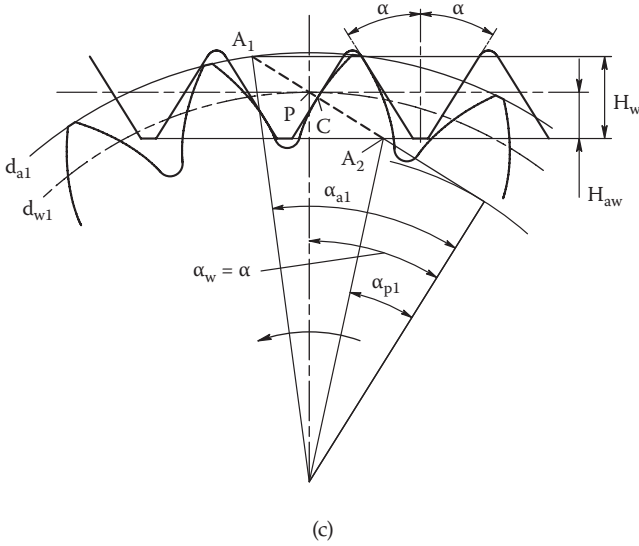


FIGURE 3.4 (continued)

tooth addendum  $H_{aw} = 0$  that can be described by Equations (3.24) or (3.25) when a gear ratio  $u = \infty$ .

$$inv(\nu_1) - inv(\nu_2) - \frac{\pi - m_{a2}}{z_1} = 0. \tag{3.26}$$

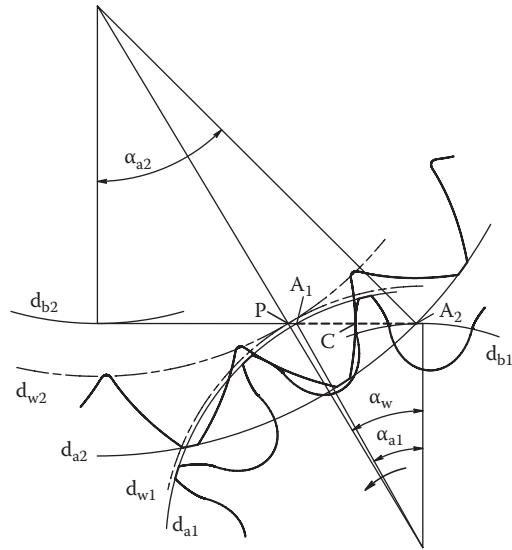
The isograms of the pitch point location are situated between isograms  $\alpha_{a1} = 0^\circ$ ,  $\alpha_{a2} = 0^\circ$ , and  $\alpha_w = 0^\circ$ . Most gear applications use the conventional action gearing, because it provides better performance parameters, such as high mesh efficiency (minimal tooth profile sliding), tooth surface durability, bending stress balance, etc. However, the approach and recess action gearings also may have rational areas of applications. For example, the recess action gearing is used for the self-locking gears (Section 6.3).

### 3.1.5 Performance Parameters' Isograms

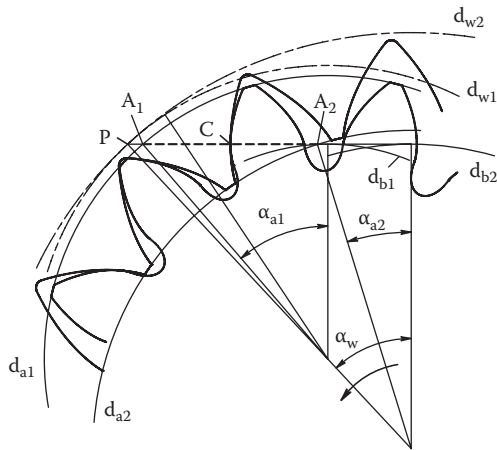
There are many other isograms that can be drawn in the area of existence. This section presents a few of them, which define gear pairs with certain constant performance characteristics.

Gear transmission power density and its load capacity in many cases are defined by the tooth surface durability. This requires minimization of the contact (Hertz) stress  $\sigma_H$ . Gear pairs with the minimal contact stress should have the maximum transverse contact ratio  $\epsilon_w$ , if the operating pressure angle  $\alpha_w$  is given, or the maximum operating pressure angle  $\alpha_w$ , if the transverse contact





(a)



(b)

**FIGURE 3.5**

Approach action gearing: (a) external gears, (b) internal gears, (c) rack and pinion.

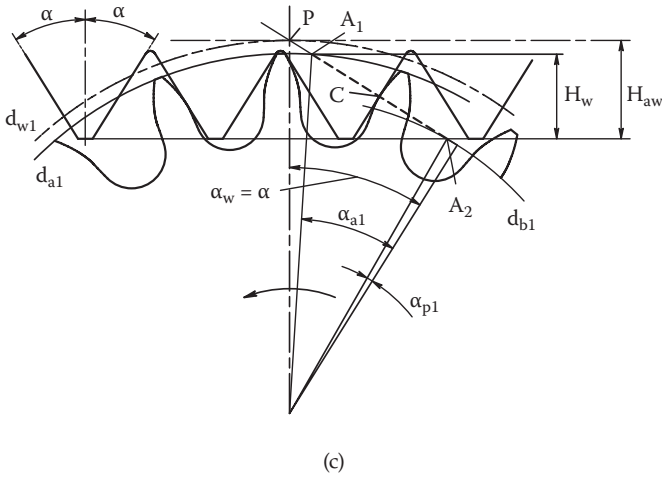


FIGURE 3.5 (continued)

ratio  $\epsilon_\alpha$  is given. These conditions occur when isograms  $\alpha_w = \text{const}$  and  $\epsilon_\alpha = \text{const}$  are tangent. The  $\sigma_{H_{\min}}$  isogram (see Figure 3.8) presents the gear meshes that correspond to the tangent points of isograms  $\alpha_w = \text{const}$  and  $\epsilon_\alpha = \text{const}$ .

Maximization of gear efficiency is critically important for many gear applications. Gear efficiency depends on gear mesh losses that for a pair of spur gears is defined as [38]

$$P_t = \frac{50f}{\cos \alpha_w} \times \frac{H_s^2 + H_t^2}{H_s + H_t}, \quad (3.27)$$

where  $f$  is the average friction coefficient,  $H_s$  is the specific sliding velocity at the start of the approach action, and  $H_t$  is the specific sliding velocity at the end of the recess action.

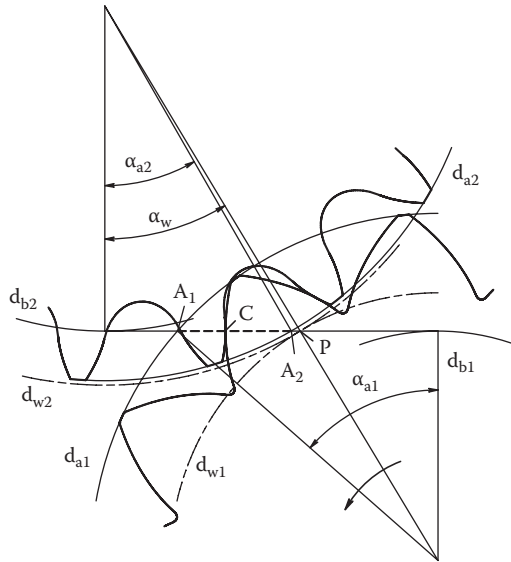
$H_s$  and  $H_t$  are ratios of the sliding velocity to the rolling velocity. They can be defined for the external and internal gears as follows:

$$H_s = (u \pm 1) \times \cos \alpha_w \times (\pm \tan \alpha_{a2} \mp \tan \alpha_w), \quad (3.28)$$

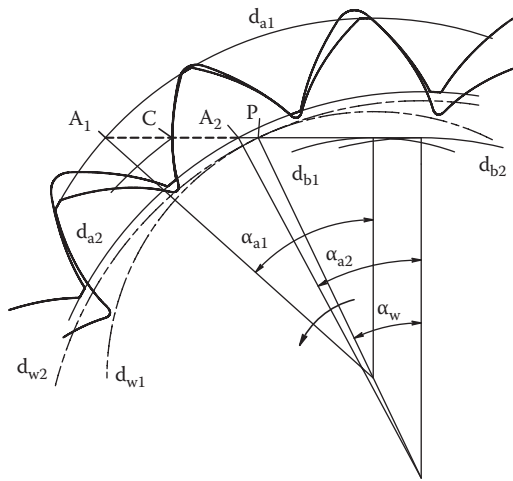
$$H_t = \frac{u \pm 1}{u} \times \cos \alpha_w \times (\tan \alpha_{a1} - \tan \alpha_w), \quad (3.29)$$

where the signs  $\pm$  and  $\mp$  are for the external gears and internal gears, respectively.

Alternatively, from (3.28), (2.60), or (2.62), and from (3.29), (2.59), or (2.61), accordingly, specific sliding velocities are



(a)



(b)

**FIGURE 3.6**  
 Recess action gearing: (a) external gears, (b) internal gears, (c) rack and pinion.

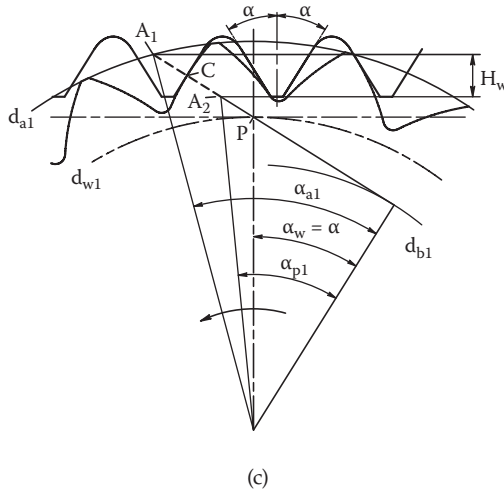


FIGURE 3.6 (continued)

$$H_s = \frac{u \pm 1}{u} \times \cos \alpha_w \times (\tan \alpha_w - \tan \alpha_{p1}), \quad (3.30)$$

$$H_t = (u \pm 1) \times \cos \alpha_w \times (\pm \tan \alpha_w \mp \tan \alpha_{p2}). \quad (3.31)$$

The gear rack number of teeth is  $z_2 = \infty$ , and as a result, the gear ratio is  $u = \infty$ . Then from (3.30) the specific sliding velocity at the start of approach action is

$$H_s = \cos \alpha_w \times (\tan \alpha_w - \tan \alpha_{p1}), \quad (3.32)$$

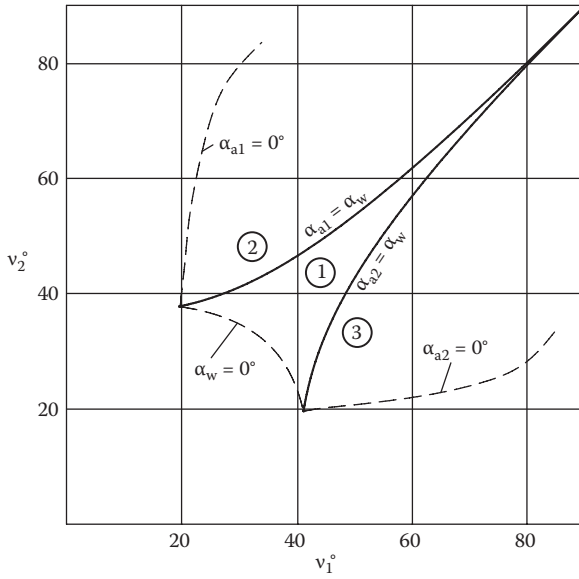
and from (3.29) the specific sliding velocity at the start of recess action is

$$H_t = \cos \alpha_w \times (\tan \alpha_{a1} - \tan \alpha_w). \quad (3.33)$$

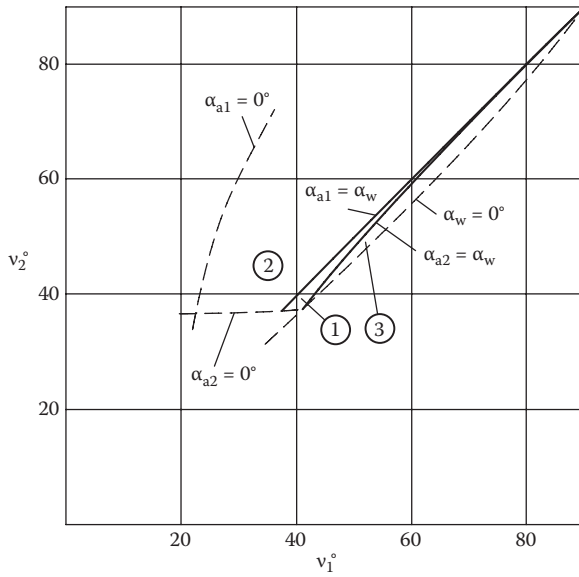
From Equation (3.27) a minimum of the gear mesh losses happens when  $H_s = H_t$ . This means that a maximum of the gear mesh efficiency  $E_{\max}$  can be defined for the external and internal gearings from (3.28) and (3.29) as

$$\tan \alpha_{a1} \mp u \tan \alpha_{a2} \pm (u \mp 1) \tan \alpha_w = 0. \quad (3.34)$$

Equations of maximum gear mesh efficiency  $E_{\max}$  value isograms (Figure 3.8) are defined as a solution of Equations (3.34) and (3.4) for the external gearing, and Equations (3.34) and (3.5) for the internal gearing.



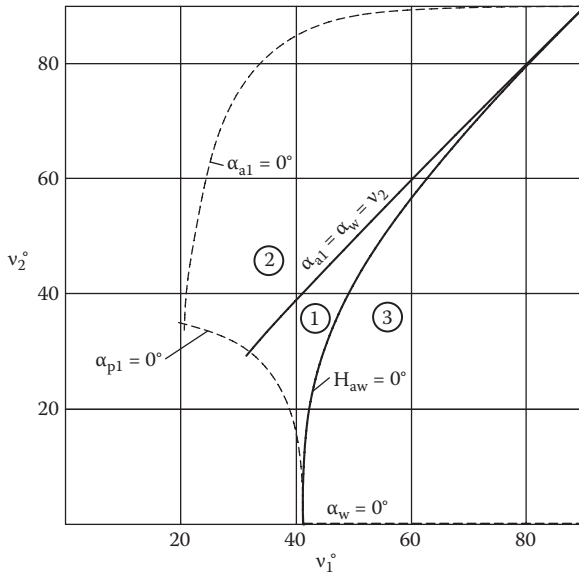
(a)



(b)

**FIGURE 3.7**

Pitch point location isograms: (a) for external gears, (b) for internal gears, (c) for rack and pinion. 1 - area of conventional action gearing; 2 - area of the approach action gearing; 3 - area of the recess action gearing.



(c)

FIGURE 3.7 (continued)

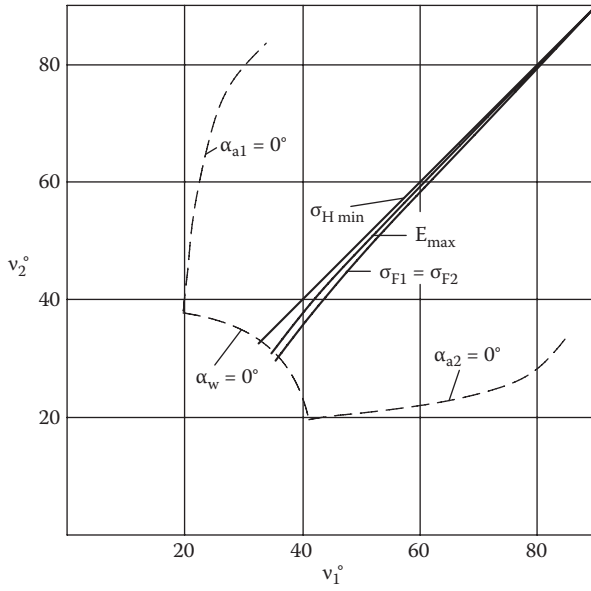
For the rack and pinion gearing a condition  $H_s = H_t$  that defines a maximum of the gear mesh efficiency  $E_{max}$  is from (3.32) and (3.33)

$$\tan \alpha_{a1} + \tan \alpha_{p1} - 2 \tan \alpha_w = 0 . \tag{3.35}$$

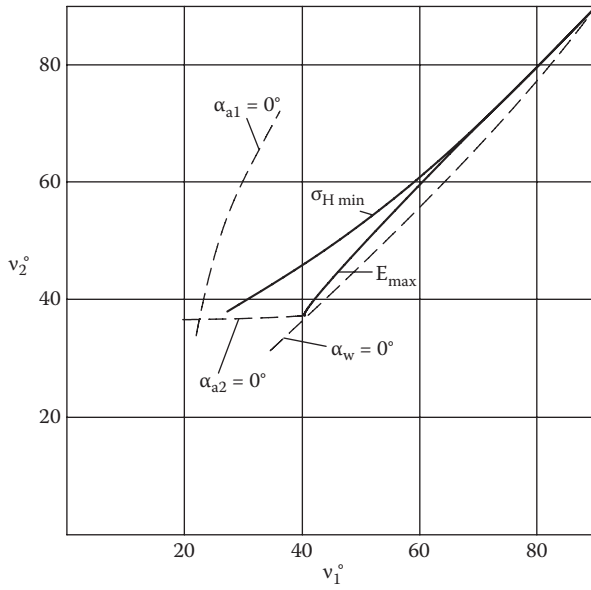
The maximum of the gear mesh efficiency  $E_{max}$  isogram for the rack and pinion gearing is defined as a solution of Equations (3.35), (3.4), (2.63), and (3.9) or (3.10).

Gear tooth geometry, including the tooth flanks and root fillet, affect the maximum bending stress level. The bending stress balance equalizes the tooth root strength of mating gears. If gears are made of similar materials and have a relatively close number of load cycles, the maximum bending stresses of mating gears should be equalized. The equal bending stress isogram  $\sigma_{F1} = \sigma_{F2}$  is defined assuming that the mating gears have identical face widths. This isogram (Figure 3.8) allows preliminary selection of a pair of gears with the equalized bending strength. Then during final gear design the mating gear face widths can be adjusted also considering a number of load cycles of each gear to achieve more accurate bending strength equalization.

In traditional gear design the tooth fillet profile is typically a trajectory of the generating tooling gear rack. Any point of the block contour (see Figure 1.5) presents the gear pair with completely described tooth profiles that include the root fillets. In Direct Gear Design the tooth flanks and root



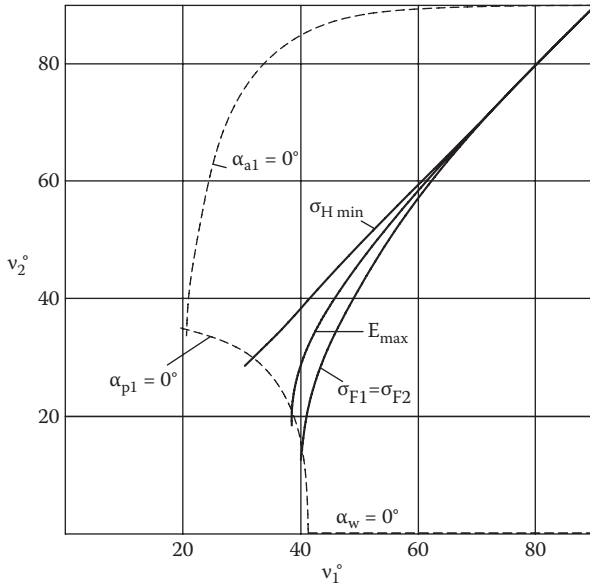
(a)



(b)

**FIGURE 3.8**

Performance parameter isograms: (a) for external gears, (b) for internal gears, (c) for rack and pinion.



(c)

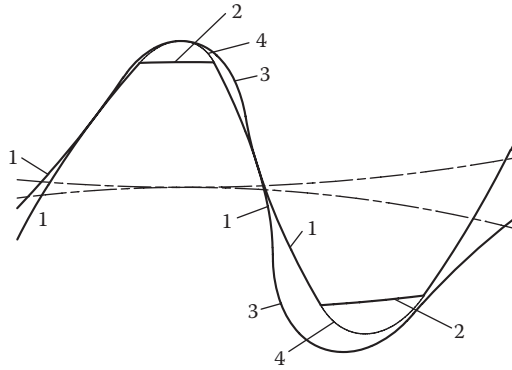
FIGURE 3.8 (continued)

fillets are constructed independently, and the tooth fillet profile is optimized to minimize bending stress concentration (see Section 5.3). However, the tooth fillet profile optimization is a time-consuming process that is used for the final stage of gear design. It is not practical for browsing the area of existence analyzing many sets of gear pairs. For preliminary construction of the interference-free tooth root fillet profile that also provides relatively low bending stress concentration, the virtual ellipsis arc is built into the tooth tip that is tangent to the involute profiles at the tip of the tooth [39]. This makes the root fillet profile a trajectory of the mating gear tooth tip virtual ellipsis arc (see Figure 3.9). The ellipsis arc is chosen because it fits both symmetric and asymmetric tooth profiles and results in lower bending stress level. This fillet profile can be considered pre-optimized because it provides lower bending stress concentration than the full tip radius rack generated fillet profile commonly used for bending stress reduction in traditional gear design.

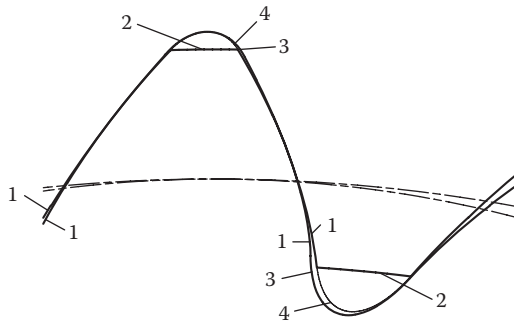
When the gear tooth with the root fillet is defined, the bending stress is calculated by the finite element analysis (FEA) method.

The equal maximum bending stress isogram  $\sigma_{F1max} = \sigma_{F2max}$  is shown in Figure 3.8. This isogram is typical for the external gearing and the rack and pinion gearing. The internal gear tooth with the equal face width with its external mating gear usually has significantly lower bending stress, because its root tooth thickness is typically much greater. It is why the equal bending

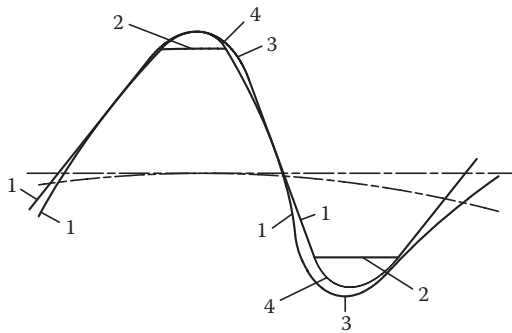




(a)



(b)



(c)

**FIGURE 3.9**

Tooth root fillet profile construction: (a) for external gears, (b) for internal gears, (c) for rack and pinion. 1 - involute profiles; 2 - tooth tip lands; 3 - fillet profiles; 4 - ellipsis arcs. ((a) and (b) from Kapelevich, A.L., and Y.V. Shekhtman, *Gear Technology*, January/February 2010, 69. With permission.)

stress isogram  $\sigma_{F1} = \sigma_{F2}$  for internal gears is not presented in Figure 3.8b. In this case, the bending stress balance can be achieved by the internal gear face width reduction.

### 3.1.6 Area of Existence and Gear Tooth Profiles

Summation of all the above-mentioned and other possible parameter or condition isograms forms an area of existence. Every point of the area of existence presents the gear pair with a certain set of parameters and gear tooth profiles. Figure 3.10 presents areas of existence of the external, internal, and rack and pinion gearings with the gear pair tooth profiles corresponding to certain points of those areas.

Some of those gear pair tooth profiles have a kind of exotic shape and present rather theoretical interest. However, even they may find practical applications for some unconventional gear drives.

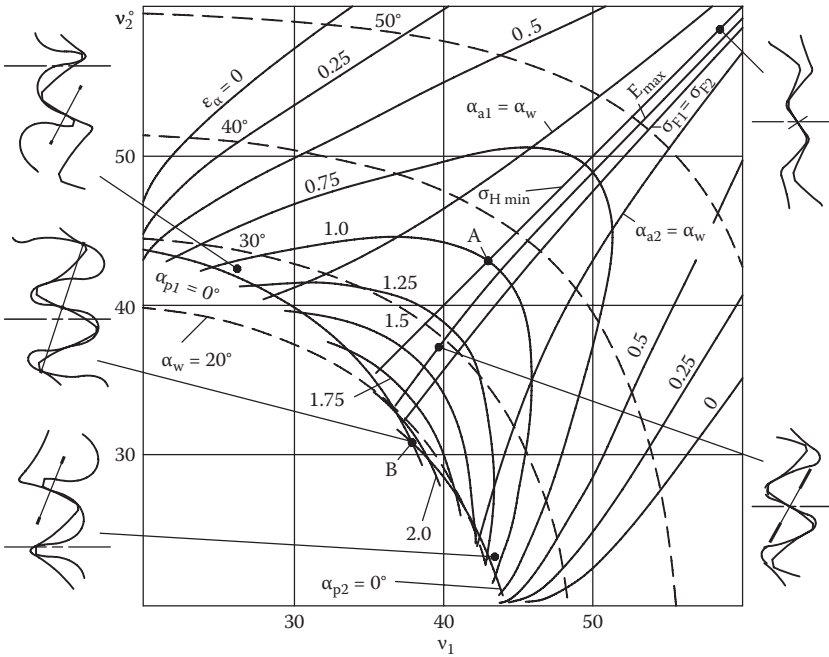
The maximum pressure angle for spur external gearing is achieved in point *A* (Figure 3.10a), where the contact ratio  $\epsilon_\alpha = 1.0$ . Pressure angle and area of existence coordinates at point *A* are defined by the combined solution of Equations (2.56), (2.75), and (3.4). The minimum pressure angle is at point *B* at the intersection of the interference isograms  $\alpha_{p1} = 0^\circ$  and  $\alpha_{p2} = 0^\circ$ . This pressure angle and the tooth tip profile angles at point *B* for external gearing are defined from a combined solution of Equations (2.56), (2.59), (2.75), (2.60), and (3.4):

$$\alpha_w^B = \arctan \frac{2\pi\epsilon_\alpha}{z_1(1+u)}, \quad (3.36)$$

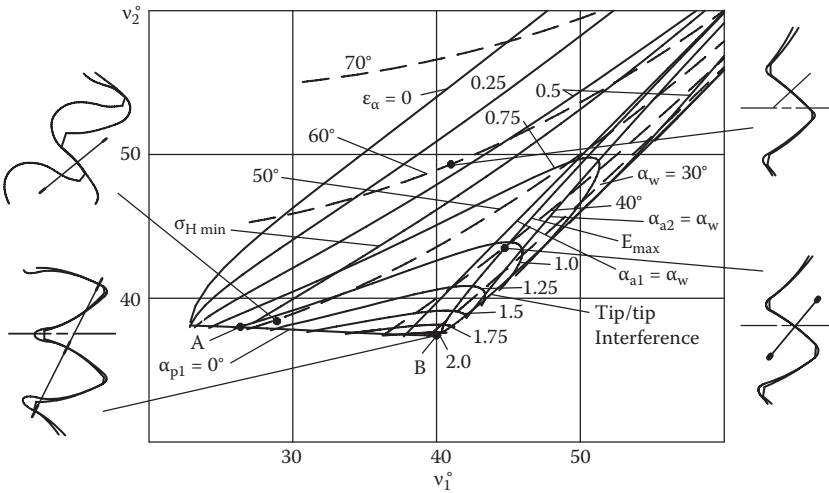
$$\alpha_{a1}^B = \arctan \frac{2\pi\epsilon_\alpha}{z_1}, \quad (3.37)$$

$$\alpha_{a2}^B = \arctan \frac{2\pi\epsilon_\alpha}{z_2}. \quad (3.38)$$

In the spur internal gearing area of existence point *A* (Figure 3.10b) is also present in the gear pair with the maximum for spur gears pressure angle. Its location depends on the gear ratio  $u = z_2/z_1$ . A point *A* typically lies at the intersection of the  $\epsilon_\alpha = 1.0$  and  $\alpha_{p1} = 0^\circ$  isograms. Then the gear mesh parameters at point *A* are defined by Equations (2.57), (2.60), (2.76), and (3.4). However, in some cases a point *A* is at the tangent point of the  $\epsilon_\alpha = 1.0$  isogram and the pressure angle isogram where its value is maximum for spur gears. This case is illustrated in Figure 3.13 (gear set 3). Then the gear mesh parameters at point *A* are defined by Equations (2.57), (2.76), and (3.4). Point *B* is at the intersection of the interference isogram  $\alpha_{p1} = 0^\circ$  and the tip/tip



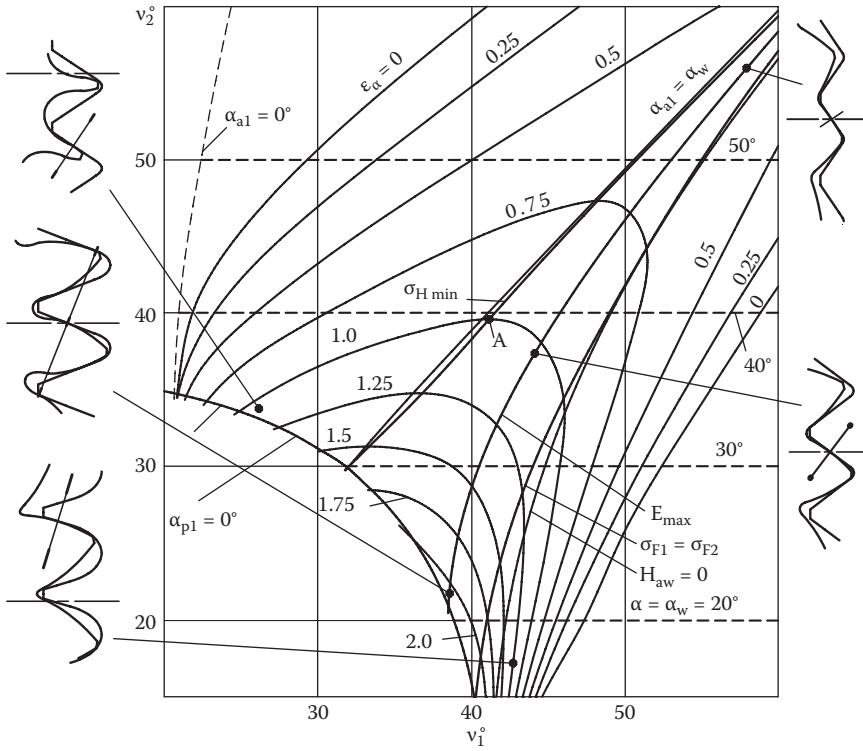
(a)



(b)

FIGURE 3.10

Area of existence for the pinion and gear with  $z_1 = 18$  and  $z_2 = 25$ ,  $m_{a1} = 0.25$  and  $m_{a2} = 0.35$ ; (a) for external gears, (b) for internal gears, (c) for rack and pinion.



(c)

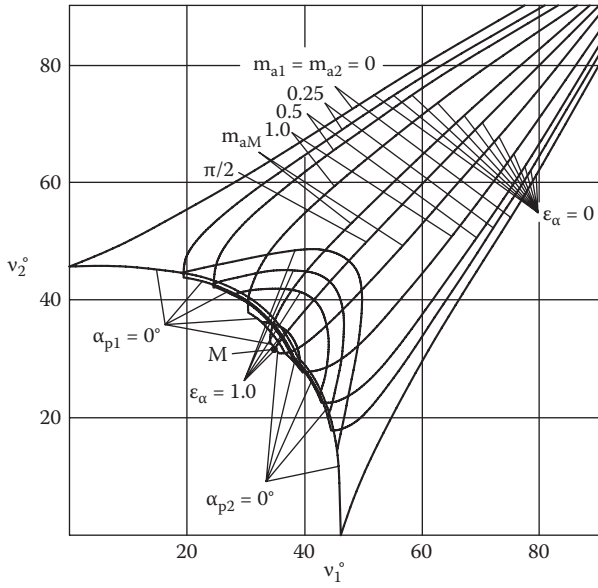
FIGURE 3.10 (continued)

interference isogram. Its gear mesh parameters are defined from the combined solution of Equations (2.70) to (2.73), (3.4), and (3.5).

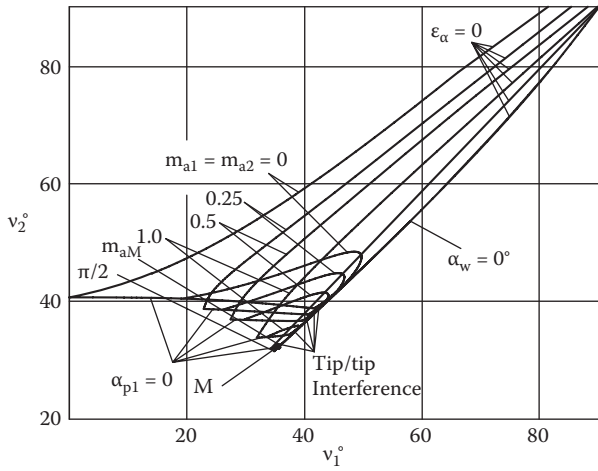
In the spur rack and pinion gearing area of existence the point A (Figure 3.10c) location depends on the pinion number of teeth  $z_1$ . For a low number of teeth ( $z_1 \leq 10$ ), point A is at the intersection of the  $\epsilon_\alpha = 1.0$  and  $\alpha_{p1} = 0^\circ$  isograms. If the pinion number of teeth  $z_1 > 10$ , point A is at the highest point of the  $\epsilon_\alpha = 1.0$  isogram, where the horizontal pressure angle isogram reaches its value maximum for spur gears. This case is illustrated in Figure 3.14 (gear sets 2 and 3). The maximum contact ratio for spur rack and pinion is achieved at the intersection of the horizontal axis  $v_2 = 0^\circ$  and the interference isogram  $\alpha_{p1} = 0^\circ$ .

### 3.1.7 Areas of Existence for Gear Pairs with Different Relative Tooth Tip Thicknesses

An area of existence of the involute gearing is limited by the interference isograms, and isogram  $\epsilon_\alpha = 1.0$  for spur gears and isograms  $\epsilon_\alpha = 0$  for helical gears.



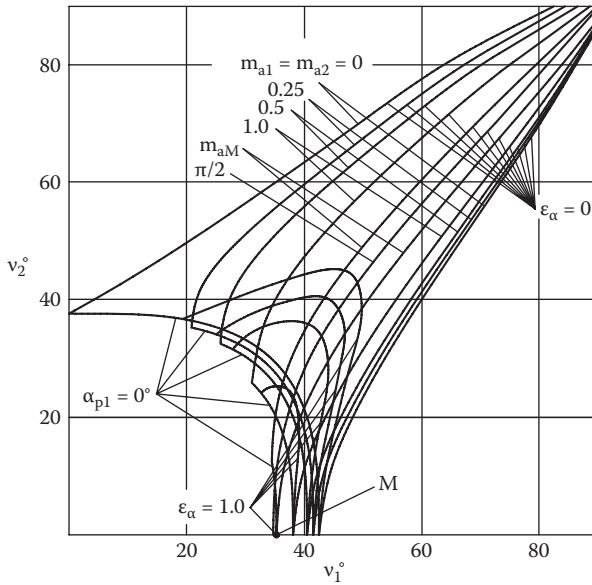
(a)



(b)

FIGURE 3.11

Areas of existence of gears with number of teeth  $z_1 = 18$ ,  $z_2 = 25$ , and different values of the relative tooth tip thicknesses  $m_{a1}$  and  $m_{a2}$ ; (a) for external gears, (b) for internal gears, (c) for rack and pinion.



(c)

FIGURE 3.11 (continued)

These border isograms depend on the relative tooth tip thickness values  $m_{a1}$  and  $m_{a2}$ . These thicknesses can vary from  $m_{a1} = m_{a2} = 0$  (sharp tooth tips) to their maximum values  $m_{a1max}$  and  $m_{a2max}$ . The higher the relative tooth tip thicknesses  $m_{a1}$  and  $m_{a2}$ , the smaller the area of existence (Figure 3.11). When the relative tooth tip thickness has its maximum for spur external gear values  $m_{aM1}$  and  $m_{aM1}$ , an area of existence is shrunk to point  $M$  (Figure 3.11a) at the intersection of the interference isograms  $\alpha_{p1} = 0^\circ$  and  $\alpha_{p2} = 0^\circ$ , when the transverse contact ratio is  $\epsilon_\alpha = 1.0$ .

For spur internal gears point  $M$  (Figure 3.11b) of the area of existence is at the intersection of isogram  $\alpha_{p1} = 0^\circ$  and the tip/tip interference isogram, when the transverse contact ratio is  $\epsilon_\alpha = 1.0$ .

For spur rack and pinion point  $M$  (Figure 3.11c) of the area of existence lies at the intersection of isogram  $\alpha_{p1} = 0^\circ$  and the axis  $v_2 = 0^\circ$ , when the transverse contact ratio is  $\epsilon_\alpha = 1.0$ .

For gear pairs with the relative tooth tip thicknesses  $m_{a1,2} > m_{aM1,2}$ , the transverse contact ratio is always  $\epsilon_\alpha < 1.0$  and only helical gearing is possible. A theoretical minimum of the transverse contact ratio is  $\epsilon_\alpha = 0$ . This means that a sum of the tooth tip thicknesses is equal to the operating circular pitch or

$$S_{a1} + S_{a2} = p_w \quad (3.39)$$

or considering (3.3), the maximum relative tooth tip thicknesses are defined from

$$m_{a1\max} + m_{a2\max} = \pi \cdot \tag{3.40}$$

A summation of the areas of existence for the gear pair with a given number of teeth with all possible values of the relative tooth tip thicknesses  $0 \leq m_{a1,2} \leq m_{a1,2\max}$  forms the so-called generalized area of existence [7]. Figure 1.7 shows an example of such a generalized area of existence for spur gears. It is much greater than any generating rack block contour. It actually includes any gear pairs, generated by all possible racks, and also the gear pairs, which require two different dedicated racks to generate the mating gears. This comparison demonstrates how many gear pair combinations available with Direct Gear Design are not even considered by the traditional gear design approach.

**3.1.8 Areas of Existence for Gear Pairs with Different Numbers of Teeth**

Isograms of an area of existence of involute gearing depend on the number of teeth. Figures 3.12 to 3.14 present the overlaid areas of existence for gear pairs with different numbers of teeth. A part of areas of existence that present spur gears and are limited by the transverse contact ratio isogram  $\epsilon_\alpha = 1.0$  is significantly smaller for gear pairs with a low number of teeth. Values of

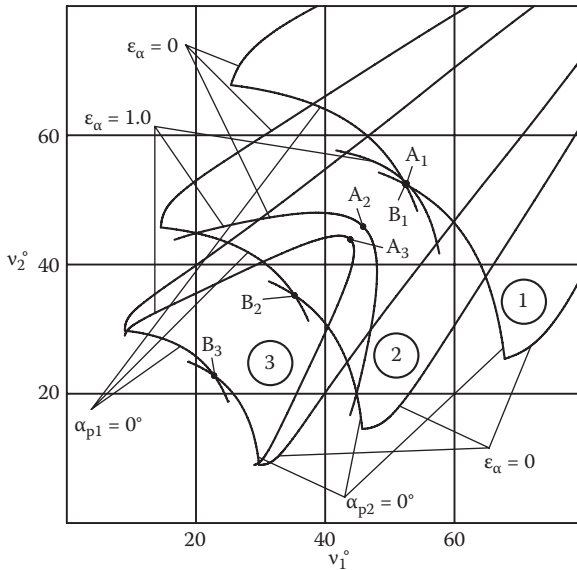


**FIGURE 3.12** Areas of existence of external gears with different number of teeth: 1 -  $z_{1,2} = 5$ , 2 -  $z_{1,2} = 20$ , 3 -  $z_{1,2} = 80$ ;  $m_{a1,2} = 0.1$ .

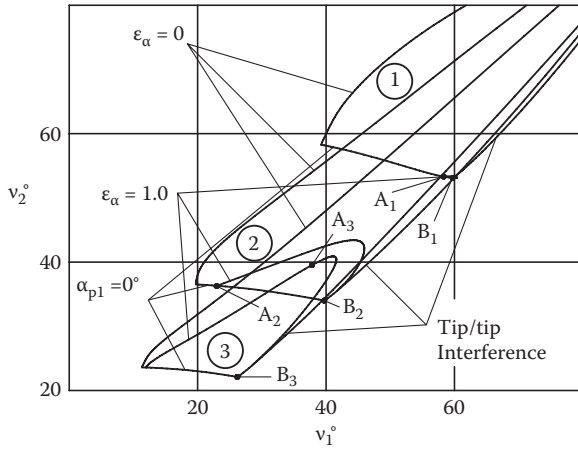


**FIGURE 3.13**

Areas of existence of internal gears with different number of teeth: 1 -  $z_1 = 4, z_2 = 7$ , 2 -  $z_1 = 20, z_2 = 35$ , 3 -  $z_1 = 80, z_2 = 140$ ;  $m_{a1} = 0.2, m_{a2} = 0.3$ .

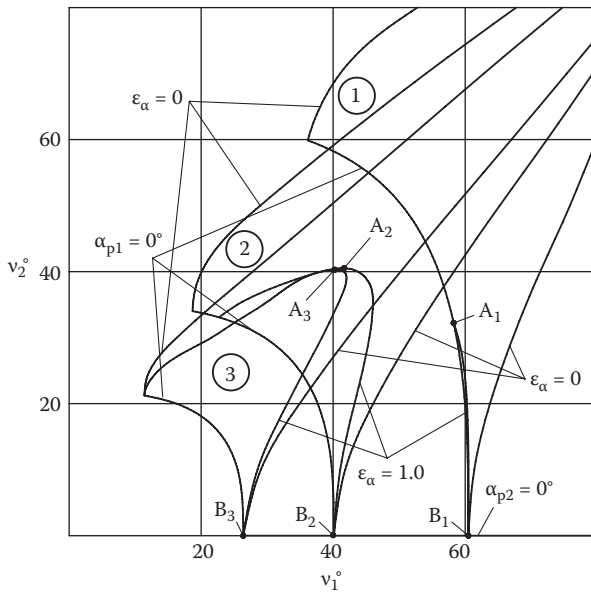


**FIGURE 3.14**

Areas of existence of rack and pinions with different number of teeth: 1 -  $z_1 = 4, z_2 = \infty$ , 2 -  $z_1 = 20, z_2 = \infty$ , 3 -  $z_1 = 80, z_2 = \infty$ ;  $m_{a1} = 0.2, m_{a2} = 0.3$ .



**TABLE 3.1**Pressure Angle and Contact Ratio in Points *A* and *B* of Area of Existence

Gearings		External (Figure 3.12)			Internal (Figure 3.13)			Rack and Pinion (Figure 3.14)		
		1	2	3	1	2	3	1	2	3
Area of existence no.		1	2	3	1	2	3	1	2	3
Number of teeth	Pinion	5	20	80	4	20	80	4	20	80
	Gear	5	20	80	7	35	140	∞	∞	∞
Pressure angle, °	Point <i>A</i>	33.18	40.80	43.85	35.50	44.18	41.24	33.36	40.52	40.29
	Point <i>B</i>	32.52	19.12	11.66	29.85	14.75	9.05	0.0	0.0	0.0
Contact ratio	Point <i>A</i>	1.0	1.0	1.0	1.0	1.0	1.0	1.0	1.0	1.0
	Point <i>B</i>	1.02	2.21	5.26	1.01	2.37	5.82	1.10	2.62	6.16

the pressure angles and the transverse contact ratios for spur gears in points *A* and *B* of these areas of existence are shown in Table 3.1.

## 3.2 Area of Existence of Asymmetric Gears

An area of existence of asymmetric gears is constructed similarly to an area of existence of symmetric gears. The drive flank profile angles  $v_{d1,2}$  at the involute intersection point are used as coordinates of the area of existence of asymmetric gears. It basically presents an overlay of two areas of existence: one for the drive flanks and another for the coast flanks of asymmetric gears. It is built with preselected values of the relative tooth tip thicknesses  $m_{a1,2}$  and the asymmetry factor  $K$ .

### 3.2.1 Area of Existence and Gear Tooth Profiles

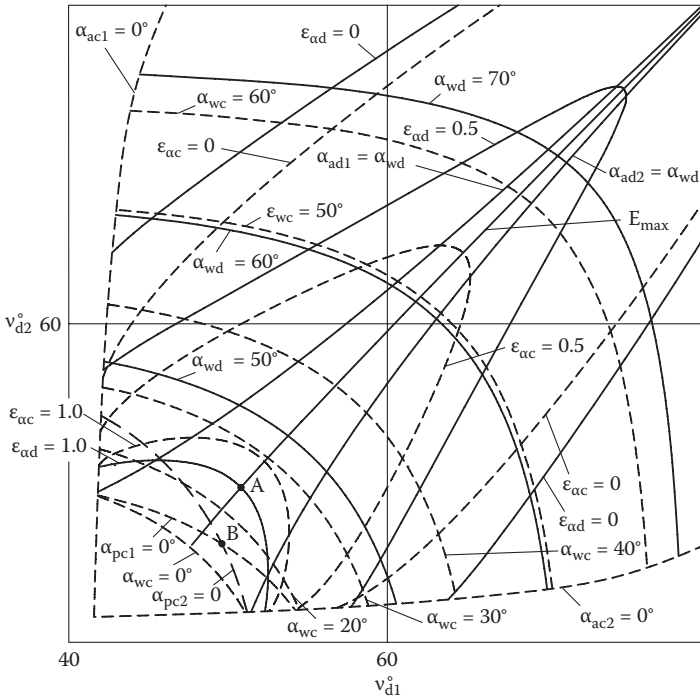
The areas of existence of asymmetric external, internal, and rack and pinion gearings are shown in Figure 3.15. Figure 3.16 presents the areas of existence of the spur asymmetric gears (fragments of the areas of existence from Figure 3.15) and the tooth profiles at their different points.

Most of the isogram equations for asymmetric gears are the same as the equations for the symmetric gears. They define constant parameter values or mesh conditions separately for the drive and coast gear flanks.

Similar to the area of existence of symmetric gears, in the area of existence of asymmetric gears the gear pairs have the constant preselected relative tooth tip thicknesses  $m_{a1,2}$  that can be described as:

For external gears:

$$m_{a1,2} = \frac{z_{1,2} \cos \alpha_{wd}}{2 \cos \alpha_{ad1,2}} \times (inv(v_{d1,2}) + inv(v_{c1,2}) - inv(\alpha_{ad1,2}) - inv(\alpha_{ac1,2})). \quad (3.41)$$



(a)

FIGURE 3.15

Area of existence of asymmetric external gears:  $z_1 = 18, z_2 = 25; K = 1.3; m_{a1} = 0.25, m_{a2} = 0.35$ . Solid isograms are for the drive flanks, dashed isograms are for the coast flanks; (a) for external gears, (b) for internal gears, (c) for rack and pinion.

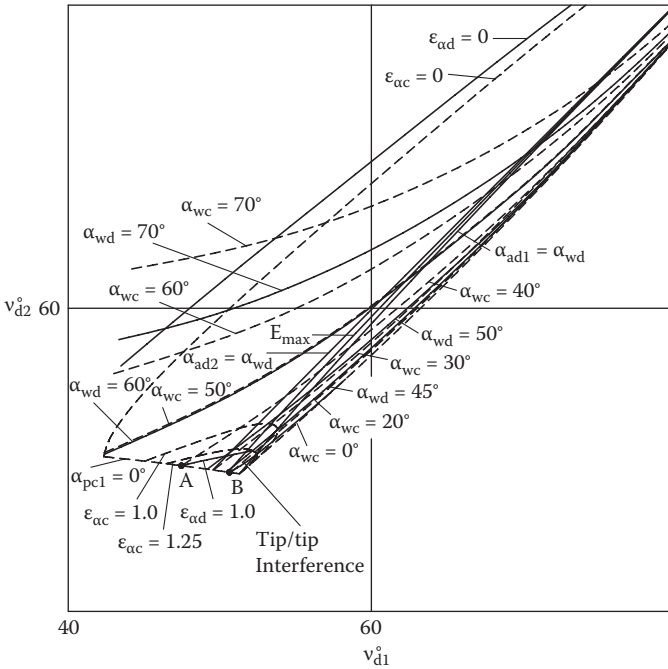
For internal gears:

$$m_{a2} = \frac{z_2 \cos \alpha_{wd}}{2 \cos \alpha_{ad2}} \times (2\pi / z_2 - \text{inv}(v_{d2}) - \text{inv}(v_{c2}) + \text{inv}(\alpha_{ad2}) + \text{inv}(\alpha_{ac2})) . \quad (3.42)$$

For gear racks:

$$m_{a2} = \frac{\pi}{2} - h_a (\tan \alpha_d + \tan \alpha_c) . \quad (3.43)$$

In most cases gears with asymmetric teeth are designed reversible, capable of transmitting torque or motion in both rotation directions. For this reason, their area of existence contains only reversible gear combinations. Typically the coast tooth flank has lower involute profile angles than the drive one, and the area of existence of asymmetric gears is limited by the coast flank interference isograms  $\alpha_{pc1} = 0^\circ$  and  $\alpha_{pc2} = 0^\circ$ . The spur gears must have a contact



(b)

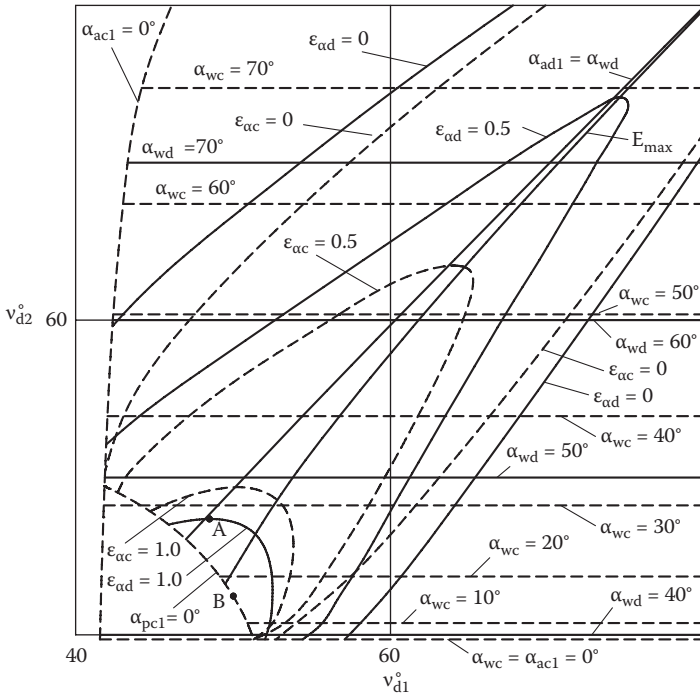
FIGURE 3.15 (continued)

ratio greater than 1.0. Therefore the area of existence of asymmetric reversible spur gears is limited by the drive flank contact ratio isogram  $\epsilon_{ad} = 1.0$  that is inside the coast flank contact ratio isogram  $\epsilon_{ac} = 1.0$ . Helical gears can have a contact ratio lower than 1.0, and because the coast flank contact ratio isogram  $\epsilon_{ac} = 0$  is inside the drive flank contact ratio isogram  $\epsilon_{ad} = 0$ , it limits the area of existence of asymmetric reversible helical gears.

The irreversible asymmetric gear geometry solutions can be found between the coast and drive flank interference isograms, between the contact ratio isograms  $\epsilon_{ad} = 1.0$  and  $\epsilon_{ac} = 1.0$  for spur gears, and between the contact ratio isograms  $\epsilon_{ac} = 0$  and  $\epsilon_{ad} = 0$  for helical gears.

The maximum of the drive flank pressure angle for the external spur gears is achieved in point A where its isogram is tangent to the drive flank contact ratio isogram  $\epsilon_{ad} = 1.0$ . The maximum of the drive flank contact ratio for external spur or helical gears is at point B at the intersection of the coast flank interference isograms  $\alpha_{pc1} = 0^\circ$  and  $\alpha_{pc2} = 0^\circ$ .

For the internal spur asymmetric gears, the same as for the internal spur symmetric gears, the point A location can be at the tangent point of the isograms of the drive flank pressure angle and the drive flank contact ratio  $\epsilon_{ad} = 1.0$  or at an intersection point of the  $\epsilon_{ad} = 1.0$  isogram and the pinion



(c)

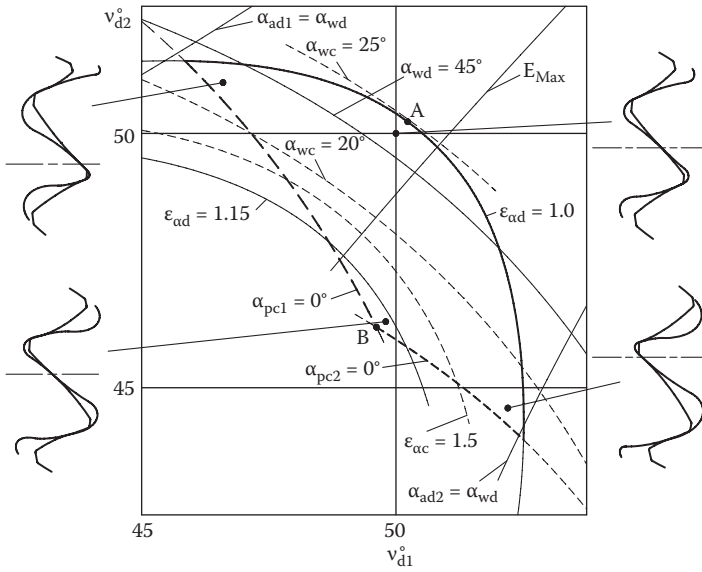
FIGURE 3.15 (continued)

coast flank interference isogram  $\alpha_{pc1} = 0^{\circ}$ . Point B of an area of existence of the internal asymmetric gears is at the intersection of the pinion coast flank interference isogram  $\alpha_{pc1} = 0^{\circ}$  and the tip/tip interference isogram.

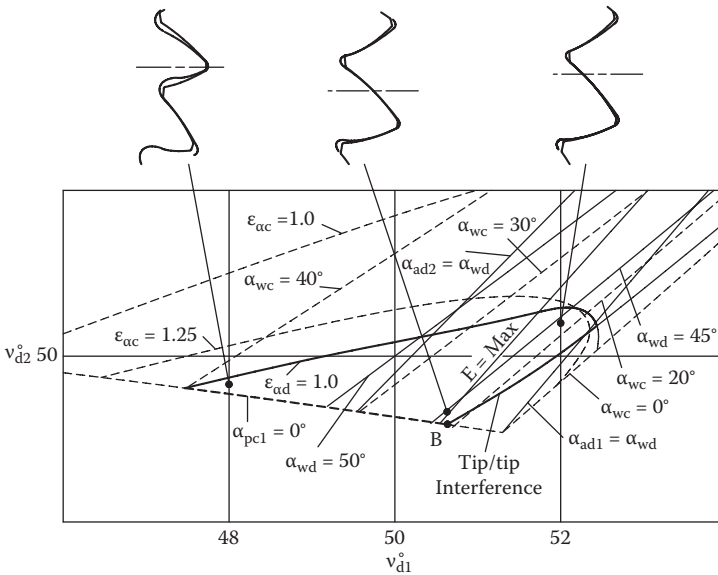
Similar to the symmetric spur rack and pinion gearing, point A in an area of existence of the asymmetric spur rack and pinion gearing can be located either at the highest point of the drive flank contact ratio isogram  $\epsilon_{od} = 1.0$ , where the horizontal isogram of the drive flank pressure angle reaches its maximum value, or at an intersection of the  $\epsilon_{od} = 1.0$  isogram and an isogram of the pinion drive flank interference  $\alpha_{pd1} = 0^{\circ}$ , depending on the pinion number of teeth. Point B is located where the drive flank contact ratio isogram is tangent to the pinion coast flank interference isogram  $\alpha_{pc1} = 0^{\circ}$  (Figures 3.15c and 3.16c).

### 3.2.2 Areas of Existence for Gear Pairs with Different Asymmetry Factors

Shape and size of an area of existence of asymmetric gears greatly depend on the asymmetry factor  $K$  [40]. An overlay of areas of existence of the spur



(a)



(b)

**FIGURE 3.16** Area of existence and gear teeth profiles of spur asymmetric external gears:  $z_1 = 18, z_2 = 25$ ;  $K = 1.3$ ;  $m_{a1} = 0.25, m_{a2} = 0.35$ . Solid line isograms are for the drive flanks, dashed line isograms are for the coast flanks. (a) For external gears, (b) for internal gears, (c) for rack and pinion.

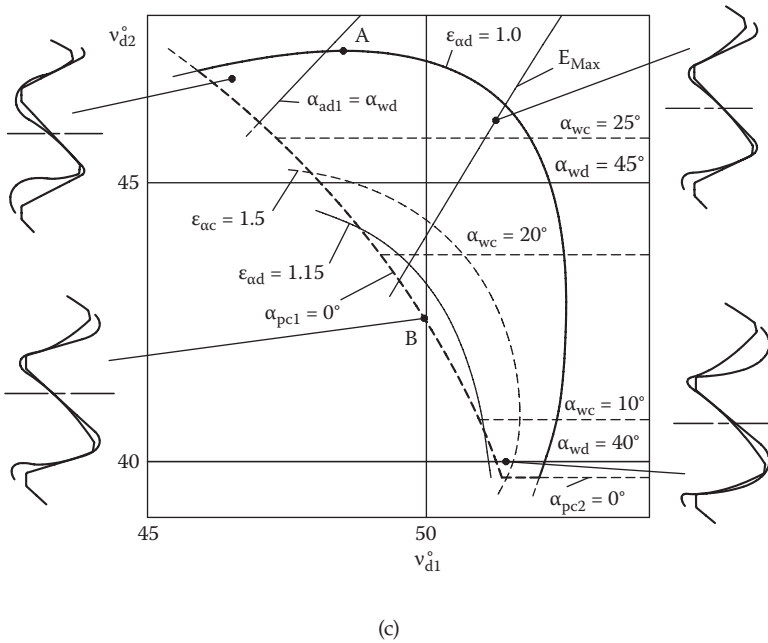


FIGURE 3.16 (continued)

asymmetric gears with different values of the asymmetry factor  $K$  is shown in Figure 3.17. When the asymmetry factor  $K = 1.0$ , gears are symmetric and their area of existence is largest. When the  $K$  factor increases, the pressure angle also increases but the area of existence decreases. At the maximum value of the factor  $K$  for spur asymmetric gears the area of existence presents a point where the drive contact ratio isogram  $\epsilon_{cd} = 1.0$  passes through an intersection of the coast flank interference isograms  $\alpha_{pc1} = 0^{\circ}$  and  $\alpha_{pc2} = 0^{\circ}$ . Here points  $A$  and points  $B$  coincide. Table 3.2 presents values of the drive and coast pressure angles and contact ratios at points  $A$  and  $B$  of areas of existence of the reversible spur asymmetric gears with different asymmetry factors, which are shown in Figure 3.17. It demonstrates potentials of asymmetric gears in increasing the drive pressure angle. Limits of the asymmetry factor  $K$  and drive pressure angle selection are described in Chapter 4. Rational selection of the asymmetry factor  $K$  are considered in Section 5.12.

### 3.3 Area of Existence and Pitch Factors

In the previous section areas of existence of asymmetric gears are considered with the given constant asymmetry factor  $K$ , and the relative tooth

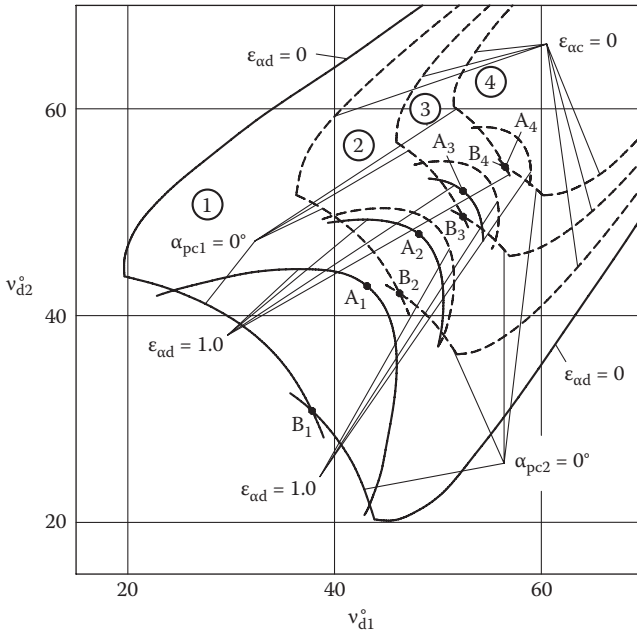


FIGURE 3.17

Areas of existence of external asymmetric gears with number of teeth  $z_1 = 18, z_2 = 25$  and relative tooth tip thicknesses  $m_{a1} = 0.25, m_{a2} = 0.35$  with different asymmetry coefficients  $K$ . Solid line isograms are for the drive flanks, dashed line isograms are for the coast flanks. 1 –  $K = 1.0$ , 2 –  $K = 1.2$ , 3 –  $K = 1.4$ , 4 –  $K = 1.575$ .

TABLE 3.2

Pressure Angle and Contact Ratio in Points A and B of Area of Existence of Asymmetric Gears

Gears		Symmetric		Asymmetric	
Asymmetry Coefficient		1.0	1.2	1.4	1.575
Pressure angle, °	Point A	37.07	43.08/28.78 <sup>a</sup>	48.10/20.79 <sup>a</sup>	51.54/12.76 <sup>a</sup>
	Point B	17.40	36.42/15.07 <sup>a</sup>	46.05/13.66 <sup>a</sup>	51.54/12.76 <sup>a</sup>
Contact ratio	Point A	1.0	1.0/1.10 <sup>a</sup>	1.0/1.26 <sup>a</sup>	1.0/1.55 <sup>a</sup>
	Point B	2.14	1.31/1.84 <sup>a</sup>	1.09/1.66 <sup>a</sup>	1.0/1.55 <sup>a</sup>

<sup>a</sup> Drive flank/coast flank.

tip thicknesses  $m_{a1}$  and  $m_{a2}$ . The pitch factors  $\theta_d, \theta_{dr}$  and  $\theta_v$  (see Section 2.3) in this case are varying. Figure 3.18 presents the overlaid areas of existence of spur external gears with the different constant drive flank pitch factors  $\theta_d$ . This type of area of existence of involute gears defines only the drive flank gear meshes. If  $\theta_d \leq 0.5$ , the gears can have symmetric or asymmetric teeth. If  $\theta_d > 0.5$ , the gears can have only asymmetric teeth.

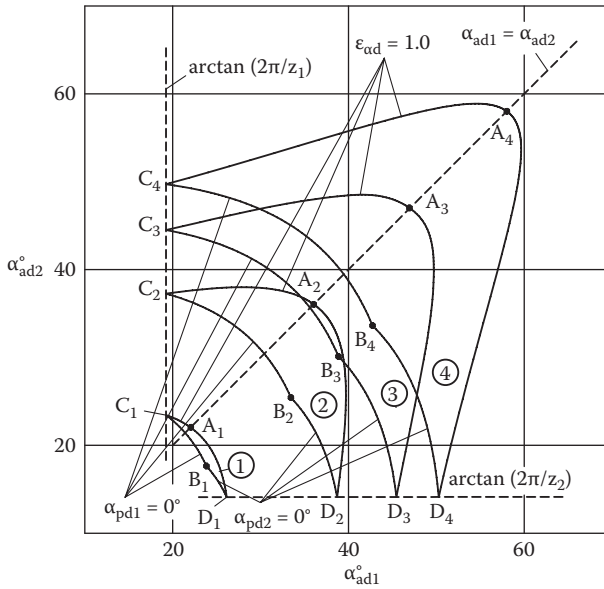


**FIGURE 3.18**

Areas of existence of external spur gears with  $z_1 = 18$ ,  $z_2 = 25$  and different values of the pitch factor  $\theta_d$ ; 1 -  $\theta_d = 0.1$ , 2 -  $\theta_d = 0.3$ , 3 -  $\theta_d = 0.5$ , 4 -  $\theta_d = 0.7$ .

The gears with symmetric teeth are always reversible. The gears with asymmetric teeth can be reversible or irreversible, depending on the coast flank pitch factor  $\theta_c$  selection.

For the drive flanks of the external gears the pressure angle isogram equation is defined from Equation (2.151) considering the tooth tip radii equal to zero. Then the effective tooth tip angles  $\alpha_{ed1,2}$  should be replaced by the tooth tip angles  $\alpha_{ad1,2}$

$$\text{inv}(\alpha_{ad1}) + u \text{inv}(\alpha_{ad2}) - (1 + u) \text{inv}(\alpha_{wd}) - \frac{2\pi\theta_d}{z_1} = 0. \quad (3.44)$$

The contact ratio isogram is defined by Equation (3.44) and

$$\tan \alpha_{ad1} + u \tan \alpha_{ad2} - (1 + u) \tan \alpha_{wd} - \frac{2\pi\epsilon_{cd}}{z_1} = 0. \quad (3.45)$$

A result of subtracting Equation (3.44) from Equation (3.45) is

$$\alpha_{ad1} + u\alpha_{ad2} - (1 + u)\alpha_{wd} - \frac{2\pi(\epsilon_{cd} - \theta_d)}{z_1} = 0. \quad (3.46)$$



The interference isograms  $\alpha_{pd1} = 0^\circ$  and  $\alpha_{pd2} = 0^\circ$  are defined by Equation (3.44) and

$$u \tan \alpha_{ad2} - (1 + u) \tan \alpha_{wd} = 0 \quad (3.47)$$

and

$$\tan \alpha_{ad1} - (1 + u) \tan \alpha_{wd} = 0. \quad (3.48)$$

In point *A* of the area of existence, where the drive flank pressure angle  $\alpha_{wd}$  is maximum and the contact ratio  $\epsilon_{cd} = 1.0$ , the pressure angle and contact ratio isograms have a common tangent point and the first derivatives of these isogram functions should be equal:

$$\frac{d(\alpha_{ad2})}{d(\alpha_{ad1})_{\alpha_{wd}=\text{const}}} = \frac{d(\alpha_{ad2})}{d(\alpha_{ad1})_{\epsilon_{cd}=1.0}}, \quad (3.49)$$

or with (3.44) and (3.45),

$$\frac{(\tan \alpha_{ad2})^2}{(\tan \alpha_{ad1})^2} = \frac{(\tan \alpha_{ad2})^2 + 1}{(\tan \alpha_{ad1})^2 + 1} \text{ or} \quad (3.50)$$

$$\alpha_{ad1} = \alpha_{ad2}. \quad (3.51)$$

This means points *A* of the areas of existence lie on the straight line  $\alpha_{ad1} = \alpha_{ad2}$ . The pressure angle equation at point *A* is defined as a solution of Equations (3.44), (3.45), and (3.51):

$$\tan \alpha_{wd} + \frac{2\pi}{z_t} - \tan\left(\alpha_{wd} + \frac{2\pi(1 - \theta_d)}{z_t}\right) = 0, \quad (3.52)$$

where  $z_t = z_1 + z_2$  is the total number of teeth of mating gears.

Its solution is [29]

$$\alpha_{wd}^A = \arctan\left(\sqrt{\frac{\pi^2}{z_t^2} + \frac{2\pi}{z_t \tan \frac{2\pi(1 - \theta_d)}{z_t}} - 1 - \frac{\pi}{z_t}}\right). \quad (3.53)$$

Then from (3.45) the coordinates of point *A* at the area of existence are

$$\alpha_{ad1}^A = \alpha_{ad2}^A = \arctan\left(\sqrt{\frac{\pi^2}{z_t^2} + \frac{2\pi}{z_t \tan \frac{2\pi(1 - \theta_d)}{z_t}} - 1 + \frac{\pi}{z_t}}\right). \quad (3.54)$$

In point  $B$  at the intersection of the interference isograms  $\alpha_{pd1} = 0^\circ$  and  $\alpha_{pd2} = 0^\circ$  the pressure angle is minimum and the contact ratio is maximum. This maximum contact ratio is defined as a solution of Equations (3.45), (3.46), (3.47), and (3.48):

$$\arctan\left(\frac{2\pi\epsilon_{od}}{z_1}\right) + u \arctan\left(\frac{2\pi\epsilon_{od}}{z_2}\right) - (1+u) \arctan\left(\frac{2\pi\epsilon_{od}}{z_t}\right) - \frac{2\pi(\epsilon_{od} - \theta_d)}{z_1} = 0. \quad (3.55)$$

Then the coordinate angles  $\alpha_{ad1}$  and  $\alpha_{ad2}$ , and drive pressure angle  $\alpha_{wd}$  at point  $B$ , are defined from Equations (3.36), (3.37), and (3.38) presented for drive flanks:

$$\alpha_{ad1}^B = \arctan\left(\frac{2\pi\epsilon_{od}}{z_1}\right), \quad (3.56)$$

$$\alpha_{ad2}^B = \arctan\left(\frac{2\pi\epsilon_{od}}{z_2}\right), \quad (3.57)$$

and

$$\alpha_{wd}^B = \arctan\left(\frac{2\pi\epsilon_{od}}{z_t}\right). \quad (3.58)$$

The coordinate angle  $\alpha_{ad1}$  at intersection point  $C$  of isograms  $\epsilon_{od} = 1.0$  and  $\alpha_{pd1} = 0^\circ$  from Equations (3.46) and (3.47) is

$$\alpha_{ad1}^C = \arctan(2\pi / z_1). \quad (3.59)$$

The coordinate angle  $\alpha_{ad2}$  and pressure angle  $\alpha_{wd}$  at point  $C$  are defined from

$$\arctan\left(\frac{2\pi}{z_1}\right) + u\alpha_{ad2} - (1+u) \arctan\left(\frac{u}{1+u} \tan \alpha_{ad2}\right) - \frac{2\pi(1-\theta_d)}{z_1} = 0 \quad (3.60)$$

and

$$\arctan\left(\frac{2\pi}{z_1}\right) + u \arctan\left(\frac{1+u}{u} \tan \alpha_{wd}\right) - (1+u)\alpha_{wd} - \frac{2\pi(1-\theta_d)}{z_1} = 0. \quad (3.61)$$

The coordinate angle  $\alpha_{ad2}$  at intersection point  $D$  of isograms  $\epsilon_{od} = 1.0$  and  $\alpha_{pd2} = 0^\circ$  from Equations (3.46) and (3.48) is

$$\alpha_{ad2}^D = \arctan(2\pi / z_2). \quad (3.62)$$

TABLE 3.3

Gear Parameters in Points *A*, *B*, *C*, and *D* of Area of Existence

Drive Flank Pitch Factor		0.1	0.3	0.5	0.7
Point A	$\alpha_{wd}$ , °	14.5	30.19	42.86	55.51
	$\epsilon_{cd}$	1.0	1.0	1.0	1.0
	$\alpha_{ad1}$ , °	22.04	36.05	47.04	58.02
	$\alpha_{ad2}$ , °	22.04	36.05	47.04	58.02
Point B	$\alpha_{wd}$ , °	10.48	15.46	18.64	21.14
	$\epsilon_{cd}$	1.27	1.89	2.31	2.65
	$\alpha_{ad1}$ , °	23.84	33.45	38.86	42.73
	$\alpha_{ad2}$ , °	17.65	25.44	30.12	33.63
Point C	$\alpha_{wd}$ , °	14.15	23.86	29.74	34.45
	$\epsilon_{cd}$	1.0	1.0	1.0	1.0
	$\alpha_{ad1}$ , °	19.24	19.24	19.24	19.24
	$\alpha_{ad2}$ , °	23.44	37.26	44.5	49.72
Point D	$\alpha_{wd}$ , °	11.61	18.55	23.05	26.73
	$\epsilon_{cd}$	1.0	1.0	1.0	1.0
	$\alpha_{ad1}$ , °	26.15	38.71	45.47	50.27
	$\alpha_{ad2}$ , °	14.11	14.11	14.11	14.11

The coordinate angle  $\alpha_{ad1}$  and pressure angle  $\alpha_{wd}$  at point *D* are defined from equations

$$\alpha_{ad1} + u \arctan\left(\frac{2\pi}{z_2}\right) - (1+u) \arctan\left(\frac{1}{1+u} \tan \alpha_{ad1}\right) - \frac{2\pi(1-\theta_d)}{z_1} = 0 \quad (3.63)$$

and

$$\arctan((1+u) \tan \alpha_{wd}) + u \arctan\left(\frac{2\pi}{z_2}\right) - (1+u)\alpha_{wd} - \frac{2\pi(1-\theta_d)}{z_1} = 0. \quad (3.64)$$

The pressure angles  $\alpha_{wd}$ , contact ratios  $\epsilon_{cd}$ , and coordinate angles  $\alpha_{ad1}$  and  $\alpha_{ad2}$  of points *A*, *B*, *C*, and *D* of the areas of existence from Figure 3.18 are presented in Table 3.3.

Points of the area of existence with the constant drive flank pitch factor do not define complete mating gear teeth, but just their drive flanks. This allows independent selection of the tooth tip thicknesses and the coast tooth flank parameters of asymmetric gears. Considering the tooth tip radii and backlash equal to zero, the noncontact pitch factor  $\theta_v$  from (2.150) is

$$\theta_v = \frac{m_{a1} \cos \alpha_{ad1} + m_{a2} \cos \alpha_{ad2}}{\pi \cos \alpha_{wd}}. \quad (3.65)$$

When some point of the area of existence with coordinates  $\alpha_{ad1}$  and  $\alpha_{ad2}$  is chosen, the pressure angle  $\alpha_{wd}$  is calculated by Equation (3.44). Then after selection of the relative tooth tip thicknesses  $m_{a1}$  and  $m_{a2}$ , the noncontact pitch factor  $\theta_v$  is calculated by Equation (3.65). This allows defining the coast flank pitch factor as

$$\theta_c = 1 - \theta_d - \theta_v. \quad (3.66)$$

If the tooth tip radii are equal to zero that makes  $\alpha_{ed1,2} = \alpha_{ad1,2}$  and  $\alpha_{ec1,2} = \alpha_{ac1,2}$ , the asymmetry factor  $K$  can be defined as a solution of Equations (2.93) and (2.153):

$$(1 + u) \operatorname{inv}(\operatorname{arc} \cos(K \cos \alpha_{wd})) = \operatorname{inv}(\operatorname{arc} \cos(K \cos \alpha_{ad1})) \\ + u \operatorname{inv}(\operatorname{arc} \cos(K \cos \alpha_{ad2})) - \frac{2\pi\theta_c}{z_1}. \quad (3.67)$$

Now the pressure angle and the coast flank tooth tip angles can be defined:

$$\alpha_{wc} = \operatorname{arc} \cos(K \cos \alpha_{wd}), \quad (3.68)$$

$$\alpha_{ac1,2} = \operatorname{arc} \cos(K \cos \alpha_{ad1,2}). \quad (3.69)$$

Equation (2.110) defines the coast flank contact ratio. The profile angles at the lowest points of contact near the root fillet for the drive and coast tooth flanks are described by Equations (2.95) and (2.96), and (2.97) and (2.98), accordingly.

### 3.4 Application of Area of Existence

Area of existence of involute gears is a research tool that can be used to find some exotic gear mesh solutions that were not known before. It also allows locating gear pairs with certain characteristics. Its practical purpose is to define the gear pair parameters that satisfy specific performance requirements before detailed design and calculations. This involute gear research tool is incorporated into the preliminary design program with the finite element analysis (FEA) subroutine. Such a program is able not just to generate all isograms for gears with the given numbers of teeth  $z_1$  and  $z_2$ , relative tooth tip thicknesses  $m_{a1}$  and  $m_{a2}$ , and asymmetry coefficient  $K$ , but also, with input of module or diametral pitch, gear face widths, and material properties (the modulus of elasticity and Poisson ratio), promptly define the relative sliding

velocities, gear mesh efficiency, bending and Hertzian contact stresses, and create the gear mesh animation of any point of area of existence [39]. Such software allows limits of parameter selection of involute gears to be defined quickly, feasible gear pairs to be located and animated, and their geometry and stress levels to be reviewed. Benefits of using the area of existence are:

- Consideration of all possible gear combinations
- Instant definition of limits of the gear performance parameters
- Awareness about nontraditional uncommon gear design options
- Quick localization of gear sets suitable for particular application
- Preliminary gear design optimization

# 4

---

## *Involute Gearing Limits*

---

The previous chapters have demonstrated how the Direct Gear Design® approach expands the involute gearing limits in comparison with the traditional gear design that is based on the rack generation. This chapter is dedicated to definition of the gear parameter limits for the spur and helical gears with symmetric and asymmetric teeth. Some of the tooth shapes and gear mesh combinations presented below look rather unusual and may not have rational practical applications. A goal of this chapter is to show boundaries of the involute gearing parameters.

---

### **4.1 Number of Teeth**

Selection of numbers of teeth of mating gears is critically important. First, it provides the required gear ratio. Second, when the gear ratio and center distance are specified, selected numbers of teeth define the gear tooth size that is described by a module in the metric system of a diametral pitch in the English system. The gear tooth size is a main parameter in the definition of the bending stress. Third, the number of gear teeth is a major factor in the definition of gear mesh efficiency. Along with the gear mesh geometry parameters (pressure angle, contact ratio, etc.), a tooth number selection allows providing sufficient safety factors for bending and contact stresses, and wear resistance to optimize a gear pair design.

The maximum number of gear teeth is limited by application practicality and manufacturing technology. Most mechanically controlled gear hobbing machines can produce gears with a number of teeth up to 400 using one-start hobs. Usage of multistart hobs increases this limit accordingly. Some computer numerical control (CNC) gear hobbing machines can produce gears with a number of teeth up to 1000 using one-start hobs. Other gear fabrication technologies like, for example, profile cutting or injection molding can provide gears with an even greater number of teeth.

From the application point, the maximum number of gear teeth may also be limited by tolerance sensitivity and operating conditions. If the gear pitch diameter is constant, an increase in the number of teeth leads to their size reduction, to the point where the size of the tooth becomes comparable with tolerance values. Gear operating conditions may result in a similar effect for

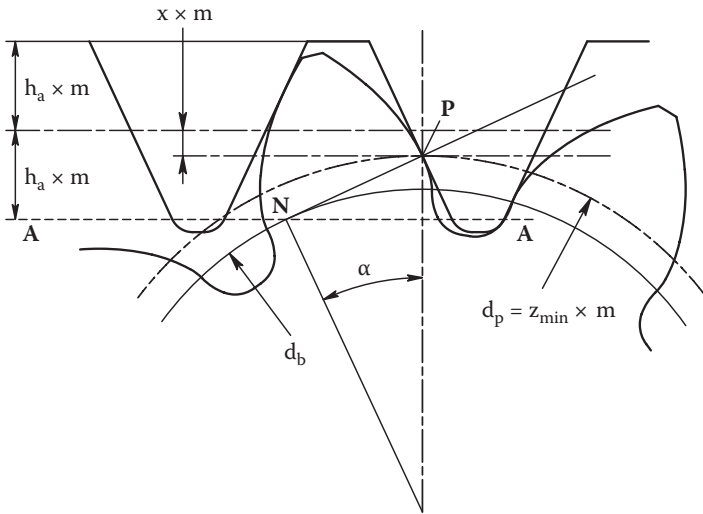


**FIGURE 4.1**  
Minimum number of teeth definition.

fine pitch gears. For example, wide operating temperature range and application of dissimilar gear and housing materials may lead to noticeable gear sizes and center distance changes also comparable to the tooth size.

#### 4.1.1 Symmetric Gearing

Gear handbooks give a conservative minimum number of teeth to avoid the tooth root undercut by the tooling generating rack and reduce tooth flank sliding. For example, the gear handbook [38] indicates that the tooth root undercut occurs for the  $14\frac{1}{2}^\circ$  pressure angle spur gears with a number of teeth lower than 32, for the  $20^\circ$  pressure angle spur gears with a number of teeth lower than 17, and for the  $25^\circ$  pressure angle spur gears with a number of teeth lower than 12. These numbers of teeth are defined by the beginning of the undercut condition when the standard addendum coefficient  $h_a = 1.0$  and the rack shift coefficient  $x = 0$ .

Figure 4.1 explains the minimum number of teeth definition. The tooth root undercut occurs when the generating rack addendum trajectory line A-A is below the tangent point N, where the normal to the rack profile at the pitch point touches the base diameter  $d_b$ .

Then the undercut avoidance condition is

$$\frac{z_{\min} m}{2} \sin^2 \alpha \geq (h_a - x)m, \quad (4.1)$$

where  $m$  is a module and  $\alpha$  is the rack pressure angle. From here

$$z_{\min} \geq \frac{2(h_a - x)}{\sin^2 \alpha}. \tag{4.2}$$

Application of the rack shift coefficient  $x > 0$  or the nonstandard generating rack with high-pressure angle  $\alpha$  and low addendum coefficient  $h_a$  allows achievement of a significantly lower minimum tooth number without tooth root undercut. The spur gears with a number of teeth as low as 6 are used in the external gear pumps.

Directly designed spur symmetric gears are not constrained by limitations imposed by the generating rack and its X-shift. Minimum numbers of teeth of external spur gears depend on the gear ratio and are defined by the simultaneous conditions: the involute profile angles at the lowest contact points  $\alpha_{p1,2} = 0^\circ$  (point *B* of an area of existence) and the contact ratio  $\epsilon_\alpha = 1.0$ . The book [7] described a minimum number of teeth of external spur gears (Figure 4.2). Parameters of these gear pairs are presented in Table 4.1.

The pinion and gear tooth tip profile angles, and the pressure angle for these gears are from Equations (3.36), (3.37), and (3.38) when  $\epsilon_\alpha = 1.0$ . Then the flank pitch factor  $\theta$  is from Equation (2.163) and the noncontact pitch factor  $\theta_v$  can be defined from (2.169) as

$$\theta_v = 1 - 2\theta. \tag{4.3}$$

Assuming equal relative tooth tip thicknesses  $m_{a1} = m_{a2}$ , they are from (3.65)

$$m_{a1} = m_{a2} = \frac{\pi\theta_v \cos \alpha_w}{\cos \alpha_{a1} + \cos \alpha_{a2}}. \tag{4.4}$$

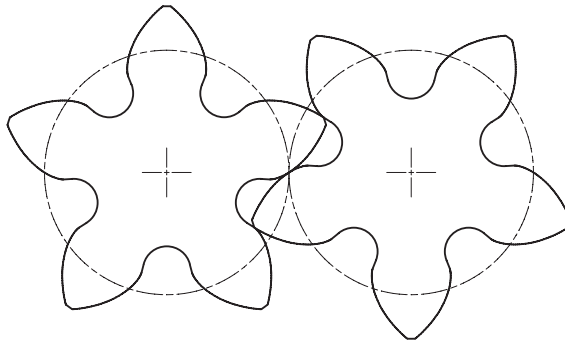
The minimum numbers of teeth of internal spur gears are defined by the simultaneous conditions: the pinion involute profile angle at the lowest contact points  $\alpha_{pd1} = 0^\circ$  and the beginning of the tip/tip interference that is described by Equation (2.70) (point *B* of an area of existence) and the contact ratio  $\epsilon_\alpha = 1.0$ . Internal spur gears with minimum numbers of teeth are shown in Figure 4.3. Their parameters are in Table 4.2.

In the rack and pinion mesh a minimum number of the pinion teeth is three, and the rack's number of teeth is considered infinite.

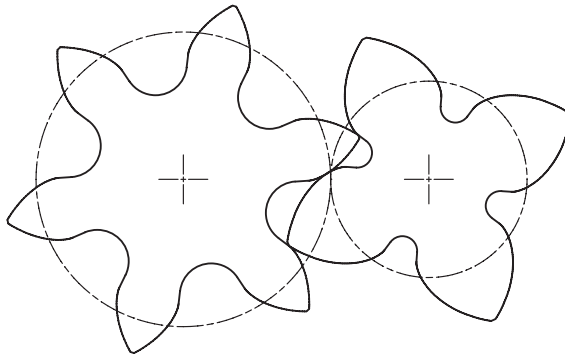
Figure 4.4 presents an unusual but kinematically possible epicyclic symmetric spur gear stage with a one-tooth sun gear, two idler gears, also with one tooth, and three-tooth ring gear.

Work of this gear stage is also quite unusual. Normally in an epicyclic gear stage all idler gears transmitting motion from the sun gear to the planet gear are constantly and simultaneously engaged with both of them. If this case, in position  $0^\circ$  (Figure 4.4a) the sun gear is engaged with both idler gears, and they are engaged with the ring gear. Then while moving from position

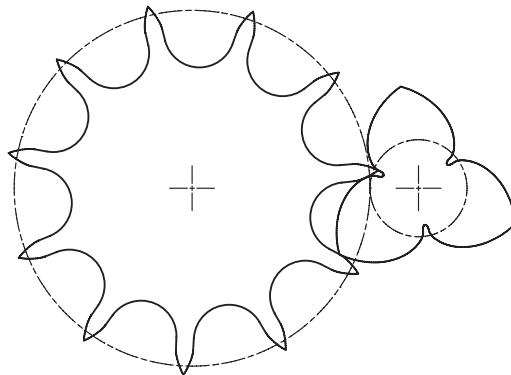




(a)



(b)



(c)

**FIGURE 4.2**

External symmetric spur gears with low number of teeth: (a)  $z_{1,2} = 5$ , (b)  $z_1 = 4, z_2 = 6$ , (c)  $z_1 = 3, z_2 = 11$ . (From Kapelevich, A.L., and R.E. Kleiss, *Gear Technology*, September/October 2002, 29–35. With permission.)

**TABLE 4.1**

External Symmetric Spur Gears with Low Number of Teeth

Pinion number of teeth, $z_1$	5	4	3
Gear number of teeth, $z_2$	5	6	11
Flank pitch factor, $\theta$	0.46	0.48	0.495
Relative tooth tip thickness, $m_{a1,2}$	0.17	0.09	0.02
Pressure angle, $\alpha_w^\circ$	32.07	32.1	24.19
Contact ratio, $\epsilon_\alpha$	1.0	1.0	1.0
Pinion tooth tip profile angle, $\alpha_{a1}^\circ$	51.41	57.47	64.5
Gear tooth tip profile angle, $\alpha_{a2}^\circ$	51.41	46.27	29.76

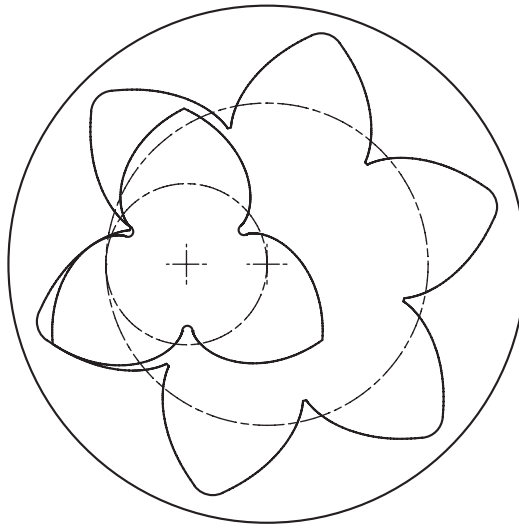


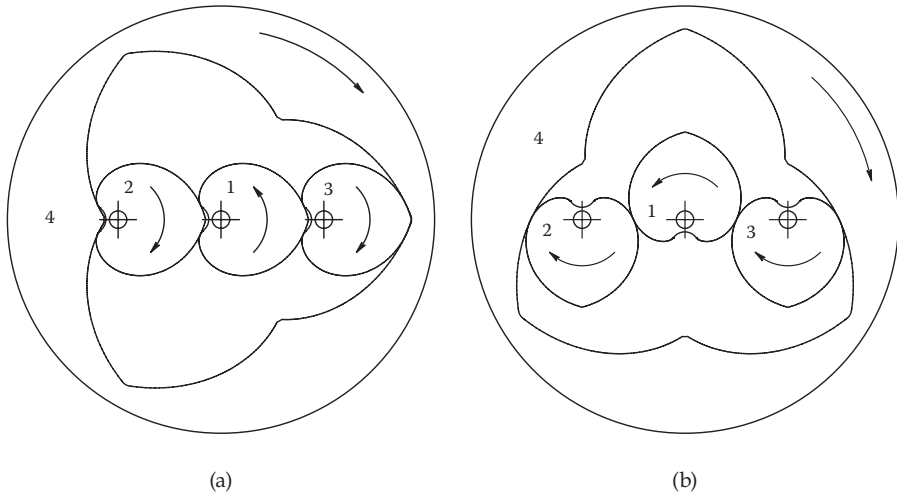
**FIGURE 4.3**

Internal symmetric spur gears with minimum number of teeth:  $z_1 = 3, z_2 = 6$ .

**TABLE 4.2**

Internal Symmetric Spur Gears with Minimum Number of Teeth

Gear	External	Internal
Number of teeth, $z$	3	6
Transverse pressure angle, $\alpha_w^\circ$		33.62
Transverse contact ratio, $\epsilon_\alpha$		1.0
Tooth tip profile angle, $\alpha_a^\circ$	64.5	18.4

**FIGURE 4.4**

Epicyclic symmetric spur gear stage with minimum number of teeth: (a) position  $0^\circ$ , (b) position  $+90^\circ$ . 1 - sun gear; 2 - left idler gear; 3 - right idler gear; 4 - ring gear.

**TABLE 4.3**

Epicyclic Symmetric Spur Gears with Minimum Number of Teeth

Gear	Sun	Idler	Ring
Number of teeth, $z$	1	1	3
Transverse pressure angle, $\alpha_w$ , $^\circ$		65	65
Transverse contact ratio, $\epsilon_\alpha$		0.56	0.59
Tooth tip profile angle, $\alpha_a$ , $^\circ$	75.6	75.6	56.1

$0^\circ$  to position  $+90^\circ$  (Figure 4.4b), the sun gear is driving only the left idler gear, which transmits motion to the ring gear. The right idler gear does not transmit motion, but it is moved by the ring gear. When gears pass position  $+180^\circ$ , the left and right idler gear motion transmission roles are changed, i.e., during one half of revolution of the sun gear, one idler gear transmits motion, then another one. It allows transmittal of motion despite the contact ratios in both sun/planet and planet/ring gear meshes being lower than 1.0. Parameters of such an epicyclic gear stage are shown in Table 4.3.

Helical gears also have an axial contact ratio  $\epsilon_\beta$  that compensates for the lack of a transverse contact ratio  $\epsilon_\alpha$  (see Section 2.2.3), which can be reduced to zero. This makes it possible to have a minimum number of teeth  $z_1 = z_2 = 1$  [35]. Figure 4.5 shows specimens of the external helical symmetric gears with numbers of teeth equal 1 and 2. Main parameters of these gears are in Table 4.4. Figure 4.6 presents their areas of existence.

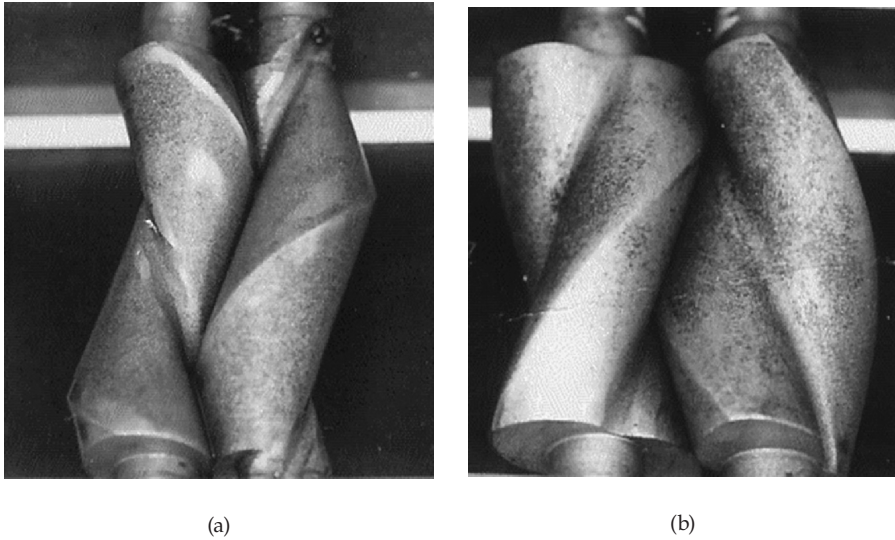


**FIGURE 4.5** External symmetric helical gears with low number of teeth: (a)  $z_{1,2} = 1$ , (b)  $z_{1,2} = 2$ . ((a) from Kapelevich, A.L., and R.E. Kleiss, *Gear Technology*, September/October 2002, 29–35. With permission.)

**TABLE 4.4**

External Symmetric Helical Gears with Low Number of Teeth

Number of teeth, $z_{1,2}$	1	2
Transverse pressure angle, $\alpha_w^\circ$	65.0	65.3
Helix angle at pitch diameter, $\beta_w^\circ$	29.2	29.5
Transverse contact ratio, $\epsilon_\alpha$	0.56	0.58
Axial contact ratio, $\epsilon_\beta$	1.0	0.5
Total contact ratio, $\epsilon_\gamma$	1.56	1.08
Tooth tip profile angle, $\alpha_{t1,2}^\circ$	75.6	73.0

Figure 4.7 shows the internal helical symmetric gears with a minimum number of teeth. The main parameters of these gears are in Table 4.5.

### 4.1.2 Asymmetric Gearing

Many asymmetric gear applications require reversibility, when the coast flanks of the tooth are engaged in motion and limited (compare to the drive flanks) load transmission. For spur gears it means that the coast contact ratio  $\epsilon_{\alpha c} \geq 1.0$ . Minimum numbers of teeth of such reversible spur asymmetric gears are the same as for the spur symmetric gears.

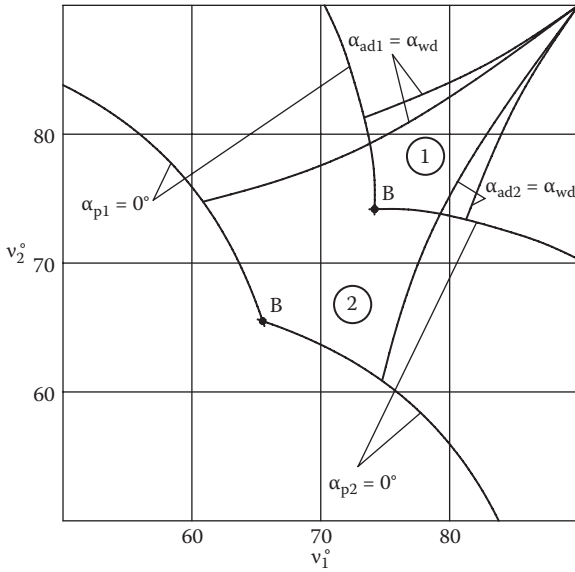


**FIGURE 4.6**  
 Areas of existence of external symmetric helical gears with minimum number of teeth:  
 1,  $z_{1,2} = 1$ ; 2,  $z_{1,2} = 2$ .

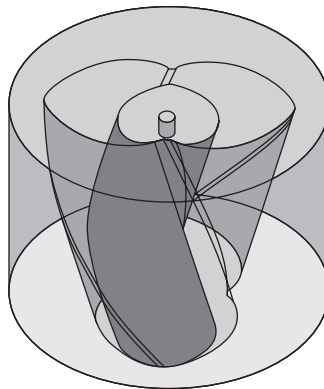


**FIGURE 4.7**  
 Internal symmetric helical gears with minimum number of teeth  $z_1 = 1, z_2 = 2$ .

The paper [41] described the asymmetric spur gears with numbers of teeth 1, 2, and 3, and gear ratio  $u = 1$ . Those gears have the drive contact ratio  $\epsilon_{oc} \geq 1.0$ , but the coast contact ratio  $\epsilon_{cc} < 1.0$  that makes them irreversible. Such gears may not have the coast flank involute profiles at all. Examples of such irreversible asymmetric spur gears with number of teeth  $z_{1,2} = 1$  and  $z_{1,2} = 2$  are shown in Figure 4.8. The main parameters of these gears are shown in Table 4.6.

**TABLE 4.5**

Internal Symmetric Helical Gears with Minimum Number of Teeth

Gear	Pinion	Gear
Number of teeth	1	2
Transverse pressure angle, $\alpha_w$ , °		65.0
Helix angle at pitch diameter, $\beta_w$ , °		61.0
Transverse contact ratio, $\epsilon_\alpha$		0.61
Axial contact ratio, $\epsilon_\beta$		0.5
Total contact ratio, $\epsilon_\gamma$		1.11
Tooth tip profile angle, $\alpha_{a1,2}$ , °	75.6	48.2

**TABLE 4.6**

Irreversible Asymmetric Spur Gears with Low Number of Teeth

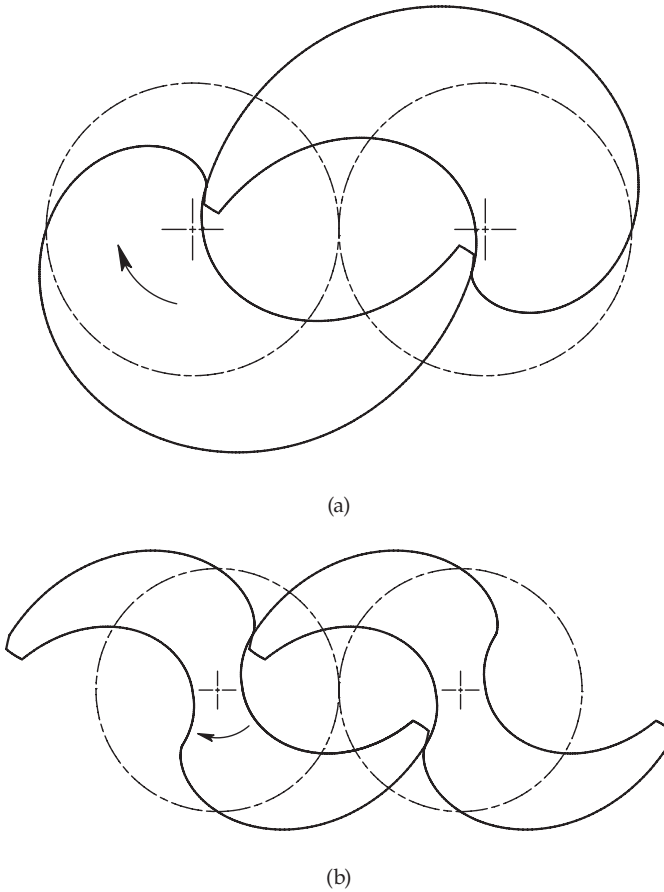
Number of teeth, $z_{1,2}$	1	2
Drive flank pitch factor, $\theta_d$	0.952	0.835
Drive flank pressure angle, $\alpha_{wd}$ , °	72.34	57.52
Drive flank contact ratio, $\epsilon_{ad}$	1.0	1.0
Drive flank tooth tip profile angle, $\alpha_{ad1,2}$ , °	80.95	72.34

## 4.2 Pressure Angle

The vast majority of gears are designed with standard tooth proportions. One of the main tooth proportion parameters is a pressure angle. Most gears are designed with the standard 20° pressure angle. The old standard pressure angle of 14½° is still in use. In some industries like, for example, aerospace, the 25° and 28° pressure angles are used [5, 42]. The term *pressure angle*, in this case, is actually related not to the gear mesh, but to the basic or generating rack that is used for design or as a cutter profile, accordingly. The gear (except the gear rack) involute profile angle varies from the form diameter to the tooth tip diameter. This section describes the transverse operating pressure angle, which is defined for a pair of mating gears as

$$\alpha_w = \arccos\left(\frac{d_{b1}(u \pm 1)}{2a_w}\right). \tag{4.5}$$

For spur gears with symmetric or asymmetric teeth the minimum pressure angle is defined at point *B* of the area of existence constructed with the constant drive pitch factor  $\theta_d$  (see Section 3.3), where the transverse contact ratio is  $\epsilon_{ad} = 1.0$ . For external spur gears it can be found from Equation (3.58)

**FIGURE 4.8**

External irreversible asymmetric spur gears with low number of teeth: (a)  $z_{1,2} = 1$ , (b)  $z_{1,2} = 2$ .

$$\alpha_{\text{wd}}^B = \arctan\left(\frac{2\pi}{z_t}\right). \quad (4.6)$$

The higher the number of teeth and gear ratio, the lower the pressure angle at point B. The tooth tip profile angles in this case are from Equations (3.56) and (3.57):

$$\alpha_{\text{ad1}}^B = \arctan\left(\frac{2\pi}{z_1}\right), \quad (4.7)$$

$$\alpha_{\text{ad2}}^B = \arctan\left(\frac{2\pi}{z_2}\right). \quad (4.8)$$

**TABLE 4.7**

Minimum Pressure Angle for External Spur Gears ( $u = 1.0$ )

Number of teeth, $z_{1,2}$	5	10	20	50	100
Drive flank pitch factor, $\theta_d$	0.46	0.18	0.05	0.009	0.002
Contact ratio, $\epsilon_{\alpha d}$	1.0	1.0	1.0	1.0	1.0
Minimum pressure angle, $\alpha_{wd}^\circ$	32.14	17.44	8.93	3.6	1.8
Tooth tip profile angle, $\alpha_{ad1,2}^\circ$	51.49	32.14	17.44	7.16	3.6

Then the drive flank pitch factor is from (3.44)

$$\theta_d = \frac{z_1}{2\pi} (inv(\alpha_{ad1}) + uinv(\alpha_{ad2}) - (1 + u)inv(\alpha_{wd})). \tag{4.9}$$

Table 4.7 presents the minimum pressure angles for gears with the gear ratio  $u = 1.0$  and different numbers of teeth.

For helical gears with symmetric or asymmetric teeth the theoretical minimum pressure angle is  $\alpha_w = 0^\circ$ .

The maximum pressure angle for external spur gears with symmetric teeth is defined at point *A* of the area of existence, where the pressure angle isogram is tangent to the transverse contact ratio isogram  $\epsilon_\alpha = 1.0$ . It depends on the number of teeth of mating gears  $z_{1,2}$  and also on the relative tooth tip thicknesses  $m_{a1,2}$ . The theoretical maximum pressure angle is achieved for a gear pair with the pointed teeth when  $m_{a1,2} = 0$  and is defined as [7]

$$\alpha_{w\max} = \arctan\left(\sqrt{\frac{\pi^2}{z_t^2} + \frac{2\pi}{z_t \tan \frac{\pi}{z_t}} - 1} - \frac{\pi}{z_t}\right). \tag{4.10}$$

From (4.10) is clear that when the total number of teeth is increasing and approaches infinity ( $z_t \rightarrow \infty$ ), the pressure angle limit for external spur gears with symmetric teeth is  $\alpha_{w\lim} = 45^\circ$ .

The general solution for the maximum pressure angle for both symmetric and asymmetric gears is presented in Equation (3.53). When  $z_t \rightarrow \infty$ , the pressure angle limit for external spur gears from this equation is defined as [29]

$$\alpha_{w\lim} = \arctan\sqrt{\frac{\theta}{1 - \theta}}. \tag{4.11}$$

A chart of the maximum pressure angles  $\alpha_{w\max}$  for different total numbers of teeth and drive pitch factors is shown in Figure 4.9.

If the tooth asymmetry is defined by the factor  $K$ , the minimum and maximum drive pressure angles are defined in points *B* and *A* of the area of existence, accordingly. Figure 4.10 presents ranges of the drive pressure angles for different numbers of teeth and asymmetry factors.



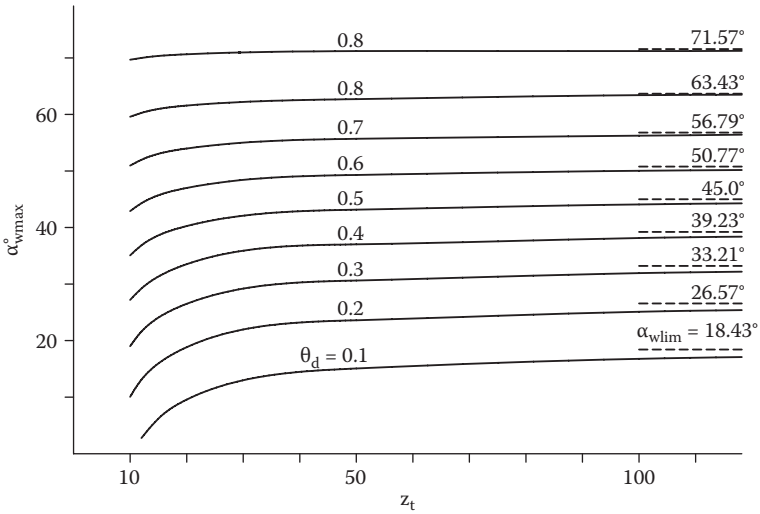


**FIGURE 4.9**  
Maximum pressure angles of external spur gears.

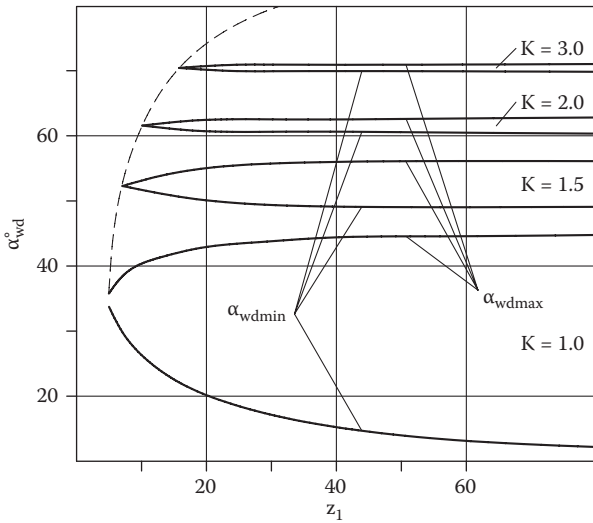


**FIGURE 4.10**  
Minimum and maximum pressure angles for external spur gears with gear ratio  $u = 1$  and relative tooth tip thicknesses  $m_{a1,2} = 0$ .

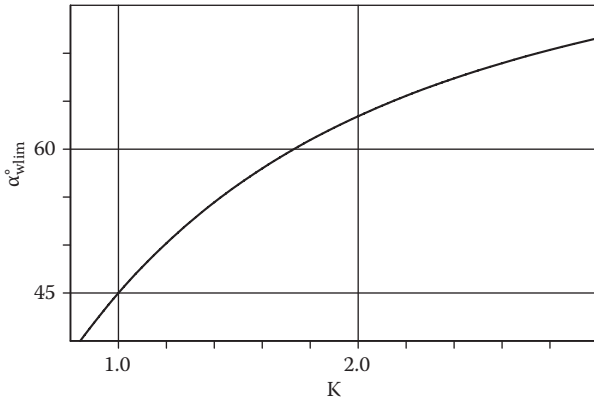


**FIGURE 4.11**  
Pressure angle limits for external spur gears.

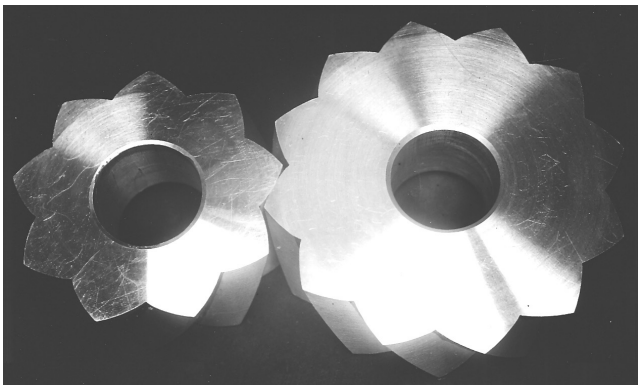


**FIGURE 4.12**  
Helical gears with high-pressure angle. (From Kapelevich, A.L., and R.E. Kleiss, *Gear Technology*, September/October 2002, 29–35. With permission.)

The pressure angle limit for the external spur gears with  $z_t \rightarrow \infty$  is [29]

$$\alpha_{w\text{lim}} = \arctan K . \tag{4.12}$$

A chart of the pressure angle limit  $\alpha_{w\text{lim}}$  as a function of the asymmetry factor  $K$  is shown in Figure 4.11.

Helical gears can have the transverse contact ratio  $0 < \epsilon_\alpha < 1.0$ . This expands a theoretical range of the transverse pressure angle to  $0^\circ < \alpha_w < 90^\circ$ .

Figure 4.12 shows the helical gear models with a high-pressure angle of  $\alpha_w = 70^\circ$  and transverse contact ratio  $\epsilon_\alpha = 0.5$ . A practical application of gears with very high transverse pressure angles ( $75^\circ$  to  $85^\circ$ ) is the self-locking gears (Section 6.3).

### 4.3 Contact Ratio

The theoretical minimum transverse contact ratio for involute helical gears is  $\epsilon_\alpha = 0$ . In this case the active involute profiles of the mating gear flanks are shrunk to the point. Helical gears with theoretically pointed contact have found practical application in noninvolute Wildhaber-Novikov gears [43, 44].

In traditional gear design the maximum transverse contact ratio is defined by the selected basic or generating rack and its X-shifts for a pinion and gear. The contact ratio limit, in this case, is achieved when the number of teeth of mating gears approaches infinity:  $z_{1,2} \rightarrow \infty$ . This limit can be defined as (see Figure 4.13)

$$\epsilon_{\alpha \text{lim}} = \frac{H_w}{p_b \sin \alpha} \tag{4.13}$$

or

$$\epsilon_{\alpha \text{lim}} = \frac{2h_w}{\pi \sin(2\alpha)} \tag{4.14}$$

Table 4.8 presents the contact ratio limits for different generating racks.

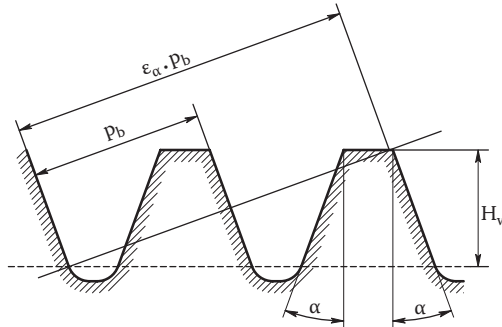


FIGURE 4.13 Contact ratio limit definition for traditionally designed gears.

TABLE 4.8 Contact Ratio Limits for Traditionally Designed Gears

Generating Rack	Pressure Angle, $\alpha$	Active Depth Coefficient, $h_w$	Contact Ratio Limit, $\epsilon_{\alpha \text{lim}}$
Standard	$14\frac{1}{2}^\circ$	2.0	2.63
Standard	$20^\circ$	2.0	1.98
Standard	$25^\circ$	2.0	1.66
Nonstandard	$28^\circ$	1.8	1.38
Nonstandard	$20^\circ$	2.3	2.28

Direct Gear Design expands the transverse contact ratio range. Its maximum value depends on the type of gearing (external, internal, or rack and pinion), tooth profile (symmetric or asymmetric), number of teeth, and relative tooth tip thicknesses.

The highest contact ratio for gear pairs with a particular number of teeth and the relative tooth tip thicknesses is achieved at point *B* of area of existence at the intersection of the interference isograms. The lower the relative tooth tip thicknesses  $m_{a1,2}$ , the higher the contact ratio at point *B*. It has its maximum value when the relative tooth tip thicknesses  $m_{a1,2} = 0$ . For external symmetric gears it is defined from Equation (3.55):

$$\arctan\left(\frac{2\pi\epsilon_\alpha}{z_1}\right) + u \arctan\left(\frac{2\pi\epsilon_\alpha}{z_2}\right) - (1 + u) \arctan\left(\frac{2\pi\epsilon_\alpha}{z_t}\right) - \frac{\pi(2\epsilon_\alpha - 1)}{z_1} = 0. \quad (4.15)$$

Maximum transverse contact ratios for external gears with symmetric teeth (Figure 4.14) are shown in Table 4.9.

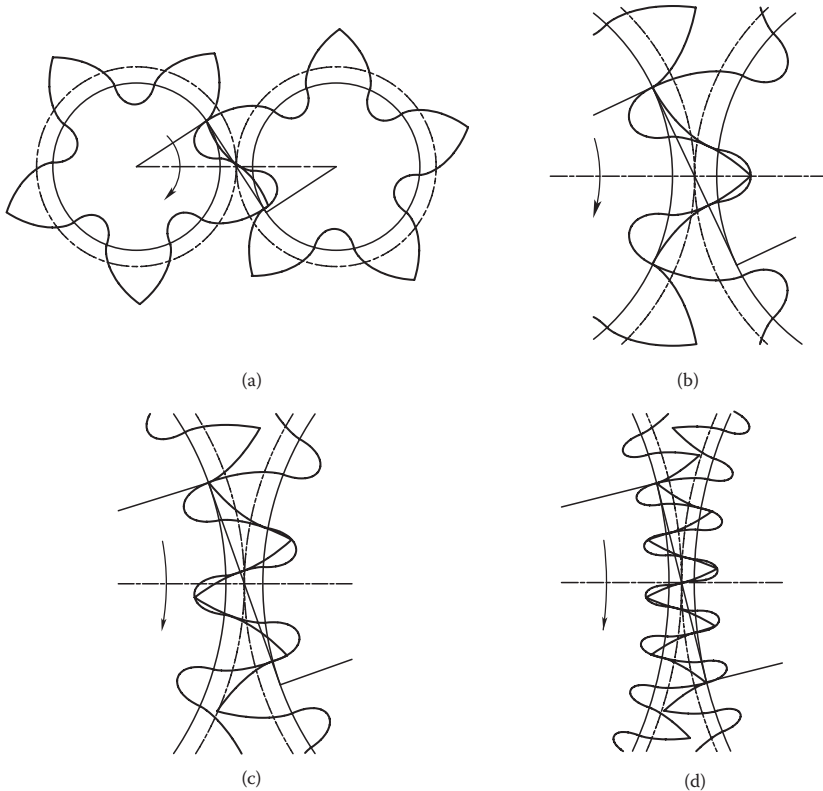


**FIGURE 4.14** External symmetric gears with maximum contact ratio: (a) number of teeth  $z_{1,2} = 5$ , (b)  $z_{1,2} = 10$ , (c)  $z_{1,2} = 20$ , (d)  $z_{1,2} = 50$ .

**TABLE 4.9**

Maximum Contact Ratios for Gears with Symmetric Teeth

Number of teeth, $z_{1,2}$	5	10	15	20	30	40	50
Maximum contact ratio, $\epsilon_\alpha$	1.04	1.51	1.9	2.26	2.89	3.46	3.98
Pressure angle, $\alpha_w^\circ$	33.14	25.31	21.72	19.53	16.85	15.21	14.05
Tooth tip angle, $\alpha_{t1,2}^\circ$	52.56	43.4	38.55	35.35	31.21	28.53	26.59
Lowest involute angle, $\alpha_{p1,2}$	0.0	0.0	0.0	0.0	0.0	0.0	0.0

**TABLE 4.10**

Maximum Drive Contact Ratios for Reversible Asymmetric Gears

Number of teeth, $z_{1,2}$	10	15	20	30	40	50
Drive contact ratio, $\epsilon_{out}$	1.53	1.931	2.288	2.924	3.49	4.015
Coast contact ratio, $\epsilon_{oc}$	1.0	1.0	1.0	1.0	1.0	1.0
Drive flank pressure angle, $\alpha_{wd}^\circ$	25.67	22.02	19.77	17.02	15.34	14.157
Coast flank pressure angle, $\alpha_{wc}^\circ$	20.58	15.79	13.19	10.47	8.73	7.692
Drive flank tooth tip angle, $\alpha_{td1,2}^\circ$	43.87	38.97	35.71	31.48	28.75	26.77
Coast flank tooth tip angle, $\alpha_{tc1,2}^\circ$	41.51	36.19	32.85	28.71	26.03	24.147
Drive flank lowest involute angle, $\alpha_{pd1,2}^\circ$	0.0	0.0	0.0	0.0	0.0	0.0
Coast flank undercut angle, $\alpha_{uc1,2}^\circ$	3.54	4.21	4.38	4.29	4.252	4.124
Drive flank pitch factor, $\theta_d$	0.519	0.519	0.517	0.514	0.512	0.511
Coast flank pitch factor, $\theta_c$	0.481	0.481	0.483	0.486	0.488	0.489
Noncontact pitch factor, $\theta_v$	0.0	0.0	0.0	0.0	0.0	0.0
Asymmetry factor, $K$	1.039	1.038	1.035	1.028	1.025	1.022

Spur reversible asymmetric gears require the coast flank contact ratio to be  $\epsilon_{oc} \geq 1.0$ . The highest contact ratio is achieved at point  $B$  of area of existence at the intersection of the drive tooth flank interference isograms. Below this point the coast flank interference occurs, resulting in involute profile undercut. Such undercut is permissible if the coast flank contact ratio is  $\epsilon_{oc} \geq 1.0$ . The condition  $\epsilon_{oc} = 1.0$  defines the coast flank undercut profile angles  $\alpha_{uc1,2}$ , drive and coast flank pitch factors  $\theta_d$  and  $\theta_c$ , and asymmetry factor  $K$ . Maximum transverse contact ratios for spur external reversible asymmetric gears with the relative tooth tip thicknesses  $m_{a1,2} = 0$  are shown in Table 4.10.

Table 4.10 data indicated that the maximum drive contact ratio of the reversible asymmetric gears is just slightly greater than it is for the symmetric gears, and asymmetry of such gears is very low. Therefore application of asymmetric reversible gears for drive contact ratio maximization is not practical.

Irreversible asymmetric gears present more theoretical rather than practical interest, because benefits of their applications are not apparent. Table 4.11 and Figure 4.15 present such gears.

Figure 4.16 shows a comparison chart of maximum contact ratio and related pressure angle for symmetric and asymmetric (reversible and irreversible)

**TABLE 4.11**

Maximum Drive Contact Ratios for Irreversible Asymmetric Gears

Number of teeth, $z_{1,2}$	1	3	5	10	20	33	48
Contact ratio, $\epsilon_{\text{cld}}$	1.05	1.27	1.52	2.08	3.01	4.02	5.04
Pressure angle, $\alpha_{\text{wd}}^\circ$	73.07	53.1	43.66	33.15	25.31	20.97	18.27
Tooth tip angle, $\alpha_{\text{td}1,2}^\circ$	81.35	69.43	62.35	52.56	43.41	37.46	33.44
Lowest involute angle, $\alpha_{\text{pd}1,2}$	0	0	0	0	0	0	0

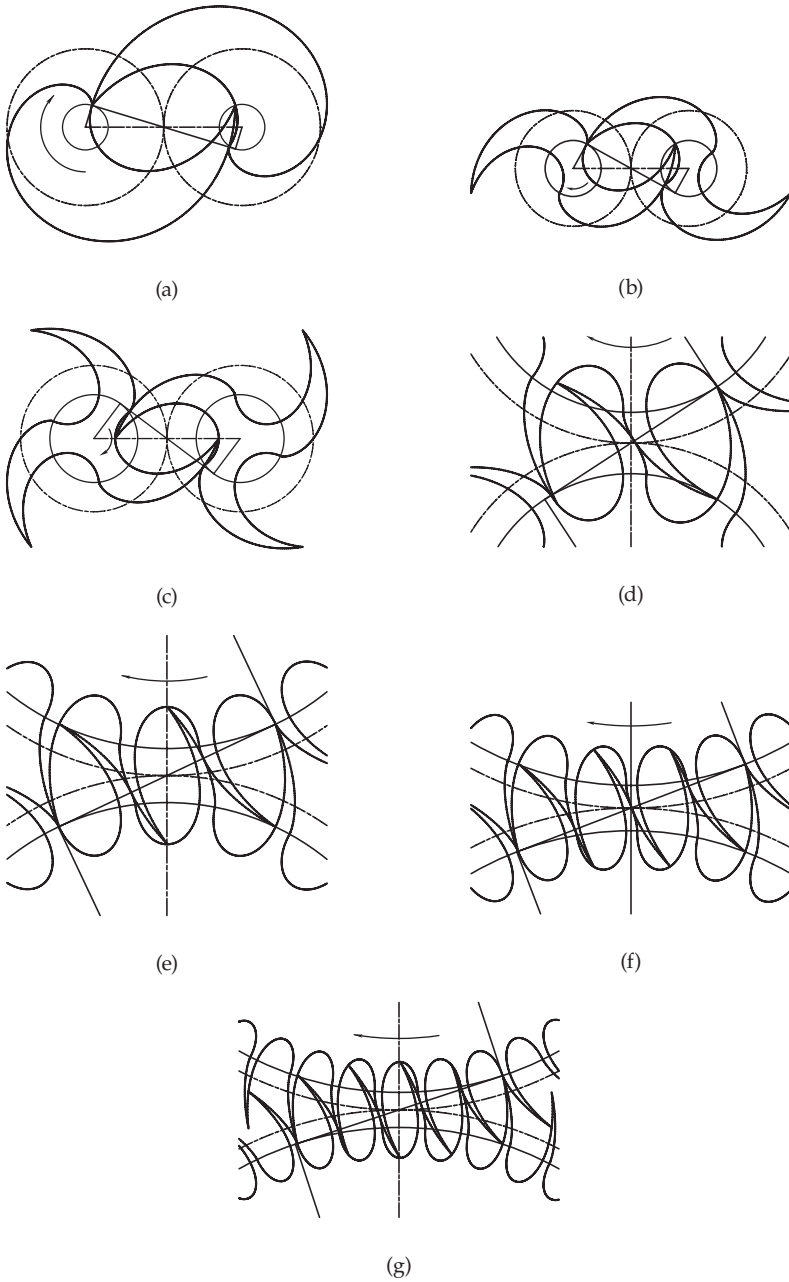
gears. It indicates that irreversible asymmetric gears allow realization of a significantly higher contact ratio.

The contact ratio for rack and pinion and internal gearings is noticeably higher than that for external gearing with the same pinion and pressure angle  $\alpha_w$  (see Figure 4.17).

#### 4.4 Practical Range of Involute Gear Parameters

Direct Gear Design significantly expands boundaries of involute gearing. However, in most cases the gear tooth and mesh geometry parameters do not reach their theoretical limits, because of, first, specific gear application performance requirements and, second, some material and technological constraints. For example, application of gears with a very low number of teeth is limited by increased specific sliding velocities, resulting in low mesh efficiency, higher gear mesh temperature, and tooth flank scuffing probability. At the same time, this reduces tooth deflection under the operating load and flank impact damping, resulting in higher noise and vibration. On the contrary, gears with a given pitch diameter and very high number of teeth have a very small tooth size. This leads to reduced bending strength and increases gear drive assembly tolerance sensitivity, when at a certain tolerance combination the contact ratio can be reduced to  $\epsilon_\alpha < 1.0$ , which also results in increased noise and vibration, and degrades gear drive performance.

A practical maximum pressure angle and transverse contact ratio are limited by the minimum tooth tip thickness. For a case of hardened teeth, it should be sufficient to avoid the hardening through the tooth tip. For gears out of soft metals and plastics it should be sufficient to exclude tooth tip bending. The minimum relative tooth tip thickness typically is  $m_{t1,2} = 0.25\text{--}0.3$ . A practical minimal contact ratio for conventional spur gears is about  $\epsilon_{\text{omin}} = 1.1\text{--}1.15$ . For high contact ratio (HCR) gears it is about  $\epsilon_{\text{omin}} = 2.05\text{--}2.1$ . These minimal contact ratio values are chosen to avoid its reduction below 1.0 for conventional spur gears and below 2.0 for HCR spur gears, because of manufacturing and assembly tolerances, and tooth tip chamfers or radii. These conditions also identify the practical maximum pressure angle. The

**FIGURE 4.15**

External asymmetric irreversible gears with maximum contact ratio: (a) number of teeth  $z_{1,2} = 1$ , (b)  $z_{1,2} = 3$ , (c)  $z_{1,2} = 5$ , (d)  $z_{1,2} = 10$ , (e)  $z_{1,2} = 20$ , (f)  $z_{1,2} = 33$ , (g)  $z_{1,2} = 48$ .

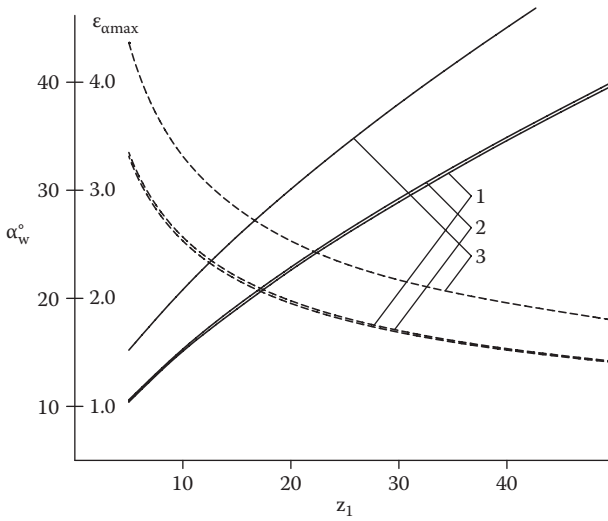


**FIGURE 4.16**

Maximum contact ratio  $\epsilon_{\alpha_{max}}$  (solid curves) and related pressure angle (dashed curves) of directly designed gears: 1 - with symmetric teeth; 2 and 3 - for reversible and irreversible asymmetric gears, accordingly.

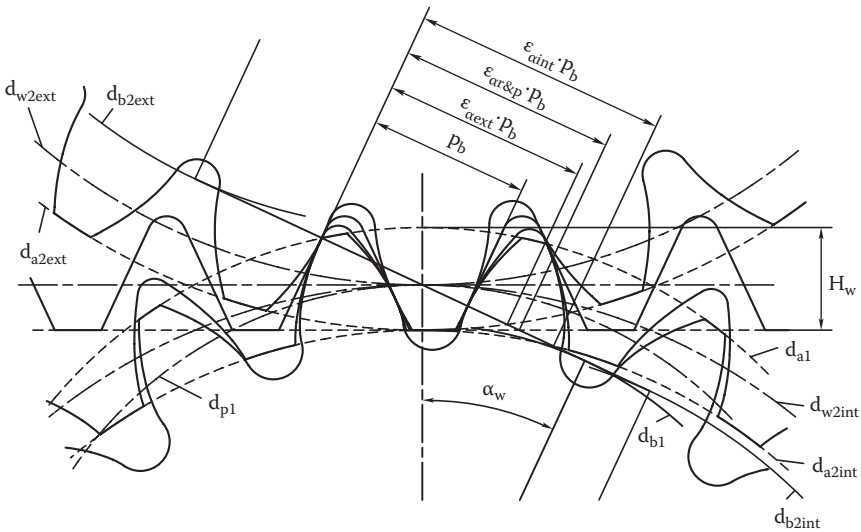


**FIGURE 4.17**

Contact ratio for external (ext), rack and pinion (r&p), and internal (int) mesh.



practical minimal pressure angle for symmetric gears is defined by the beginning of the tooth involute undercut, when the involute profile angles at the lowest contact points  $\alpha_{pd1,2} = 0^\circ$ , where the transverse contact ratio reaches its maximum value  $\epsilon_{\alpha_{max}}$ . Table 4.12 presents a practical range of pressure angles and contact ratios for spur external gears with symmetric teeth.

Application of gears with asymmetric teeth allows increasing the drive flank pressure angle in comparison with gears with symmetric teeth by the coast flank pressure angle reduction. If the coast flanks are not normally used for load transmission and may just occasionally be engaged in contact (as a result of tooth bouncing, inertial load during gear drive deceleration, etc.), the coast flank pressure angle can be as  $\alpha_{wc} = 10^\circ$  to  $-15^\circ$ . Practical maximum drive flank pressure angles for conventional and HCR asymmetric gears are shown in Tables 4.13 and 4.14.

The maximum drive pressure angle values in Tables 4.13 and 4.14 assume some possible small undercut of the coast flank near the root, especially for gears with a low number of teeth (15–30). However, this does not reduce the coast flank contact below  $\epsilon_{cc} = 1.0$ . This undercut can be reduced or completely eliminated by using the slanted tooth tips (Figure 4.18) [28]. It increases the tooth tip land and reduces bending stress. These slanted tooth tips can be produced by the special topping gear cutter (hob) or by the secondary (after the tooth hobbing) tooth tip milling operation.

If the coast flanks are used in normal operating load transmission, as in, for example, idler or planet gears (in epicycling drives), asymmetry factor  $K$  and practical range of pressure angles and contact ratios are defined based on specific application requirements (see Section 5.1.2).



**TABLE 4.13**

Practical  $\alpha_{wdmax}$  for Conventional Asymmetric Gears  
 ( $m_{a1,2} = 0.3, \epsilon_{od} = 1.1, \alpha_{wc} = 15^\circ$ )

$z_2$	$z_1$						
	15	20	30	40	50	70	100
15	43.5						
20	44.5	45.5					
30	45.9	46.4	47.3				
40	47	47.3	47.7	48.2			
50	47.6	47.8	48	48.3	48.9		
70	48	48.2	48.6	48.7	49	49.5	
100	48.7	48.9	49.2	49.5	49.1	49.6	50

**TABLE 4.14**

Practical  $\alpha_{wdmax}$  for the HCR Asymmetric Gears  
 ( $m_{a1,2} = 0.3, \epsilon_{od} = 2.1, \alpha_{wc} = 15^\circ$ )

$z_2$	$z_1$						
	20	25	30	40	50	70	100
20	19.3						
25	20.5	21.5					
30	21.5	22.4	23				
40	23	23.6	24.1	25			
50	24.1	24.6	25	25.6	26.1		
70	25.5	25.8	26.1	26.6	26.9	27.5	
100	26.7	27	27.2	27.5	27.7	28.1	28.5

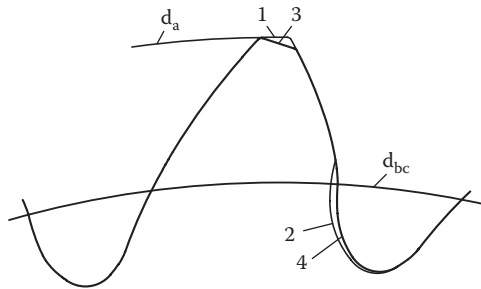


**FIGURE 4.18**

Asymmetric tooth with slanted tip:  $d_a$  - gear outer diameter;  $d_{bc}$  - coast flank base diameter; 1 - circular tooth tip land; 2 - slanted tooth tip land; 3 - fillet profile with undercut optimized from a trajectory of the mating tooth with the circular tip; 4 - fillet profile optimized from a trajectory of the mating tooth with the slanted tip.

# 5

---

## *Tooth Geometry Optimization*

---

Direct Gear Design® is not limited by any preselected tooling parameters or fabrication process requirements. Its tooth geometry boundaries are considerably expanded in comparison to the traditional gear design method. This allows definition of an optimal tooth shape for specific custom gear application.

Gear tooth geometry optimization is a part of gear drive optimization that also includes optimization of the gear arrangement of multistage gear drives, rational material and manufacturing technology selection, choice of lubrication system, etc. A starting point of gear tooth geometry optimization is to establish a set of priorities for specific gear drive applications. This “wish list” may include, for example:

- Gear transmission density maximization that requires minimizing gear drive size and weight for a given transmitted load and gear ratio, or maximizing the transmitted load for a given gear drive size
- Accommodation into the given space or envelope (typically for integrated gear drives)
- Noise and vibration reduction
- Cost reduction
- Increased life and reliability
- Other performance enhancement requirements

These application priorities dictate the Direct Gear Design tooth geometry optimization directions. As a part of the gear drive design it should be done in combination with other gear transmission component optimization.

---

### **5.1 Involute Profile Optimization**

Involute tooth flank profiles influence many gear drive performance characteristics, affecting contact surface endurance (pitting and scuffing resistance), tooth bending fatigue resistance, profile sliding and gear efficiency, tooth flexibility and load sharing, vibrations and noise, etc.

### 5.1.1 Gear Pair Size Reduction

Gear pair size reduction is typically limited by the tooth flank surface endurance defined by pitting and scuffing resistance. Both types of tooth surface defects depend on contact stress and tooth profile sliding velocity. Application of higher operating pressure angle ( $\alpha_w = 25\text{--}30^\circ$  for gears with symmetric teeth and  $\alpha_{wd} = 30\text{--}45^\circ$  for drive flank of gears with asymmetric teeth) leads to the Hertz contact stress reduction. This allows increasing transmitted torque and/or reducing gear size (diameter, face width, or both), maintaining an acceptable contact stress level. This also makes gear teeth stubby, with the reduced whole depth and increased thickness at the root area reducing the bending stress. High-pressure angle gear pairs have a relatively low contact ratio of  $\epsilon_\alpha = 1.1\text{--}1.5$  and profile sliding that reduces scuffing probability. Drawbacks of a high-pressure angle gear application are higher separating load taken by bearings and higher stiffness of symmetric teeth tooth that reduces tooth engagement impact absorbing and leads to higher noise and vibration. In asymmetric teeth with high drive pressure angle the coast flank is designed independently, which allows reduction of the tooth stiffness, noise, and vibration.

Another way for the tooth profile optimization to reduce gear pair size is application of gears with high contact ratio (HCR). Conventional spur involute gears have a transverse contact ratio  $1.0 < \epsilon_\alpha < 2.0$  when one or two tooth pairs are in contact. The HCR spur gears have a transverse contact ratio  $\epsilon_\alpha \geq 2.0$  (typically 2.05–2.2) when two or three tooth pairs are in contact. The HCR gears provide load sharing between gear pairs in contact, and according to [5] the maximum gear pair load does not exceed about 60% of the total load. The HCR gears have a relatively low operating pressure angle ( $\alpha_w = 18\text{--}23^\circ$  for gears with symmetric teeth and  $\alpha_{wd} = 23\text{--}28^\circ$  for drive flank of gears with asymmetric teeth), higher tooth addendum and whole depth, and reduced thickness at the tooth root. As a result, they have increased tooth deflection, providing a better load sharing between engaged tooth pairs and allowing reduction of contact and bending stresses, and also a noise and vibration level that makes them applicable for aerospace gear transmissions [5, 45]. However, the HCR gears must be accurate enough to have the base pitch variation lower than the tooth deflection under operating load to provide load sharing. These gears also have some drawbacks. The minimum number of teeth of the HCR gears should be at least 20 or more to provide the transverse contact ratio  $\epsilon_\alpha \geq 2.0$ . Long tooth addendum and low operating pressure angle result in higher sliding velocity that increases scuffing probability and mesh power losses. However, according to [46], “despite their higher sliding velocities high contact ratio gears can be designed to levels of efficiency comparable to those of conventional gears while retaining their advantages through proper selection of gear geometry.”

Attempts to use the buttress asymmetric HRC gears in the sun/planet mesh of the planetary gear stage for noise and vibration reduction were not

successful [25, 26]. This could be explained by high stiffness of the buttress teeth that have low drive pressure angle and high coast pressure angle. It seems a more rational approach for many applications of the asymmetric gear is to have the drive tooth flanks with higher pressure angle than the coast ones. In case of the epicyclic gear stages where the planet gear has both driving flanks, the higher pressure angle should be used in the sun/planet gear mesh and the lower pressure angle in the planet/ring gear mesh (see Section 11.2). Application of this approach to the asymmetric HCR gears allows design of the coast flanks independently to reduce the gear tooth stiffness for better tooth load sharing. Table 5.1 presents samples of the gear tooth profile geometry for high-pressure angle and high contact ratio gears.

### 5.1.2 Asymmetry Factor Selection

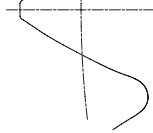
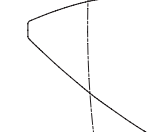


Asymmetric tooth profiles make it possible to increase the operating pressure angle (with the given transverse contact ratio) beyond the conventional symmetric gears' limits. This allows reduction of drive flank contact stress and sliding velocity. As a result, the drive flanks of asymmetric gears have higher tooth surface endurance to pitting and scuffing, providing maximized transmission density.

Selection of the asymmetry factor  $K$  depends on the gear pair operating cycle that is defined by RPM and transmitted load in the main and reversed directions, and life requirements [47]. These data allow calculation of numbers and magnitude of the tooth load cycles in each regime in both load transmission directions. If the gear tooth is equally loaded in both the main and reversed rotation directions, asymmetric tooth profiles should not be considered. Table 5.2 presents different torque transmission cases by the spur gear pairs with the identical 24 tooth mating gears to illustrate bidirectional and unidirectional drive applications.

#### 5.1.2.1 Cases 1 and 2

The gear teeth are symmetric and their surface durability is identical for both drive and coast flanks. Case 1 presents the traditionally designed 25° pressure angle gear pair with the full radius fillet. This case is considered a baseline, and its Hertz contact stress, bearing load, and specific sliding velocity are assumed as 100% for comparison with other gear pairs. This type of gear profile is used in the aerospace industry because it provides better bending strength and flank surface endurance in comparison with the standard 20° pressure angle gears typical for commercial applications. Case 2 is the high 32° pressure angle symmetric gears, optimized by the Direct Gear Design method. Its Hertzian contact stress is about 8% lower and its specific sliding velocity is about 6% lower than those for the baseline gear pair. This should provide better flank tooth surface pitting or scoring resistance. However, the bearing load is 7% higher.

**TABLE 5.1**  
 Gear Geometry Parameters for High Pressure Angle and High Contact Ratio Gears

Tooth Form	High-Pressure Angle		High Contact Ratio (HCR)	
	Symmetric	Asymmetric	Symmetric	Asymmetric
Tooth profile				
Number of teeth	35	35	35	35
Pinion and gear $z_{1,2}$				
Pressure angle	$\alpha_{std}$ 30°	42°	22°	26°
	$\alpha_{uc}$ 30°	14°	22°	12°
Asymmetry factor $K$	1.0	1.3	1.0	1.09
Transverse contact ratio	$\epsilon_{std}$ 1.39	1.25	2.04	2.02
	$\epsilon_{oc}$ 1.39	2.02	2.04	2.16

**TABLE 5.2**  
Gear Parameters of Bidirectional and Unidirectional Gear Drives

Case No.	1		2		3		4		5	
	Bidirectional		Both		Mostly unidirectional		Unidirectional			
Load transmission	Both		Both		Drive, lower coast load		Drive, very low coast load		Drive flank only	
Loaded flanks	Symmetric (baseline)		Symmetric		Asymmetric		Asymmetric		Asymmetric	
Tooth profile										
Gear mesh										
Pressure angle	$\alpha_{add}$	25°	32°	32°	40°	46°	60°			
Asymmetry coefficient K	$\alpha_{mic}$	25°	32°	32°	24°	10°	—*			
Transverse contact ratio	1.0	1.0	1.0	1.0	1.19	1.42	—*			
Hertz contact stress, %	$\epsilon_{add}$	1.35	1.2	1.2	1.2	1.2	1.2			
Bearing load, %	$\epsilon_{oc}$	1.35	1.2	1.2	1.44	1.0	—*			
	Drive flank	100	92	92	88	86	94			
	Coast flank	100	92	102	102	150	—*			
	Drive flank	100	107	118	118	130	181			
	Coast flank	100	107	99	99	92	—*			
Specific sliding velocity, %	Drive flank	100	94	94	75	68	49			
	Coast flank	100	94	108	108	97	—*			

Source: Graphics from Kapelevich, A.L., *Gear Technology*, June/July 2012, 48–51. With permission.  
\* Coast flank mesh does not exist.



### 5.1.2.2 Case 3

These asymmetric gears are for mostly unidirectional load transmission with a 40° pressure angle driving tooth flanks providing 12% contact stress and 25% sliding velocity reduction. At the same time, the contact stress and sliding velocity of the coast flanks are close to these parameters of the baseline gears and should provide a tooth surface load capacity similar to that for the baseline gears. This type of gear may find applications for drives with one main load transmission direction, but it should be capable to carry a lighter load for shorter periods of time in the opposite load transmission direction.

### 5.1.2.3 Case 4

These asymmetric gears have a 46° drive pressure angle that allows reduction of the contact stress by 14% and sliding velocity by 32%. The disadvantage of such gear teeth is a high (+30%) bearing load. These types of gears are only for unidirectional load transmission. Their 10° coast pressure angle flanks have insignificant load capacity. They may find applications for drives with only one load transmission direction that may occasionally have a very low load coast flank tooth contact, like in the case of a tooth bouncing in high-speed transmissions.

### 5.1.2.4 Case 5

These asymmetric gears have only driving tooth flanks with the extreme 60° pressure angle with no involute coast tooth flanks at all. As a result, the bearing load is significant.

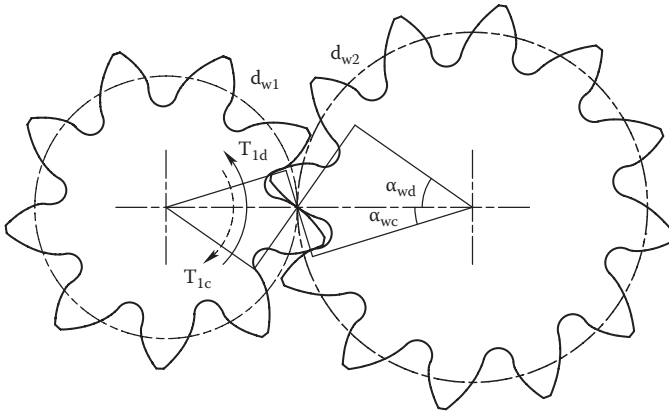
There are many applications, as described in a Case 3, where a gear pair transmits load in both load directions, but with significantly different magnitude and duration (Figure 5.1). In this case, the asymmetry factor  $K$  for a gear pair is defined by equalizing potential accumulated tooth surface damage defined by operating contact stress and number of tooth flank load cycles. In other words, the contact stress safety factor  $S_H$  should be the same for the drive and coast tooth flanks. This condition can be presented as

$$S_H = \frac{\sigma_{HPd}}{\sigma_{Hd}} = \frac{\sigma_{HPc}}{\sigma_{Hc}}, \quad (5.1)$$

where  $\sigma_{Hd}$  and  $\sigma_{Hc}$  are the operating contact stresses for the drive and coast tooth flanks, and  $\sigma_{HPd}$  and  $\sigma_{HPc}$  are the permissible contact stresses for the drive and coast tooth flanks that depend on the number of load cycles.

Then from (5.1)

$$\frac{\sigma_{Hd}}{\sigma_{Hc}} = \frac{\sigma_{HPd}}{\sigma_{HPc}}. \quad (5.2)$$

**FIGURE 5.1**

Asymmetric gear pair,  $T_{1d}$  and  $T_{1c}$ , pinion torque applied to the drive and coast tooth flanks. (From Kapelevich, A.L., *Gear Technology*, June/July 2012, 48–51. With permission.)

The contact stress at the pitch point [48] is

$$\sigma_H = z_H z_E z_\varepsilon z_\beta \sqrt{\frac{F_t}{d_{w1} b_w} \frac{u \pm 1}{u}}, \quad (5.3)$$

where

$$z_H = \sqrt{\frac{2 \cos(\beta_b) \cos(\alpha_{wt})}{\cos(\alpha_t)^2 \sin(\alpha_{wt})}}$$

is the zone factor that for the directly designed spur gears is

$$z_H = \frac{2}{\sqrt{\sin(2\alpha_w)}}; \quad (5.4)$$

$z_E$  is the elasticity factor that takes into account gear material properties (modulus of elasticity and Poisson's ratio);  $z_\varepsilon$  is the contact ratio factor, its conservative value for spur gears is  $z_\varepsilon = 1.0$ ;  $z_\beta$  is the helix factor, for spur gears  $z_\beta = 1.0$ ;  $F_t$  is the nominal tangent load, which at the pitch diameter  $d_{w1}$  is  $F_t = \frac{2T_1}{d_{w1}}$ ;  $T_1$  is the pinion torque;  $b_w$  is the contact face width; and + is for external gearing and – for external gearing.

Then for the directly designed spur gears the contact stress at the pitch point can be presented as

$$\sigma_H = z_E \frac{2}{d_{w1}} \sqrt{\frac{2T_1}{b_w \sin(2\alpha_w)} \frac{u \pm 1}{u}}. \quad (5.5)$$

Some parameters of this equation,  $Z_E, d_{w1}, b_{wv}$  and  $u$ , do not depend on the rotation direction, and Equation (5.2) for the pitch point contact can be presented as

$$\frac{\sin(2\alpha_{wc})}{\sin(2\alpha_{wd})} = A, \quad (5.6)$$

where a parameter  $A$  is

$$A = \frac{T_{1c}}{T_{1d}} \left( \frac{\sigma_{HPd}}{\sigma_{HPc}} \right)^2. \quad (5.7)$$

According to [48], “the permissible stress at limited service life or the safety factor in the limited life stress range is determined using life factor  $Z_{NT}$ .” This allows replacement of the permissible contact stresses in Equation (5.7) for the life factors

$$A = \frac{T_{1c}}{T_{1d}} \left( \frac{Z_{NTd}}{Z_{NTc}} \right)^2. \quad (5.8)$$

When parameter  $A$  is defined and the drive pressure angle is selected, the coast pressure angle is calculated by Equation (5.6) and the asymmetry coefficient  $K$  from a common solution of (5.6) and (2.93):

$$K = \frac{\sqrt{1 + \sqrt{1 - A^2 (\sin 2\alpha_{wd})^2}}}{\sqrt{2} \cos \alpha_{wd}}. \quad (5.9)$$

If the gear tooth is equally loaded in both the main and reversed load application directions, then both the coefficient  $A$  and the asymmetry factor  $K$  are equal to 1.0 and gear teeth are symmetric.

#### Example 1

The drive pinion torque  $T_{1d}$  is two times greater than the coast pinion torque  $T_{1c}$ . The drive tooth flank has  $10^9$  load cycles, and the coast tooth flank has  $10^6$  load cycles during the life of the gear drive. From the  $S$ - $N$  curve [48] for steel gears an approximate ratio of the life factors  $Z_{NTd}/Z_{NTc} = 0.85$ . Then the coefficient  $A = 0.85^2/2 = 0.36$ . Assuming the drive pressure angle is  $\alpha_{wd} = 36^\circ$ , the coast pressure angle from Equation (5.6) is  $\alpha_{wc} = 10^\circ$  and the asymmetry factor from Equation (5.9) is  $K = 1.22$ .

In many unidirectional gear drives like in, for example, propulsion system transmissions that seem irreversible, the coast tooth flanks are loaded because of the system inertia during the drive system deceleration or the tooth

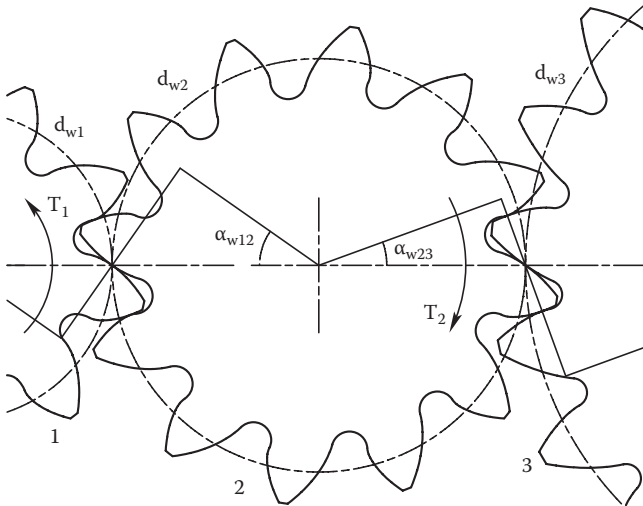


**FIGURE 5.2**

Chain gear arrangement: 1 - input pinion; 2 - idler gear; 3 - output gear. (From Kapelevich, A.L., *Gear Technology*, June/July 2012, 48–51. With permission.)

bouncing in the high RPM drives. This coast tooth flank load can be significant and should be taken in consideration while defining the asymmetry factor  $K$ .

If the gear drive is completely irreversible and the coast tooth flanks never transmit any load (Case 4), the asymmetry factor is defined only by the drive flank geometry. In this case, increase of the drive flank pressure could be limited by a minimum selected contact ratio and a separating load applied to the bearings. Application of a very high drive flank pressure angle results in the reduced coast flank pressure angle and possibly its involute profile undercut near the tooth root. Another limitation of the asymmetry factor of the irreversible gear drive is growing compressive bending stress at the coast flank root. Usually for conventional symmetric gears compressive bending stress does not present a problem, because its allowable limit is significantly higher than for the tensile bending stress. However, for asymmetric gears it may become an issue, especially for gears with thin rims.

In the unidirectional chain gear drives (Figure 5.2), the idler gear transmits the same load by both tooth flanks. This arrangement seems unsuitable for asymmetric gear application. However, in many cases, the idler's mating gears have significantly different numbers of teeth. This allows equalizing contact stresses on opposite flanks of the asymmetric teeth to achieve maximum load capacity.

Equation (5.5) is used to define the pitch point contact stress in the pinion/idler gear mesh,

$$\sigma_{H12} = z_E \frac{2}{d_{w1}} \sqrt{\frac{2T_1}{b_{w12} \sin(2\alpha_{w12})} \frac{u_{12} + 1}{u_{12}}}, \quad (5.10)$$

and in the idler/output gear mesh,

$$\sigma_{H23} = z_E \frac{2}{d_{w2}} \sqrt{\frac{2T_2}{b_{w23} \sin(2\alpha_{w23})} \frac{u_{23} + 1}{u_{23}}}, \quad (5.11)$$

or, ignoring gear mesh losses,

$$\sigma_{H23} = z_E \frac{2}{u_{12} d_{w1}} \sqrt{\frac{2u_{12} T_1}{b_{w23} \sin(2\alpha_{w23})} \frac{u_{23} + 1}{u_{23}}}, \quad (5.12)$$

where  $b_{w12}$  and  $b_{w23}$  are the contact face widths in the pinion/idler gear and the idler/output gear meshes, accordingly;  $u_{12} = z_2/z_1$  is the gear ratio in the pinion/idler gear mesh;  $u_{23} = z_3/z_2$  is the gear ratio in the idler/output gear mesh; and  $z_1$ ,  $z_2$ , and  $z_3$  are the number of teeth of the input, idler, and output gears.

Numbers of the idler gear tooth load cycles and permissible contact stresses in this case are equal in both meshes, and Equation (5.2) can be presented as  $\sigma_{H12} = \sigma_{H23}$ . Then considering that all gears are made from the same material, the idler gear pressure angle ratio is defined by

$$\frac{\sin(2\alpha_{w23})}{\sin(2\alpha_{w12})} = B \quad (5.13)$$

where

$$B = \frac{b_{w12}}{b_{w23}} \frac{u_{23} + 1}{u_{23}(u_{12} + 1)} \quad (5.14)$$

is a parameter that reflects the gear ratios  $u_{12}$  and  $u_{23}$ , and contact face widths  $b_{w12}$  and  $b_{w23}$  in the pinion/idler gear and idler/output gear meshes, accordingly.

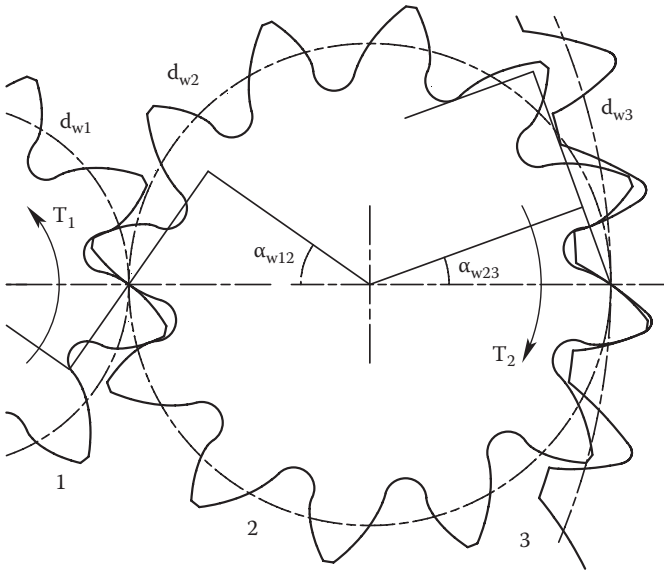
Then considering Equation (2.93) the asymmetry factor  $K$  can be presented as

$$K = \frac{\sqrt{1 + \sqrt{1 - B^2 (\sin 2\alpha_{wd})^2}}}{\sqrt{2} \cos \alpha_{wd}}. \quad (5.15)$$

If  $z_1 = z_3$  and  $b_{w12} = b_{w23}$ , then both the coefficient  $B$  and the asymmetry factor  $K$  are equal to 1.0 and gear teeth are symmetric. If  $z_1 \neq z_3$  or  $b_{w12} \neq b_{w23}$ , application of asymmetric gears can be considered.

### Example 2

The pinion number of teeth is  $n_1 = 9$ , the idler gear number of teeth is  $n_2 = 12$ , the output gear number of teeth is  $n_3 = 20$ , the contact face width ratio is  $b_{w12}/b_{w23} = 1.2$ . This makes parameter  $B = 0.82$ . Then assuming the pinion/idler gear mesh pressure angle is  $\alpha_{w12} = 35^\circ$ , the idler/output pressure angle from (5.13) is  $25.32^\circ$  and the asymmetry factor from Equation (5.15) is  $K = 1.10$ .

**FIGURE 5.3**

Planetary gear arrangement: 1 - sun gear; 2 - planet gear; 3 - ring gear. (From Kapelevich, A.L., *Gear Technology*, June/July 2012, 48–51. With permission.)

Similarly, the contact stress equalization technique can be applied for the unidirectional epicyclic gear stage (Figure 5.3), because the planet gear can be considered as the idler gear engaged with the sun gear and ring gear.

In this case, the asymmetry factor  $K$  is also defined by Equation (5.15), where parameter  $B$  is

$$B = \frac{b_{w12}}{b_{w23}} \frac{u_{23} - 1}{u_{23}(u_{12} + 1)}, \quad (5.16)$$

$b_{w12}$  and  $b_{w23}$  are the contact face widths of the sun/planet gear and planet/ring gear meshes;  $u_{12} = z_2/z_1$  is the gear ratio in the sun/planet gear mesh;  $u_{23} = z_3/z_2$  is the gear ratio in the planet/ring gear mesh; and  $z_1$ ,  $z_2$ , and  $z_3$  are the number of teeth of the sun, planet, and ring gears.

In a typical epicyclic gear stage  $z_2 = (z_3 - z_1)/2$ . This allows simplification of Equation (5.16):

$$B = \frac{b_{w12}}{u_{13}b_{w23}}, \quad (5.17)$$

where  $u_{13} = z_3/z_1$  is the epicyclic stage gear ratio. This gear ratio is always greater than 1.0, which makes an epicyclic gear stage suitable for asymmetric gear application.

**Example 3**

The sun gear number of teeth is  $n_1 = 9$ , the planet gear number of teeth is  $n_2 = 12$ , the output gear number of teeth is  $n_3 = 33$ , and the contact face width ratio is  $b_{w12}/b_{w23} = 1.8$ . This makes parameter  $B = 0.49$ . Then assuming the pinion/idler gear pressure angle is  $\alpha_{w12} = 40^\circ$ , the idler/output pressure angle from (5.13) is  $14.5^\circ$  and the asymmetry factor from Equation (5.15) is  $K = 1.26$ .

**5.1.3 Mesh Efficiency Maximization**

Gear mesh power losses depend on the gear tooth geometry and friction coefficient. For spur gears, the percent of mesh losses is defined in Equation (3.27). Maximum gear mesh efficiency (minimum of mesh losses) is achieved if the specific sliding velocities at the start of the approach action and at the end of the recess action are equalized:  $H = H_s = H_t$ . Then Equation (3.27) can be presented as

$$P_t = \frac{50fH}{\cos \alpha_w}. \quad (5.18)$$

If this equation is solved with Equations (2.75), (2.76), (3.30), and (3.31) the mesh power loss percent for spur gears can be defined as

$$P_t = 50f\pi\epsilon_\alpha \left( \frac{1}{z_1} \pm \frac{1}{z_2} \right), \quad (5.19)$$

and the maximized gear mesh efficiency as

$$E_{\max} = 100 - P_t = 100 - 50f\pi\epsilon_\alpha \left( \frac{1}{z_1} \pm \frac{1}{z_2} \right), \quad (5.20)$$

where (in Equations (5.20), (5.21), and (5.22)) signs  $\pm$  are for external gears and internal gears, respectively.

Equation (5.20) indicates that for spur gears the optimized maximum efficiency gear geometry depends only on the type of gearing (external or internal), numbers of teeth, and transverse contact ratio  $\epsilon_\alpha$ . For helical gears the mesh power losses are [38]

$$P_t = \frac{50f \cos^2 \beta_w}{\cos \alpha_w} \times \frac{H_s^2 + H_t^2}{H_s + H_t}. \quad (5.21)$$

With the optimized gear geometry they are

$$P_t = 50f\pi\epsilon_\alpha \cos^2 \beta_w \left( \frac{1}{z_1} \pm \frac{1}{z_2} \right). \quad (5.22)$$

The maximum gear mesh efficiency of the spur gears is limited by the minimum transverse contact ratio  $\epsilon_\alpha = 1.0$ . Helical gears make it possible

to increase the gear mesh efficiency by reducing  $\varepsilon_\alpha < 1.0$  and increasing the operating helix angle  $\beta_{opt}$ , although such gear geometry might not be practical for many gear applications.

---

## 5.2 Tooth Modeling and Bending Stress Calculation

The gear design standards [48, 49] recommend calculating the nominal tooth root bending stress using the analytical Lewis equation [50], although Method A of the International Organization for Standardization (ISO) standard [48] allows for use of numerical calculation methods: “finite element analysis, integral equations, conformal mapping procedures, ..., etc.” These numerical methods are more suitable for Direct Gear Design, because the Lewis equation-based method may not be sufficient for a broad variety of its possible tooth profile configurations, including asymmetric ones.

Examples of the two-dimensional (2D) finite element analysis (FEA) tooth mesh models and stress isograms are shown in Figures 5.4 and 5.5. Here the triangle linear finite elements are used, although other kinds of finite elements can be used for this purpose.

An area at the fillet profile, where high stress is expected, has a higher finite element node density and the elements are smaller than in the rest of the tooth profile to achieve a more accurate stress calculation result within a short period of time. For conventional gears with the transverse contact ratio  $1.0 < \varepsilon_\alpha < 2.0$  a force is initially applied at the highest point of single-tooth contact, and for the HCR gears with the transverse contact ratio  $\varepsilon_\alpha \geq 2.0$  a force is applied at the highest point of double-tooth contact. Typically the force application point is located between two finite element nodes. In this case the force is replaced with two force components applied to these two closest nodes. A sum of the node-applied forces is equal to the initial force, and their values are defined in inverse proportion to the distances from the initial force application point to the loaded finite element nodes.

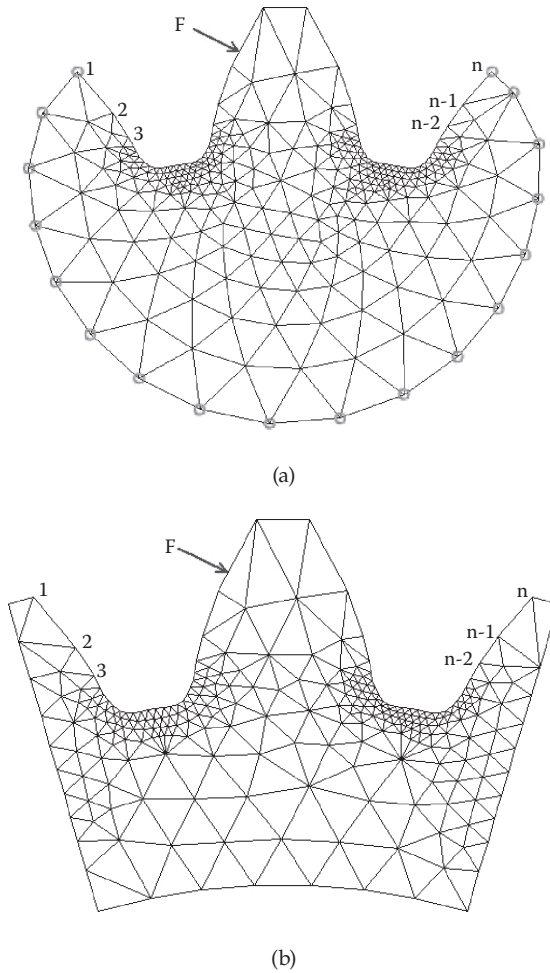
Figure 5.6 presents a typical stress distribution along the whole tooth profile with the conventional (not optimized) trochoidal fillet from the finite element nodes 1 to  $n$ . Figure 5.7 presents the asymmetric tooth FEA mesh model and stress isograms.

---

## 5.3 Root Fillet Optimization

Historically gear tooth geometry improvement efforts were concentrated on the involute flanks. Although the gear tooth root fillet is an area of maximum

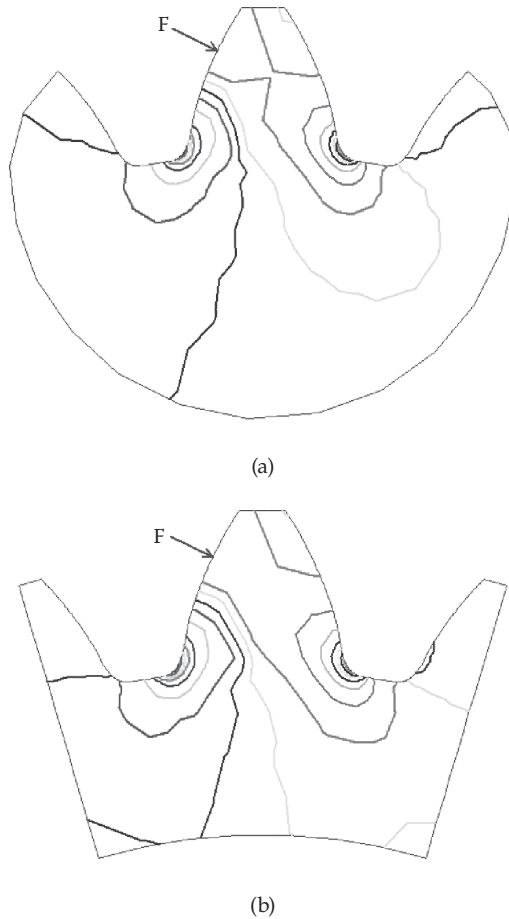


**FIGURE 5.4**

FEA tooth models: (a) with solid gear body, (b) with thin rim.  $F$  - applied force;  $n$  - number of FEA nodes on the tooth profile.

bending stress concentration, its profile and accuracy are marginally defined on the gear drawing by typically very generous root diameter tolerance and, in some cases, by the minimum fillet radius, which is not easy to accurately inspect. In fact, tooth bending strength is usually provided by material and heat treatment improvement rather than gear geometry enhancement. The gear tooth root fillet profile is typically a trochoidal curve determined by the generating tool (gear hob or shaper cutter, for example) tooth tip trajectory (Figure 5.8).

The cutter tooth parameters, such as the profile (pressure) angle, addendum, and whole depth, are designed to generate, first of all, the involute

**FIGURE 5.5**

Stress isograms: (a) with solid gear body, (b) with thin rim.

tooth flank profile. But the root fillet profile is basically a by-product of the cutter edge motion. The fillet profile and, as a result, bending stress level are dependent on the cutter radial clearance and tip radius. The standard radial clearance usually is  $(0.20 - 0.35) \times m$  or  $(0.20 - 0.35)/DP$ , where  $m$  is a module and  $DP$  is a diametral pitch. The standard cutter tooth radius for the coarse pitch gears is  $0.30 \times m$  or  $0.30/DP$ . For fine pitch gears the standard cutter tooth radius may not be specified and could be equal to zero [38].

Unlike the contact Hertz stress, the bending stress typically does not define the major gear pair dimensions such as pitch diameters or center distance. If the calculated bending stress is unacceptably high, the coarser diametral pitch (larger module) can be applied. The number of teeth, in this case, is proportionally reduced to keep original pitch diameters and center distance, and the same (or close) gear ratio. This makes the gear tooth larger

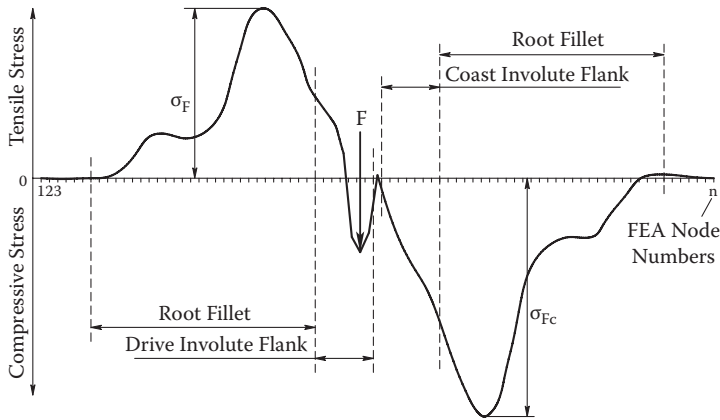


**FIGURE 5.6**  
Stress distribution along the tooth profile.

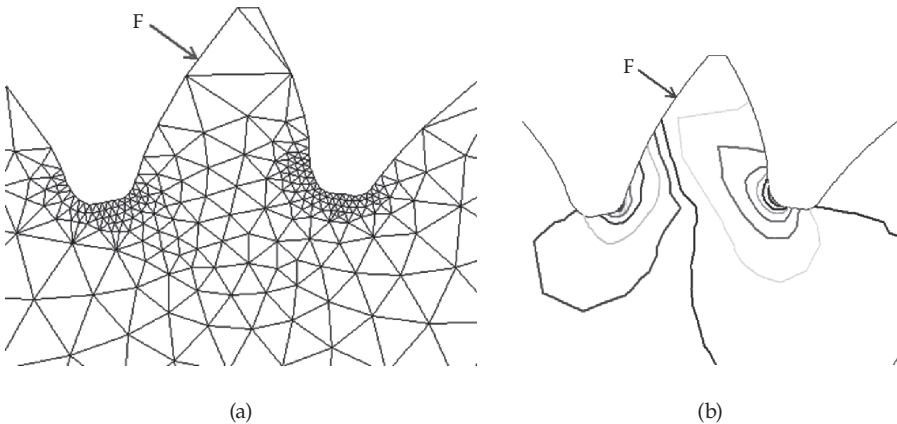


**FIGURE 5.7**  
Asymmetric tooth FEA: (a) mesh model, (b) stress isograms.

and reduces bending stress to an acceptable level, although this increases tooth stiffness and specific sliding velocity, and reduces gear mesh efficiency.

There are two general approaches for reducing bending stress for the given tooth size. One of them is to alter the generating cutter tooth tip profile [51, 52]. The most common application of such an approach is the tooling rack with the full tip radius. Another approach is to alter the gear tooth fillet profile [53–56]. The most common application of such an approach is using the circular arc root fillet profile. Further development of both these approaches is based on a mathematical function fitting technique where the cutter tip radius or the gear tooth trochoid fillet profile is replaced by a parabola, ellipse, chain curve, or other curve, reducing the bending stress. Bending stress reduction achieved by these fillet profile improvement methods varies greatly

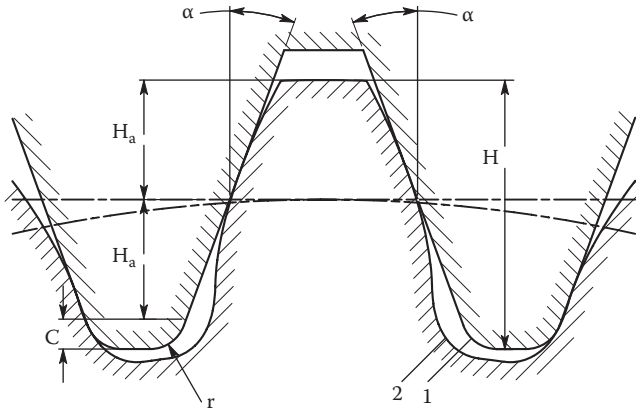


**FIGURE 5.8**

Gear tooth fillet generation by the rack cutter (gear hob). 1 - cutter tooth tip; 2 - gear tooth root fillet;  $\alpha$  - rack profile (pressure) angle;  $H$  - whole depth;  $H_a$  - addendum;  $C$ , radial clearance;  $r$  - cutter tip radius. (From Kapelevich, A.L., and Y.V. Shekhtman, *Gear Technology*, September/October 2009, 73–79. With permission.)

depending on the cutter and/or gear mesh parameters. The resulting tooth fillet profile must be checked for interference with the mating gear tooth tip.

### 5.3.1 Root Fillet Optimization Method

In Direct Gear Design the tooth fillet is designed after the involute flank parameters are completely defined. A goal is to achieve a minimum of stress concentration on the tooth fillet profile. In other words, the maximum bending stress should be evenly distributed along the large portion of the root fillet profile. The initial fillet profile is a trajectory of the mating gear tooth tip in the tight (zero-backlash) mesh. This allows interference with the mating gear tooth tip to be avoided.

The fillet optimization method that is used in Direct Gear Design was developed by Dr. Y.V. Shekhtman [57, 58]. It utilizes the following calculation processes:

- Definition of a set of mathematical functions that are used to describe the optimized fillet profile. Such a set may contain the trigonometric, polynomial, hyperbolic, exponential, and other functions and their combinations. Parameters of these functions are defined during the optimization process.
- FEA with the triangle linear elements is used to calculate stress. This kind of finite element allows achievement of satisfactory optimization results within reasonable time. In [59] the boundary element method (BEM) is used for stress analysis of the optimized tooth root fillet.

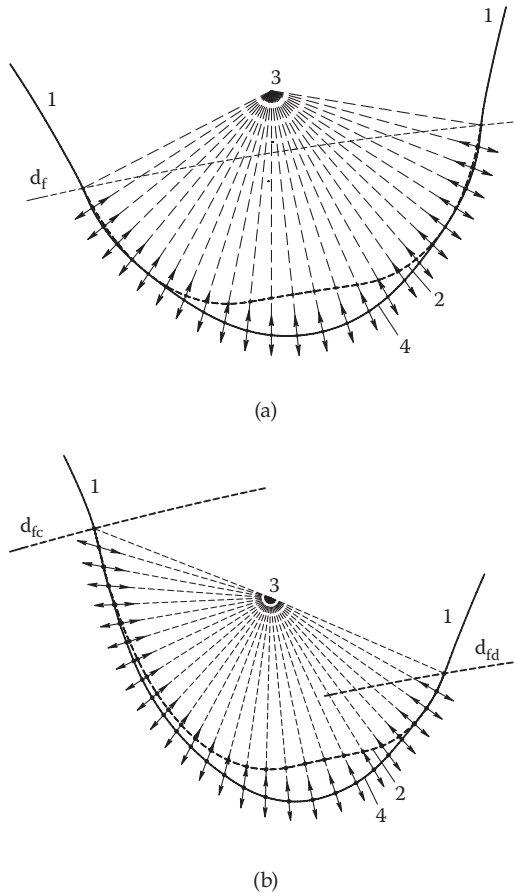


**FIGURE 5.9**

Tooth fillet profile optimization: (a) symmetric tooth fillet, (b) asymmetric tooth fillet. 1 - involute tooth flanks; 2 - initial fillet profile; 3 - fillet center; 4 - optimized fillet profile;  $d_f$ ,  $d_{fd}$ ,  $d_{fc}$  - form circle diameter of symmetric tooth, and drive and coast flanks of asymmetric tooth, accordingly. ((a) from Kapelevich, A.L., and Y.V. Shekhtman, *Gear Technology*, September/October 2009, 73–79. With permission.)

- A random search method [60] is used to define the next step in the multiparametric iteration process of the root fillet profile optimization.

This fillet optimization method establishes the approximate fillet center (Figure 5.9). It is defined as the center of the best-fitted circular arc, and it is connected to the finite element nodes located on the initial fillet profile [57, 58]. The first and last finite element nodes of the initial fillet profile located on the form diameter circle cannot be moved during the optimization process. The rest of the initial fillet finite element nodes are moved along the straight lines (beams) that connect through the fillet center. The bending stresses are

calculated for every fillet profile configuration iteration. Variable parameters of mathematical functions that describe the fillet profile for the next iteration are defined depending on stress calculation results of the previous iteration. If it provided stress reduction, the optimization process moves the fillet nodes along their beams in the same direction. If stress was increased, the nodes are moved in the opposite direction. After the specified number of iterations the optimization process stops, resulting in the optimized fillet profile. The more finite element nodes that are placed on the fillet profile, the more accurate are the stress calculation results, but this requires more iterations and the fillet profile optimization takes more time. During the optimization process the fillet nodes cannot be moved inside the initial fillet profile because this may cause interference with the mating gear tooth tip. This is a main constraint for fillet optimization, although there are other possible additional constraints (Figure 5.10). One of them is a minimum radial clearance. The optimized fillet typically results in low radial clearance, much less than in conventional standard or custom gear drives. The concern here is that the radial clearance can be so small that the lubricant could be trapped in the fillet space, resulting in additional power losses and gear efficiency reduction. In this case, the root diameter providing the acceptable radial clearance should be established and the optimized fillet profile must be tangent to this root diameter. Another such constraint is the thin gear rim (Figures 5.4b and 5.5b). In this case, the optimized fillet profile and maximum root stress depend on the rim thickness and type of the gear rim design. There are three different rim design options that can be considered. The first is a “free” rim support with its possible radial deflection. This is typical for idler gears when the rim surface is used as the roll (or ball) bearing race, or for gears with the spokes connecting the rim with the hob. The second option of rim design is typical for gears that have the sliding fit or the glue fit on the rim surface with very small clearance. This restrains the rim radial deflections, but does not create additional hoop stress. The third type of rim design is a press (or heat) fit. It imposes additional hoop stress depending on press fit interference. If press fit interference is significant or rim thickness is low, resulting in high hoop stress, the root fillet optimization may not be possible. One more additional fillet optimization constraint is related to manufacturability of the gears with the optimized fillet. It is typical for external gears with a low ( $<20$ ) number of teeth. The fillet optimization process tries to create minimum curvature (maximum radius) at the maximum stress fillet area to minimize its concentration. For gears with a low number of teeth this may result in a small fillet radius near the form diameter creating the undercut. Unlike the undercut that occurs in conventional gears, this one is made for a purpose, and it does not affect the active involute flank profile. However, to make such an optimized fillet profile could be difficult or even impossible by some gear fabrication methods, such as profile cutting, hobbing, etc. In order to make the root fillet profile manufacturable using these fabrication methods, the fillet profile undercut should be limited or eliminated. This

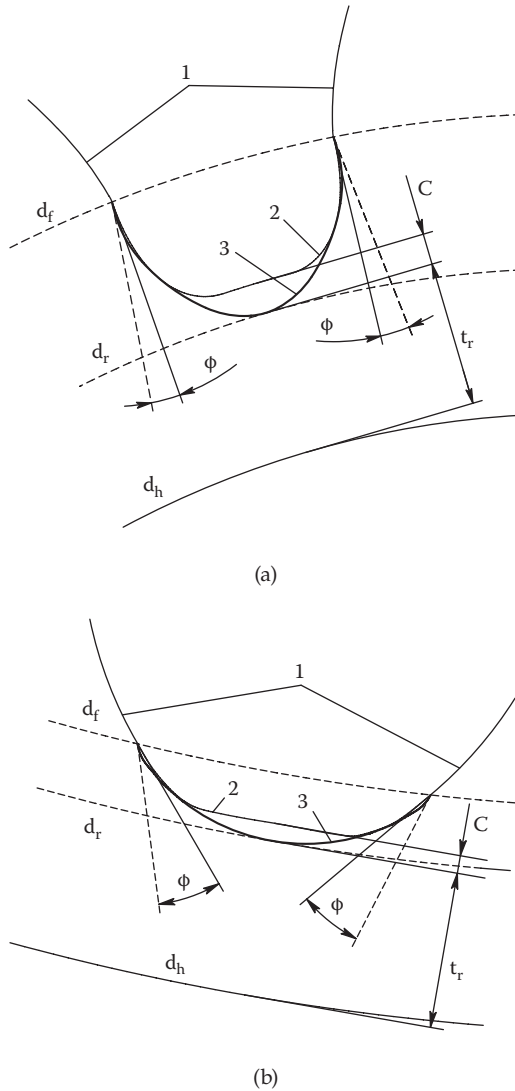


**FIGURE 5.10**

Tooth fillet optimization constraints (dashed lines): (a) external gear fillet, (b) internal gear fillet. 1 - involute tooth flanks; 2 - initial fillet profile; 3 - optimized fillet profile;  $d_f$  - form circle diameter;  $d_r$  - specified root diameter;  $d_h$  - rim diameter;  $C$  - radial clearance;  $t_r$  - rim thickness.

constrains the angle  $\phi$  (Figure 5.10) between tangents to the initial and optimized fillet profiles at their beginning and endpoints. These additional fillet optimization constraints compromise root stress concentration reduction in comparison to the optimized fillet constrained only by the initial fillet profile. Figure 5.11 presents the gear tooth stress distribution comparison before and after root fillet optimization.

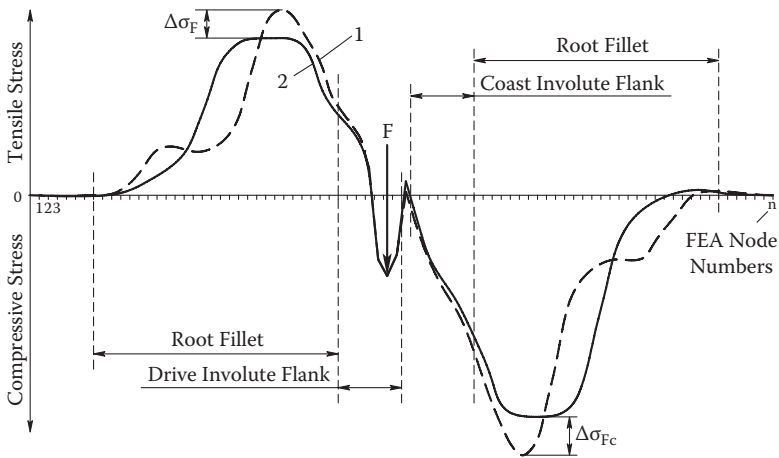


**FIGURE 5.11**

Tooth profile stress distribution charts before (1) and after (2) root fillet optimization.  $\Delta\sigma_F$  - tensile stress reduction;  $\Delta\sigma_{Fc}$  - compressive stress reduction.

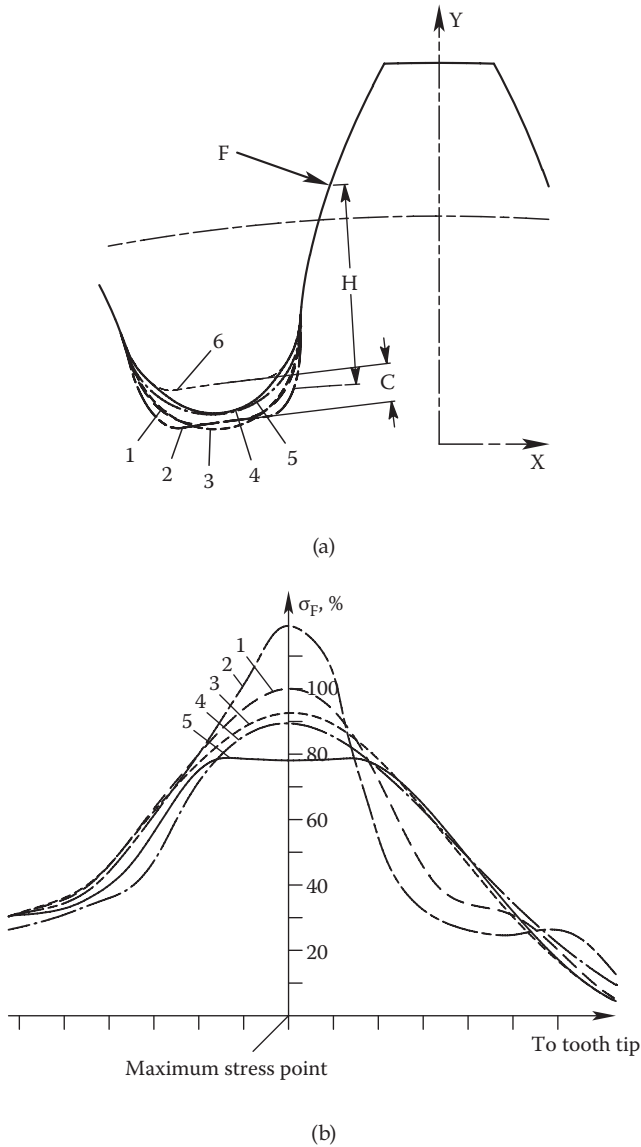
### 5.3.2 Fillet Optimization Analysis

Figure 5.12 presents a comparison of different tooth root fillet profile options. The involute flanks, face widths, tooth load, and its application point are the same for all fillet profile options. Results of the FEA stress calculation along with other root fillet parameters are shown in Table 5.3. Calculation results for fillet profile option 1 generated by the standard  $20^\circ$  pressure angle rack profile are considered the 100% benchmark values. Parameters of other fillet profile options are defined relative to the option 1 parameters.

Root fillet profile comparison results presented in Table 5.3 indicate considerable root stress concentration reduction provided by the fillet optimization. At the maximum tensile stress point the optimized fillet has a significantly larger fillet radius  $R_f$ , and a smaller distance  $H$  and root clearance  $C$ . It has the lowest maximum bending stress, which is evenly distributed along the large portion of the fillet profile. Other fillet profiles have significantly greater and sharply concentrated maximum stress.

Analysis of the fillet optimization results has indicated that the optimized fillet profile practically does not depend on the force value and its application point on the involute flank, except in the case where the application point is located very close to the form diameter. In this case, compression under the applied force may affect the optimized fillet profile. Such load application should not be considered for fillet optimization, because it induces minimal tensile stress in the root fillet in comparison to other load application points along the tooth flank. The gears with the optimized root fillets are shown in Figure 5.13.



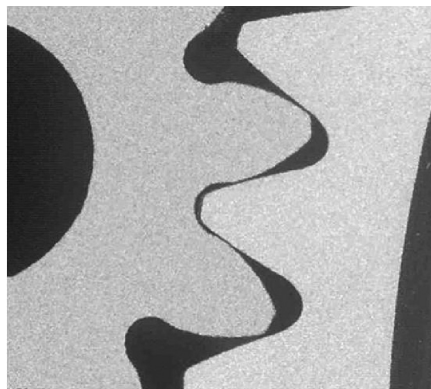
**FIGURE 5.12**

Root fillet comparison: (a) gear tooth with different fillet profiles, (b) stress chart along the fillet. 1 - fillet profile generated by the standard coarse pitch rack with the tip radius 0.3m (or 0.3 DP); 2 - fillet profile generated by the standard fine diametral pitch rack with the tip radius equal to zero; 3 - fillet profile generated by the full tip radius rack; 4 - circular fillet profile; 5 - optimized fillet profile; 6 - trajectory of the mating gear tooth tip in tight (zero backlash) mesh;  $F$  - applied load;  $H$  - radial distance between load application and maximum stress points;  $C$  - radial clearance;  $R_f$  - fillet curvature radius at the maximum stress point;  $\sigma_f$  - tensile stress. (From Kapelevich, A.L., and Y.V. Shekhtman, *Gear Technology*, September/October 2009, 73–79. With permission.)

**TABLE 5.3**

Fillet Profile Comparison (Figure 5.12)

	Rack with Tip Radius $R = 0.3m$	Rack with Tip Radius $R = 0$	Rack with Full Tip Radius	Circular Fillet Profile	Optimized Fillet
Fillet Profile No.	1	2	3	4	5
$R_f$ , %	100	58	118	121	273
$H$ , %	100	103	100	88	82
$C$ , %	100	100	118	79	76
$\sigma_{Fmax}$ , %	100	119	90	88	78

**FIGURE 5.13**

Gears with the optimized root fillets. (From Kapelevich, A.L., and Y.V. Shekhtman, *Gear Technology*, September/October 2009, 73–79. With permission.)

### 5.3.3 Benefits of Fillet Optimization

A goal and main benefit of the root fillet optimization is the bending stress concentration reduction. If the load capacity of gears with conventional (trochoidal or circular) root fillet profiles is limited by maximum tooth bending stress, fillet profile optimization increases gear load capacity proportionally to the bending stress reduction. However, quite often, gear load capacity, and consequently possible gear drive size and weight reduction, is limited by the tooth surface durability defined by pitting and scuffing resistance, which greatly depends on the contact stress, profile sliding, and contact (flash) temperature. Then potential bending stress reduction provided by the fillet optimization can be used to improve other gear drive performance parameters.

Figure 5.14 presents the charts of the bending and contact stresses (dashed curve), calculated for the gear pairs with the standard involute profiles. These gear pairs contain identical mating gears that make a gear ratio  $u = 1.0$ . They all have the same center distance  $a_w = 60$  mm, and the face width of

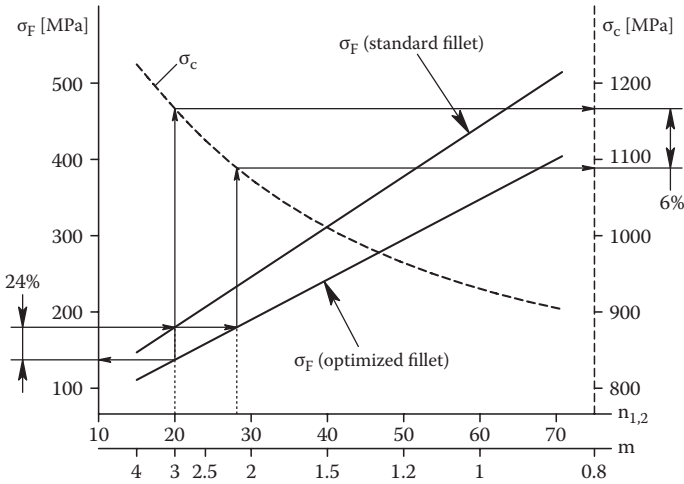


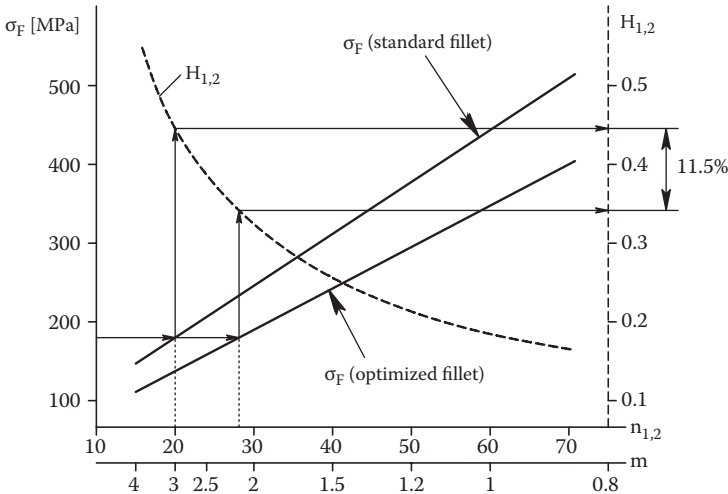
**FIGURE 5.14**

Conversion of potential bending stress reduction into contact stress reduction. (From Kapelevich, A.L., and Y.V. Shekhtman, *Gear Technology*, September/October 2009, 73–79. With permission.)

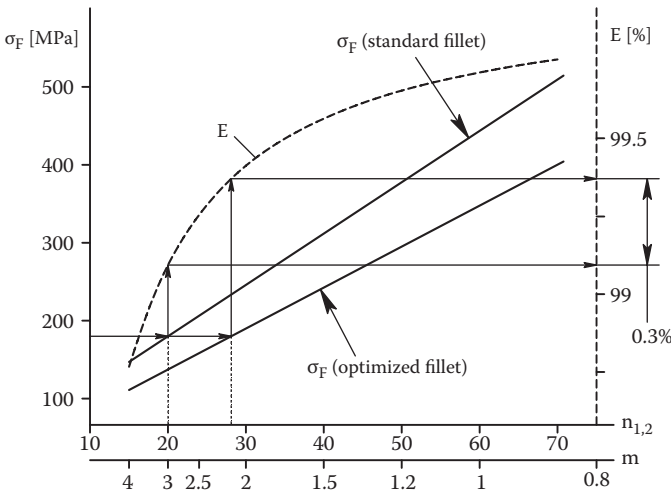
each gear is  $b = 10$  mm. Applied driving torque is  $T = 50$  Nm. The number of teeth varies from 12 to 75, and module varies accordingly from 5 to 0.8 mm to keep the constant center distance. The bending stresses are presented in two charts: The top one is for the gears with the standard (generated by  $20^\circ$  pressure angle rack) trochoidal fillet profiles, and the bottom one is for the same gears but with the optimized fillet profiles. For example, the bending stress level of 180 MPa is considered acceptable. This level is achievable for the 20-tooth gears with the standard fillet or for the 28-tooth gears (with lower module) with the optimized fillet. However, the 28-tooth gear pair has a higher contact ratio and, as a result, lower contact stress. The root fillet optimization allows trading of potential 24% bending stress reduction for 6% contact stress reduction by using the gears with a greater number of teeth and lower module. This 6% contact stress reduction could be used to increase gear drive life or for its size and weight reduction.

Similarly, the fillet optimization that makes it possible to increase the number of teeth and reduce their module allows reduction of specific sliding velocities (Figure 5.15), because the tooth addendum and tooth tip profile angles, in this case, are also reduced. This also leads to increased mesh efficiency (Figure 5.16), and reduced contact (flash) temperature (Figure 5.17) and scuffing probability (Figure 5.18).\*

\* Calculations of the contact (flash) temperature and scuffing probability were done using the mesh scuffing risk analysis subroutine of the GearWin software package developed by Charles E. Long.

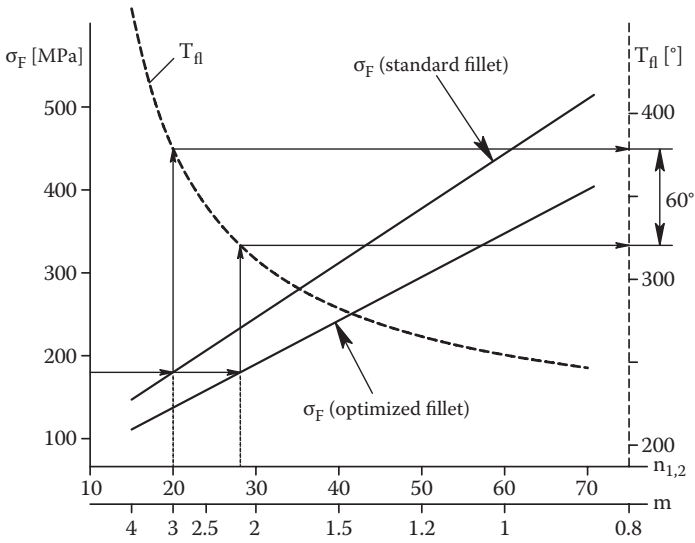


**FIGURE 5.15**  
Conversion of potential bending stress reduction into specific sliding reduction.

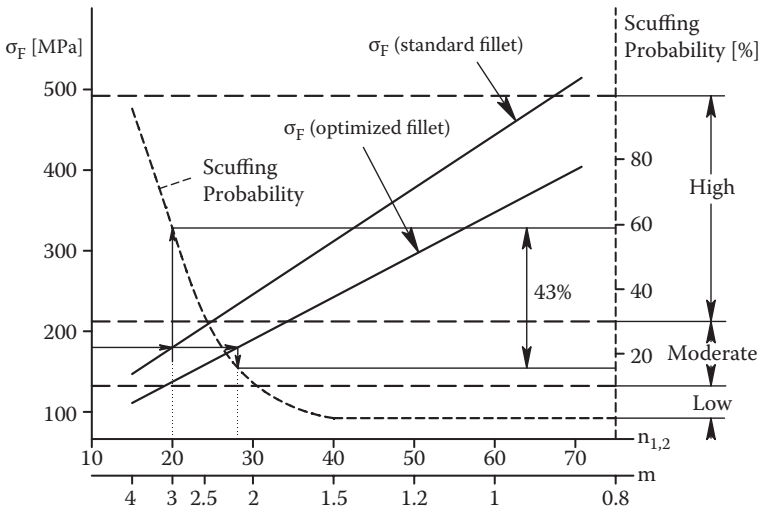


**FIGURE 5.16**  
Conversion of potential bending stress reduction into increased gear mesh efficiency. (From Kapelevich, A.L., and Y.V. Shekhtman, *Gear Technology*, September/October 2009, 73–79. With permission.)

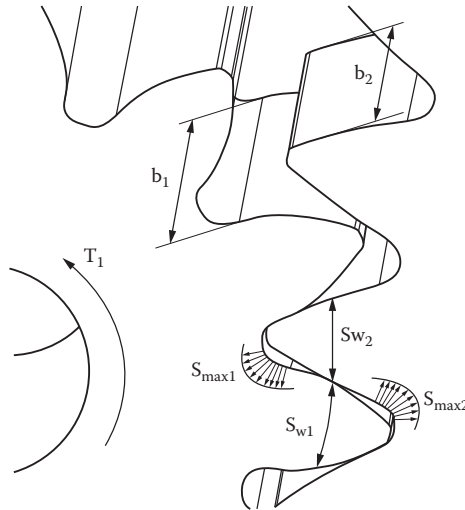
Potential benefits of the bending stress concentration reduction by the tooth fillet profile optimization can be extended. For example, this also allows use of gears with a greater number of teeth and lower module for noise and vibration reduction and allows increase of the elastohydrodynamic lubricant (EHL) film thickness also because of the reduced flash temperature and profile sliding.



**FIGURE 5.17**  
Conversion of potential bending stress reduction into contact (flash) temperature reduction.



**FIGURE 5.18**  
Conversion of potential bending stress reduction into scuffing probability reduction.

**FIGURE 5.19**

Bending stress balance. (From Kapelevich, A.L., and Y.V. Shekhtman, *Gear Technology*, September/October 2003, 45. With permission.)

## 5.4 Bending Strength Balance

The mating gears typically have different tooth shapes and face widths, and they could be made out of different materials, have different heat treatments, etc. In order to provide equally strong teeth of a pinion and gear, their maximum bending stress should be balanced or safety factors should be equalized [57]. This balance condition can be presented as

$$|\sigma_{F_{\max 1}} - C_b \sigma_{F_{\max 2}}| \leq \delta_F, \quad (5.23)$$

where  $\sigma_{F_{\max 1}}$  and  $\sigma_{F_{\max 2}}$  are maximum bending stresses in the fillet area of the pinion and the gear,  $C_b$  is the bending stress balance coefficient reflecting the difference in material properties and in a number of tooth load cycles for the pinion and the gear that defined their allowable bending stresses, and  $\delta_F$  is the permissible stress balance tolerance (typically less than 2–3%). Direct Gear Design uses the stress balance approach that utilizes a combination of an iteration method with the FEA stress calculation to satisfy the bending stress balance condition (5.23) by adjusting the tooth thickness ratio:

$$C_{tt} = S_{w1} / S_{w2}, \quad (5.24)$$

where  $S_{w1}$  and  $S_{w2}$  are tooth thicknesses on operating pitch diameters (Figure 5.19). This bending stress balance procedure should work in combination with the tooth profile and root fillet optimization.

---

## 5.5 Final Stress Definition

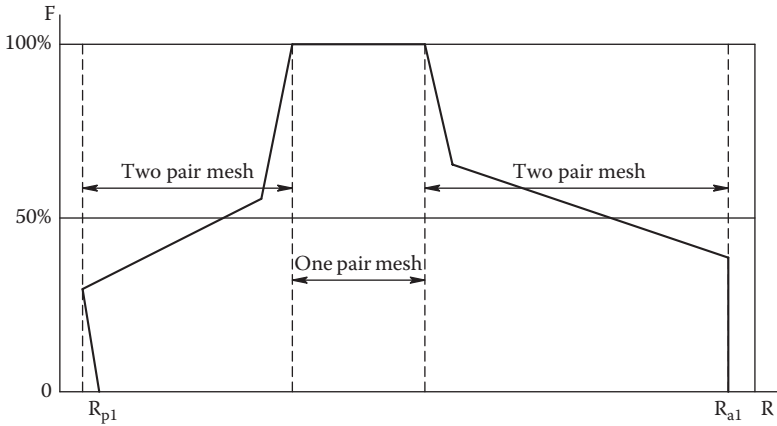
After the tooth geometry of mating gears is finalized the nominal bending and contact stresses are defined considering the tooth deflection under the applied load. In this case, the tooth load value is defined at different contact points of the involute tooth flank. Positions of these points are affected by the tooth bending deflection and the contact deflection of the involute flank. The FEA models of mating gears loaded by the driving torque at different angular positions allow load and stress distributions to be defined during the tooth pair engagement. Gear material properties like modulus of elasticity and Poisson ratio are used for deflection calculations. The FEA procedure defines bending stress. The Hertz equation is used for contact stress definition. This approach allows maximum contact and bending stresses to be defined. Typical charts of the driving gear tooth load, and contact and bending stress distribution along the involute tooth profile are presented in Figures 5.20 to 5.22 for conventional (a) and HCR (b) gears.

Conventional spur gears with the contact ratio  $1.0 < \epsilon_\alpha \leq 2.0$  have three tooth engagement phases:

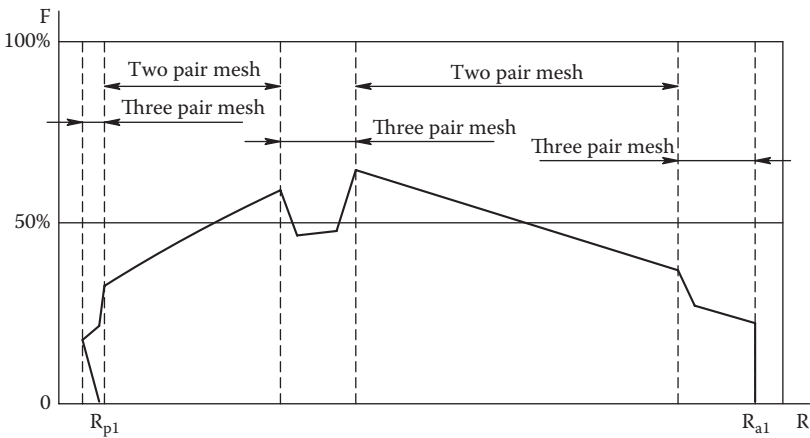
- Two-pair contact near the driving gear tooth root when a tooth load is partially shared with the previous tooth pair
- One-pair contact near the middle section of a tooth when a full load is taken by the engaged pair of teeth
- Two-pair contact near the driving gear tooth tip when a tooth load is partially shared with the following tooth pair

The HCR spur gears with the contact ratio  $\epsilon_\alpha > 2.0$  have five tooth engagement phases:

- Three-pair contact near the driving gear tooth root when a tooth load is partially shared with two previous tooth pairs
- Two-pair contact between the tooth root and the middle of the tooth when a tooth load is partially shared with the previous tooth pair
- Three-pair contact in a middle of the tooth when a tooth load is partially shared with one previous tooth pair and another following tooth pair
- Two-pair contact between a middle of the tooth and the tooth tip when a tooth load is partially shared with one following tooth pair
- Three-pair contact near the driving gear tip of the tooth when a tooth load is partially shared with two following tooth pairs



(a)



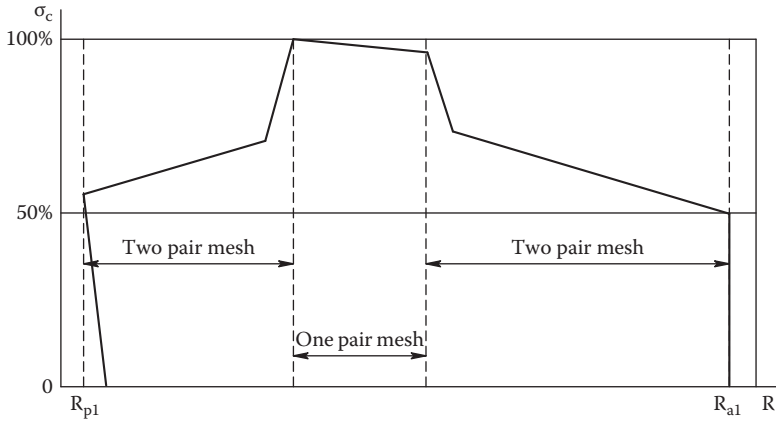
(b)

**FIGURE 5.20**

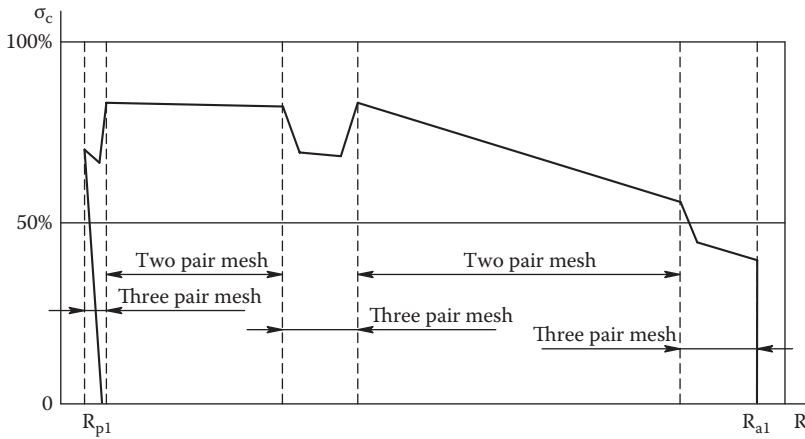
Tooth load distribution: (a) for conventional gears, (b) for HCR gears.  $R_{p1}$  and  $R_{a1}$  are radii at beginning and end of driving gear tooth engagement in contact with driven gear tooth.

Figures 5.20 to 5.22 have graphs that are defined considering the mating gear tooth deflections. Manufacturing tolerances, assembly misalignments, other gear drive components' (housing, shafts, bearings, etc.) deflections, and operating conditions (temperature, humidity, etc.) also affect the gear tooth load and stress distribution.





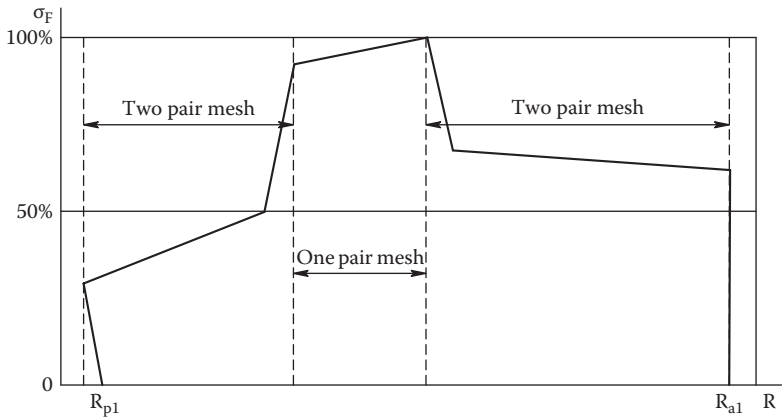
(a)



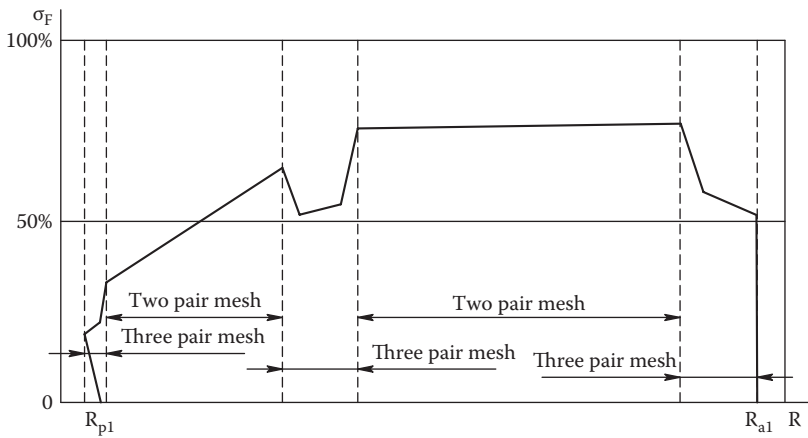
(b)

FIGURE 5.21

Contact stress distribution: (a) for conventional gears, (b) for HCR gears.



(a)



(b)

**FIGURE 5.22**  
Bending stress distribution: (a) for conventional gears, (b) for HCR gears.



# 6

---

## *Gear Design Details*

---

This chapter addresses various specific tasks of gear design, such as transmission density maximization, achieving high gear ratio in the planetary drives, self-locking gear design, some plastic gear design issues, and tooth modeling technique.

---

### 6.1 Gear Transmission Density Maximization

Maximization of the gear transmission density allows the output torque to be increased within given gear drive dimensional constraints or to reduce gear drive size and weight with a given output torque to be reduced. Size and weight reduction often also accompanies cost reduction.

This chapter presents an approach that allows optimizing gearbox kinematic arrangement and gear tooth geometry to achieve high gear transmission density. This approach uses dimensionless gearbox volume functions, which can be minimized by the gear drive internal gear ratio optimization [61].

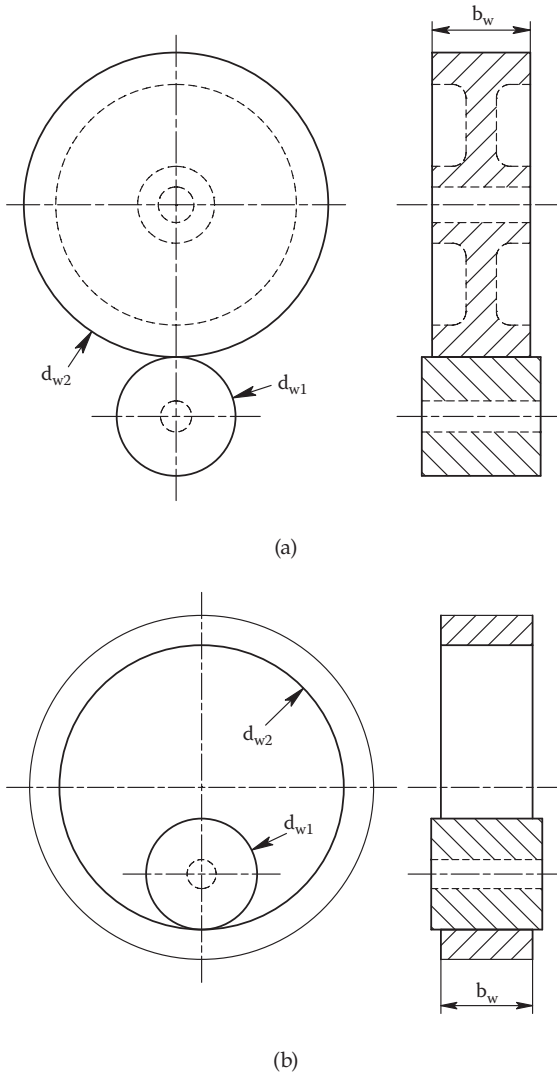
#### 6.1.1 Introduction of Volume Function

Load capacity or transmission density is defined by the gear tooth working flank surface durability that is limited, as a rule, by allowable contact stress level. For a pair of mating gears the gear transmission density coefficient  $K_o$  (also known as the  $K$ -factor) [5, 38] is

$$K_o = \frac{2 \times T_1}{d_{w1}^2 \times b_w} \times \frac{u \pm 1}{u}, \quad (6.1)$$

where  $T_1$  is the driving pinion torque,  $d_{w1}$  is the pinion operating pitch diameter,  $b_w$  is the effective gear face width in mesh,  $u = z_2/z_1$  is the gear pair ratio,  $z_1$  is the driving pinion number of teeth,  $z_2$  is the driven gear number of teeth, + is for external gear mesh, and – is for internal gear mesh.

The gear pair transmission density coefficient  $K_o$  statistically varies about 0.5–4.0 MPa for commercial drives and about 4.0–12.0 MPa for more demanding applications such as aerospace, racing, and automotive drives. So a wide range of  $K_o$  can be explained by the gear drive design (arrangement,

**FIGURE 6.1**

Gear pair volume definition: (a) external gearing, (b) internal gearing. (From Kapelevich, A.L., and V.M. Ananiev, *Gear Technology*, November/December 2011, 46–52. With permission.)

materials, heat treatment, lubrication, etc.), its application, operating conditions, and performance priorities, which may include size and weight, reliability, life, cost, noise and vibration, and many other characteristics. The gear pair volume definition is illustrated in Figure 6.1.

Weight of the pinion can be presented as

$$w_1 = \rho \times V_1 \times K_{v1}, \quad (6.2)$$

where  $\rho$  is the material density,  $K_{v1}$  is the volume utilization coefficient of the pinion (a ratio of the pinion volume to its operating pitch cylinder volume), and  $V_1$  is the operating pitch cylinder volume, which is equal to

$$V_1 = \frac{\pi}{4} \times d_{w1}^2 \times b_w, \quad (6.3)$$

which, considering Equation (6.1), also can be presented as

$$V_1 = \frac{\pi}{2} \times \frac{T_1}{K_o} \times \frac{u \pm 1}{u}. \quad (6.4)$$

The operating pitch cylinder volume of the mating gear is

$$V_2 = \frac{\pi}{4} \times d_{w2}^2 \times b_w = u^2 \times V_1, \quad (6.5)$$

where  $d_{w2}$  is the gear operating pitch diameter.

Assuming identical material density of both mating gears, the total weight of a gear pair is

$$w = w_1 + w_2 = \rho \times (V_1 \times K_{v1} + V_2 \times K_{v2}), \quad (6.6)$$

where  $K_{v2}$  is the volume utilization coefficient of the mating gear.

The volume utilization coefficients  $K_{v1}$  and  $K_{v2}$  depend on the gear body shape (solid body or with central or lightening holes, rim, web, spokes, etc.). Their values for driving pinions (sun gears) statistically vary in a range of 0.8–1.0; for driven (or planet) gears, 0.3–0.7, and for internal (or ring) gears, 0.05–0.1.

Then applying (6.5) the gear pair weight is

$$w = \rho \times V_1 \times (K_{v1} + u^2 \times K_{v2}), \quad (6.7)$$

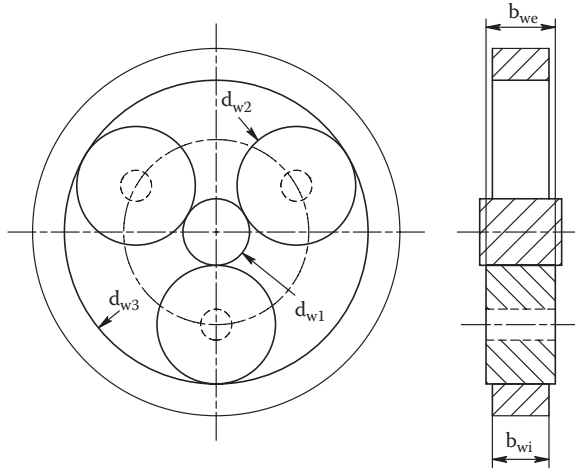
or with (6.4),

$$w = \rho \times \frac{\pi}{2} \times \frac{T_1}{K_o} \times F_v, \quad (6.8)$$

where  $F_v$  is the dimensionless volume function.

For the cylindrical pair of gears the volume function is

$$F_v = F_{v1} + F_{v2} = \frac{u \pm 1}{u} \times (K_{v1} + u^2 \times K_{v2}), \quad (6.9)$$

**FIGURE 6.2**

Epicyclic gear stage volume definition. (From Kapelevich, A.L., and V.M. Ananiev, *Gear Technology*, November/December 2011, 46–52. With permission.)

where

$$F_{v1} = \frac{u \pm 1}{u} \times K_{v1} \quad (6.10)$$

is the pinion volume function, and

$$F_{v2} = (u \pm 1) \times u \times K_{v2} \quad (6.11)$$

is the mating gear volume function.

The epicyclic gear stage volume definition is illustrated in Figure 6.2. In this case the subscript indexes 1, 2, and 3 are related to the sun gear, planet gear, and ring gear, respectively.

Operating pitch cylinder volume of the sun gear is defined by Equation (6.4) with the + sign, because the sun gear is in the external mesh with the planet gear. The planet gear operating pitch cylinder volume is defined by Equation (6.5). The operating pitch cylinder volume of the ring gear is

$$V_3 = \frac{\pi}{4} \times d_{w3}^2 \times b_{wi} = p^2 \times V_1 \times K_{bw}, \quad (6.12)$$

where  $d_{w3}$  is the ring gear operating pitch diameter,  $K_{bw} = b_{wi}/b_{we}$  is the effective gear face width ratio in the epicyclic gear stage,  $b_{we}$  is the effective gear face width in the sun/planet gear mesh,  $b_{wi}$  is the effective gear face width in the planet/ring gear mesh,  $p = z_3/z_1$  is the ring/sun gear ratio in the epicyclic stage, and  $z_3$  is the ring gear number of teeth.

Unlike the convex-convex sun/planet gear mesh tooth flank contact, the planet/ring gear mesh has the convex-concave tooth flank contact, resulting in significantly lower contact stress. This allows reducing the effective gear face width in the planet/ring gear mesh to achieve a similar level of contact stress as in the sun/planet gear mesh. This makes the effective gear face width ratio  $K_{bw} < 1.0$ . Typically it is 0.7–0.9.

Assuming the same density material for all gears, the total weight of gears in the epicyclic gear stage is

$$w = w_1 + n_p \times w_2 + w_3 = \rho \times (V_1 \times K_{v1} + n_p \times V_2 \times K_{v2} + V_3 \times K_{v3}), \quad (6.13)$$

where  $K_{v3}$  is the volume utilization coefficient of the ring gear, and  $n_p$  is the number of planet gears.

Applying Equations (6.5) and (6.12) the total weight is

$$w = \rho \times V_1 \times (K_{v1} + u^2 \times n_p \times K_{v2} + p^2 \times K_{v3} \times K_{bw}). \quad (6.14)$$

Then considering Equation (6.4) the epicyclic gear stage volume function is

$$\begin{aligned} F_{ve} &= F_{ve1} + n_p \times F_{ve2} + F_{ve3} \\ &= \frac{u+1}{u \times n_p} \times (K_{v1} + u^2 \times n_p \times K_{v2} + p^2 \times K_{v3} \times K_{bw}). \end{aligned} \quad (6.15)$$

where

$$F_{ve1} = \frac{u+1}{u \times n_p} \times K_{v1} \quad (6.16)$$

is the sun gear volume function,

$$F_{ve2} = \frac{u+1}{n_p} \times u \times K_{v2} \quad (6.17)$$

is the planet gear volume function, and

$$F_{ve3} = \frac{u+1}{u \times n_p} \times p^2 \times K_{v3} \times K_{bw} \quad (6.18)$$

is the ring gear volume function.

The more planet gears in the epicyclic gear stage, the lower its volume function and more compact the gear stage.

When the input torque and gear ratio are given and the gear transmission density coefficient  $K_o$  is selected according to the application, volume functions allow estimating the size and weight of the gearbox at a very preliminary stage of design for different gear arrangement options.



## 6.1.2 Volume Functions for Two-Stage Gear Drives

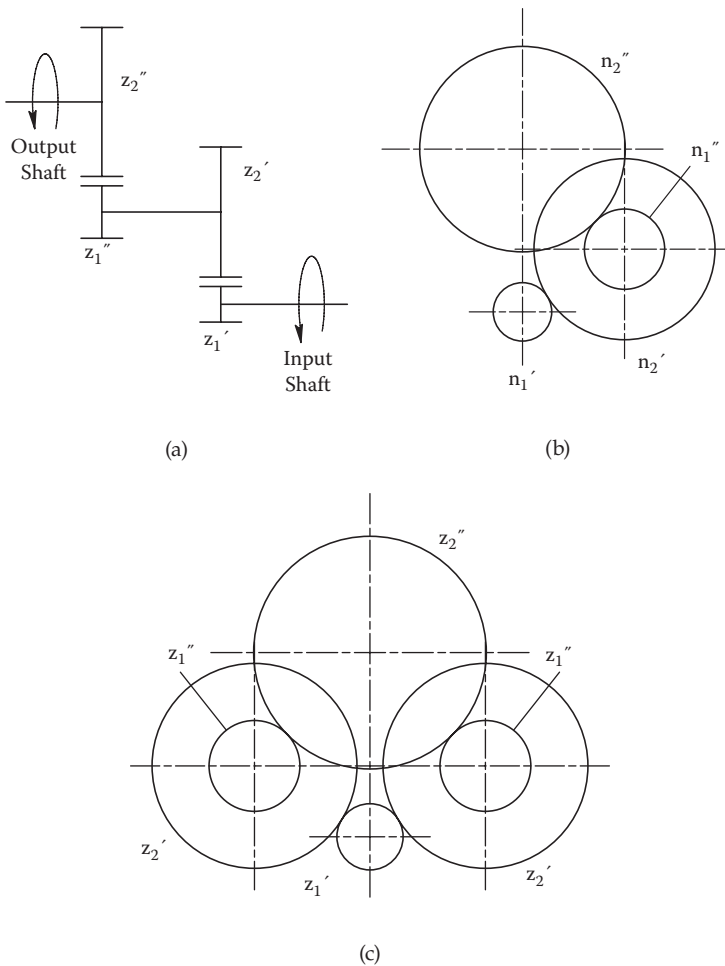
### 6.1.2.1 External Gear Arrangement

Figure 6.3 presents the two-stage gear drive arrangements with one (b) and two (c) load transmission branches.

Their total gear ratio is

$$u_t = u^I \times u^{II}, \quad (6.19)$$

where indexes I and II are for the first and second stages, accordingly.



**FIGURE 6.3**

(a) Two-stage external gear train, (b) one-transmission-branch arrangement, (c) two-transmission-branch arrangement. (From Kapelevich, A.L., and V.M. Ananiev, *Gear Technology*, November/December 2011, 46–52. With permission.)

The volume function for such arrangements is

$$F_v = \frac{u^I + 1}{n_b} \times \left( \frac{K_{v1}^I}{u^I} + n_b \times u^I \times K_{v2}^I \right) + \frac{u^I(u^{II} + 1)}{n_b} \times \left( \frac{n_b \times K_{v1}^{II}}{u^{II}} + u^{II} \times K_{v2}^{II} \right), \quad (6.20)$$

where  $K_{v3}$  is the volume utilization coefficient of the sun gear, and  $n_b$  is the number of transmission branches.

**6.1.2.2 Epicyclic Star Arrangement**

The two-stage epicyclic star gear arrangement is shown in Figure 6.4. This gear arrangement provides a more compact and lighter gear drive in comparison with the gear arrangements shown in Figure 6.3, because the number of transmission branches (planet gears) per stage is typically three or more, and also because of internal gear meshes of planet and ring gears. The planet (idler) gears in this arrangement are rotated around their stationary axis. A total gear ratio is

$$u_t = p^I \times p^{II}. \quad (6.21)$$

The volume function for this arrangement is

$$F_v = F_{ve}^I + p^I \times F_{ve}^{II}. \quad (6.22)$$

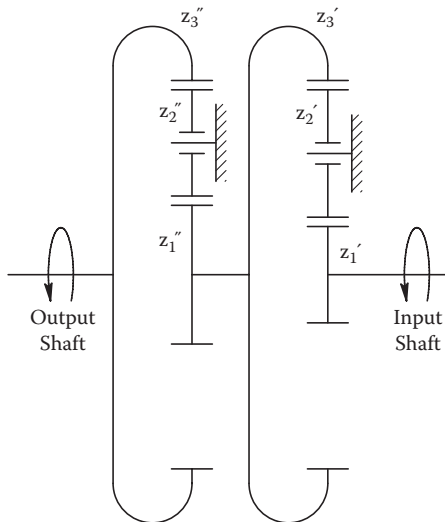


**FIGURE 6.4** Two-stage epicyclic star gear arrangement. (From Kapelevich, A.L., and V.M. Ananiev, *Gear Technology*, November/December 2011, 46–52. With permission.)

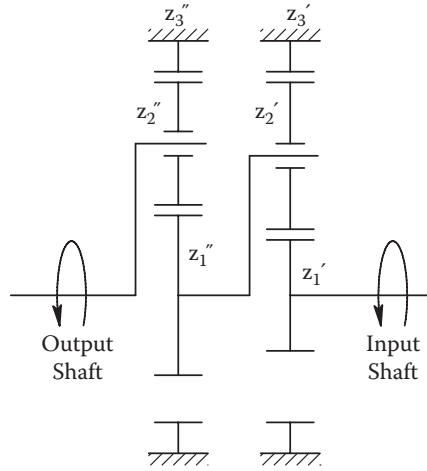


**FIGURE 6.5** Two-stage epicyclic planetary gear arrangement. (From Kapelevich, A.L., and V.M. Ananiev, *Gear Technology*, November/December 2011, 46–52. With permission.)

**6.1.2.3 Epicyclic Planetary Arrangement**

This epicyclic planetary gear arrangement (Figure 6.5) is more compact than the star one (Figure 6.4), because the planet gears are installed on the carrier and involved in the planetary motion around the sun gear. The total gear ratio is

$$u_t = (1 + p^I) \times (1 + p^{II}) . \tag{6.23}$$

The volume function for this arrangement is

$$F_v = F_{ve}^I + (1 + p^I) \times F_{ve}^{II} . \tag{6.24}$$

**6.1.2.4 Epicyclic Split Power Arrangement**

The split power arrangement [62] is shown in Figure 6.6. The first stage is differential. The second stage has the star arrangement. A part of the transmitted power goes from the first-stage carrier directly to the output shaft bypassing the second stage. The rest of the transmitted power goes from the first-stage ring gear to the second-stage sun gear, and then through the planets to the second-stage ring gear that is also connected to the output shaft. This allows reduction of the size and weight of the second stage and makes a gearbox even more compact and lighter than a gearbox with the planetary arrangement (Figure 6.5). The total gear ratio is

$$u_t = 1 + p^I + p^I \times p^{II} . \tag{6.25}$$

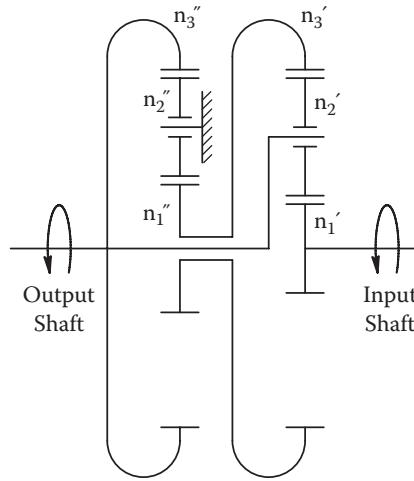


**FIGURE 6.6**

Two-stage epicyclic split power arrangement. (From Kapelevich, A.L., and V.M. Ananiev, *Gear Technology*, November/December 2011, 46–52. With permission.)

The volume function for this arrangement is

$$F_v = F_{ve}^I + \frac{p^I}{1 + p^I} \times F_{ve}^{II} . \tag{6.26}$$

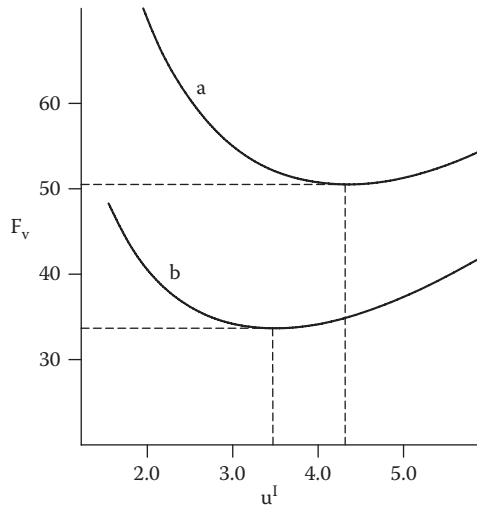
### 6.1.3 Internal Gear Ratio Optimization

The internal gear ratio distribution for multistage gearboxes can be optimized to achieve the minimum of the volume function [63]. For the two-stage gearboxes a minimum of the volume function  $F_v = f(u^I, u^{II})$  is achieved when the first derivatives  $d(F_v)/d(u^I)$  and  $d(F_v)/d(u^{II})$  are equal to zero.

Figure 6.7 presents a chart of the volume function vs. the first-stage gear ratio for the two-stage gear arrangements with one and two transmission branches with the total gear ratio of  $u = 15:1$ . The volume utilization coefficients are assumed for the pinions (driving gears)  $K_{v1} = 0.8$  and for the driven mating gears  $K_{v2} = 0.5$ .

A minimum of the volume function of the two-branch arrangement is significantly lower than for the one-branch arrangement because of load sharing between branches. Results of the volume function minimization and the optimal stage gear ratios are presented in Table 6.1.

Figure 6.8 shows the volume function vs. first-stage gear ratio charts for the two-stage epicyclic gear arrangements (Figures 6.4 to 6.6) with the total gear ratio of  $u = 15:1$ . Both stages have three planet gears. The volume utilization coefficients are assumed for the sun gears  $K_{v1} = 0.8$ , for the planet gears

**FIGURE 6.7**

Two-stage external gear train volume function charts: (a) with one transmission branch (Figure 6.3b), (b) with two transmission branches (Figure 6.3c). (From Kapelevich, A.L., and V.M. Ananiev, *Gear Technology*, November/December 2011, 46–52. With permission.)

**TABLE 6.1**

Volume Function Minimization for Two-Stage External Gear Arrangements

Total gear ratio	15:1	
Gear arrangement (Figure 6.7)	a	b
Number of branches	1	2
Minimum total volume function	50.469	33.697
First-stage volume function	12.476	8.303
Second-stage volume function	37.993	25.394
First-stage gear ratio	4.320:1	3.465:1
Second-stage gear ratio	3.472:1	4.329:1

$K_{v2} = 0.5$ , and for the ring gears  $K_{v3} = 0.1$ . The effective gear face width ratio in the epicyclic gear stages is assumed  $K_b = 0.75$ .

A minimum of the volume function for the split power arrangement has advantages in comparison with the star and planetary arrangements, because part of the transmitted power goes from the first-stage carrier directly to the output shaft and the second stage is less loaded. Results of the volume function minimization and the optimal stage gear ratios for the two-stage epicyclic gear trains are presented in Table 6.2.

After definition of the minimal total volume function and the stage gear ratios, the individual gear volume functions can be defined using Equations (6.10), (6.11), (6.16), (6.17), and (6.18). Then the pitch cylinder volume of an individual gear, considering (6.4), is

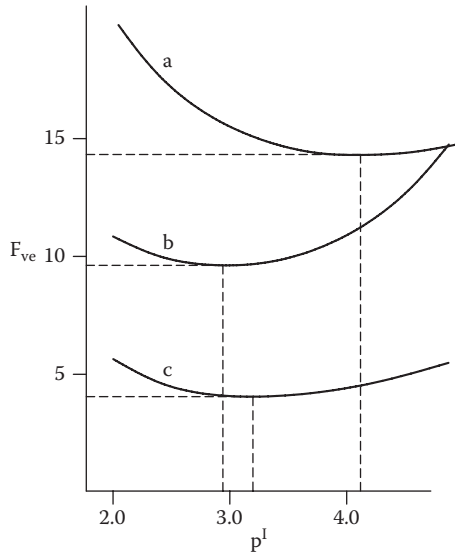


**FIGURE 6.8** Two-stage epicyclic gear train volume function charts: (a) star arrangement (Figure 6.4), (b) planetary arrangement (Figure 6.5), (c) split power arrangement (Figure 6.6). (From Kapelevich, A.L., and V.M. Ananiev, *Gear Technology*, November/December 2011, 46–52. With permission.)

**TABLE 6.2**  
Volume Function Minimization for Two-Stage Epicyclic Gear Arrangements

Total gear ratio	15:1		
Gear arrangement (Figure 6.8)	a	b	c
Minimum total volume function	14.32	9.66	4.09
First-stage volume function	3.22	2.03	2.24
Second-stage volume function	11.09	7.63	1.85
First-stage planet/sun gear ratio	1.55:1	0.97:1	1.09:1
Second-stage planet/sun gear ratio	1.33:1	0.91:1	1.20:1
First-stage ring/sun gear ratio	4.11:1	2.93:1	3.19:1
Second-stage ring/sun gear ratio	3.65:1	2.82:1	3.40:1

$$V = \frac{\pi}{2} \times \frac{T_1}{K_0} \times F_v \tag{6.27}$$

From here

$$d_w^2 \times b_w = \frac{4}{\pi} \times V = \frac{2 \times T_1}{K_v \times K_0} \times F_v \tag{6.28}$$

or

$$d_w = \sqrt[3]{\frac{2 \times T_1 \times F_v}{K_v \times K_0 \times \Psi}} \quad (6.29)$$

where  $K_v$  is the volume utilization coefficient, and  $\Psi = b_w/d_w$  is the aspect ratio that varies in a range of 0.05–1.2 or higher [5]. This allows the pitch diameters and face widths of all gears to be defined.

However, the total volume and weight of a gear transmission are not in direct proportion to its volume function  $F_v$ . A share of gear volume is usually higher for simple arrangements like the external gear train. In more complicated epicyclic gear arrangements this share could be much lower, because of a higher number and volume of other gearbox parts and components, such as carriers, bearings, shafts, lubrication system parts, etc. Statistical data of a gear volume share for a selected type of gear arrangement help to define the approximate size of a gearbox. In many cases, a gearbox is built in the overall mechanism assembly, and its size and weight minimization should be considered to achieve minimal size and weight of the whole mechanism.

The approach presented in this chapter utilizes volume functions, and allows estimation of volume and weight of a gearbox at the very early stages of product development.

---

## 6.2 High Gear Ratio Planetary Drives

Epicyclic gear stages provide high load capacity and compactness to gear drives. There is a huge variety of different combinations of planetary gear arrangements [64, 65]. Although some of them are quite complicated, they typically contain simple epicyclic stages (Figure 6.9a) or epicyclic stages with the compound planet gear (Figure 6.9b). These stages, however, have limited gear ratios. For simple epicyclic planetary stages when the ring gear is stationary, the practical gear ratio varies from 3:1 to 9:1 [66]. For epicyclic planetary stages with compound planet gears, the practical gear ratio varies from 8:1 to 30:1 [66].

### 6.2.1 One-Stage Arrangements

There are one-stage differential planetary arrangements that provide much higher gear ratios. In these arrangements the output shaft is connected to the second rotating ring gear instead of to the carrier, like in the epicyclic planetary stages. A carrier in this case does not transmit torque, and it is called a cage because it is used just to support planet gears.

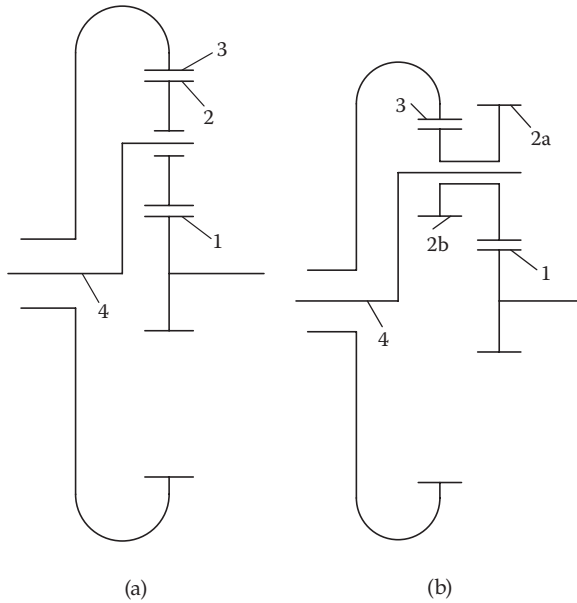


**FIGURE 6.9**

Epicyclic gear stages: (a) simple, (b) with compound planet gears. 1 - sun gear; 2 - planet gear; 2a and 2b - two portions of compound planet gear; 3 - ring gear; 4 - planet carrier.

Figure 6.10a and 6.10b presents differential planetary arrangements with compound planet gears. In the arrangement in Figure 6.10a the sun gear is engaged with a portion of the planet gear that is in mesh with the stationary ring gear. In this case the gear ratio is

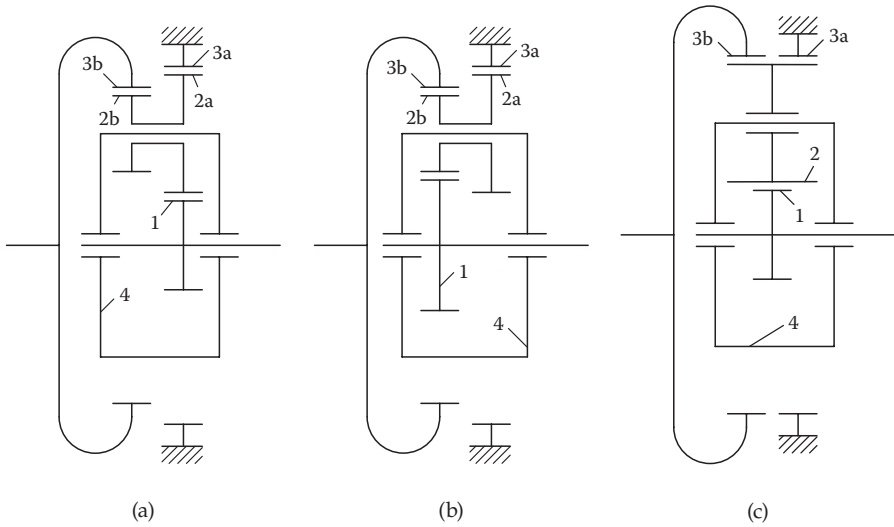
$$u = \frac{1 + \frac{z_{3a}}{z_1}}{1 - \frac{z_{2b}z_{3a}}{z_{2a}z_{3b}}}, \tag{6.30}$$

where  $z_1$  is the sun gear number of teeth,  $z_{2a}$  is the number of teeth the planet gear engaged with the sun gear and stationary ring gear,  $z_{2b}$  is the number of teeth the planet gear engaged with the rotating ring gear,  $z_{3a}$  is the stationary ring gear number of teeth, and  $z_{3b}$  is the rotating ring gear number of teeth.

In the arrangement in Figure 6.10b the sun gear is engaged with a portion of the planet gear that is in mesh with the rotating ring gear. In this case the gear ratio is

$$u = \frac{1 + \frac{z_{3a}z_{2b}}{z_1z_{2a}}}{1 - \frac{z_{3a}z_{2b}}{z_{3b}z_{2a}}}. \tag{6.31}$$



**FIGURE 6.10**

Differential planetary arrangements: (a, b) with compound planet gears, (c) with singular planet gears. 1 - sun gear; 2 - planet gear; 2a and 2b - two portions of compound planet gear; 3a - stationary ring gear; 3b - rotating ring gear; 4 - planet cage.

If a gear ratio is negative, the input and output shaft rotation directions are opposite.

All gear meshes in differential planetary arrangements have the same center distance. This condition from Equation (2.43) allows definition of relations between the operating modules  $m_w$  (metric system) or diametral pitches  $DP_w$  (English system). For the arrangement in Figure 6.10a they are

$$m_{w12a}(z_1 + z_{2a}) = m_{w2a3a}(z_{3a} - z_{2a}) = m_{w2b3b}(z_{3b} - z_{2b}) \quad (6.32)$$

and

$$\frac{z_1 + z_{2a}}{DP_{w12a}} = \frac{z_{3a} - z_{2a}}{DP_{w2a3a}} = \frac{z_{3b} - z_{2b}}{DP_{w2b3b}}. \quad (6.33)$$

The relation between operating pressure angles in the gear meshes of sun gear  $z_1$  with planet gear  $z_{2a}$  and planet gear  $z_{2a}$  with ring gear  $z_{3a}$  is defined by

$$\frac{\cos(\alpha_{w2a-3a})}{\cos(\alpha_{w1-2a})} = \frac{z_1 + z_{2a}}{z_{3a} - z_{2a}}, \quad (6.34)$$

where  $\alpha_{w1-2a}$  is the operating pressure angle in a mesh of the sun gear and the planet gear engaged with the stationary ring gear, and  $\alpha_{w2a-3a}$  is the operating pressure angle in the planet/stationary ring gear mesh.

Similar for the arrangement in Figure 6.10b,

$$m_{w12b}(z_1 + z_{2b}) = m_{w2b3b}(z_{3b} - z_{2b}) = m_{w2a3a}(z_{3a} - z_{2a}) \quad (6.35)$$

and

$$\frac{z_1 + z_{2b}}{DP_{w12b}} = \frac{z_{3b} - z_{2b}}{DP_{w2b3b}} = \frac{z_{3a} - z_{2a}}{DP_{w2a3a}}. \quad (6.36)$$

The relation between operating pressure angles in the gear meshes of sun gear  $z_1$  with planet gear  $z_{2b}$  and planet gear  $z_{2b}$  with ring gear  $z_{3b}$  is defined by

$$\frac{\cos(\alpha_{w2b-3b})}{\cos(\alpha_{w1-2b})} = \frac{z_1 + z_{2b}}{z_{3a} - z_{2b}}, \quad (6.37)$$

where  $\alpha_{w1-2b}$  is the operating pressure angle in a mesh of the sun gear and the planet gear engaged with the rotating ring gear, and  $\alpha_{w2b-3b}$  is the operating pressure angle in the planet/rotating ring gear mesh.

In the differential planetary arrangements with compound planet gears, operating pressure angles in the planet/stationary ring gear mesh and in the planet the planet/rotating ring gear mesh can be selected independently. This allows specific sliding velocities in these meshes to be balanced to maximize gear efficiency. These differential planetary arrangements with compound planet gears allow achievement of very high gear ratios up to 500:1 and more with relatively high gear mesh efficiencies of 80–90% [66].

The assembly condition for these arrangements is

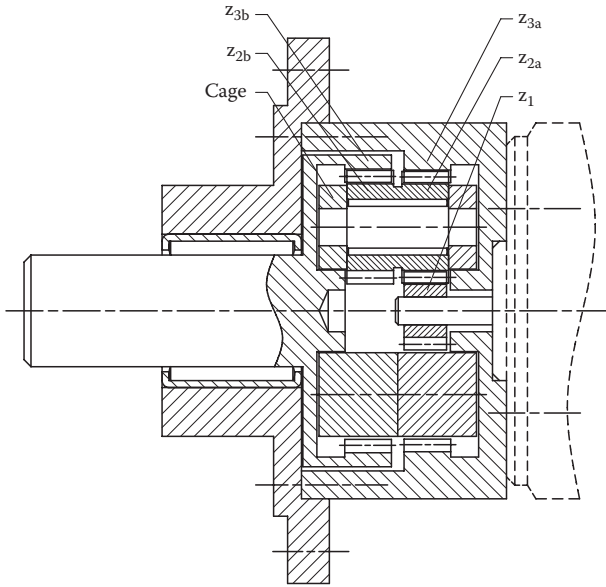
$$\frac{z_{3a} - z_{3b}}{n_w} = \text{integer}, \quad (6.38)$$

where  $n_w$  is the number of planet gears.

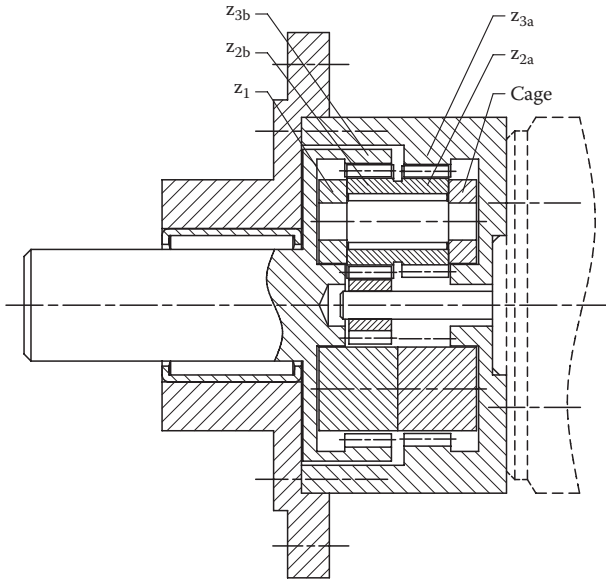
Two parts of a compound planet gear should be angularly aligned. This is typically achieved by aligning the axes of one tooth of each part of the compound planet gear, which makes its fabrication more complicated. Assembly of such gear drives requires certain angular positioning of planet gears. All this increases the cost of this type of gear drive.

Examples of the differential planetary gear actuators with compound planet gears are shown in Figure 6.11.

A simplified version of the one-stage differential planetary arrangement is shown in Figure 6.10c. This arrangement does not use the compound planet gear. All three gear meshes should have the same center distance. The plain planet gear is engaged with the sun gear, and both stationary and rotating ring gears. This does not allow specific sliding velocities in each mesh to



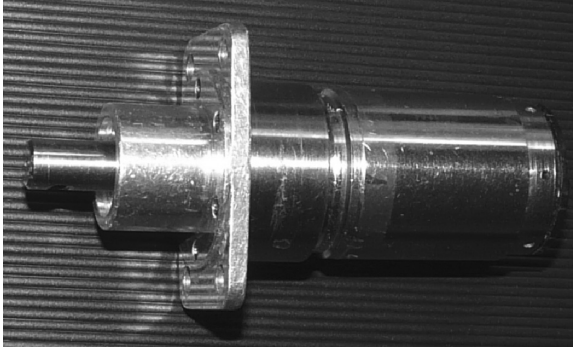
(a)



(b)

**FIGURE 6.11**

Differential planetary gear actuators: (a, b) cross sections, (c) photo. (Courtesy of Leigh Aerosystems Corp., Carlsbad, California.)



(c)

FIGURE 6.11 (continued)

be equalized, resulting in some gear efficiency reduction. Relations between operating pressure angles in the gear meshes are defined by

$$\frac{\cos(\alpha_{w2-3a})}{\cos(\alpha_{w1-2})} = \frac{z_1 + z_2}{z_{3a} - z_2}, \tag{6.39}$$

$$\frac{\cos(\alpha_{w2-3b})}{\cos(\alpha_{w1-2})} = \frac{z_1 + z_2}{z_{3b} - z_2}, \tag{6.40}$$

and

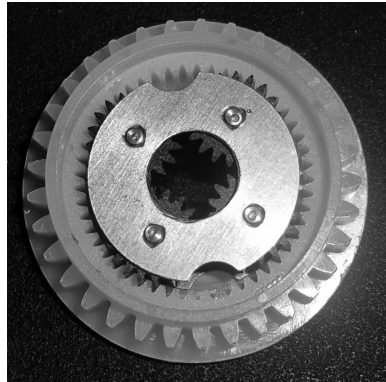
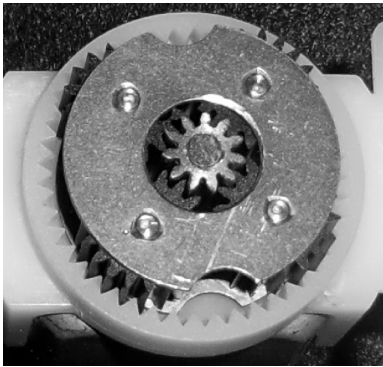
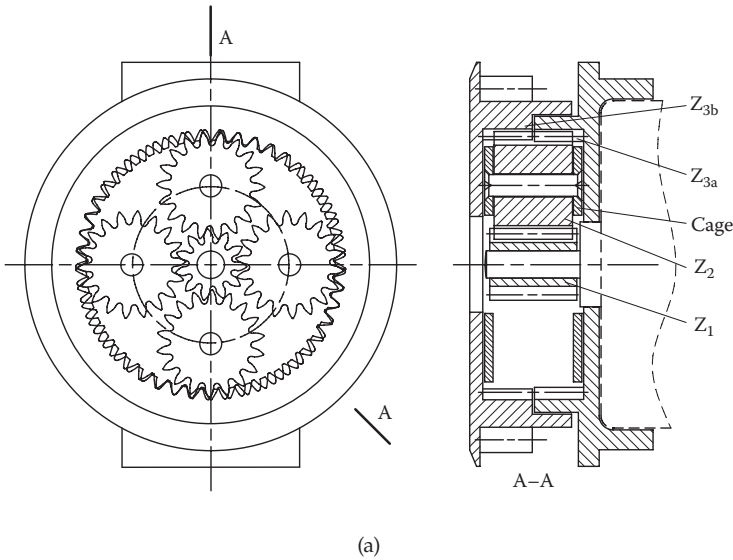
$$\frac{\cos(\alpha_{w2-3b})}{\cos(\alpha_{w2-3a})} = \frac{z_{3a} - z_2}{z_{3b} - z_2}, \tag{6.41}$$

where  $\alpha_{w1-2}$  is the operating pressure angle in sun/planet gear mesh,  $\alpha_{w2-3a}$  is the operating pressure angle in planet/stationary ring gear mesh, and  $\alpha_{w2-3b}$  is the operating pressure angle in planet/rotating ring gear mesh.

A gear ratio is

$$u = \frac{1 + \frac{z_{3a}}{z_1}}{1 - \frac{z_{3a}}{z_{3b}}}. \tag{6.42}$$

This gear arrangement with three planet gears allows achievement of a gear ratio over 200:1 in one stage. Gear mesh efficiency of this type of gear drives is typically lower in comparison with differential planetary gear drives with compound gears (Figure 6.10a and b) with the same gear ratio

**FIGURE 6.12**

Differential planetary gear actuator: (a) sketch with cross section, (b, c) gearbox component photos. (Courtesy of Thermotech Co., Hopkins, Minnesota.)

due to unequalized specific sliding velocities. Depending on the gear ratio, it is 70–84% [66]. However, such an arrangement provides a compact package. It also simplifies planet gear fabrication and does not require angular positioning of planet gears in assembly, reducing gear drive cost. An example of the differential planetary gearbox with four simple planet gears is shown in Figure 6.12.

In differential planetary arrangements (Figure 6.10) tangent forces applied to the planet gear teeth from the stationary and rotating ring gears are unbalanced, because they lie on different parallel planes and have opposite

directions. The sturdy planet cage is required to avoid severe planet gear mesh misalignment. There are gear drives that use the differential planetary arrangements with the balanced planet gear tangent forces (Figure 6.13). In this case, the triple-compound planet gears (Figure 6.13a and 6.13b) are used. They have identical gear profiles on their ends that are engaged with two identical stationary ring gears. The middle portion of such planet gears has a different profile than those on the ends and is engaged with the rotating ring gear. The arrangement in Figure 6.13c has plain planet gears engaged with the sun gear, two stationary ring gears, and one rotating ring gear. These types of differential planetary drives typically do not have the cage and bearings, because the planet gear forces are balanced and planet gears themselves work like the roll bearings for radial support of the rotating ring gear.

### 6.2.2 Two-Stage Arrangements

In most conventional two-stage planetary arrangements the gear ratio usually does not exceed 100:1, although there are possible arrangements that allow a significant increase in the gear ratio. Two examples of such two-stage planetary gear trains are described in [67]. Figure 6.14 shows the gear arrangement A with the sun gears of the first and second stages connected together and the compound cage supporting the planet gears of both first and second stages. A sketch of the gearbox with arrangement A is presented in Figure 6.15.

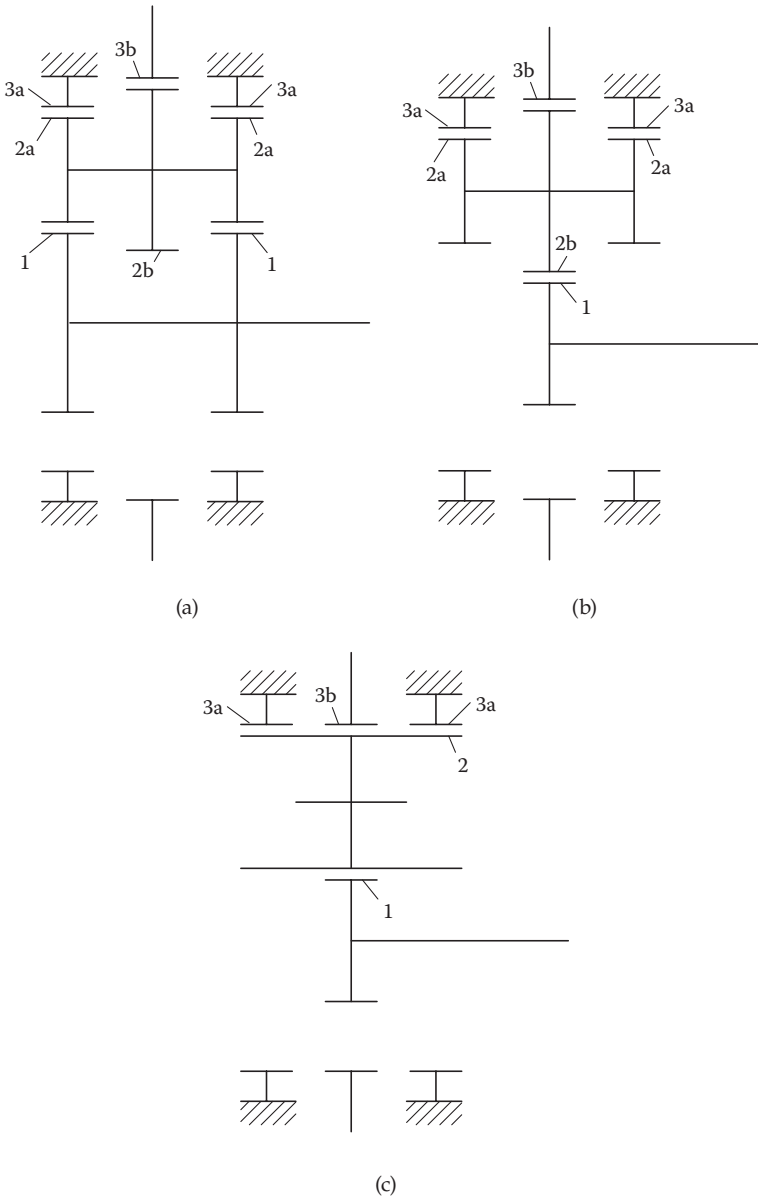
Both sun gears are connected to the input shaft and engaged with the planet gears of the first and second stages accordingly. The first-stage ring gear is stationary and connected with the gearbox housing. It is engaged with the first-stage planet gears. The compound cage practically contains the first- and second-stage cages connected together. The ring gear of the second stage is engaged with the second-stage planet gears and connected to the output shaft.

The gear ratio of arrangement A is

$$u = \frac{z_3^{\text{II}} \times (z_1^{\text{I}} + z_3^{\text{I}})}{z_1^{\text{I}} \times z_3^{\text{II}} - z_1^{\text{II}} \times z_3^{\text{I}}}, \quad (6.43)$$

where  $z_1^{\text{I}}$  and  $z_1^{\text{II}}$  are numbers of teeth of the sun gears of the first and second stages,  $z_2^{\text{I}}$  and  $z_2^{\text{II}}$  are numbers of teeth of the planet gears of the first and second stages, and  $z_3^{\text{I}}$  and  $z_3^{\text{II}}$  are numbers of teeth of the ring gears of the first and second stages.

Figure 6.16 shows the alternative gear arrangement B with the sun gears of both stages connected together and the ring gears of both stages also connected together. A sketch of the gearbox with the alternative arrangement B is presented in Figure 6.17.

**FIGURE 6.13**

Differential planetary arrangements without planet gear cage: (a, b) with triple-compound planet gears, (c) with simple planet gears. 1 - sun gear; 2 - planet gear; 2a and 2b - two portions of triple-compound planet gear; 3a - stationary ring gear; 3b - rotating ring gear.

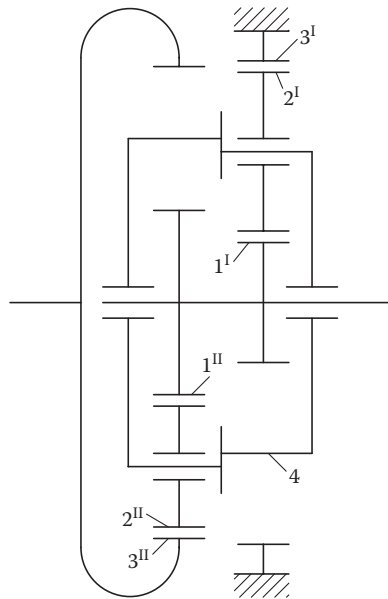


**FIGURE 6.14**

Two-stage planetary arrangement A with connected sun gears of first and second stages and compound cage. 1<sup>I</sup> and 1<sup>II</sup> - sun gears; 2<sup>I</sup> and 2<sup>II</sup> - planet gears; 3<sup>I</sup> - stationary ring gear of first stage; 3<sup>II</sup> - rotating ring gear of second stage; 4 - compound cage. Indexes I and II are for first and second stages accordingly.

Both sun gears are connected to the input shaft and engaged with the planet gears of the first and second stages accordingly. The shafts supporting the first-stage planet gears are connected (pressed in, for example) to the gearbox housing. Both ring gears are connected together and engaged with the planet gears of the first and second stages accordingly. The second-stage carrier is connected to the output shaft.

The gear ratio of arrangement B is

$$u = \frac{z_3^I \times (z_1^{II} + z_3^{II})}{z_1^{II} \times z_3^I - z_1^I \times z_3^{II}} \quad (6.44)$$

The maximum gear ratios of these two-stage planetary arrangements A and B are achieved when the denominator of Equations (6.43) and (6.44) is equal to 1 or -1. This condition can be presented as

$$|z_1^I \times z_3^{II} - z_1^{II} \times z_3^I| = 1 \quad (6.45)$$

When this denominator is 1, the input and output shafts are rotating in the same direction. When it is -1, the input and output shafts are rotating in



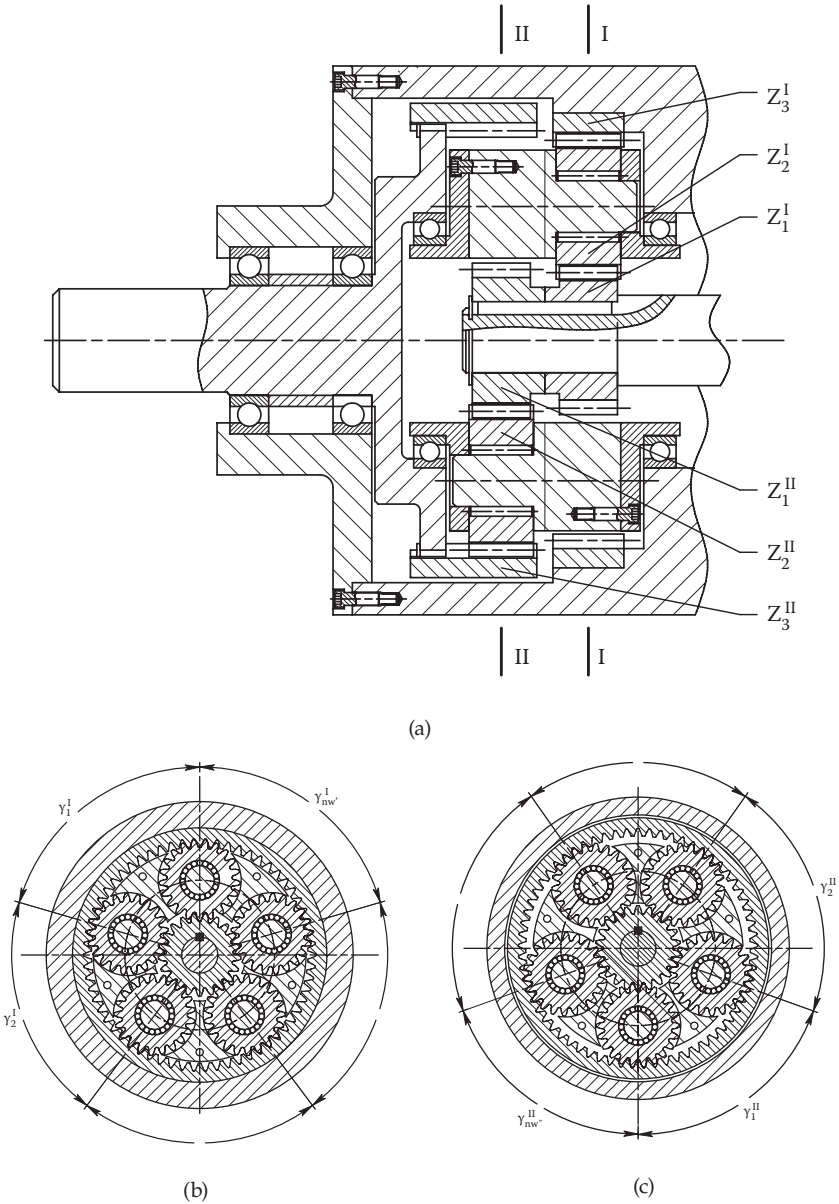


**FIGURE 6.15**

Two-stage planetary gearbox (arrangement A) with connected sun gears of first and second stages and compound cage: (a) axial cross section, (b) section I-I, (c) section II-II.  $\gamma_i$  - central location angles between planet gears. Indexes I and II are for first and second stages.

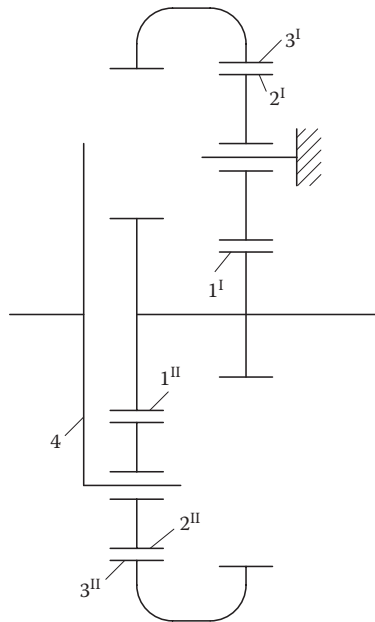


**FIGURE 6.16**

Two-stage planetary arrangement B with sun gears and ring gears of first and second stages connected together. 1<sup>I</sup> and 1<sup>II</sup> - sun gears; 2<sup>I</sup> and 2<sup>II</sup> - planet gears; 3<sup>I</sup> and 3<sup>II</sup> - ring gears; 4 - second-stage carrier. Indexes I and II are for first and second stages.

opposite directions. If a number of planet gears are more than one ( $nw^I > 1$  and  $nw^{II} > 1$ ), the condition (6.45) requires irregular angular positioning of the planet gears in one or both planetary stages. This means that the central location angles  $\gamma_i$  between planet gears in one or both stages are not identical (see Figures 6.15b and c and 6.17b and c).

The following method is used to define the central location angles  $\gamma_i$  between planet gears for irregular angular positioning of the planet gears in one or both planetary stages. The planet gear location factor is

$$F_{nw} = \frac{z_1 + z_3}{nw} . \tag{6.46}$$

If the factor  $F_{nw}$  is a whole number, the planet gears have identical central location angles between the planet gears equal to  $360^\circ/nw$ . Otherwise, if the factor  $F_{nw}$  is not a whole number, the initial central angles in radians are

$$\phi_i = \frac{2\pi(i - 1)}{nw} , \tag{6.47}$$

where  $i$  is a planet gear number from 1 to  $nw$ .

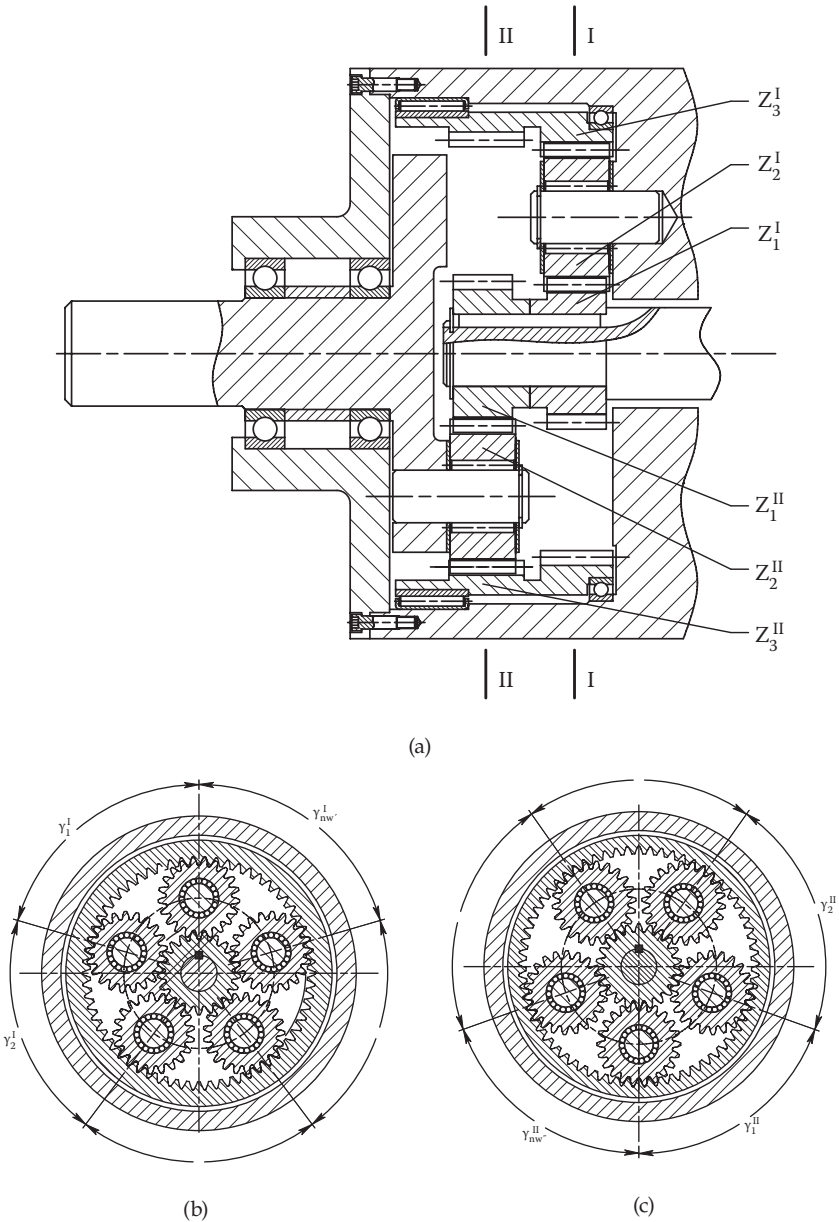


**FIGURE 6.17**

Two-stage planetary gearbox (arrangement B) with sun gears and ring gears of first and second stages connected together: (a) axial cross section, (b) section I-I, (c) section II-II.  $\gamma_i$  - central location angles between planet gears;  $nw$  - number of planet gears. Indexes I and II are for first and second stages.

The ring gear position angles in radians are

$$\varphi_i = \phi_i \left(1 + \frac{z_1}{z_3}\right). \quad (6.48)$$

The numbers of the ring gear teeth per each position angle are

$$z_{3ai} = \varphi_i \frac{z_3}{2\pi}. \quad (6.49)$$

Rounded numbers of the ring gear teeth per each position angle are

$$z_{3ri} = \text{round}(z_{3ai}). \quad (6.50)$$

The adjusted central angles in radians are

$$\phi a_i = \frac{2\pi z_{3ri}}{z_1 + z_3}. \quad (6.51)$$

The central angles between planet in radians gears are

$$\gamma_j = \phi a_{j+1} - \phi a_j, \quad (6.52)$$

where  $\phi a_{m+1} = 2\pi$ .

For example, if a number of the sun gear teeth is  $z_1 = 21$ ; planet gear,  $z_2 = 20$ ; ring gear,  $z_3 = 61$ ; and a number of planet gears is 5, the central angles between planet gears are  $\gamma_1 = 70.244^\circ$ ,  $\gamma_2 = 74.634^\circ$ ,  $\gamma_3 = 70.244^\circ$ ,  $\gamma_4 = 74.634^\circ$ , and  $\gamma_5 = 70.244^\circ$ .

The neighboring planet gears located at the minimum central angles must be checked for the possibility of tip/tip interference. Irregular angular positioning of the planet gears may result in an imbalance in the planetary stage. This must be avoided by the carrier assembly balancing.

Application of the two-stage planetary arrangements A and B with the number of gear teeth satisfying a condition (6.45) allows very high gear ratio values to be achieved. Practically these values are limited only by numbers of teeth of the ring gears  $z_3^I$  and  $z_3^{II}$ . Table 6.3 presents maximum achievable gear ratios depending on numbers of teeth of the ring gears  $z_3^I$  and  $z_3^{II}$ .

Unlike in conventional two-stage planetary arrangements (Figures 6.4 to 6.6), in the planetary arrangements A and B a total gear ratio does not depend on internal gear ratios in each stage. This allows increase of a number of planet gears. An example of the gear ratio calculation for the planetary arrangements A and B is shown in Table 6.4.

Efficiency of these two-stage planetary gear arrangements is in opposite proportion to gear ratio and noticeably lower than for conventional two-stage

**TABLE 6.3**

Maximum Achievable Gear Ratios in Two-Stage Planetary Gear Arrangements A and B

Ring Gear Number of Teeth, $z_3^I$ and $z_3^{II}$	Maximum Gear Ratio*
100	$\pm 14,000:1$
200	$\pm 66,000:1$
300	$\pm 160,000:1$
400	$\pm 280,000:1$

\* +, if rotation directions of the input and output shafts are the same;  
 -, if rotation directions of the input and output shafts are opposite.

**TABLE 6.4**

Gear Ratio Calculation Examples

Arrangement		A (Figure 6.15)	B (Figure 6.17)
First stage	Sun gear number of teeth	21	21
	Planet gear number of teeth	21	21
	Ring gear number of teeth	62	62
	Number of planet gears	5	5
Second stage	Sun gear number of teeth	22	22
	Planet gear number of teeth	22	22
	Ring gear number of teeth	65	65
	Number of planet gears	5	5
Gear ratio		5395:1	-5394:1

planetary gear arrangements. One of the potential areas of application is in different positioning systems that need very low-output RPM and typically do not require high-output torque.

### 6.3 Self-Locking Gears

In most gear drives, when driving torque is suddenly reduced as a result of power outage or any mechanical failure at the transmission input, gears are rotating either in the same direction driven by inertia or in the opposite direction driven by the resistant load, applied to the output shaft. The latter condition is known as backdriving. During inertial motion or backdriving, a driven output shaft becomes a driving one and a driving input shaft becomes a driven one. There are many gear drive applications where such operating mode is not acceptable. In order to prevent it, different types of brake or clutch devices are used. However, there are solutions that prevent inertial motion or backdriving using self-locking gears without any

additional devices. The most common one is a worm gear drive with a low lead angle. In a self-locking worm gear drive, the torque applied to the worm gear is blocked by friction force preventing its rotation. However, worm gear drives have some constraints. They require a crossed axis shaft arrangement and relatively high gear ratio. They also have low gear mesh efficiency.

There are parallel axis self-locking gears [68, 69]. These gears, unlike worm gears, can utilize practically any gear ratio. They have a driving mode and a self-locking mode when inertial or backdriving torque is applied to the output gear. Earlier these gears had a low (<50%) driving efficiency that limited their application. Then it was proved [70] that a higher driving efficiency in such gear drives is possible. The self-locking conditions were analyzed [71].

### 6.3.1 Self-Locking Conditions

Figure 6.18 presents conventional gears (a) and self-locking gears (b) in driving and backdriving modes. Figure 6.19 presents conventional gears (a) and self-locking gears (b) in driving and inertial driving modes. Conventional gear drives usually have the pitch point  $P$  located on an active portion of the contact line  $B_1$ - $B_2$  (Figures 6.18a and 6.19a). This pitch point location provides low specific sliding velocities and as a result, high driving efficiency. In the case where such gears are driven by a resistant load or inertia applied to output shaft, they are rotating freely.

In Figures 6.18 and 6.19:

$T_1$  = driving pinion torque

$T_2$  = driven gear torque

$T'_2$  = driving torque, applied to the gear

$T'_1$  = driven torque, applied to the pinion

$F$  = driving force

$F'$  = driving force, when the backdriving or inertial torque is applied to the gear

$\alpha_w$  = operating transverse pressure angle

$\gamma = \arctan(f)$ , friction angle

$f$  = average friction coefficient

In order to achieve self-locking, pitch point  $P$  should be located off the active portion of the contact line  $B_1$ - $B_2$ . There are two options. Option 1 is when point  $P$  is placed between a center of the pinion  $O_1$  and point  $B_2$ , where the outer diameter of the gear intersects the line contact. This makes the self-locking possible, but the driving efficiency will be low under 50% [70]. Option 2 (Figures 6.18b and 6.19b) is when point  $P$  is placed between point  $B_1$ , where the outer diameter of the pinion intersects the line contact, and a center of the gear  $O_2$ . This type of self-locking gear has a relatively high driving efficiency of >50%.

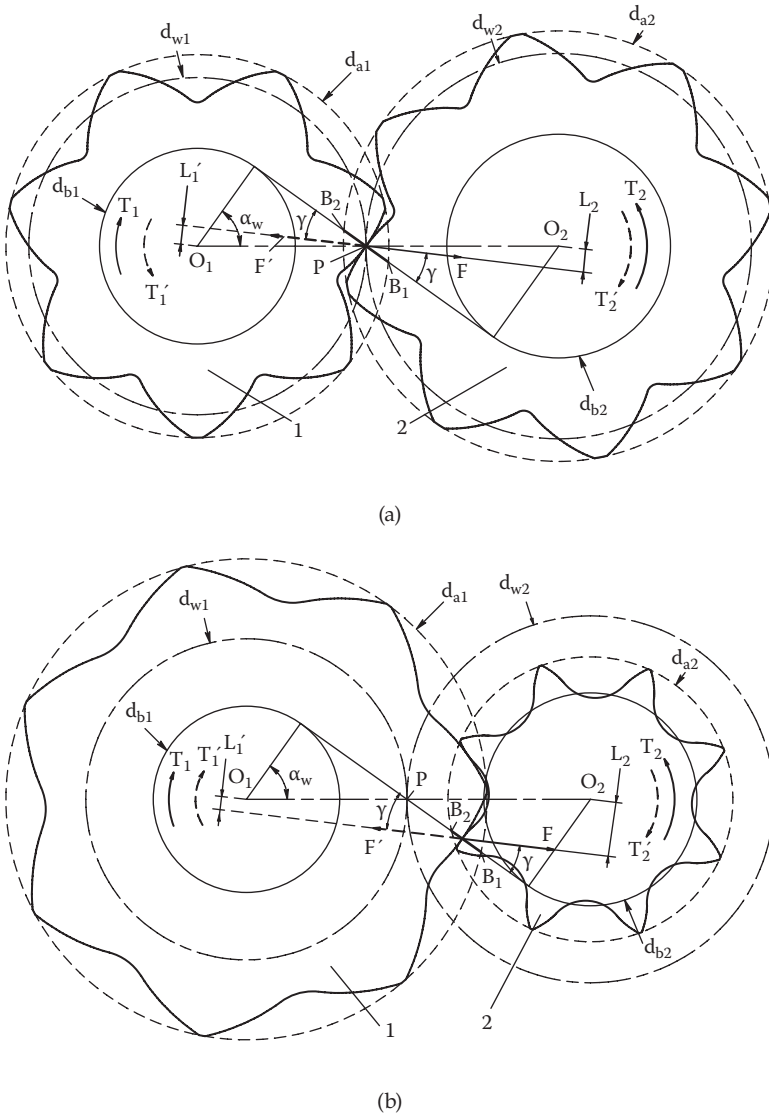


**FIGURE 6.18**

Conventional (a) and self-locking (b) gears. 1 - driving pinion; 2 - driven gear. Solid lines show normal driving operation, dashed lines show the case when driven gear 2 becomes driven by resistant load. (From Kapelevich, A.L., and E. Taye, *Gear Solutions*, May 2012, 53–58. With permission.)

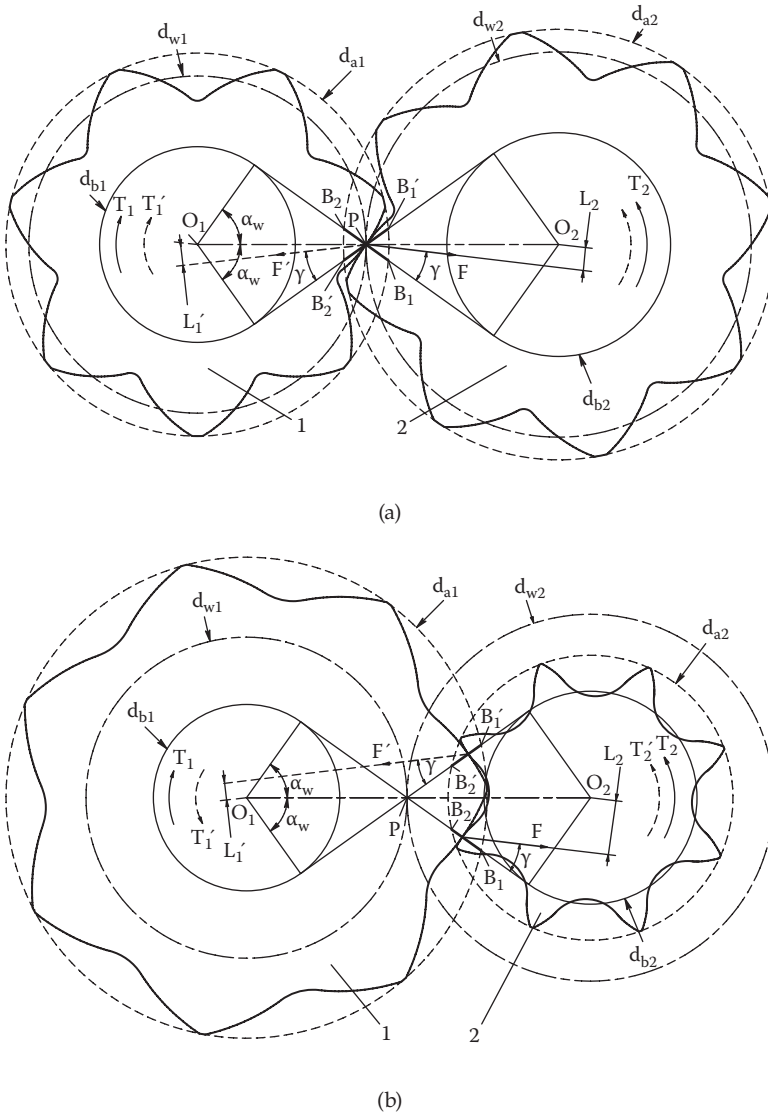


**FIGURE 6.19**

Conventional (a) and self-locking (b) gears. 1 - driving pinion; 2 - driven gear. Solid lines show normal driving operation, dashed lines show the case when driven gear 2 becomes driven by inertia. (From Kapelevich, A.L., and E. Taye, *Gear Solutions*, May 2012, 53–58. With permission.)



An additional necessary condition of self-locking is to have a sufficient friction angle  $\gamma$  to deflect the force  $F'$  beyond the center of the pinion  $O_1$ . It creates the resisting self-locking moment (torque)  $T'_1 = F' \times L'_1$ ;  $L'_1$  is a lever of the force  $F'_1$ . This condition can be presented as  $L'_{1min} > 0$  or

$$\gamma > \arctan\left[\frac{1}{(1 + u) \times \tan \alpha_w - u \times \tan \alpha_{a2}}\right] \tag{6.53}$$

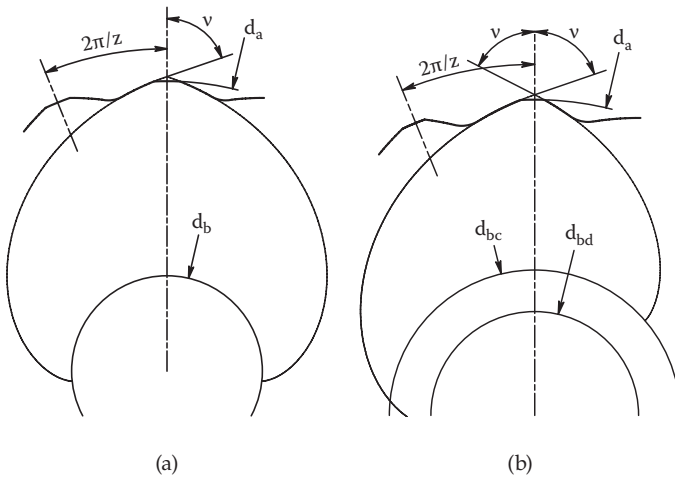
or

$$f > \frac{1}{(1 + u) \times \tan \alpha_w - u \times \tan \alpha_{a2}}, \tag{6.54}$$

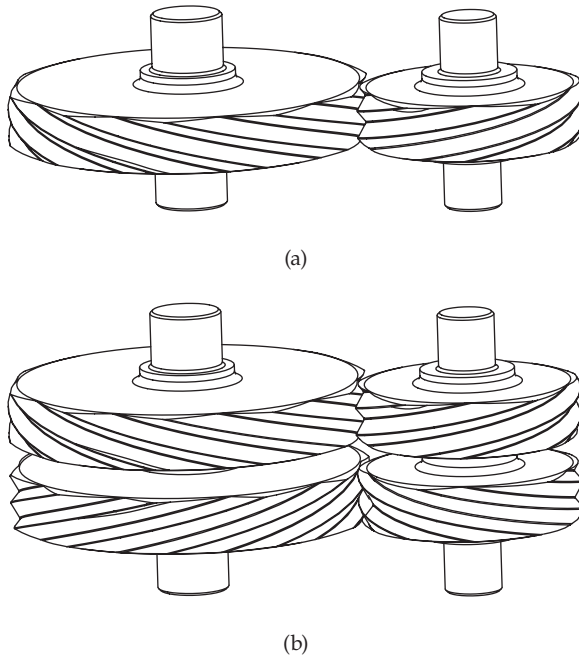
where  $u = z_2/z_1$  is the gear ratio,  $z_1$  and  $z_2$  are the pinion and gear number of teeth, and  $\alpha_{a2} = \arccos \frac{d_{b2}}{d_{a2}}$  is the involute profile angle at the tip of the gear tooth.

### 6.3.2 Self-Locking Gear Design

Self-locking gears are custom and suitable for Direct Gear Design® application to define the gear tooth geometry (Figure 6.20) [72]. Self-locking conditions (6.53) and (6.54) require high pressure angle and high sliding friction in the tooth contact. If the sliding friction coefficient is  $f = 0.1 - 0.3$ , it requires the transverse operating pressure angle to be  $\alpha_w = 75 - 85^\circ$ . As a result,



**FIGURE 6.20** Self-locking gear tooth geometry: (a) symmetric tooth profile, (b) asymmetric tooth profile.  $d_a$  - tooth tip circle diameter;  $d_b$  - base circle diameter;  $v$  - involute intersection profile angle;  $z$  - number of teeth. Subscripts  $d$  and  $c$  are for the drive and coast flanks of the asymmetric tooth. (From Kapelevich, A.L., and E. Taye, *Gear Solutions*, May 2012, 53–58. With permission.)

**FIGURE 6.21**

Helical (a) and double-helical (b) self-locking gears. (From Kapelevich, A.L., and E. Taye, *Gear Solutions*, May 2012, 53–58. With permission.)

a transverse contact ratio  $\epsilon_\alpha < 1.0$  (typically 0.4–0.6). Lack of a transverse contact ratio should be compensated by the axial contact ratio  $\epsilon_\beta$  to guarantee the total contact ratio  $\epsilon_\gamma = \epsilon_\alpha + \epsilon_\beta \geq 1.0$ . This can be achieved by using helical gears (Figure 6.21a). However, helical gears generate high axial force that is applied to bearings. Double-helical (or herringbone) gears (Figure 6.21b) allow this force to be neutralized.

Another axial force free self-locking gear design option is application of laminated gears (Figure 6.22). They have several layers assembled with an angular shift. These layers are engaged in gear mesh with the mating gear layers consecutively. The rational number of layers is three or more. They provide necessary axial contact ratio, like in helical gears, but without axial force. Since these gears are engaged in mesh one layer at a time, every layer face width must provide sufficient tooth surface endurance in both driving and self-locking modes. This is especially important considering very high transverse pressure angles resulting in increased bearing loads that could be up to four to five times higher than for conventional  $20^\circ$  pressure angle gears with the same driving torque. Bearing selection, and shafts and gear-box housing design should be done accordingly to hold this increased load.

Application of asymmetric teeth for conventional unidirectional drives allows improvement of their performance. In self-locking gears that should

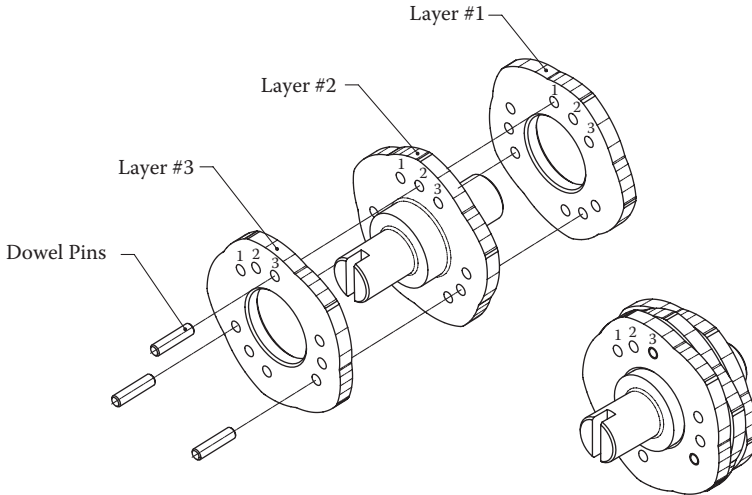


**FIGURE 6.22**  
Laminated self-locking gears.

prevent backdriving, the same tooth flank is loaded in both driving and locking modes (Figure 6.18b). In this case, the asymmetric tooth profile allows increase of the drive transverse contact ratio in comparison with the symmetric tooth profile. It makes it possible to reduce the helix angle and axial load. The article [73] describes the self-locking gear arrangement to prevent backdriving, which allows the use of different tooth flanks to increase the driving mode efficiency, although such an arrangement requires a special gear mechanism that changes rotation direction for the self-locking mode.

In self-locking gears that should prevent inertial driving, different tooth flanks are used for driving and locking modes (Figure 6.19b). In this case, an asymmetric tooth profile with a low-pressure angle provides higher efficiency for the driving mode and the opposite high-pressure angle tooth profile is used for reliable self-locking.

An example of the self-locking gear is shown in Figure 6.23. These gears were designed, made, and tested to explore their driving and locking performance [72]. The gear data are presented in Table 6.5.

Average driving efficiency of the self-locking gear obtained during testing was above 85%. This gear set testing has confirmed the self-locking condition in the backdriving mode.

Initially self-locking gears were used in the textile industry [69]. However, this type of gear has many potential applications, like in lifting mechanisms, assembly tooling, and other gear drives where the backdriving or inertial driving is not permissible. One such potential application of the self-locking gears is for an automotive engine continuously variable valve lift system [74].

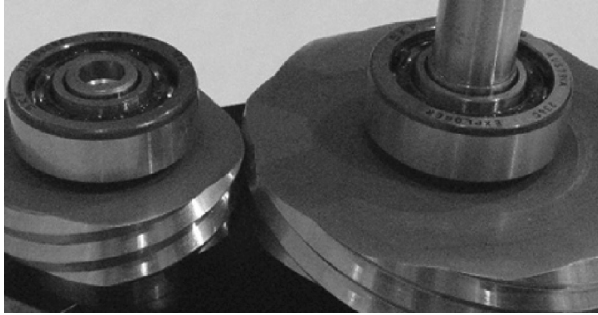


**FIGURE 6.23**  
Helical self-locking gears. (From Kapelevich, A.L., and E. Taye, *Gear Solutions*, May 2012, 53–58. With permission.)

**TABLE 6.5**  
Self-Locking Gear Data

Gear	Input	Output
Number of teeth	6	11
Normal module, mm	1.500	
Normal pressure angle	63°	
Helix angle on the pitch diameter	75°	
Transverse pressure angle	82.5°	
Transverse contact ratio	0.50	
Axial contact ratio	2.00	
Driving torque, Nm	0.5	

## 6.4 Plastic Gear Design Specifics

Just a few decades ago plastic gears were considered for use mainly for low-demand applications: toys, some consumer product transmissions, etc. Nowadays progress in polymer materials and injection molding processing has allowed drastic expansion of plastic gear application areas. They are used not only for motion transmissions, but also in moderate load power drives in automotive, medical, defense, agriculture, and many other industries.

Comprehensive books about plastic gears are written by C. Adams [75] and V.E. Starzhinsky with coauthors [76]. The AGMA standards [77, 78] present tooth proportions for plastic gears and the AGMA standard [79] gives a polymer material selection guideline. The paper [80] describes polymer gear wear behavior and its performance prediction based on the extensive investigations on the gear thermal mechanical contact both numerically and experimentally. The papers [81, 82] study asymmetric plastic spur gears.

### 6.4.1 Polymer Benefits and Limitations

Benefits of polymer gears in comparison to metal ones include:

- Low cost of injection molding process for high-volume production gear drive components
- Low vibration and noise
- Low weight and inertia
- No corrosion
- No electric current conductivity
- In some cases they can work without external (oil or grease) lubrication

These advantages made possible usage of polymers for a wide variety of gear drives. However, there are limitations that must be taken into account considering plastic gears instead of metal ones:

- Low strength and wear resistance
- Low thermal conductivity and maximum operating temperature
- Wide deviation of material property parameters
- Sensitivity to operating conditions (temperature and humidity)
- Low modulus of elasticity and increased tooth deflection
- Limited injection molding process accuracy
- Creep

Main polymer gear materials are acetals (POM) and nylons (6, 66, 610), polyesters, and polycarbonates. They can be used with operating temperatures up to 150°C. For elevated temperature (<170°C) suitable gear polymers are polyphthalamide (PPA), nylon 46, and similar. High-temperature (<200°C) plastic materials include polyetherimide (PEI), polyetheretherketone (PEEK), and liquid crystal polymers (LCPs).

Some drawbacks of gear plastics properties can be improved by different additives to polymer composition. Additives for higher flexural strength include glass, carbon, and aramid (Kevlar) fibers. Tooth flank wear resistance of nonlubricated plastic gears can be increased by antiwear and antifriction additives: silicone, polytetrafluoroethylene (PTFE), graphite powders, molybdenum disulfide (MoS<sub>2</sub>), etc.

### 6.4.2 Direct Gear Design of Polymer Gears

Although there are machined plastic gears, the most common and cost-effective plastic gear fabrication technology is injection molding. This process does not use the generating rack type tooling to form gear teeth. Besides, molding

tool cavity shape is unique for every gear profile. This makes plastic molded gears more acceptable for Direct Gear Design that maximizes performance of plastic gearing [83] by compensating some polymer property limitations. Its guidelines for polymer gears include:

- Increased safety factors to guarantee sufficient tooth strength considering a wide range of material properties deviation, depending on molding process parameters, operating temperature, humidity, etc.
- Increased tooth size (larger module or coarser diametral pitch) to reduce bending stress
- Lower number of teeth to fit the increased tooth size into required center distance with given gear ratio
- Higher operating pressure angle and contact ratio to reduce bending and contact stress, and increase tooth flank wear resistance
- Bending stress balance that equalizes safety factors of mating gears
- Specific sliding balance for higher efficiency and tooth flank wear resistance
- Root fillet profile optimization for bending stress reduction
- Asymmetric tooth profile for unidirectional gear drives

#### 6.4.3 Metal-to-Plastic Conversion

Besides original plastic gear designs, applications of plastic gears are often considered to replace relatively lightly loaded metal gears usually for cost and noise reduction. In this case exact replication of metal gear design typically does not work, because of material property difference, especially the low strength of polymers in comparison with metals. Design of plastic gears should compensate for the lack of polymer strength following guidelines described in the previous section. Table 6.6 presents an example of metal-to-plastic gear conversion. It shows how Direct Gear Design makes it possible to replace metal machined gears with plastic ones providing required performance and sufficient safety factors.



---

## 6.5 Gear Tooth Profile Modeling

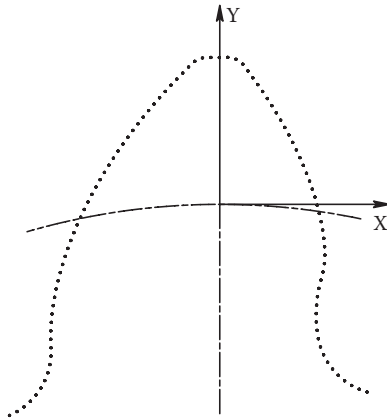
A gear tooth profile includes involute flanks, root fillets, tooth tip lands, and tooth tip radii or chamfers. As a result of the Direct Gear Design geometry calculation procedure, a tooth profile is defined by  $X,Y$ -coordinate points (Figure 6.24). Usually a number of these points vary from several hundred to several thousand.

**TABLE 6.6**

Example of Metal-to-Plastic Gear Conversion

Design Method	Metal Gear Pair		Plastic Gear Pair	
	Traditional (Standard 20° Pressure Angle Tool)		Direct	
	Driving	Driven	Driving	Driven
Number of teeth	34	54	17	27
Module, mm		0.5		1.0
Pitch diameter, mm	17.0	27.0	17.0	27.0
Center distance, mm		22.0		22.0
Face width, mm	6.0	6.0	6.0	6.0
Operating pressure angle, °		20.0		27.0
Operating contact ratio		1.56		1.27
Root fillet	Trochoidal	Trochoidal	Optimized	Optimized
Mesh efficiency, %		98.8		98.2
Maximum temperature, °C		110		110
Maximum driving torque, Nm	1.0		1.0	
Maximum bending stress, MPa	128	130	45	45
Gear material	Steel 4140 normalized		Amodel AS-1133 HS	
Yield tensing strength, MPa		635		193
Minimum bending safety factor	5.0	4.9	4.3	4.3
Image of driving gear				

For computer-aided design (CAD) gear modeling, and computer numerical control (CNC) machining, the coordinate point presentation of the tooth profile coordinate points should be replaced by some mathematical curves, for example, using the B-spline interpolation [84]. N.J. Kleiss [85] has applied the tangent circular arc approximation for gear tooth modeling. Y.V. Shekhtman used this approximation approach and developed an algorithm of fitting the tangent circular arc with given accuracy, a maximum deviation from initial  $X,Y$ -coordinate points. Circular arcs describing the tooth profile are consequently connected and have equal first derivatives at the connection point for smooth transition from one arc to another. A number of these arcs depend on the tooth size (module or diametral pitch), its profile, number of initial points, and required approximation accuracy. This accuracy is deviation  $\Delta$  from the coordinate point to the closest point of the arc (Figure 6.25a).

**FIGURE 6.24**

Tooth profile coordinate points.

Deviation  $\Delta$  must be much less than the tooth profile tolerance. Typically  $\Delta$  is about 0.0005 mm (or 0.00002 in.), which makes it virtually undetectable by the tooth profile inspection. Then this approximation does not affect tooth flank accuracy. The number of arcs per one gear tooth usually varies from 10 to 30 or more. Application of the tangent circular arc approximation in comparison with the B-spline interpolation for gear tooth modeling allows creation of more compact CAD files.

The tooth tip and root areas of the tooth profile usually require correction, because the tangent arcs lie in proximity of the  $X,Y$ -coordinate points. The tooth tip land arcs may have its centers not coinciding with the center of the gear. In order to fix it, the top land is replaced with the tooth tip diameter arc and tooth tip radii or chamfers (Figure 6.26).

Polar duplication of the tooth profile is used to create a whole gear profile. The ends of the connected tooth profiles may not coincide exactly. Then the tangent arc should be fit to connect the neighboring tooth profiles (Figure 6.27).

If the tangent arc approximation technique is applied to the whole symmetric tooth, the left and right tooth flank arcs are not exactly symmetric. It makes sense to fit tangent arcs to only one-half of the tooth profile and then mirror it also fixing the tooth tip and root areas (Figure 6.28).



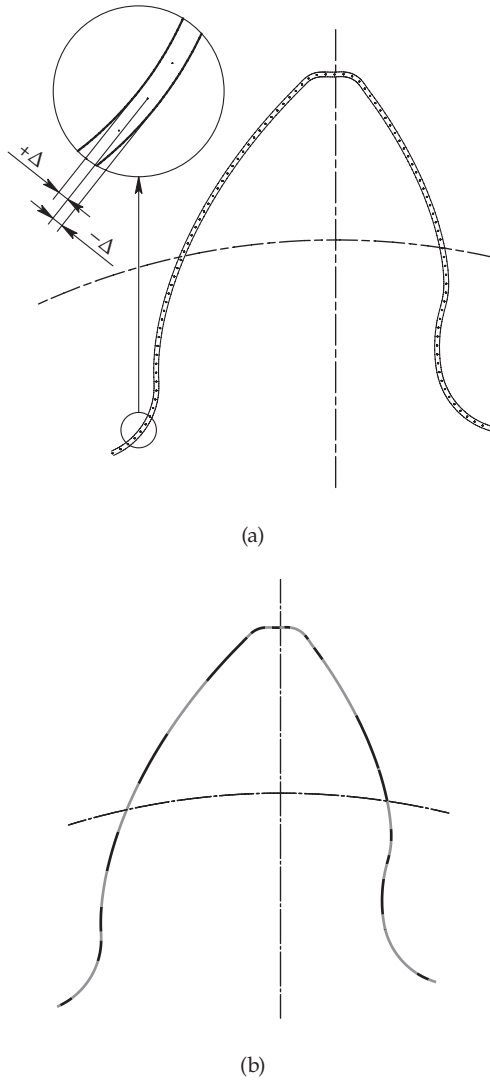


**FIGURE 6.25** Tangent circular arc approximation: (a) deviation  $\Delta$  from coordinate points, (b) resulting tooth profile.

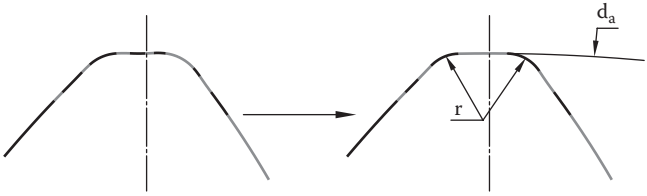


**FIGURE 6.26**  
Tooth tip correction.

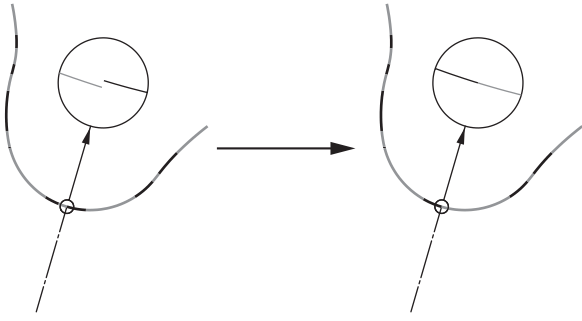


**FIGURE 6.27**  
Tooth root correction.

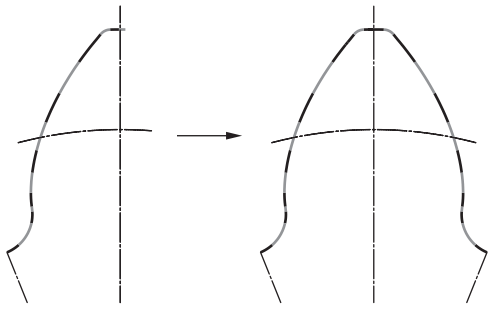


**FIGURE 6.28**  
Symmetric tooth root construction.



# 7

---

## *Tolerancing and Tolerance Analysis*

---

Every engineer should be aware that “the devil is in the details.” Assigned manufacturing tolerances are some of those details of gear drive design. Tolerances that are seemingly negligibly small in comparison to nominal gear dimensions greatly affect gear drive performance and product cost. Incorrect tolerancing can turn a potentially successful project into a total failure.

This chapter considers tolerance selection approach and shows how tolerancing influences some gear pair performance parameters.

---

### **7.1 Gear Specification**

Comprehensive gear drawing specification is critically important. With a noncompletely specified drawing a designer practically delegates his responsibilities to a gear supplier, letting him guess about the designer’s actual intentions. A main problem here is that a supplier is not in a position to do this, even if he has gear design experience, because he usually does not know enough about gear drive application specifics, loads, RPMs, operating cycle and conditions, etc. As a result of such guessing, gears are typically made the most cost-efficient for a supplier in a way that may compromise gear drive performance. The 3D CAD gear model also cannot replace a properly specified gear drawing.

A gear drawing specification must completely define gear geometry, accuracy level (standard accuracy grade or accuracy parameters), reference dimensions, all critical dimensions with tolerances, gear inspection dimensions (for example, measurement over/between pins or balls, span measurement, etc.), surface finish, material data including its grade, heat treatment (surface and core hardness, harden case depth), and post-machining surface treatment (for example, shot peening, super finishing, coating, etc.). It may also describe gear tooth flank microgeometry (tip and root relief, lead crowing) and contain information about tooling, processing, material specimen condition, and some additional information. Most gear geometry and inspection dimensions are included in the gear specification tables. Examples of proper gear drawing specification tables for most types of involute gears are described in [86, 87].

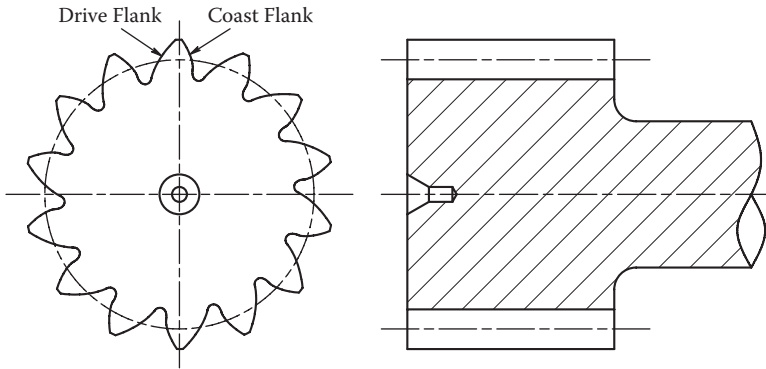


**FIGURE 7.1**

Asymmetric tooth flank identification in the gear drawing.

The Direct Gear Design<sup>®</sup> method provides a sufficient gear drawing specification that is very similar to a proper drawing specification for traditionally designed gears to make it understandable to a gear supplier and exclude any guesswork or confusion, although this specification typically has some additional data. For example, it should have a description of the optimized root fillet profile (as a coordinate point table or as part of the CAD tooth profile that accompanies a gear drawing) and its tolerance. Tooth flanks of an asymmetric gear should clearly be identified in the gear drawing to avoid potential assembly problems (Figure 7.1). A gear specification table for gears with asymmetric teeth contains geometry parameters of both drive and coast tooth flanks (see for example Table 7.1).

---

## 7.2 Accuracy Selection

Gear accuracy selection, defined by gear tolerances, depends on gear drive application, operating conditions, and technical and market performance requirements. This selection is also affected by chosen gear fabrication technology, materials, heat treatment, etc. Gear accuracy is defined by a set of tolerances. Types of gear tolerances and their effects on fabrication, cost, and function of a gear drive are described in [38]. For high-performance gear drives, such as, for example, aerospace and racing transmissions, the functional requirements are primary factors for tolerance selection. For less demanding gear drive applications, other factors, such as cost, manufacturability, availability of fabrication equipment, and tooling, prevail. In many cases gear accuracy standards, like, for example, [88–91], are used for tolerance selection. There are also gear dimensions, for which tolerances are not defined by accuracy standards. Such dimensions are the tooth tip diameter,

**TABLE 7.1**  
Gear Specification Table Example

Number of teeth		a
Module		b
Reference diameter		b
Pressure angle at reference pitch diameter	Drive flank	b
	Coast flank	b
Base diameter	Drive flank	b
	Coast flank	b
Form diameter	Drive flank	Min/max <sup>a</sup>
	Coast flank	Min/max <sup>a</sup>
Tooth tip diameter		Min/max <sup>a</sup>
Root diameter		Min/max <sup>a</sup>
Tooth thickness at reference pitch diameter		Min/max <sup>a</sup>
Tooth tip radius		Min/max <sup>a</sup>
Face width		Min/max <sup>a</sup>
Pin diameter		b
Measurement over two pins		Min/max <sup>a</sup>
Accuracy grade per AGMA 2015-A01		b
Run-out tolerance, $F_r$		a
Total cumulative pitch tolerance, $F_p$		a
Single pitch tolerance, $f_{pt}$		a
Profile tolerance	Total, $F_\alpha$	a
	Form, $f_{f\alpha}$	a
	Slope, $f_{H\alpha}$	a
Helix tolerance	Total, $F_\beta$	a
	Form, $f_{f\beta}$	a
	Slope, $f_{H\beta}$	a
Root fillet profile tolerance		a, c
Mating gear part number		b
Mating gear number of teeth		b
Center distance		Min/max <sup>b</sup>

<sup>a</sup> Critical parameter or dimension.

<sup>b</sup> Reference parameter or dimension.

<sup>c</sup> Root fillet profile tolerance is not defined by gear accuracy standards and should be assigned by designer.

root diameter, form diameter, gear face width, tooth tip radius or chamfer, etc. The standards also do not cover the tooth microgeometry tolerances defining acceptable limits of the tooth tip and root relief, and lead crowning. This tolerance selection is based on gear drive application, operating conditions, experience with the previously designed similar drives, and the prototype performance testing results.

Direct Gear Design utilizes the same tolerance selection criteria and the same standards as traditional gear design. At the same time, it may add its

own specific tolerance requirements. One such requirement is the root fillet profile tolerancing. Although the gear tooth root fillet is an area of maximum bending stress concentration, existing gear accuracy standards do not define the fillet profile tolerances, and in traditional gear design its profile and accuracy are marginally defined on the gear drawing by typically very generous root diameter tolerance and, in some cases, by the minimum fillet radius.

Direct Gear Design optimizes the gear tooth root fillet profile for minimum bending stress concentration. This requires that the root fillet profile must be comprehensibly specified, toleranced, and then inspected. If the whole gear profile, including the root fillet, is shaped by the same fabrication process and tooling, the fillet profile tolerance can be the same as the involute flank tolerance that is specified by the standards. However, some gear fabrication methods apply separate machining processes and tooling for final machining of the tooth involute flank and the root fillet. One such method uses the gear cutters (hobs or shaper cutters) with protuberances for final machining of the tooth root fillet profile and preliminary machining of the tooth flanks, leaving a stock for grinding or shaving after heat treatment. As a result, the involute tooth flank and root fillet accuracy are very different. In this case, the fillet profile tolerance is selected according to accuracy grade achievable by the fillet profile machining. The root diameter tolerance of directly designed gears is defined considering the root fillet profile tolerance.

---

### 7.3 Tolerance Analysis

A goal of a tolerance analysis is to verify the mating gear pair design data in order to guarantee the adequate normal backlash, sufficient root clearance, and minimal acceptable contact ratio at any possible tolerance combinations and operating conditions.

Operating conditions include operating temperature and humidity ranges. A wide operating temperature range noticeably changes gear drive dimensions (particularly for large gear transmissions) and may greatly affect tolerance analysis results in case of dissimilar material applications for gears, gear housing, shafts, etc. This is especially critical for gear drives made with polymer components. Besides, some gear polymers like nylons absorb moisture, resulting in increased gear dimensions. Typical input data for a tolerance analysis are presented in Table 7.2. Tolerance analysis defines the mating gear normal backlash, contact ratio, and root clearances at two extreme (minimum and maximum) value combinations of tolerances and parameters presented in Table 7.2.

**TABLE 7.2**

Tolerance Analysis Input Data

Dimensions and Tolerances	Symbol	Units
Number of teeth of mating gears	$z_1, z_2$	—
Normal module or diametral pitch at reference pitch diameter	$m_n$ or $DP_n$	mm or 1/in.
Normal pressure angle at reference pitch diameter	$\alpha$	°
(for asymmetric gears: drive and coast pressure angles)	$\alpha_d$ and $\alpha_c$	°
Helix angle at reference pitch diameter	$\beta$	°
Tooth tip diameters (minimum/maximum values)	$d_{amin1}, d_{amax1},$ $d_{amin2}, d_{amax2}$	mm or in. mm or in.
Root diameters (minimum/maximum values)	$d_{rmin1}, d_{rmax1},$ $d_{rmin2}, d_{rmax2}$	mm or in. mm or in.
Normal tooth thickness at reference pitch diameter (minimum/maximum values)	$S_{nmin1}, S_{nmax1},$ $S_{nmin2}, S_{nmax2}$	mm or in. mm or in.
Tooth tip radius (minimum/maximum values)	$R_{amin1}, R_{amax1},$ $R_{amin2}, R_{amax2}$	mm or in. mm or in.
Gear face width (minimum/maximum values)	$b_{min1}, b_{max1},$ $b_{min2}, b_{max2}$	mm or in. mm or in.
Run-out tolerance <sup>a</sup>	$F_{r1}, F_{r2}$	mm or in.
Single pitch tolerance	$f_{p1}, f_{p2}$	mm or in.
Total profile tolerance	$F_{\alpha1}, F_{\alpha2}$	mm or in.
Total helix tolerance	$F_{\beta1}, F_{\beta2}$	mm or in.
Housing center distance	$a_{min}, a_{max}$	mm or in.
Bearing radial gap	$\delta_{min1}, \delta_{max1},$ $\delta_{min2}, \delta_{max2}$	mm or in. mm or in.
<i>Operating Conditions</i>		
Temperature (minimum/ambient <sup>b</sup> /maximum values)	$T_{min}, T_{amb}, T_{max}$	°C or °F
Humidity (minimum/ambient <sup>b</sup> /maximum values)	$RH_{min},$ $RH_{amb},$ $RH_{max}$	% % %
<i>Material Properties</i>		
Linear coefficient of thermal expansion (CTE)	$\delta_l$	mm/mm/°C or in./in./°F
Moisture expansion coefficient (CME) <sup>c</sup>	$\delta_m$	mm/mm/% or in./in./%

<sup>a</sup> In some cases the total radial composite deviation ( $F_r''$ ), which is also known as the total composite error (TCE), is used instead of the run-out tolerance.

<sup>b</sup> Ambient temperature or humidity in this content is inspection lab temperature or humidity. Typical ambient temperature is 20°C or 68°F and ambient humidity is about 50% RH.

<sup>c</sup> For moisture absorbing materials.



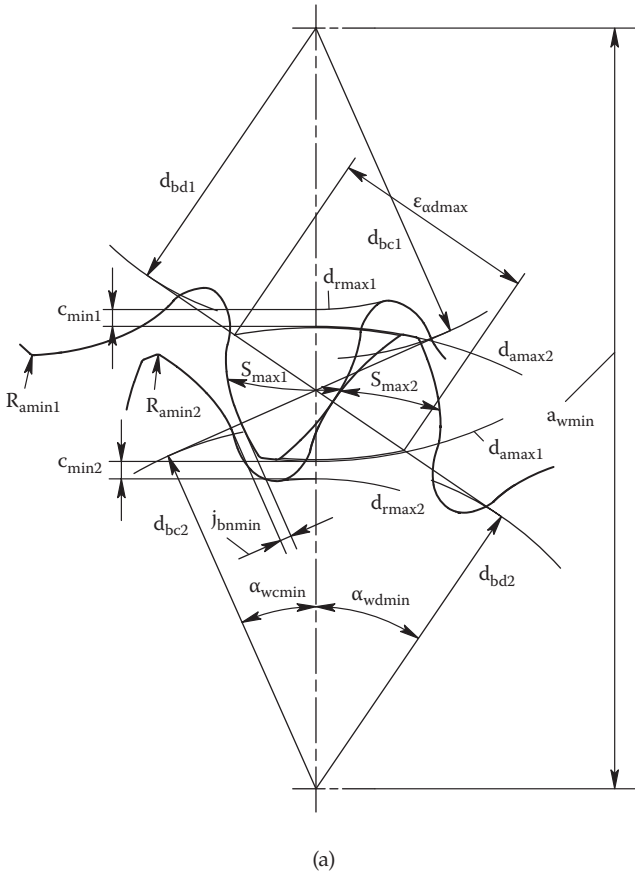
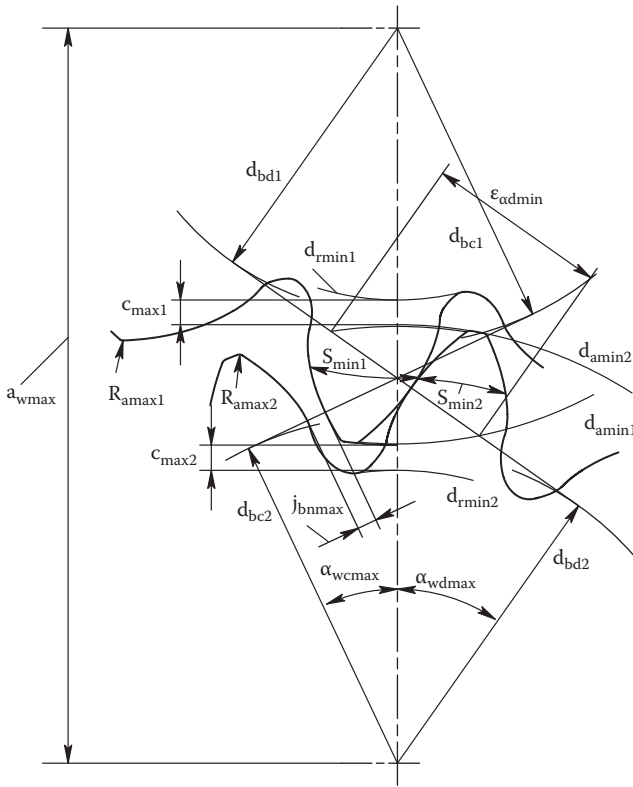


**FIGURE 7.2**

Cases 1 (a) and 2 (b) of extreme tolerance combinations for external gear pair with asymmetric teeth.

Tolerance analysis for an external gear pair considers two cases:

*Case 1* (Figure 7.2a): Resulting in minimum normal backlash and radial clearances, and maximum contact ratio. This gear tolerance buildup includes the minimum housing center distance, bearing radial plays, and tooth tip radii, and the maximum tooth tip diameters, root diameters, and normal tooth thicknesses of mating gears. In this case, run-outs of both mating gears should reduce the effective center distance, and the tooth profile, pitch, and helix maximum tolerance combination increases the effective tooth thickness. Minimum or maximum operating temperature value is selected depending on gear and housing material combination to reduce the effective center distance. If, for example, the material combination is the steel gears and aluminum housing, the minimum effective center distance is



(b)

FIGURE 7.2 (continued)

achieved at the minimum operating temperature, because the CTE of steel is lower than that of aluminum. If the material combination is the plastic gears and aluminum housing, the minimum effective center distance is achieved at the maximum operating temperature, because the CTE of plastics is higher than that of aluminum. If gears or gear drive housing are made out of the moisture absorbing materials (nylon, for example), the minimum or maximum value of operating humidity is selected depending on the gear and housing material combination to reduce the effective center distance.

Case 2 (Figure 7.2b): Resulting in the maximum normal backlash and radial clearances, and minimum contact ratio. This gear tolerance buildup includes the maximum housing center distance, bearing radial plays, and tooth tip radii, and the minimum tooth tip diameters, root diameters, and normal tooth thicknesses of mating gears. In this case, run-out of both mating gears should increase the effective center distance, and the tooth profile, pitch, and helix

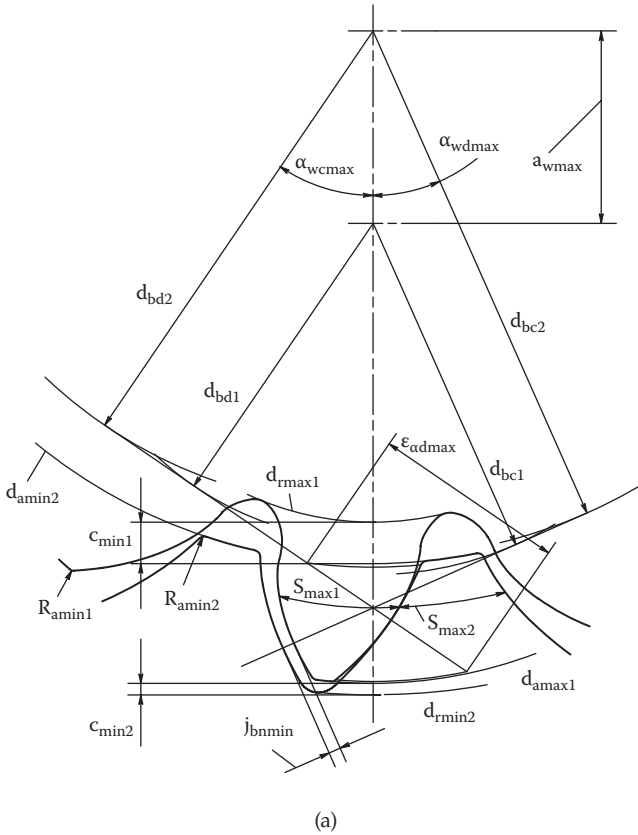


**FIGURE 7.3**  
Cases 1 (a) and 2 (b) of extreme tolerance combinations for internal gear pair with asymmetric teeth.

tolerances combination does not change the effective tooth thickness. Minimum or maximum operating temperature and humidity values are selected depending on gear and housing material combination to increase the effective center distance.

For an internal gear pair, a tolerance analysis approach is the same, but selection of parameters limits is different.

*Case 1* (Figure 7.3a): Resulting in the minimum normal backlash and radial clearances, and maximum contact ratio. This gear tolerance buildup includes the maximum housing center distance, minimum bearing radial plays and tooth tip radii, maximum pinion tooth tip and root diameters of the pinion, minimum ring gear tooth tip and root diameters, and maximum normal tooth thickness. In this case, the gear run-outs should increase the effective center distance, and

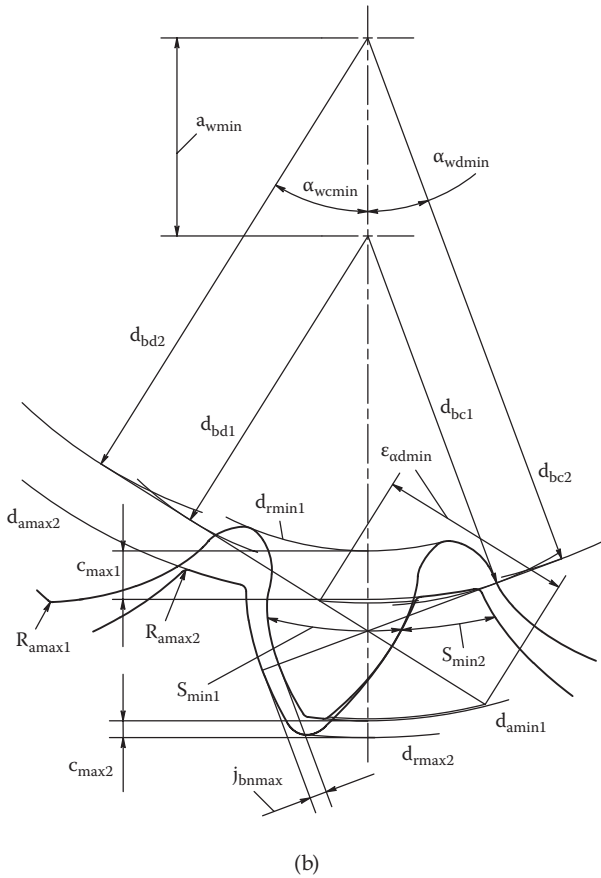


FIGURE 7.3 (continued)

the tooth profile, pitch, and helix tolerances combination increases the effective tooth thickness. Minimum or maximum operating temperature and humidity values are selected depending on the gear and housing material combination to increase the effective center distance.

Case 2 (Figure 7.3b): Resulting in the maximum normal backlash and radial clearances, and minimum contact ratio. This gear tolerance buildup includes the minimum housing center distance, maximum bearing radial plays and tooth tip radii, minimum pinion tooth tip and root diameters of the pinion, maximum ring gear tooth tip and root diameters, and minimum normal tooth thickness. In this case, the gear run-outs should reduce the effective center distance, and the tooth profile, pitch, and helix tolerances combination does not affect the effective tooth thickness. Minimum or maximum operating temperature and humidity values are selected depending on the gear and housing material combination to reduce the effective center distance.

The tolerance analysis set of equations that allows definition of the minimum and maximum values of the normal backlash, radial clearances, and minimum contact ratio is presented below. It is described for helical gears with asymmetric teeth. For spur gears these equations are used with the zero helix angle, and in the case of symmetric teeth, the pressure angles of the opposite tooth flanks are equal. Here is an assumption that the mating gears and gear drive housing are made out of different materials, and those materials could be moisture absorbing. The operating condition coefficients are:

For gears:

$$\lambda_{o1,2} = 1 + \delta_{t1,2}(T_o - T_{amb}) + \delta_{m1,2}(RH_o - RH_{amb}) . \quad (7.1)$$

For gear drive housing:

$$\lambda_{oh} = 1 + \delta_{th}(T_o - T_{amb}) + \delta_{mth}(RH_o - RH_{amb}) , \quad (7.2)$$

where  $T_o$  and  $RH_o$  are operating temperature and humidity, which can have minimum, ambient, or maximum values. Symbols 1,2 and  $h$  are for the pinion, gear, and housing, accordingly.

For ambient conditions coefficients  $\lambda_{o1,2}$  and  $\lambda_{oh}$  are equal to 1.0. For real operating conditions major gear and housing dimensions should be adjusted by these coefficients:

Center distance:

$$a_{\min} = \lambda_{oh} \times a_{\min} \quad \text{and} \quad a_{\max} = \lambda_{oh} \times a_{\max} . \quad (7.3)$$

Tooth tip diameters:

$$d_{a\min1,2} = \lambda_{o1,2} \times d_{a\min1,2} \quad \text{and} \quad d_{a\max1,2} = \lambda_{o1,2} \times d_{a\max1,2} . \quad (7.4)$$

Root diameters:

$$d_{r\min1,2} = \lambda_{o1,2} \times d_{r\min1,2} \quad \text{and} \quad d_{r\max1,2} = \lambda_{o1,2} \times d_{r\max1,2} . \quad (7.5)$$

Normal tooth thicknesses:

$$s_{n\min1,2} = \lambda_{o1,2} \times s_{n\min1,2}$$

and

$$s_{n\max1,2} = \lambda_{o1,2} \times s_{n\max1,2} + f_{pt1,2} + F_{\alpha1,2} + F_{\beta1,2} . \quad (7.6)$$

Gear face widths:

$$b_{\min 1,2} = \lambda_{o1,2} \times b_{\min 1,2} \text{ and } b_{\max 1,2} = \lambda_{o1,2} \times b_{\max 1,2} . \quad (7.7)$$

It is not necessary to apply operating condition coefficients  $\lambda_{o1,2}$  and  $\lambda_{oh}$  to small dimensions like the tooth tip radii, the bearing radial gaps, or accuracy tolerances for operating conditions, because typically it does not make any noticeable difference.

Then the operating center distance values  $a_{w\min}$  and  $a_{w\max}$  are:

For external gearing:

$$a_{w\min} = a_{\min} - \frac{F_{r1}}{2} - \frac{F_{r2}}{2} + \frac{\delta_{\min 1}}{2} + \frac{\delta_{\min 2}}{2}$$

and

$$a_{w\max} = a_{\max} + \frac{F_{r1}}{2} + \frac{F_{r2}}{2} + \frac{\delta_{\max 1}}{2} + \frac{\delta_{\max 2}}{2} . \quad (7.8)$$

For internal gearing:

$$a_{w\min} = a_{\min} - \frac{F_{r1}}{2} - \frac{F_{r2}}{2} - \frac{\delta_{\max 1}}{2} - \frac{\delta_{\max 2}}{2}$$

and

$$a_{w\max} = a_{\min} + \frac{F_{r1}}{2} + \frac{F_{r2}}{2} - \frac{\delta_{\min 1}}{2} - \frac{\delta_{\min 2}}{2} . \quad (7.9)$$

The reference pitch diameters  $d_{p1,2}$  are:

In the metric system:

$$d_{p1,2} = \frac{m_n z_{1,2} \lambda_{o1,2}}{\cos \beta} . \quad (7.10)$$

In the English system:

$$d_{p1,2} = \frac{z_{1,2} \lambda_{o1,2}}{DP_n \cos \beta} . \quad (7.11)$$

The transverse pressure angles  $\alpha_{td}$  and  $\alpha_{tc}$  at the reference pitch diameters are:

For drive flanks:

$$\alpha_{td} = \arctan\left(\frac{\tan \alpha_d}{\cos \beta}\right). \quad (7.12)$$

For coast flanks:

$$\alpha_{tc} = \arctan\left(\frac{\tan \alpha_c}{\cos \beta}\right). \quad (7.13)$$

The base diameters  $d_{b1,2}$  are:

For drive flanks:

$$d_{bd1,2} = d_{p1,2} \cos \alpha_{td}. \quad (7.14)$$

For coast flanks:

$$d_{bc1,2} = d_{p1,2} \cos \alpha_{tc}. \quad (7.15)$$

The helix angles  $\beta_{bd}$  and  $\beta_{bc}$  at the base diameters are:

For drive flanks:

$$\beta_{bd} = \arctan(\tan \beta \cos \alpha_{td}). \quad (7.16)$$

For coast flanks:

$$\beta_{bc} = \arctan(\tan \beta \cos \alpha_{tc}). \quad (7.17)$$

The tooth tip involute angles  $\alpha_{ad\min 1,2}$  and  $\alpha_{ad\max 1,2}$  are

$$\alpha_{ad\min 1,2} = \arccos\left(\frac{d_{bd1,2}}{d_{a\min 1,2}}\right)$$

and

$$\alpha_{ad\max 1,2} = \arccos\left(\frac{d_{bd1,2}}{d_{a\max 1,2}}\right). \quad (7.18)$$

The helix angles at the tooth tip diameters  $\beta_{a\min 1,2}$  and  $\beta_{a\max 1,2}$  are

$$\beta_{a\min 1,2} = \arctan\left(\tan \beta \frac{\cos \alpha_{td}}{\cos \alpha_{ad\min 1,2}}\right)$$

and

$$\beta_{a\max 1,2} = \arctan\left(\tan \beta \frac{\cos \alpha_{td}}{\cos \alpha_{ad\max 1,2}}\right). \quad (7.19)$$

The effective tooth tip involute angles for gears with external teeth from (2.34) and (2.35) are:

For drive flanks  $\alpha_{ed\min 1,2}$  and  $\alpha_{ed\max 1,2}$ :

$$\alpha_{ed\min 1,2} = \arctan\left(\tan\left(\arccos\left(\frac{d_{bd1,2}}{d_{a\min 1,2} - 2R_{a\max 1,2}}\right)\right) + \frac{2R_{a\max 1,2}}{d_{bd1,2}}\right)$$

and

$$\alpha_{ed\max 1,2} = \arctan\left(\tan\left(\arccos\left(\frac{d_{bd1,2}}{d_{a\max 1,2} - 2R_{a\min 1,2}}\right)\right) + \frac{2R_{a\min 1,2}}{d_{bd1,2}}\right). \quad (7.20)$$

For coast flanks  $\alpha_{ec\min 1,2}$  and  $\alpha_{ec\max 1,2}$ :

$$\alpha_{ec\min 1,2} = \arctan\left(\tan\left(\arccos\left(\frac{d_{bc1,2}}{d_{a\min 1,2} - 2R_{a\max 1,2}}\right)\right) + \frac{2R_{a\max 1,2}}{d_{bc1,2}}\right)$$

and

$$\alpha_{ec\max 1,2} = \arctan\left(\tan\left(\arccos\left(\frac{d_{bc1,2}}{d_{a\max 1,2} - 2R_{a\min 1,2}}\right)\right) + \frac{2R_{a\min 1,2}}{d_{bc1,2}}\right). \quad (7.21)$$

The tooth tip effective involute angles for a gear with internal teeth from (2.34) and (2.35) are:

For drive flanks  $\alpha_{ed\min 1,2}$  and  $\alpha_{ed\max 1,2}$ :

$$\alpha_{ed\min 2} = \arctan\left(\tan\left(\arccos\left(\frac{d_{bd2}}{d_{a\min 2} + 2R_{a\max 2}}\right)\right) - \frac{2R_{a\max 2}}{d_{bd2}}\right)$$



and

$$\alpha_{aed\max 2} = \arctan\left(\tan\left(\arccos\left(\frac{d_{bd2}}{d_{a\max 2} + 2R_{a\min 2}}\right)\right) - \frac{2R_{a\min 2}}{d_{bd2}}\right). \quad (7.22)$$

For coast flanks  $\alpha_{ec\min 1,2}$  and  $\alpha_{ec\max 1,2}$ :

$$\alpha_{ec\min 2} = \arctan\left(\tan\left(\arccos\left(\frac{d_{bc2}}{d_{a\min 2} + 2R_{a\max 2}}\right)\right) - \frac{2R_{a\max 2}}{d_{bc2}}\right)$$

and

$$\alpha_{ec\max 2} = \arctan\left(\tan\left(\arccos\left(\frac{d_{bc2}}{d_{a\max 2} + 2R_{a\min 2}}\right)\right) - \frac{2R_{a\min 2}}{d_{bc2}}\right). \quad (7.23)$$

From (2.21) the asymmetry factor  $K$  is

$$K = d_{bc1,2} / d_{bd1,2} = \cos \alpha_{tc} / \cos \alpha_{td}. \quad (7.24)$$

The involute intersection profile angles  $v_{d\min 1,2}$  and  $v_{d\max 1,2}$  for gears with external teeth are defined from a system of equations:

$$\operatorname{inv}(v_{d\min 1,2}) + \operatorname{inv}(v_{c\min 1,2}) = \operatorname{inv}(\alpha_{td}) + \operatorname{inv}(\alpha_{tc}) + \frac{2s_{n\min 1,2} \tan \alpha_{td}}{d_{bd1,2} \cos \beta} \quad (7.25)$$

and

$$\cos v_{c\min 1,2} = K \cos v_{d\min 1,2}, \quad (7.26)$$

$$\operatorname{inv}(v_{d\max 1,2}) + \operatorname{inv}(v_{c\max 1,2}) = \operatorname{inv}(\alpha_{td}) + \operatorname{inv}(\alpha_{tc}) + \frac{2s_{n\max 1,2} \tan \alpha_{td}}{d_{bd1,2} \cos \beta} \quad (7.27)$$

and

$$\cos v_{c\max 1,2} = K \cos v_{d\max 1,2}. \quad (7.28)$$

The involute intersection profile angles  $v_{d\min 2}$  and  $v_{d\max 2}$  for gears with internal teeth are defined from a system of equations:

$$\operatorname{inv}(v_{d\min 2}) + \operatorname{inv}(v_{c\min 2}) = \operatorname{inv}(\alpha_{td}) + \operatorname{inv}(\alpha_{tc}) + \frac{2(P_n - s_{n\max 1,2}) \tan \alpha_{td}}{d_{bd2} \cos \beta} \quad (7.29)$$

and (7.24), and

$$\text{inv}(v_{d\max 2}) + \text{inv}(v_{c\max 2}) = \text{inv}(\alpha_{td}) + \text{inv}(\alpha_{tc}) + \frac{2(P_n - s_{n\min 2}) \tan \alpha_{td}}{d_{bd2} \cos \beta} \quad (7.30)$$

and (7.26), where  $P_n$  is a normal circular pitch at the reference pitch diameter that is equal to  $P_n = \pi m_n$  or  $P_n = \pi / DP_n$  in the metric or English system, accordingly.

Then operating pressure angles are:

For drive flanks  $\alpha_{wd\min}$  and  $\alpha_{wd\max}$ :

$$\alpha_{wd\min} = \arccos\left(\frac{d_{bd1}(u \pm 1)}{2a_{e\min}}\right)$$

and

$$\alpha_{wd\max} = \arccos\left(\frac{d_{bd1}(u \pm 1)}{2a_{e\max}}\right), \quad (7.31)$$

where  $u = z_2/z_1$  is gear ratio, and + is for the external gearing and – is for the internal gearing.

For coast flanks  $\alpha_{wc\min}$  and  $\alpha_{wc\max}$ :

$$\alpha_{wc\min} = \arccos(K \cos \alpha_{wd\min})$$

and

$$\alpha_{wc\max} = \arccos(K \cos \alpha_{wd\max}). \quad (7.32)$$

The operating transverse tooth thicknesses  $S_{w\min 1,2}$  and  $S_{w\max 1,2}$  are:

For gears with external teeth:

$$S_{w\min 1,2} = \frac{d_{bd1,2}}{2 \cos \alpha_{wd\max}} (\text{inv}(v_{d\min 1,2}) + \text{inv}(v_{c\min 1,2}) - \text{inv}(\alpha_{wd\max}) - \text{inv}(\alpha_{wc\max}))$$

and

$$S_{w\max 1,2} = \frac{d_{bd1,2}}{2 \cos \alpha_{wd\min}} (\text{inv}(v_{d\max 1,2}) + \text{inv}(v_{c\max 1,2}) - \text{inv}(\alpha_{wd\min}) - \text{inv}(\alpha_{wc\min})). \quad (7.33)$$

For gears with internal teeth:

$$s_{w \min 2} = \frac{d_{bd2}}{2 \cos \alpha_{wd \min}} \left( \frac{2\pi}{z_2} - \text{inv}(v_{d \max 2}) - \text{inv}(v_{c \max 2}) + \text{inv}(\alpha_{wd \min}) + \text{inv}(\alpha_{wc \min}) \right)$$

and

$$s_{w \max 2} = \frac{d_{bd2}}{2 \cos \alpha_{wd \max}} \left( \frac{2\pi}{z_2} - \text{inv}(v_{d \min 2}) - \text{inv}(v_{c \min 2}) + \text{inv}(\alpha_{wd \max}) + \text{inv}(\alpha_{wc \max}) \right). \quad (7.34)$$

For gears with asymmetric teeth the normal backlash is defined between the coast tooth flanks, when the drive tooth flanks are in contact. The normal backlash values  $j_{bn \min 1,2}$  and  $j_{bn \max 1,2}$  are

$$j_{bn \min} = \left( \frac{\pi d_{bd1,2}}{z_1 \cos \alpha_{wd \min}} - s_{w \max 1} - s_{w \max 2} \right) \cos \alpha_{wc \min} \cos \beta_{bc}$$

and

$$j_{bn \max} = \left( \frac{\pi d_{bd1,2}}{z_1 \cos \alpha_{wd \max}} - s_{w \min 1} - s_{w \min 2} \right) \cos \alpha_{wc \max} \cos \beta_{bc}. \quad (7.35)$$

The normal backlash must be greater than the maximum possible gear tooth tip deflection under the load. This allows avoidance of simultaneous contact of the opposite tooth flanks with mating gear tooth flanks.

The root clearances  $c_{\min 1,2}$  and  $c_{\max 1,2}$  are:

For external gearing:

$$c_{\min 1} = a_{\min} - \frac{d_{a \min 2}}{2} - \frac{d_{r \max 1}}{2} \quad \text{and} \quad c_{\max 1} = a_{\max} - \frac{d_{a \max 2}}{2} - \frac{d_{r \min 1}}{2}, \quad (7.36)$$

$$c_{\min 2} = a_{\min} - \frac{d_{a \min 1}}{2} - \frac{d_{r \max 2}}{2} \quad \text{and} \quad c_{\max 2} = a_{\max} - \frac{d_{a \max 1}}{2} - \frac{d_{r \min 2}}{2}. \quad (7.37)$$

For internal gearing:

$$c_{\min 1} = \frac{d_{a \min 2}}{2} - \frac{d_{r \max 1}}{2} - a_{\max} \quad \text{and} \quad c_{\max 1} = \frac{d_{a \max 2}}{2} - \frac{d_{r \min 1}}{2} - a_{\min}, \quad (7.38)$$

$$c_{\min 2} = \frac{d_{r\min 2}}{2} - \frac{d_{a\max 1}}{2} - a_{\max} \quad \text{and} \quad c_{\max 2} = \frac{d_{r\max 2}}{2} - \frac{d_{a\min 1}}{2} - a_{\min}. \quad (7.39)$$

The minimal root clearances must be greater than zero to avoid the tooth tip/root interference. Actually, this condition is already taken into consideration during the tooth root fillet construction and optimization (see Section 5.3). However, operating conditions, including temperature and humidity, may reduce root clearances. Besides, low radial clearances may result with trapping lubricant in the tooth root area, increased hydraulic losses, and reduced gear efficiency, especially for relatively wide spur gears. This may require designing the tooth fillet with increased root clearances even with some compromise of bending stress reduction.

The transverse operating contact ratios are:

For drive flanks of external mesh  $\epsilon_{od\min}$  and  $\epsilon_{od\max}$ :

$$\epsilon_{od\min} = \frac{z_1}{2\pi} (\tan \alpha_{aed\min 1} + u \tan \alpha_{aed\min 2} - (u + 1) \tan \alpha_{wd\max})$$

and

$$\epsilon_{od\max} = \frac{z_1}{2\pi} (\tan \alpha_{aed\max 1} + u \tan \alpha_{aed\max 2} - (u + 1) \tan \alpha_{wd\min}). \quad (7.40)$$

For coast flanks of external mesh  $\epsilon_{oc\min}$  and  $\epsilon_{oc\max}$ :

$$\epsilon_{oc\min} = \frac{z_1}{2\pi} (\tan \alpha_{aec\min 1} + u \tan \alpha_{aec\min 2} - (u + 1) \tan \alpha_{wc\max})$$

and

$$\epsilon_{oc\max} = \frac{z_1}{2\pi} (\tan \alpha_{aec\max 1} + u \tan \alpha_{aec\max 2} - (u + 1) \tan \alpha_{wc\min}). \quad (7.41)$$

For drive flanks of internal mesh  $\epsilon_{oid\min}$  and  $\epsilon_{oid\max}$ :

$$\epsilon_{oid\min} = \frac{z_1}{2\pi} (\tan \alpha_{aed\max 1} - u \tan \alpha_{aed\min 2} + (u - 1) \tan \alpha_{wd\min})$$

and

$$\epsilon_{oid\max} = \frac{z_1}{2\pi} (\tan \alpha_{aed\min 1} - u \tan \alpha_{aed\max 2} + (u - 1) \tan \alpha_{wd\max}). \quad (7.42)$$

For coast flanks of internal mesh  $\epsilon_{\alpha c \min}$  and  $\epsilon_{\alpha c \max}$ :

$$\epsilon_{\alpha c \min} = \frac{z_1}{2\pi} (\tan \alpha_{\alpha ec \max 1} - u \tan \alpha_{\alpha ec \min 2} + (u - 1) \tan \alpha_{\alpha wc \min})$$

and

$$\epsilon_{\alpha c \max} = \frac{z_1}{2\pi} (\tan \alpha_{\alpha ec \min 1} - u \tan \alpha_{\alpha ec \max 2} + (u - 1) \tan \alpha_{\alpha wc \max}). \quad (7.43)$$

The axial operating contact ratio values  $\epsilon_{\beta \min}$  and  $\epsilon_{\beta \max}$  from (2.135) are

$$\epsilon_{\beta \min} = \frac{b_{w \min} \tan \beta_{bd}}{p_{bd}} = \frac{b_{w \min} \tan \beta_{bc}}{p_{bc}}$$

and

$$\epsilon_{\beta \max} = \frac{b_{w \max} \tan \beta_{bd}}{p_{bd}} = \frac{b_{w \min} \tan \beta_{bc}}{p_{bc}}, \quad (7.44)$$

where  $p_{bd}$  and  $p_{bc}$  are transverse base circular pitches of the drives and coast tooth flanks, accordingly, and  $b_{w \min}$  and  $b_{w \max}$  are the minimum and maximum values of the operating face width or the axial width of gear engagement (see Figure 7.4).

In asymmetric gearing the operating axial contact ratio is the same for the drive and coast tooth flanks.

The total operating contact ratios are defined from Equation (2.131):

For drive flanks  $\epsilon_{\gamma d \min}$  and  $\epsilon_{\gamma d \max}$ :

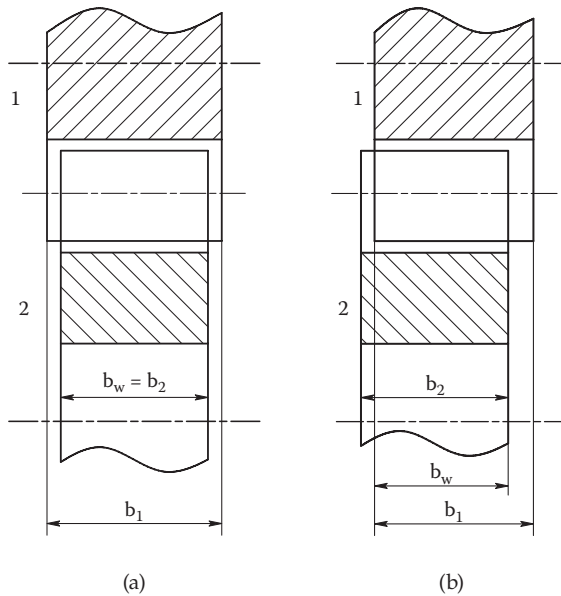
$$\epsilon_{\gamma d \min} = \epsilon_{\alpha d \min} + \epsilon_{\beta \min} \quad \text{and} \quad \epsilon_{\gamma d \max} = \epsilon_{\alpha d \max} + \epsilon_{\beta \max}. \quad (7.45)$$

For coast flanks  $\epsilon_{\gamma c \min}$  and  $\epsilon_{\gamma c \max}$ :

$$\epsilon_{\gamma c \min} = \epsilon_{\alpha c \min} + \epsilon_{\beta \min} \quad \text{and} \quad \epsilon_{\gamma c \max} = \epsilon_{\alpha c \max} + \epsilon_{\beta \max}. \quad (7.46)$$

The minimum total operating contact ratio must be greater than 1.0 for smooth tooth pair engagement.

The equations above describe the absolute tolerance analysis approach with output parameters (normal backlash, radial clearances, and contact ratio) defined at two extreme tolerance combinations, described above as cases 1 and 2. As a result, differences between these parameters' minimum and maximum values can be considerable. At the same time, a significant

**FIGURE 7.4**

Operating face width definition: (a) width  $b_w = b_2 < b_1$ , (b) width  $b_w = b_1 < b_2$ , (c) gears are assembled with axial shift.

number of dimensions involved in tolerance analysis create a very low probability of simultaneous coincidence of extreme tolerance combinations of their minimum or maximum values.

Application of the statistical tolerance analysis allows reduction of tolerance ranges of output parameters or achievement of required ranges with the larger input tolerances, which reduces production cost. According to paper [92], “statistical tolerance analysis can be used by designers and manufacturing personnel to take advantage of statistical averaging over assemblies of parts, allowing the use of less restrictive tolerances in exchange for admitting the small probability of non-assembly.” Reduction of this probability can be provided by the statistical process control (SPC) that establishes the technological tolerances for critical dimensions that are lower than the drawing tolerances. The statistical tolerance analysis approach is also described in [93, 94].



# 8

---

## *Gear Fabrication Technologies and Tooling*

---

Direct Gear Design® provides improved performance for custom gear drives. This is achieved by gear tooth macrogeometry enhancement that also requires certain customization of manufacturing technology and tooling. This chapter considers some gear manufacturing issues.

There are many gear fabrication processes. They can be divided into two groups:

- Machining processes that shape gear and tooth profiles by material removal
- Forming processes that shape gear and tooth profiles by distortion of material or changing material state

Other manufacturing processes that are used for gear as well as many other mechanical component fabrications, like heat treatment, surface engineering, coating, etc., are not considered in this book.

---

### **8.1 Gear Machining**

Table 8.1 presents main machining processes used for spur and helical gears.

#### **8.1.1 Form Machining**

In the form gear cutting or grinding process (Figure 8.1) a tool profile is the same as a space profile between gear teeth. This process is applicable for spur and helical [95] gears. A form machining tool is unique for every gear tooth profile, and its cost is practically the same for standard or custom directly designed gears with similar geometry. Accuracy of form cutting tool positioning relative to the gear blank is very important. The form end mill cutter can be used to machine only gears with symmetric teeth (Figure 8.2). The optimized root fillet profile for gears with a low number of teeth may have an undercut below the form circle. In this case two form disk cutters (Figure 8.3) can be used to machine such tooth profiles. The cutter profiles are overlapping the root fillet at its bottom, which may result in a little step.



**TABLE 8.1**  
Spur and Helical Gear Machining Processes

Type of Process		Type of Tooling
Form machining	Cutting	Form disk or end mill cutter, broach, etc.
	Grinding	Grinding wheel
Generating machining	Cutting	Hob, shaper cutter, rack cutter, shaver cutter
	Grinding	Grinding wheel
Contour machining	CNC milling	Cylinder or ball mill cutter
	Wire-cut EDM <sup>*</sup>	Wire
	Laser cutting	Laser beam
	Water jet cutting	Water or water and abrasive media mixture stream

<sup>\*</sup> EDM - elastic discharge machining.

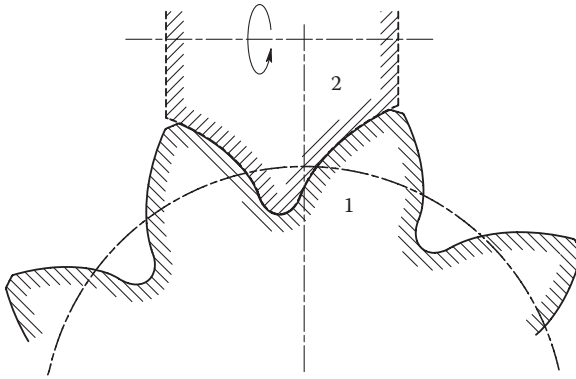


**FIGURE 8.1**  
Gear form machining. 1 - gear profile (solid contour); 2 - tool profile (dashed contour).

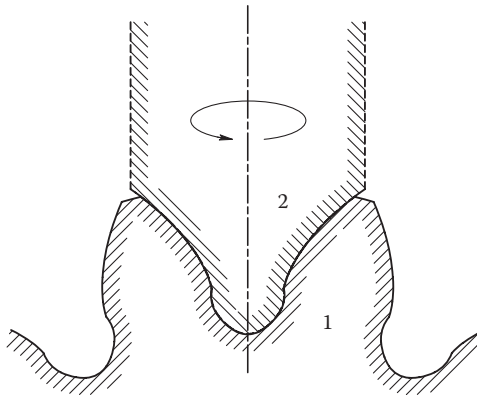


**FIGURE 8.2**  
End mill cutter machining. 1 - gear profile (solid contour); 2 - cutter profile (dashed contour).

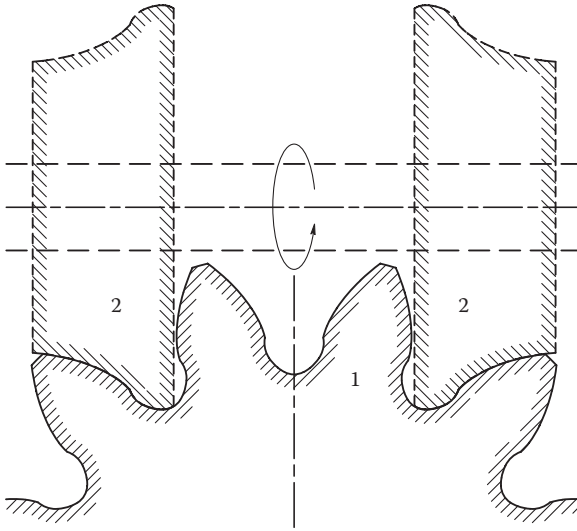


**FIGURE 8.3** Machining of teeth with undercut root fillet. 1 - gear profile (solid contour); 2- form disk cutters (dashed contour).

In gear form machining usually one tooth is machined after another. When machining of one tooth is completed the indexing device (rotary table) positions a gear blank for the next tooth cutting. But there is one type of form machining process—gear fly cutting [96] that has a tool (fly cutter) in mesh with the gear blank (Figures 8.4 and 8.5). It uses conventional gear hobbing machines that have a cutter and gear blank in constant synchronized rotation. However, unlike the gear rack generating process, a space between teeth is shaped by a whole cutter tooth profile exactly as in conventional form machining with the disk cutter (Figure 8.4).

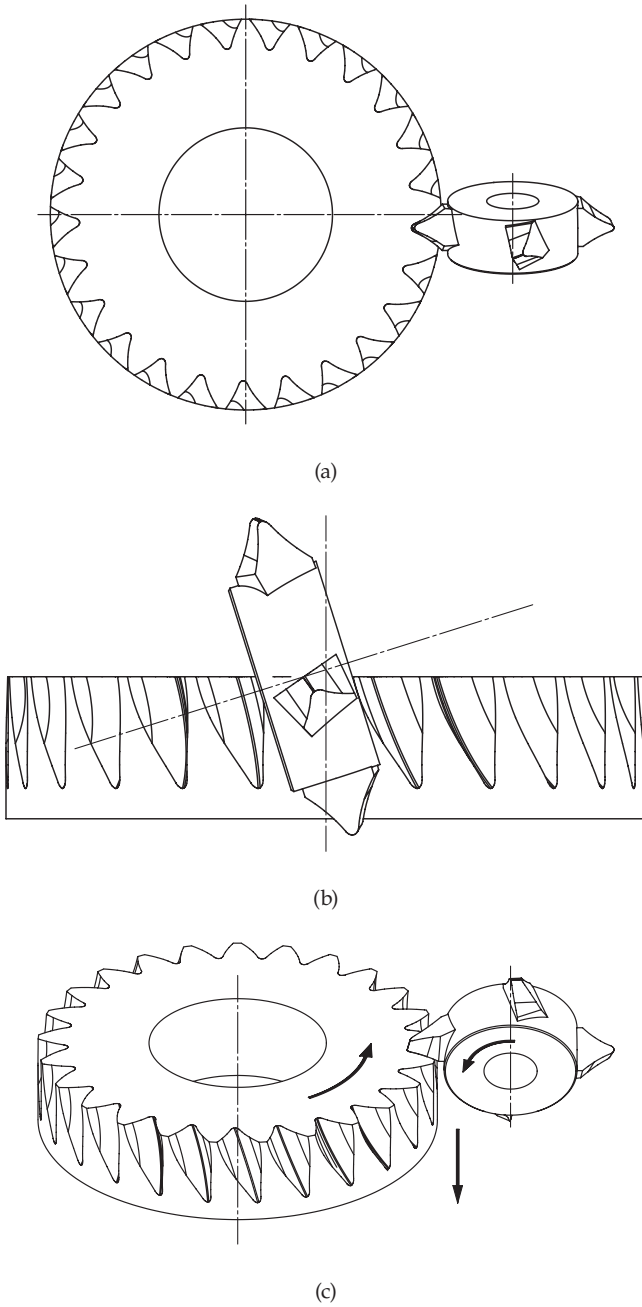
The gear fly cutter also looks similar to the conventional gear disk cutter, but all cutter edges are turned at the start angle  $\phi$ , which is defined as

$$\phi = \arcsin \frac{m_n n_t}{d_t}, \tag{8.1}$$

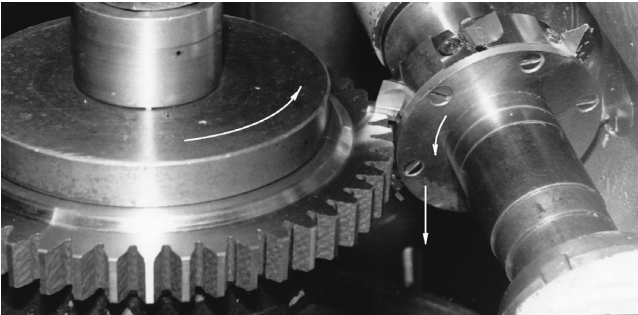
where  $m_n$  is the normal module of the gear,  $n_t$  is the number of the fly cutter teeth, and  $d_t$  is the fly cutter pitch diameter.

A gear fly cutter also can be considered the multistart gear hob that has just one tooth in each start. The cutter setup angle  $\phi$  relative to the gear plane is defined the same way as for gear hobbing;

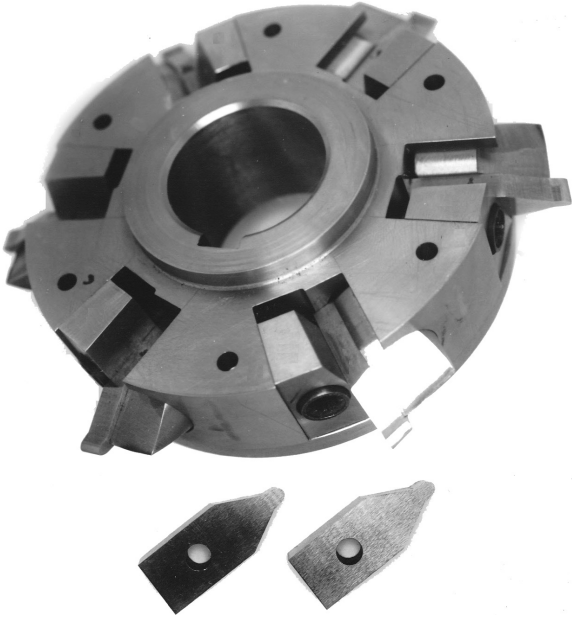
$$\phi = \beta \pm \phi \tag{8.2}$$

**FIGURE 8.4**

Gear fly cutting schematics: (a) top view, (b) right view, (c) isometric view.



(a)

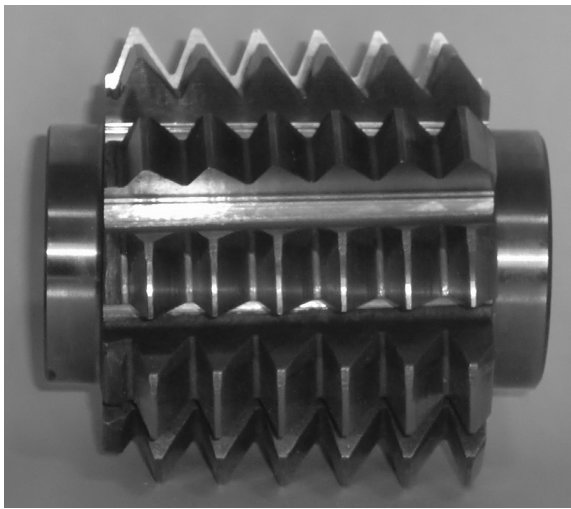
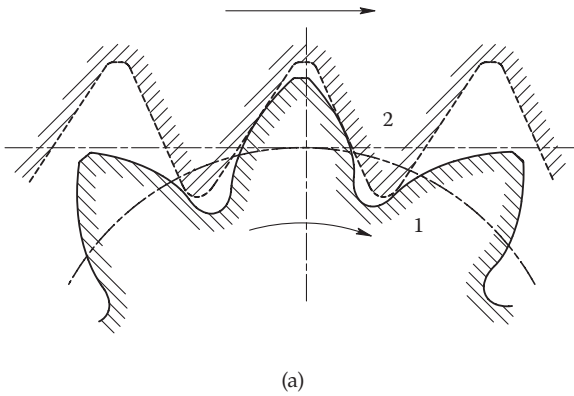


(b)

**FIGURE 8.5** Gear fly cutting: (a) hobbing machine setup, (b) universal fly cutter with inserts.

where  $\beta$  is the gear helix angle, + indicates the gear helix and cutter start angle have the same directions (right or left), and - indicates the gear helix and cutter start angle have opposite directions.

The adjustable gear fly cutter is shown in Figure 8.5b. It makes it possible to machine gear with different numbers of teeth and modules by using replaceable cutting and angle inserts.

**FIGURE 8.6**

(a) Rack generating. 1 - gear profile (solid contour); 2 - hob or rack cutter profile (dashed contour). (b) Asymmetric gear hob cutter.

### 8.1.2 Generating Machining

Schematics of the rack generating gear machining process are shown in Figure 8.6. In this process a gear blank and tool are engaged in a mesh, and all gear teeth are machined practically simultaneously. In traditional gear design the tooling (a hob or rack cutter) profile is known at an early stage of the gear design procedure. In combination with its position relative to the gear center (addendum modification or X-shift), the tooling rack profile defines the gear tooth and whole gear profiles.

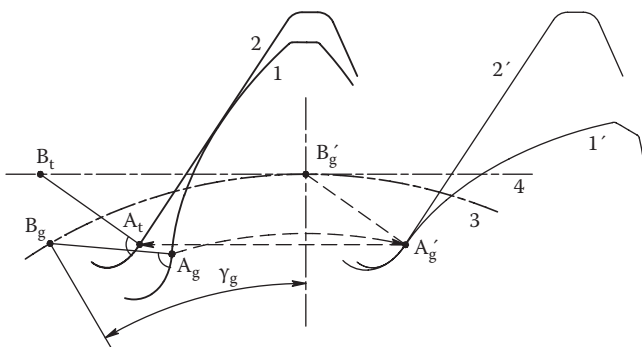


**FIGURE 8.7**

Generating rack profile definition. 1 and 1' - gear profile positions; 2 and 2' - rack cutter profile positions; 3 - gear pitch circle in mesh with rack; 4 - rack pitch line in mesh with gear.

Direct Gear Design applies a different approach. The optimized gear tooth and whole gear profiles are described without using any redefined tooling rack parameters. Then the reverse generating technique is applied to find the tooling rack profile using the known gear profile. This technique assumes that in the rack/gear mesh every point of the gear tooth profile has its mating point on the rack tooth profile. Figure 8.7 demonstrates how the tooling rack profile point  $A_t$  position is defined from the gear tooth profile point  $A_g$  position. In order to find the generating rack profile point  $A_t$  corresponding to the gear tooth profile point  $A_g$ , the line  $A_g B_g$  perpendicular to the tooth profile in point  $A_g$  is constructed. Point  $B_g$  lies in an intersection of the line  $A_g B_g$  with the gear pitch circle. The gear tooth profile and line  $A_g B_g$  are rotated on the angle  $\gamma_g$  relative to the gear center until point  $B_g$  reaches its pitch point position  $B_g'$ , where the gear pitch circle 3 is tangent to the rack pitch line 4. Then point  $A_g$  is in position  $A_g'$ , where gear tooth profile 1' is tangent to rack profile 2'. The line  $A_g' B_g'$  is moved parallel to the rack pitch line 4 on distance  $B_g' B_t$ , which is equal to the length of the arc  $B_g B_g'$ . This movement puts point  $A_g'$  in position  $A_t$  at the rack profile that corresponds to point  $A_g$  at the gear tooth profile. This approach allows definition of any generating rack profile point that is related to a certain gear tooth profile point.

In the case where a gear is made by shaping cutting, traditional gear design suggests that the shaper cutter parameters and profile are known prior to gear design. In combination with its position relative to the gear center (addendum modification or X-shift), the shaper cutter profile defines the gear tooth and whole gear profiles. Schematics of the shaper generating gear cutting process are shown in Figure 8.8.

In Direct Gear Design the shaper cutter profile is also defined after the gear profile is already known. This gear profile is used for the shaper cutter profile reverse generation using a technique similar to that for the rack type tooling profile definition. It assumes that in the shaper cutter/gear

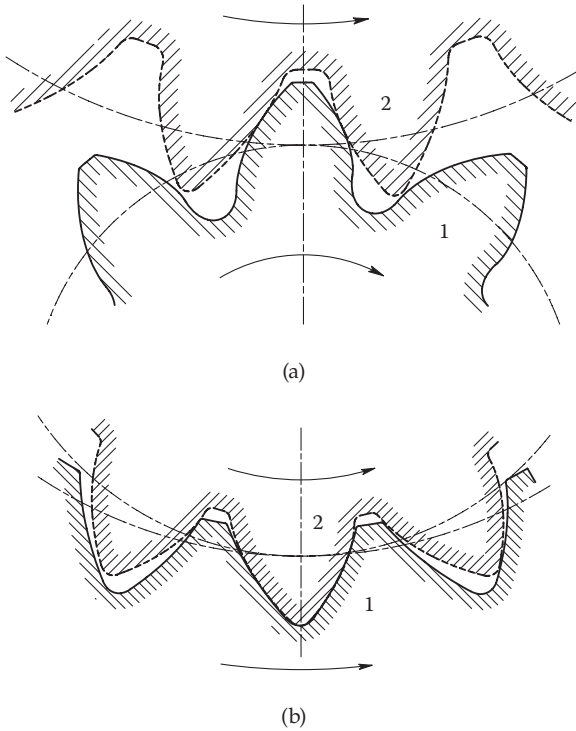


**FIGURE 8.8** Generating of external (a) and internal (b) gears. 1 - gear profile (solid contour); 2 - shaper cutter profile (dashed contour).

mesh every point of the gear tooth profile has its mating point on the shaper cutter tooth profile.

Figure 8.9 demonstrates how the shaper cutter profile point  $A_t$  position is defined from the gear tooth profile point  $A_g$  position. In order to find the shaper cutter profile point  $A_t$  corresponding to the gear tooth profile point  $A_g$ , the line  $A_g B_g$  perpendicular to the tooth profile is constructed. Point  $B_g$  lies in an intersection of the line  $A_g B_g$  with the gear pitch circle. The gear tooth profile and line  $A_g B_g$  are rotated on the angle  $\gamma_g$  relative to the gear center until point  $B_g$  reaches its pitch point position  $B'_g$ , where gear pitch circle 3 is tangent to shaper cutter pitch circle 4. The angle  $\gamma_g$  is

$$\gamma_g = \frac{2B_g B'_g}{d_{pg}}, \tag{8.3}$$

where  $B_g B'_g$  is the length of arc  $B_g B'_g$ , and  $d_{pg}$  is the gear pitch diameter in the mesh with the shaper cutter.

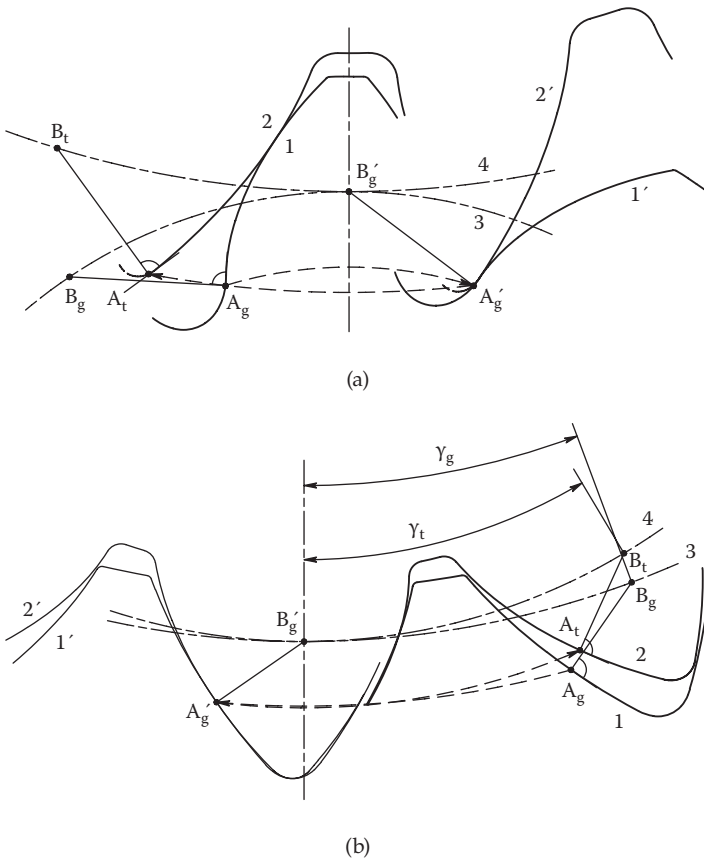


**FIGURE 8.9**

Generating gear shaper cutter profile definition for external (a) and internal (b) gears. 1 and 1' - gear profile positions; 2 and 2' - shaper cutter profile positions; 3 - gear pitch circle in mesh with shaper cutter; 4 - shaper cutter pitch circle in mesh with gear.

Point  $A_g$  is in position  $A_g'$  where gear tooth profile 1' is tangent to shaper cutter profile 2'. Line  $A_g'B_g'$  is rotated back relative to the shaper cutter center on angle  $\gamma_t$ , that is,

$$\gamma_t = \gamma_g \frac{d_{pg}}{d_{pt}}, \tag{8.4}$$

where  $d_{pg}$  is the gear pitch diameter in the mesh with the shaper cutter.

This movement puts point  $A_g'$  in position  $A_t$  at the shaper cutter profile that corresponds to point  $A_g$  at the gear tooth profile. This approach allows any shaper cutter profile point corresponding to the certain gear tooth profile point to be defined.



The gear pitch diameter in mesh with a generating tooling (hob, rack, or shaper cutters) is not necessarily equal to the operating pitch diameter with the mating gear. The pressure angle in mesh with generating tooling can be different than the operating pressure angle accordingly. The pressure angle in mesh with generating tooling selection is important. Too large of a pressure angle results in a tooling profile that will not be able to generate the required gear profile, because, for example, of the pointed tooling tooth tip or its too small radius. Too small (close to zero) of a pressure angle negatively affects the cutting condition, gear tooth profile surface finish, and tooling life.

One of the benefits of the gear generating process is the possibility of using one tool (hob, rack, or shaper cutter) for machining gears with different numbers of teeth. This allows reduction of tooling inventory and cost of low- and medium-volume gear production where a tooling share per one gear is relatively high. In general, traditionally designed mating gears are machined with the same generating gear cutter. However, in mass gear production gear cutting (or grinding) machines are typically set up to machine one gear, and they use a dedicated set of tools, including the gear cutters.

Directly designed gears require a custom dedicated generating tool for every gear with different numbers of teeth. This increases tooling inventory and gear cost when production volume is low, although, even in this case, application of directly designed gears is beneficial if their improved performance justifies some production cost increase, like, for example, in aerospace and racing transmissions. In mass gear production a share of custom dedicated machining tool per gear is low, and as a result, the cost of the directly designed gears becomes practically equal to that of the traditional ones. This makes them applicable for automotive, agriculture, and other industries.

Reverse generating of the tooling profile from the gear profile is applicable for involute as well as for noninvolute gears.

### 8.1.3 Contour Machining

Contour machining (Figure 8.10) is not a highly productive gear fabrication method, but unlike form or generating machining, it does not require special tooling. This makes it very useful for gear prototyping and quick fabrication of a relatively small quantity of gears.

Contour gear machining processes include the CNC milling, wire-cut EDM, laser cutting, water jet cutting, etc. In many cases, in order to achieve higher accuracy and surface finish, the contour machining process may require several passes. The final pass removes a tiny amount of material. Most of these processes are used only for spur gears; the CNC ball cutter milling can be used for helical gears as well. The contour cutting path (Figure 8.11) is defined with offset  $S$  from the nominal (average material condition) gear profile. This offset contains a half of the cut width  $W_c$  and some additional offset that depends on the machining process. This additional offset may

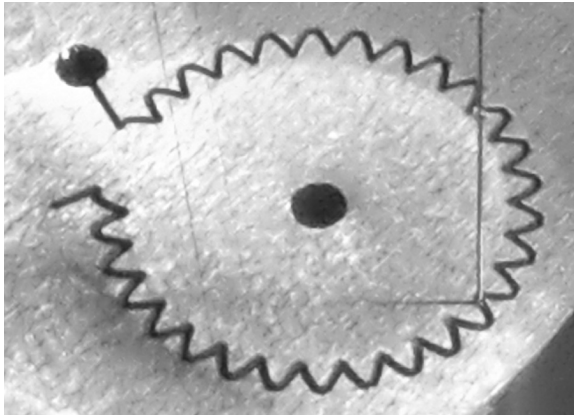
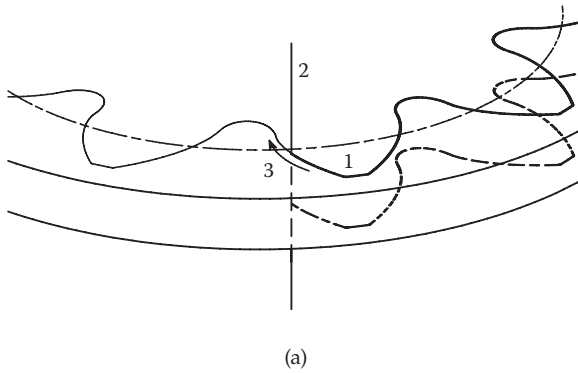


**FIGURE 8.10**

(a) Schematic of contour gear machining. 1 - gear profile; 2 - cutting tool; 3 - cutting direction.  
 (b) Wire EDM gear cutting. ((b) Courtesy of Accuprompt, Inc., Fridley, Minnesota.)

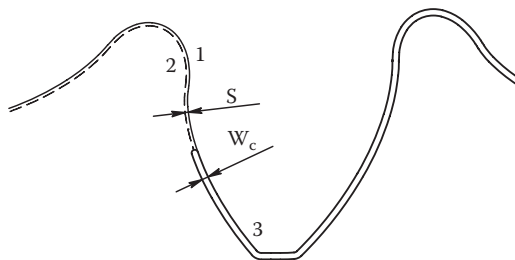


**FIGURE 8.11**

Contour cutting path: 1, nominal (average material condition) gear profile; 2 - tool path; machined gear profile;  $W_c$  - cut width;  $S$  - tool path offset.

include a stock for final machining, overcut or overburn (for wire-cut EDM and laser machining), and a defective layer that should be removed by the following tooth surface treatment operation, for example, polishing.

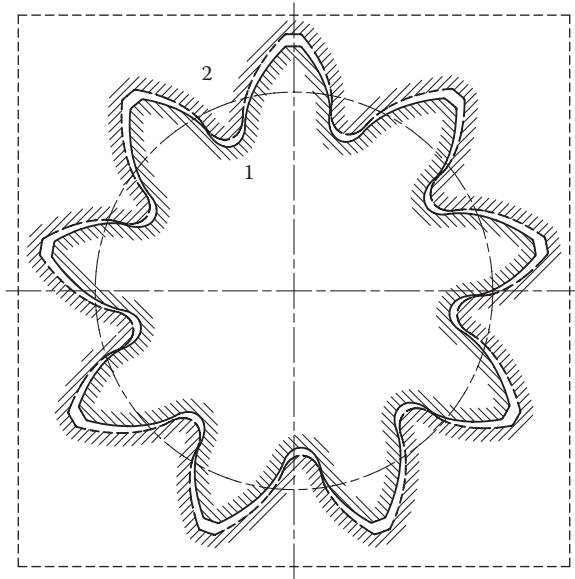
---

## 8.2 Gear Forming

Forming gear fabrication processes like plastic and metal injection molding, powder metal processing, net forging, stamping, die casting, extrusion, gear and worm rolling, etc., have gained popularity in the last few decades, providing a high benefit-cost ratio for mass-produced gear drives. Progress of these technologies allowed a significant increase in their accuracy. As a result, usage of formed gears has also increased considerably. Most of these very different forming gear fabrication processes have a similar tooling component that actually defines a gear shape and its accuracy, the tooling (mold or die) cavity. Any gear forming process cavity is dedicated to a particular gear profile. This makes Direct Gear Design very acceptable for gear forming technology, because production cost of the custom-optimized gears, in this case, is practically the same as that of the similar size standard gears [97].

The forming tool cavity has a profile similar to that of the gear, but adjusted for shrinkage and warpage (Figure 8.12), which greatly affect gear size and shape accuracy. This made proper prediction of shrinkage and warpage critical for all gear forming technologies, particularly for the plastic injection molding process. Plastic gears often have an intricate body shape, including ribs or spokes to maintain limited maximum material thickness to exclude voids, and for weight and cost reduction. They also are often incorporated as one piece with other mechanism components, like, for example, shafts, cams, etc. These design specifics, in combination with a huge variety of available gear polymers and enhancing additives (for increased strength, thermo-resistance, lubricity, etc.), make prediction of gear shrinkage and warpage an utmost difficult task. In many cases gear molders use a trial-and-error method with different degrees of success. Typically this “educated guess” method works better for gears with a relatively simple body shape (like, for example, the flat uniform disk with a small central hole) that are made out of generic unfilled polymers.

R.E. Kleiss [98] stated that “plastic does not shrink from the cavity in an isotropic fashion” and suggested using different shrinkage factors for main gear dimensions, including the tooth tip, root, and base circle diameters, and base tooth thickness. S.F. Walsh [99] analyzed effects of material crystallinity, orientation, and cooling stress relaxation for shrinkage and warpage prediction of injection molded components. The Autodesk® Moldflow® plastic injection molding simulation software [100] predicts “part shrinkage based on processing parameters and grade-specific material data.” Realization of

**FIGURE 8.12**

Gear molding. 1 - gear profile (solid contour); 2 - mold or die cavity profile (dashed contour).

these and similar approaches to adjust the mold cavity shape compensating molding process distortion requires knowledge of specific data about polymer material grade, tooling design (number of injection gates, their size and location, cooling system, etc.), molding process parameters, etc.

A totally different approach to molding distortion compensation was proposed by Y.V. Shekhtman [101]. It was called a Genetic Molding Solution®. Similar to how the DNA contains genetic information about the entire live organism, the shape of the molded part reflects the originally designed profile, polymer material properties, tooling design, and molding process parameters. The Genetic Molding Solution method is based on a mathematical prediction that defines a transformation function describing relations between the molded sample gear profile and its actual cavity profile. Once this function is defined, the target gear profile replaces the molded sample profile as the transformation function variable to calculate the final cavity profile. The transformation function is based on a system of trigonometric and polynomial equations.

The initial cavity profile coordinates are

$$M_1 = K_{sh} \times D, \quad (8.5)$$

where  $D$  is the target gear profile data set, presented as  $X,Y$ -coordinate points of the 2D CAD model constructed for average material conditions, and  $K_{sh}$  is the polymer linear mold shrinkage coefficient provided by the material supplier.

These initial cavity profile coordinates  $M_1$  can be also presented as

$$M_1 = f(P), \quad (8.6)$$

where  $P$  is the initial sample gear profile data set, presented as  $X,Y$ -coordinate points provided by the coordinate measuring machine (CMM) inspection of actual molded gear, and  $f$  is the transformation function describing relations between the initial cavity and initial sample gear profiles.

Then the final cavity profile coordinates are

$$M_2 = f(D). \quad (8.7)$$

Unlike previously mentioned approaches, the Genetic Molding Solution method is based on the “black box” concept and uses only gear and cavity inspection results and math that defines the transformation function between them. It does not require knowledge of any specific data related to polymer material, tooling (except only the linear mold shrinkage coefficient  $K_{sh}$ ), and molding process parameters.

Practical application of this method takes eight steps:

1. *Target gear profile definition* (data file 1). The  $X,Y$ -coordinate points are extracted from the gear CAD model and present a desired nominal gear profile at average material condition. A number of these coordinate points are typically several hundred per one gear tooth.
2. *Initial cavity profile definition*. Initial cavity profile is the scaled-up target gear CAD profile using the polymer linear mold shrinkage coefficient  $K_{sh}$ .
3. *Fabrication and inspection of initial mold cavity* (data file 2). CMM inspection produces the  $X,Y$ -coordinate points (several hundred per one tooth space) accurately describing the initial cavity.
4. *Molding process optimization*. Gears are molded using the initial cavity, without concern about the gear shape. A goal here is to achieve a stable and repeatable molding process with the part dimensional variation significantly lower than the required accuracy tolerances. Any material flaws like voids are not acceptable. Once this goal is reached, the molding process must be “locked in” and certified; no changes to the process are allowed. Using the optimized process, several dozen gears are molded.
5. *Representative gear specimen selection*. All molded gears are roll tested and inspection data are analyzed. Then one most representative gear specimen is selected. This specimen should have average statistical tooth-to-tooth and total composite errors (TTE and TCE).

6. *Gear specimen inspection* (data file 3). CMM inspection produces the  $X,Y$ -coordinate points (several hundred per one gear tooth) accurately describing the most representative gear specimen. Inspection data of the initial cavity and the gear specimen must have the same axes orientation to provide each gear tooth and its cavity space accordance.
7. *Final cavity profile definition, fabrication, and inspection*. The Genetic Molding Solution software uses the most representative gear specimen and initial cavity data (files 2 and 3) to generate a transformation function  $f$ . The target gear data (file 1) is then used as the variable of this transformation function to define the final cavity profile—the output data set. The same axes orientation of all three data files is absolutely critical. Any angular rotation or mirroring of the data points totally compromises the mold cavity adjustment results. The final cavity is then manufactured and given a CMM check inspection.
8. *Final gear profile*. At last, gears are molded using the final mold cavity. The CMM data of the molded gears should be identical to the specified gear profile, within the molding process accuracy variation.

For successful application of the Genetic Molding Solution method the initial and final gear molding must be done with the same batch polymer on the same molding press using the same tool. A current version of the software uses the 2D data sets and works well for spur plastic gears with relatively low face width. For helical and wide spur gears this method should be used for several (typically two or three) gear sections.

An example of this method application for the cam shaft gear is shown in Figure 8.13a. This gear is not particularly molding friendly: It has a metal over-molded shaft, two cams, six spokes, and three injecting gates located in the middle of these spokes. Mold development for this gear using traditional methods requires considerable time and guesswork, and several mold cavity iterations. The Genetic Molding Solution method develops the desired cavity in a short time by direct calculation, with only one extra (initial) cavity.

The chart in Figure 8.13c shows a comparison of roll test graphs on the initial most representative gear specimen to the final gear sample. The initial gear roll test measurements (TTE and TCE) exceed the required accuracy level, but the final gear roll test results fit well inside the TTE and TCE tolerance limits.

The Genetic Molding Solution method can significantly accelerate the injection plastic mold cavity development. It eliminates a guess component of the final cavity prediction and provides its profile definition by use of direct calculation. It is applicable not only to plastic molded gears but also to other plastic components. It also can be considered for other gear forming processes that use mold or die cavities, like power metallurgy, die casting, net forging, etc.

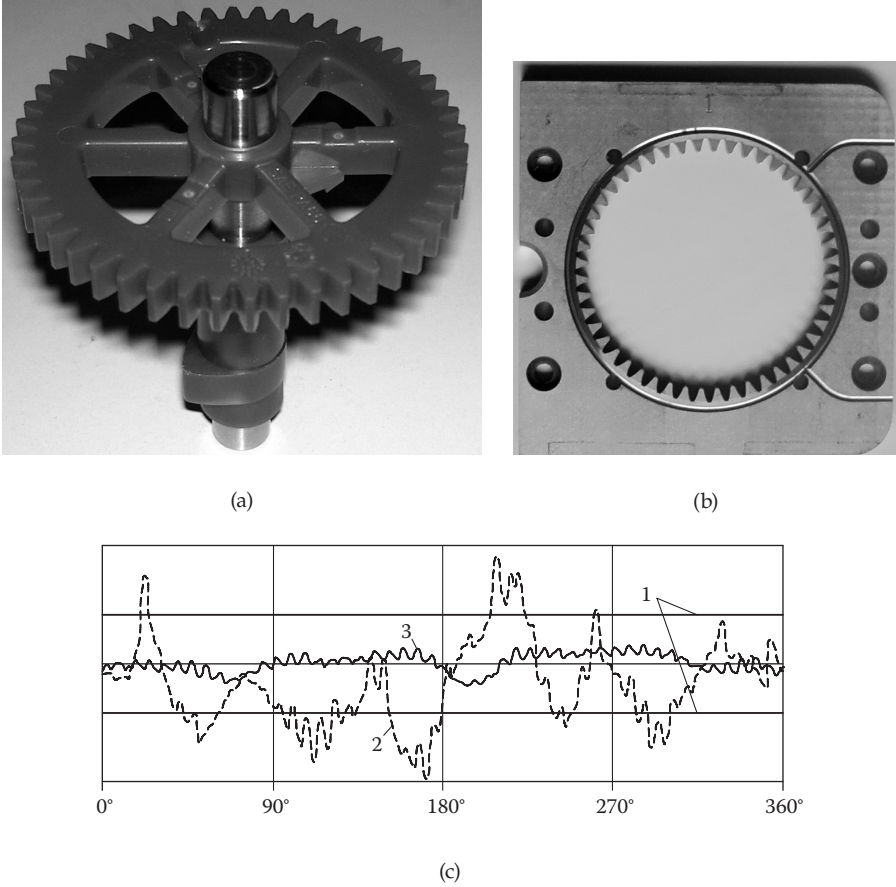


**FIGURE 8.13**

Genetic Molding Solution application: (a) cam shaft gear, (b) gear mold cavity, (c) roll rest chart overlay. 1 - total composite tolerance limits; 2 - initial specimen chart (solid contour); 3 - final gear chart (dashed contour). (Courtesy of Thermotech Co., Hopkins, Minnesota.)

# 9

---

## *Gear Measurement*

---

Inspection is a critical stage of the gear production process. It is also absolutely essential for development of new gear transmissions. Comprehensive inspection prior to assembly and prototype testing allows potential design issues to be isolated from manufacturing errors and makes it possible to draw correct conclusions based on the prototype testing results.

Manufacturing of directly designed gears not only requires custom tooling, but also affects gear measurement. This chapter presents definitions of main inspection dimensions and parameters for directly designed spur and helical, external and internal gears with symmetric and asymmetric teeth.

---

### 9.1 Measurement over (between) Balls or Pins

Measurement over (for gears with external teeth) or between (for gears with internal teeth) balls or pins is an indirect way to inspect the tooth thickness at the given reference diameter. All equations below are defined for gears with asymmetric teeth. However, they are applicable for gears with symmetric teeth, assuming that all parameters describing the opposite tooth flanks are identical.

#### 9.1.1 Spur Gears

The position of the measuring ball or pin center is shown in Figure 9.1. The involute angles  $\alpha_{gd}$  and  $\alpha_{gc}$  at the ball or pin center location circle diameter  $d_g$  are defined by [102, 103]:

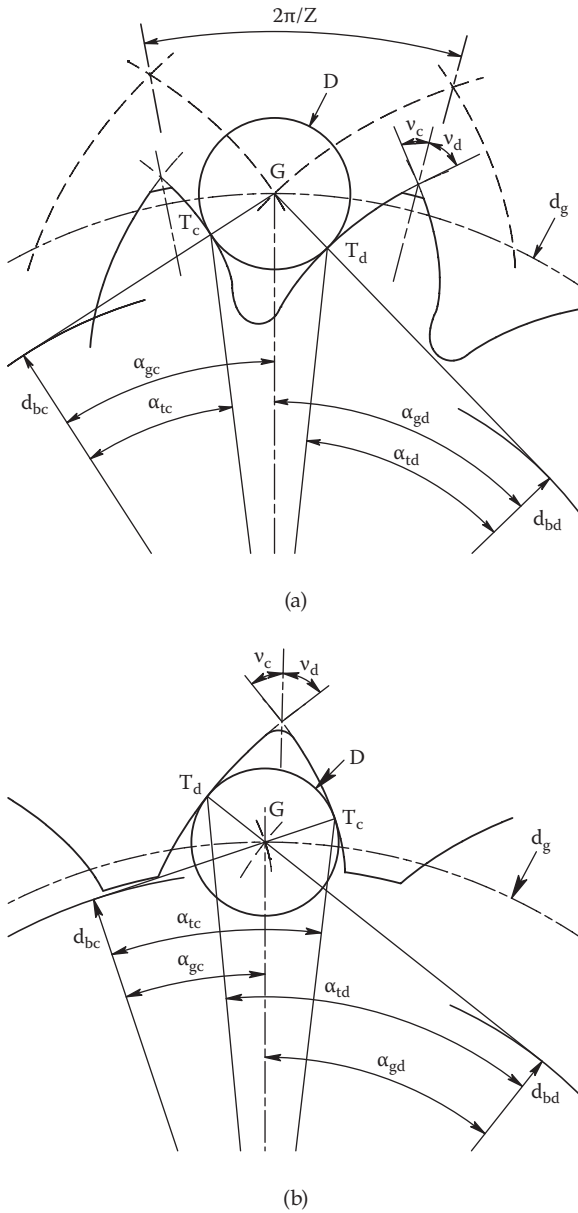
For external gear:

$$\operatorname{inv}(\alpha_{gd}) + \operatorname{inv}(\alpha_{gc}) = \operatorname{inv}(v_d) + \operatorname{inv}(v_c) + \frac{D}{d_{bd}} + \frac{D}{d_{bc}} - \frac{2\pi}{z}. \quad (9.1)$$

For internal gear:

$$\operatorname{inv}(\alpha_{gd}) + \operatorname{inv}(\alpha_{gc}) = \operatorname{inv}(v_d) + \operatorname{inv}(v_c) - \frac{D}{d_{bd}} - \frac{D}{d_{bc}}. \quad (9.2)$$



**FIGURE 9.1**

Ball or pin position: (a) external gear, (b) internal gear.  $D$  - ball or pin diameter;  $G$  - center of ball or pin. (From Kapelevich, A.L., *Gear Technology*, January/February 2011, 60–65. With permission.)

The ball or pin center location circle diameter  $d_g$  is

$$d_g = \frac{d_{bd}}{\cos \alpha_{gd}} = \frac{d_{bc}}{\cos \alpha_{gc}}. \quad (9.3)$$

The involute angles  $\alpha_{td}$  and  $\alpha_{tc}$  in the ball or pin contact points  $T_d$  and  $T_c$  are

$$\alpha_{td} = \arctan\left(\tan \alpha_{gd} \mp \frac{D}{d_{bd}}\right) \quad (9.4)$$

and

$$\alpha_{tc} = \arctan\left(\tan \alpha_{gc} \mp \frac{D}{d_{bc}}\right), \quad (9.5)$$

where – is for the external gear and + is for the internal gear.

Then a measurement over two balls or pins for the external gear is:

For even number of teeth (Figure 9.2a):

$$M = d_g + D. \quad (9.6)$$

For odd number of teeth (Figure 9.2b):

$$M = d_g \cdot \cos \frac{\pi}{2z} + D. \quad (9.7)$$

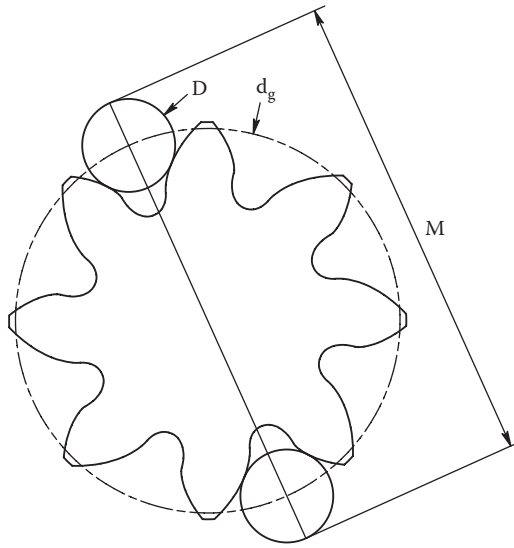
A measurement between two balls or pins for the internal gear is:

For even number of teeth (Figure 9.3a):

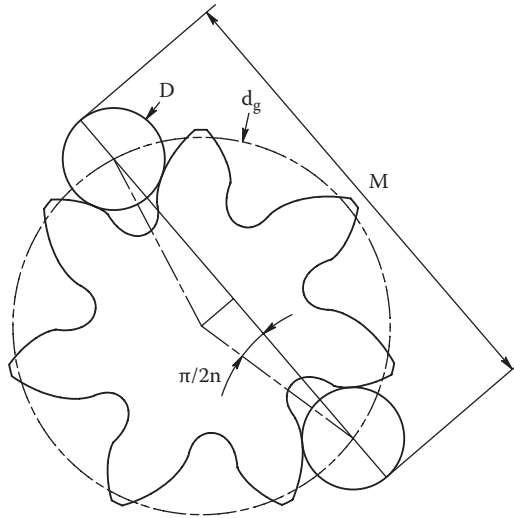
$$M = d_g - D. \quad (9.8)$$

For odd number of teeth (Figure 9.3b):

$$M = d_g \cdot \cos \frac{\pi}{2n} - D. \quad (9.9)$$



(a)



(b)

**FIGURE 9.2**

Measurement over balls or pins for external gears: (a) even number of teeth, (b) odd number of teeth. (From Kapelevich, A.L., *Gear Technology*, January/February 2011, 60–65. With permission.)

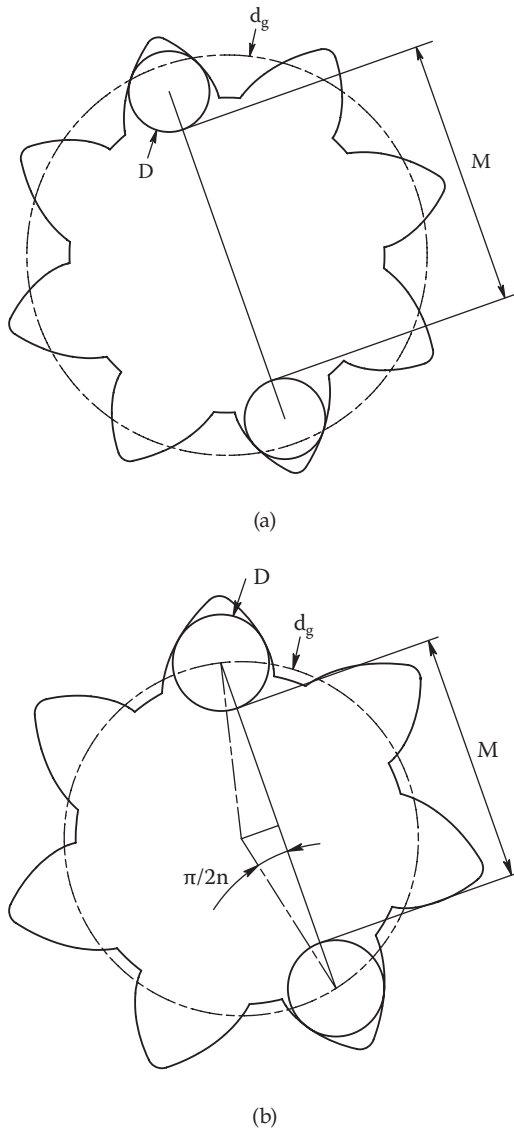


**FIGURE 9.3** Measurement between balls or pins for internal gears: (a) even number of teeth, (b) odd number of teeth. (From Kapelevich, A.L., *Gear Technology*, January/February 2011, 60–65. With permission.)

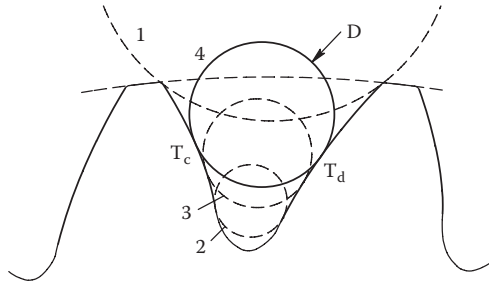


**FIGURE 9.4**

Ball or pin diameter selection. 1 - diameter too large—contact point is at the tooth tip corner; 2 - diameter too small—contact point is at the root fillet; 3 - diameter is acceptable, but the small tip caliper (or micrometer) is required to fit between gear teeth; 4 - suitable ball or pin diameter.

The ball or pin contact points  $T_d$  and  $T_c$  should always be located on the involute flanks. They must not contact the tooth profile at the tooth tip radius or chamfer and at the root fillet profile (Figure 9.4). These conditions are described by the contact point involute angle limits:

For external gears:

$$\arccos \frac{d_{bd}}{d_{fd}} < \alpha_{td} < \arccos \frac{d_{bd}}{d_a} \quad \text{and} \quad \arccos \frac{d_{bc}}{d_{fc}} < \alpha_{tc} < \arccos \frac{d_{bc}}{d_a}. \quad (9.10)$$

For internal gears:

$$\arccos \frac{d_{bd}}{d_a} < \alpha_{td} < \arccos \frac{d_{bd}}{d_{fd}} \quad \text{and} \quad \arccos \frac{d_{bc}}{d_a} < \alpha_{tc} < \arccos \frac{d_{bc}}{d_{fc}}, \quad (9.11)$$

where  $d_a$  is the tooth tip diameter, and  $d_{fd}$  and  $d_{fc}$  are the drive and coast tooth flank form diameters.

For measurement convenience the ball or pin surface should be above the gear tooth tips; otherwise the caliper (or micrometer) should have small tips to fit between gear teeth. This condition can be presented as

$$D > |d_a - d_g|. \quad (9.12)$$

For external gears this inequality should be solved with Equations (9.1) and (9.3), and for internal gear with Equations (9.2) and (9.3), to define a proper ball or pin diameter.

### 9.1.2 Helical Gears

The involute angles  $\alpha_{gd}$  and  $\alpha_{gc}$  at the ball or pin location circle diameter  $d_g$  are defined by [102]:

For external gear:

$$\text{inv}(\alpha_{gd}) + \text{inv}(\alpha_{gc}) = \text{inv}(v_d) + \text{inv}(v_c) + \frac{D}{d_{bd} \times \cos \beta_{bd}} + \frac{D}{d_{bc} \times \cos \beta_{bc}} - \frac{2\pi}{z}. \quad (9.13)$$

For internal gear:

$$\text{inv}(\alpha_{gd}) + \text{inv}(\alpha_{gc}) = \text{inv}(v_d) + \text{inv}(v_c) - \frac{D}{d_{bd} \times \cos \beta_{bd}} - \frac{D}{d_{bc} \times \cos \beta_{bc}}, \quad (9.14)$$

where  $\beta_{bd}$  and  $\beta_{bc}$  are the helix angles at the drive and coast base diameters:

$$\beta_{bd} = \arctan(\tan \beta \times \cos \alpha_d), \quad (9.15)$$

$$\beta_{bc} = \arctan(\tan \beta \times \cos \alpha_c). \quad (9.16)$$

Then the ball or pin center location circle diameter  $d_g$  is defined by (9.3). This equation is used for the pin center location circle definition only for external helical gears. Cylindrical pins cannot be used to measure the internal helical gears, because the pin surface cannot be tangent to the concave internal helical gear tooth flanks. The ball or pin diameters should also satisfy conditions (9.10) to (9.12). When diameter  $d_g$  is known, measurements over two balls for external helical gears (Figure 9.5) and between two balls for internal helical gears (Figure 9.6) are defined by Equations (9.6) and (9.7), and (9.8) and (9.9), accordingly.

Measurement over two pins for external helical gears with an even number of teeth is also defined by Equation (9.6). Measurement over two pins for external helical gears with an odd number of teeth is not convenient because the shortest distance between the pin centers does not intersect the gear axis, which makes it difficult to place the pins between the flat parallel tips of the caliper (or micrometer). However, this type of measurement is commonly used in gear production, and it is necessary to provide a correct definition of measurement over two pins for external helical gears with an odd number of teeth.

For external helical gears with an odd number of teeth, the shortest distance  $L$  between the pin centers does not lie in the transverse section of the circle diameter  $d_p$  (Figure 9.7). This distance definition is described in [104] as

$$L = \frac{d_g}{2 \times \tan \beta_g} \sqrt{\lambda^2 + 4 \times (\tan \beta_g \times \cos(\frac{\pi}{2z} + \frac{\lambda}{2}))^2}, \quad (9.17)$$

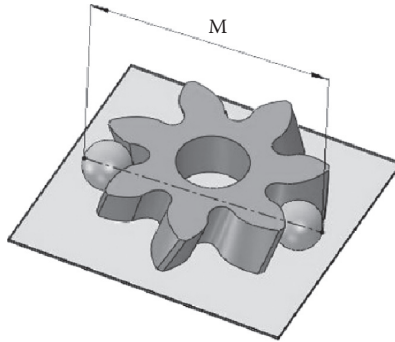


**FIGURE 9.5**  
Measurement over balls of external helical gear. (From Kapelevich, A.L., *Gear Technology*, January/February 2011, 60–65. With permission.)

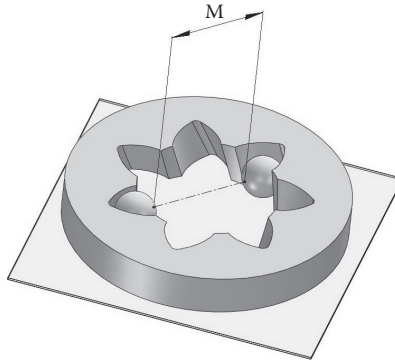


**FIGURE 9.6**  
Measurement between balls of internal helical gear. (From Kapelevich, A.L., *Gear Technology*, January/February 2011, 60–65. With permission.)

where the helix angle at the pin center diameter  $\beta_g$  is

$$\beta_g = \arctan\left(\frac{\tan \beta_{bd}}{\cos \alpha_{gd}}\right) = \arctan\left(\frac{\tan \beta_{bc}}{\cos \alpha_{gc}}\right) \tag{9.18}$$

and the angle  $\lambda$  is a solution of the equation

$$\frac{\lambda}{\tan \beta_g} - \sin\left(\frac{\pi}{z} + \lambda\right) = 0. \tag{9.19}$$

Then the measurement over two pins for external helical gears with an odd number of teeth (Figure 9.8) is

$$M = L + D. \tag{9.20}$$

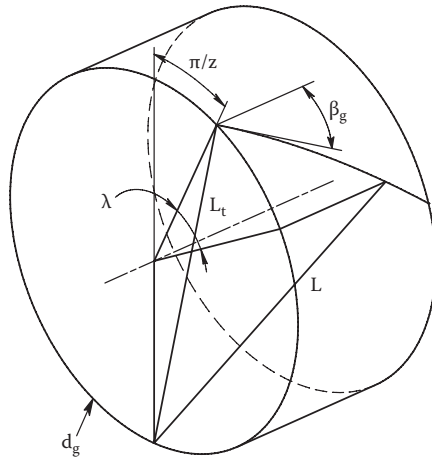


**FIGURE 9.7**

Definition of the distance between the pin centers for the helical gears with an odd number of teeth. (From Kapelevich, A.L., *Gear Technology*, January/February 2011, 60–65. With permission.)

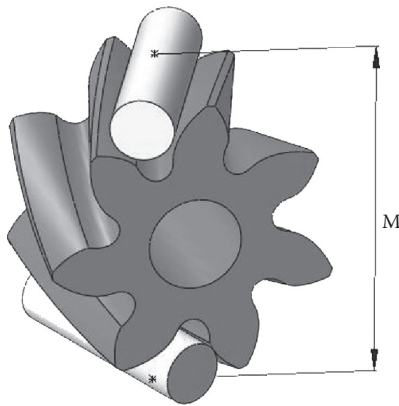


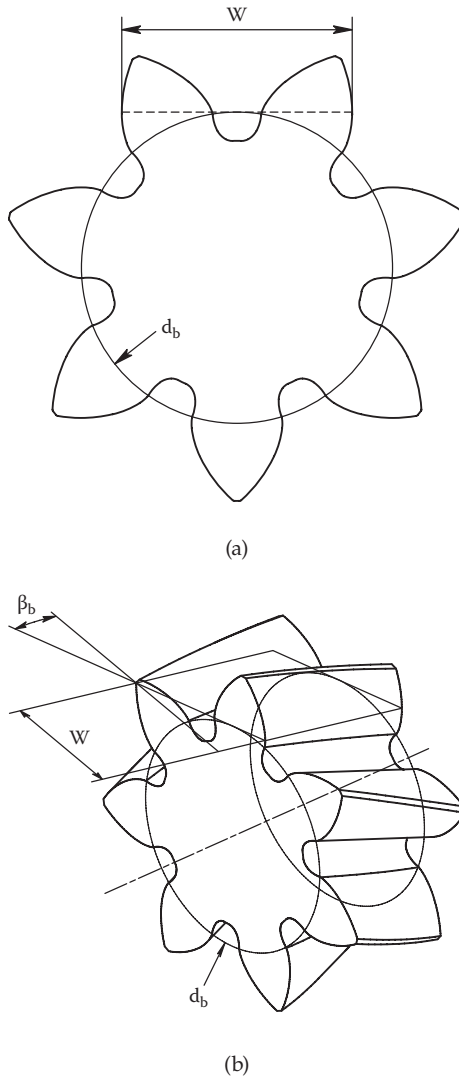
**FIGURE 9.8**

Measurement over pins of the external helical gear with an odd number of teeth. (From Kapelevich, A.L., *Gear Technology*, January/February 2011, 60–65. With permission.)

## 9.2 Span Measurement

Span measurement is another way to inspect the tooth thickness at the given reference diameter for gears with external symmetric teeth. It is the measurement of the distance across several teeth, along a line tangent to the base cylinder (Figure 9.9) [103]. It cannot be applied for gears with asymmetric teeth, because it is impossible to have a common tangent line to two concentric base cylinders of asymmetric tooth flanks.



**FIGURE 9.9**

Span measurement: (a) for spur gear, (b) for helical gear. (From Kapelevich, A.L., *Gear Technology*, January/February 2011, 60–65. With permission.)

Span measurement over  $z_w$  teeth is

$$W = (S_b + (z_w - 1) \times p_b) \times \cos \beta_b, \quad (9.21)$$

where  $S_b$  is the tooth thickness at the base diameter:

$$S_b = S \times \cos \alpha + d_b \times \text{inv}(\alpha), \quad (9.22)$$

$S$  and  $\alpha$  are gear tooth thickness and involute profile angle at the reference diameter  $d$ .

$p_b$  is the circular pitch at the base diameter:

$$p_b = \frac{\pi \times d_b}{z}, \quad (9.23)$$

$z_w$  is number of teeth for span measurement:

$$z_{w\min} < z_w < z_{w\max}, \quad (9.24)$$

$z_{w\min}$  is the minimum number of the spanned teeth:

$$z_{w\min} = \frac{\sqrt{d_f^2 - d_b^2 - S_b}}{p_b}, \quad (9.25)$$

$z_{w\max}$  is the maximum number of the spanned teeth:

$$z_{w\max} = \frac{\sqrt{d_a^2 - d_b^2 - S_b}}{p_b}. \quad (9.26)$$

Calipers, micrometers, or special gages are used for span measurement.

### 9.3 Composite Gear Inspection

There are two types of composite gear inspection: single- and double-flank composite testing [105].

Single-flank composite testing is used for the mating gears at a fixed center distance for transmission error component measurement that includes adjacent pitch variation, total accumulated pitch variation, tooth-to-tooth transmission variation, and total transmission variation. This type of testing applied to custom directly designed gears is practically the same as for conventional gears, except gears with asymmetric teeth that use both flanks for torque or motion transmission. In this case, opposite flanks require separate testing. This method provides a good indication of gear pair functionality because it checks two mating gears.

Double-flank composite testing has the inspected gear mounted on a rolling fixture (roll tester) with a tight spring-loaded mesh with a master gear. Deviations of the center distance during gear rotation indicate the tooth-to-tooth composite error (TTE) and total composite error (TCE). Modern

roll testers with a computerized data acquisition system also allow evaluation of functional tooth thickness and radial run-out. Double-flank roll testing is a quick and inexpensive way to separate acceptable and defective gears.

However, it does not indicate which gear dimension or accuracy parameter is responsible for excessive TTE and TCE. It also does not recognize which gear tooth flank is a major contributor to composite errors. Double-flank composite testing does not provide sufficient data about actual gear pair functionality because it checks only one gear in mesh with the master gear.

This type of testing is also applied to custom directly designed gears. However, it requires the custom master gears.

---

## 9.4 Elemental Gear Inspection

Coordinate measuring machines (CMM) are used for elemental gear inspection (Figure 9.10). It allows mapping a surface of all teeth, including the fillet profiles. It provides measurement results for involute flank elemental accuracy parameters: run-out tolerance, pitch variation, profile tolerance, and lead or tooth alignment tolerance. In Direct Gear Design a whole gear tooth profile, including the root fillet, is optimized. Therefore actual accuracy of the root fillet profile should be also inspected by a CMM. The gear tooth (including the root fillet) CAD profile at the average material condition is used for the CMM inspection. The data set also includes the involute flank and fillet profile tolerances that are established, depending on required gear accuracy and also the manufacturing technology. The CMM is programmed to indicate if the inspected tooth profile points lie within the corridor defined by the CAD tooth profile  $\pm$  profile tolerance. An example of the CMM inspection chart of the optimized root fillet profile is shown in Figure 9.11.

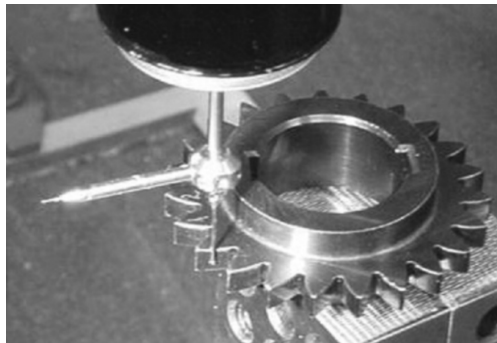


**FIGURE 9.10**

CMM measurement of asymmetric gear. (From Kapelevich, A.L., *Gear Technology*, January/February 2011, 60–65. With permission.)

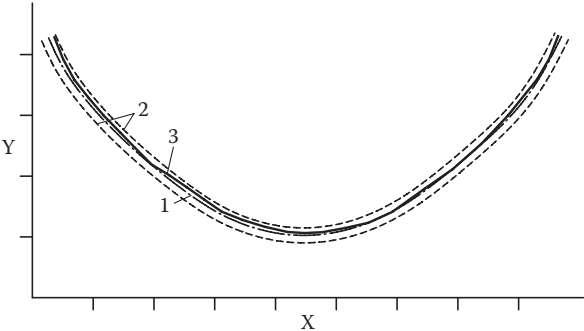


**FIGURE 9.11**  
CMM inspection chart of the optimized root fillet profile. 1 - nominal (average material condition) profile (dash-dotted contour); 2 - tolerance corridor (dashed contour); 3 - actual inspected profile (solid fat contour).



# 10

---

## *Comparison of Traditional and Direct Gear Design<sup>®</sup>*

---

The benefits of traditional gear design are well known: It is comprehensively standardized and has great availability of design software, tooling, and a massive volume of experimental data. It provides acceptable solutions for practically all types of gear drive applications. A goal of this chapter is not to undermine or criticize the traditional gear design approach, but to compare it with Direct Gear Design<sup>®</sup> to help a gear engineer choose the most suitable design method for a particular gear application.




---

### **10.1 Comparable Geometry and Stress Analysis**

In some publications dedicated to advanced gear geometry, its performance results are compared with the standard 20° pressure angle gears, indicating impressive advantages of new gear geometry. Although such comparison makes some sense, because baseline performance of the standard gears is well known, it cannot be considered a fair one. The standard gears are universally applicable, but they by no means are suitable for high-performance demanding applications. New advanced performance gear geometry should be compared with the best-known solutions to evaluate its true benefits. Such known baseline gear geometry can be found, for example, in aerospace gear transmissions. Although such a comparison approach does not usually result in very impressive numbers, indicating new gear geometry advantages, it puts this new gear geometry side by side with the best existing one to assess its true benefits. Table 10.1 presents directly designed optimized gears with symmetric and asymmetric teeth in comparison with the traditionally designed aerospace type gears that have a high 25° pressure angle and a full circular root fillet. Table 10.2 presents a comparison of the directly designed symmetric and asymmetric HCR gears with the traditionally designed HCR gears that have the high (>2.0) transverse contact ratio and the full circular root fillet. Such gears are also used in aerospace gear transmissions [106].

**TABLE 10.1**

Comparison of Directly and Traditionally Designed Conventional Gears

Design Method	Traditional (Baseline)		Direct			
	Symmetric		Symmetric		Asymmetric	
Gear mesh						
Gears	Pinion	Gear	Pinion	Gear	Pinion	Gear
Number of teeth	27	49	27	49	27	49
Module, mm	3.0		3.0		3.0	
X-shift	0.09	-0.09	N/A	N/A	N/A	N/A
Root fillet profile	Full circle		Optimized		Optimized	
Operating pressure angle	25°		27°		32°/18°*	
Drive contact ratio	1.49		1.49		1.49/1.98*	
Pitch diameter, mm	81.0	147.0	81.0	147.0	81.0	147.0
Outer diameter, mm	87.540	152.46	87.444	153.133	87.895	153.645
Root diameter, mm	74.285	138.962	74.185	139.80	73.685	139.488
Root clearance, mm	0.628	0.749	0.341	0.380	0.335	0.308
Tooth thickness at pitch diameter, mm	4.955	4.469	4.873	4.551	4.873	4.551
Tooth thickness at outer diameter, mm	1.543	1.797	1.248	1.244	1.13	1.13
Center distance, mm	114.0		114.0		114.0	
Face width, mm	30	30	30	30	30	30
Driving torque, Nm	300		300		300	
Bending stress, MPa	210	213	178	179	182	183
			(-15%)	(-16%)	(-13%)	(-14%)
Contact stress, MPa	958		937 (-2%)		886 (-7.5%)	
Drive flank specific sliding velocity	0.258	0.230	0.241	0.241	0.228	0.228
Bearing load, N	8172		8313 (+2%)		8734 (+7%)	
Maximum tooth tip deflection, mm	0.0054	0.0049	0.0047	0.0048	0.0071	0.0058

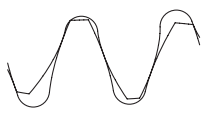





\* Drive/coast flank parameter.

## 10.2 Gear Testing Results Comparison

Experimental comparison of the traditional and Direct Gear Design approaches was done by the Rotorcraft division of the Boeing Company [107]. Directly designed gears with an asymmetric involute gear tooth form were analyzed to determine their bending and contact stresses relative to

**TABLE 10.2**

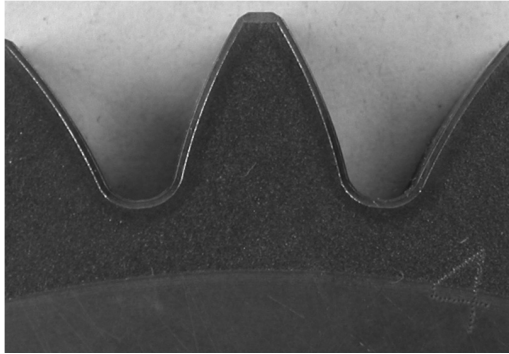
Comparison of Directly and Traditionally Designed HCR Gears

Design Method	Traditional (Baseline)		Direct			
	Symmetric		Symmetric		Asymmetric	
Tooth Shape						
Gear mesh						
Gear	Pinion	Gear	Pinion	Gear	Pinion	Gear
Number of teeth	27	49	27	49	27	49
Module, mm	3.0		3.0		3.0	
X-shift	0.15	-0.15	N/A	N/A	N/A	N/A
Root fillet profile	Full circle		Optimized		Optimized	
Operating pressure angle	20°		21.5°		24°/16°	
Drive contact ratio	2.04		2.04		2.04/2.48*	
Pitch diameter, mm	81.0	147.0	81.0	147.0	81.0	147.0
Outer diameter, mm	89.40	153.60	89.108	154.442	89.576	154.963
Root diameter, mm	73.658	137.822	73.040	138.347	72.394	137.901
Root clearance, mm	0.371	0.389	0.259	0.273	0.322	0.262
Tooth thickness at pitch diameter, mm	5.040	4.384	5.0140	4.410	5.020	4.404
Tooth thickness at outer diameter, mm	1.18	1.70	1.12	1.13	1.01	1.02
Center distance, mm	114.0		114.0		114.0	
Face width, mm	30	30	30	30	30	30
Driving torque, Nm	300		300		300	
Bending stress, MPa	147	150	122 (-17%)	123 (-18%)	126 (-14%)	126 (-16%)
Contact stress, MPa	824		808 (-2%)		774 (-6%)	
Drive flank specific sliding velocity	0.367	0.323	0.342	0.342	0.336	0.336
Bearing load, N	7882		7961 (+1%)		8108 (+3%)	
Maximum tooth tip deflection, mm	0.0071	0.0068	0.0073	0.0070	0.0084	0.0081

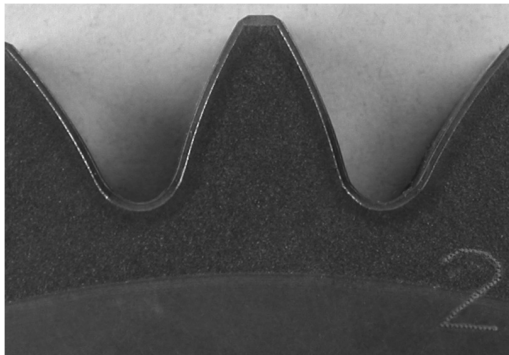
\* Drive/coast flank parameter.

the symmetric involute gear tooth form, which is representative of helicopter main drive gears. Asymmetric and baseline (symmetric) toothed gear test specimens were designed, fabricated, and tested to experimentally determine their single-tooth bending fatigue strength and scuffing resistance. Also, the directly designed symmetric gears with an analytically optimized tooth root fillet form were made and tested to determine their single-tooth bending fatigue characteristics relative to baseline specimens with a circular root fillet form. The gear test specimens are presented in Figure 10.1.

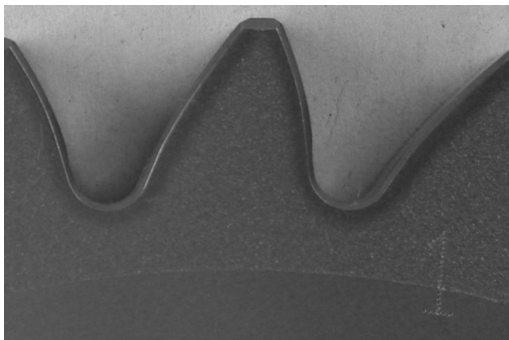




(a)



(b)



(c)

**FIGURE 10.1**

Test specimen gear tooth profiles: (a) baseline gear teeth, (b) symmetric gear teeth with optimized fillet, (c) asymmetric gear teeth. (Courtesy of Boeing Co., Philadelphia, Pennsylvania.)

The objective of this work was to evaluate the potential benefits of asymmetric involute gear teeth and optimized root fillet geometry for helicopter main transmission applications. This involved not only quantifying performance improvements achieved by these concepts, but evaluating the practicality of manufacturing gears with asymmetric teeth and optimized root fillet geometry for aerospace applications.

### **10.2.1 Test Specimen Design and Analysis**

Test specimen gears designed for this program were representative of helicopter main drive gears in diametral pitch, pressure angle, material, and processing. Standardized traditional toothed designs have been developed for bending fatigue and scuffing test rigs that Boeing Rotorcraft uses for gear research. The standardized test specimen designs were modified to incorporate the asymmetric tooth configuration, and another for the optimized fillet configuration. Specimens of each type were manufactured using aerospace production techniques and requirements. A manufacturing approach was developed with a goal of reducing material and processing variability. The test specimen gear designs were analyzed to predict their bending and contact stresses, and compared to stresses predicted for the baseline test specimens.

The single-tooth bending fatigue test gears are 32-tooth gears with groups of 4 teeth removed per quadrant to allow for assembly into the single-tooth bending fatigue (STBF) test fixture. For comparison, conventional symmetric involute gears and gears with asymmetric involute teeth were designed and tested. Both asymmetric toothed and conventional baseline specimens employ ground circular root fillets. The asymmetric gear tooth form for the STBF test specimens was nominally based on the standard STBF gear specimen. This enabled the asymmetric toothed specimen to fit the existing test fixture with only minor modifications for tooth load angle, and provided a direct comparison between asymmetric and conventional gears of the same diameter and face width. Single-tooth bending fatigue specimens with the optimized fillets share the same symmetric tooth geometry as the baseline, except for the form of the root fillet. The form of the optimized root fillet profile was determined analytically. A comparison of the geometry between the circular fillet and the optimized fillet geometries is shown in Figure 10.2.

The gear parameters and finite element analysis (FEA) calculated bending stresses for the STBF test gears are presented in Table 10.3, and the scuffing test gears are within the design experience range of typical main transmission helicopter power gears. The gear parameters for the scuffing test gear specimens are presented in Table 10.4.

### **10.2.2 Test Specimen Manufacturing**

The asymmetric gear specimens, optimized root fillet gear specimens, and baseline circular fillet test gears were fabricated by Aero Gear (South

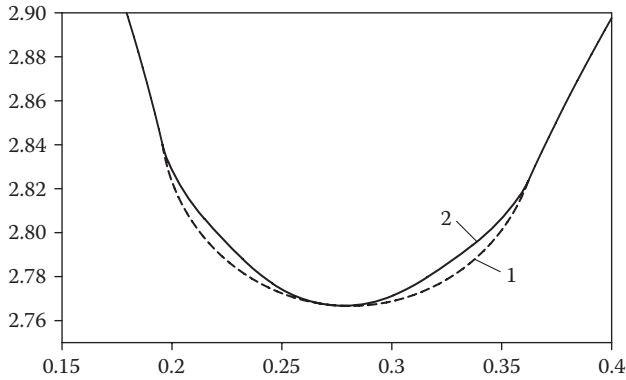


**FIGURE 10.2**

Coordinate plot of tooth fillet design geometries. 1 - circular fillet; 2 - optimized fillet. (From Brown, F.W., et al., *Gear Technology*, June/July 2011, 46–55. With permission.)

**TABLE 10.3**

STBF Test Gear Specimen Parameters

	Symmetric Gears with Circular Fillets (baseline)	Symmetric Gears with Optimized Fillets	Asymmetric Gears with Circular Fillets
Number of teeth of both mating gears	32	32	32
Diametral pitch, 1/in.	5.333	5.333	5.333
Pressure angle	25°	25°	35°/15°*
Pitch diameter, in.	6.000	6.000	6.000
Base diameter, in.	5.4378	5.4378	4.9149/5.7956*
Outside diameter, in.	6.3975	6.3975	6.3864
Root diameter, in.	5.571	5.571	5.558
Form diameter, in.	5.6939	5.6939	5.6581/5.8110*
Circular tooth thickness, in.	0.2895	0.2895	0.2895
Face width, in.	0.375	0.375	0.375
Torque, in.-lb	5000	5000	5000
Load application radius, in.	3.06	3.06	3.06
Calculated maximum bending stress, psi	57,887	48,387 (–16.4%)	54,703 (–5.5%)

\* Drive/coast flank parameter.

Windsor, Connecticut). The specimens were fabricated from aerospace quality (AGMA Grade 3) 9310 steel with all pertinent records and certifications retained. All specimens were low-pressure carburized and high-pressure gas quenched. Low-pressure carburizing and high-pressure gas quench heat treating processes were performed at Solar Atmospheres (Souderton, Pennsylvania). The material for all specimens was from the same lot and the heat treat processes, grind stock removal, and shot peening processes for all

TABLE 10.4

Scuffing Test Gear Specimen Parameters

	Symmetric Gears with Circular Fillets (baseline)	Asymmetric Gears with Circular Fillets
Number of teeth of both mating gears	30	30
Diametral pitch, 1/in.	5.000	5.000
Pressure angle	25°	35°/18°
Pitch diameter, in.	6.000	6.000
Base diameter, in.	5.4378	4.9149/5.7063*
Outside diameter, in.	6.400 max	6.403 max
Root diameter, in.	5.459 max	5.510
Form diameter, in.	5.6864	5.6415/5.7607*
Circular tooth thickness, in.	0.3096	0.3096
Face width, in.	0.50	0.50
Drive contact ratio	1.417	1.25
Torque, in.-lb	6000	6000
Calculated maximum contact stress, psi	193,180	174,100 (-9.9%)

\* Drive/coast flank parameter.

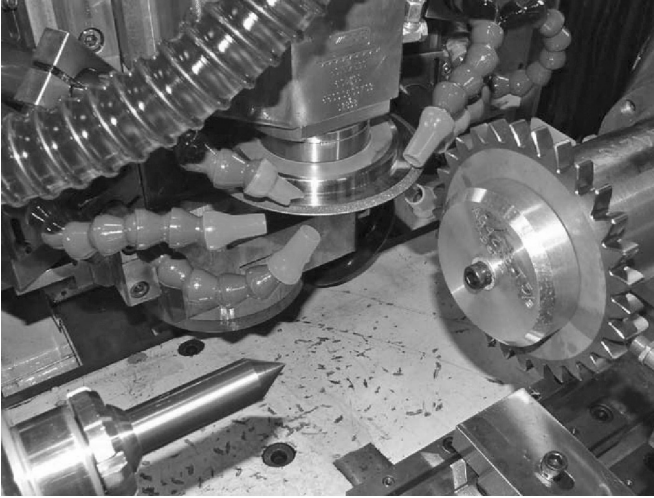
specimens were identical. All gears were surface temper etch inspected and magnetic particle inspected after the completion of machining.

All specimens produced for this project were ground using conventional gear tooth form grinding equipment, including the asymmetric tooth specimens and specimens with optimized root fillet geometry. The form grinding process is often used to grind conventional symmetric gear teeth with circular fillets in helicopter main drives. The cubic boron nitride (CBN) form grinding wheels were produced from data shown on the engineering drawings for both the asymmetric gear teeth and optimized fillet geometry. The CBN gear grinding setup is shown in Figure 10.3. Measurements of the gear teeth, including the fillet profile, were carried out using conventional CMM gear checking equipment and software.

10.2.3 Test Arrangement and Procedure

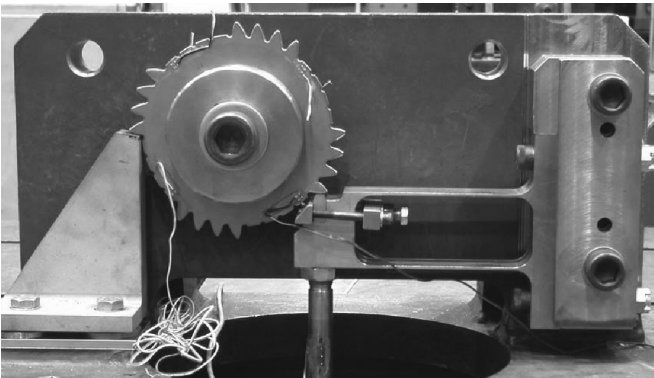
Single-tooth bending fatigue tests were performed on nonrotating STBF test fixtures, shown in Figure 10.4. These fixtures are loaded by Baldwin-Lima-Hamilton IV-20 universal fatigue machines through a series of alignment fixtures and in-line load cells. These fatigue machines are capable of 18,000 lb (10,000 lb steady load and 8,000 lb alternating load).

For the STBF testing of the subject gears, pulsating fatigue load is applied to the tooth through the load link and flexure arrangement shown in Figure 10.4. The test gear teeth were cycled at approximately 1200 cycles per minute. Prior to the start of testing, alignment of the fixture was verified with a strain-gaged baseline specimen. The specimen was instrumented



**FIGURE 10.3**

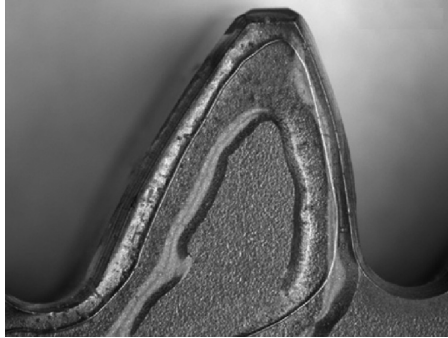
Gear form grinding setup with CBN grinding wheel. (Courtesy of Aero Gear, South Windsor, Connecticut. From Brown, F.W., et al., *Gear Technology*, June/July 2011, 46–55. With permission.)



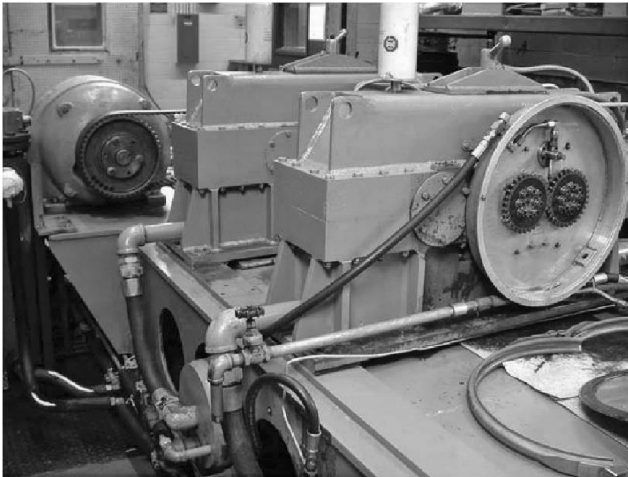
**FIGURE 10.4**

STBF test fixture with asymmetric gear installed. (Courtesy of Boeing Co., Philadelphia, Pennsylvania. From Brown, F.W., et al., *Gear Technology*, June/July 2011, 46–55. With permission.)

with three strain gages across the face width and was used to align the fixture as well as correlate load applied to stress in the fillet of the tooth. For fatigue testing, each tested tooth is instrumented with a crack-wire, as seen in Figure 10.5. Upon failure of the crack-wire due to the presence of a fatigue crack, the test machine is triggered to shut down. The crack-wire is placed so that a crack length of 0.050 in. is detected. Magnetic particle inspection is used to confirm the presence of a crack. Each tooth specimen was run continuously until failure or run-out. For this project, run-out was defined as  $1.0 \times 10^7$  cycles.

**FIGURE 10.5**

Asymmetric STBF test tooth with crack-wire installed. (Courtesy of Boeing Co., Philadelphia, Pennsylvania. From Brown, F.W., et al., *Gear Technology*, June/July 2011, 46–55. With permission.)

**FIGURE 10.6**

Scuffing test rig with cover removed and test specimen gears installed. (Courtesy of Boeing Co., Philadelphia, Pennsylvania. From Brown, F.W., et al., *Gear Technology*, June/July 2011, 46–55. With permission.)

Scuffing tests of asymmetric gear specimens and baseline specimens were conducted on a gear research test stand. The test stand is a split-coupling torque design. The test gears are outboard of the main housing and can be quickly inspected or changed by removal of a simple cover (see Figure 10.6).

A separate lubrication system serves the test specimen chamber, which was isolated from the test stand drive lubrication system. The lubricant supply to the test gears could be heated or cooled to supply lubricant at a constant temperature to the test gears. The test gears were subjected to a series of 15 min long, incrementally loaded runs. At the end of each 15 min run, a visual evaluation of the test gear teeth was conducted. If the condition of the

gears did not meet the criteria for scuffing failure, the next higher incremental load was applied. This procedure was continued until a scuffing failure was observed. For purposes of this test program, a scuffing failure was declared when 25% of the available tooth contact surface exhibited visible evidence of radial scratch marks, characteristic of scuffing, on a minimum of 10 teeth.

#### 10.2.4 Test Results

At the conclusion of the single-tooth bending fatigue tests, all crack locations were verified both visually and using magnetic particle inspection (MPI), as shown in Figure 10.7. Cracks were also opened to determine the origins and confirm the validity of the results. In Figure 10.8 the dark dashed line represents the extent of fatigue propagation, and the arrow indicates the fracture origin.

Fatigue results of the STBF tests of the asymmetric tooth, the optimized root fillet tooth, and the baseline specimens are presented in Figure 10.9. Curves for the optimized root fillet data and the asymmetric data were assumed to be parallel to the baseline curve.

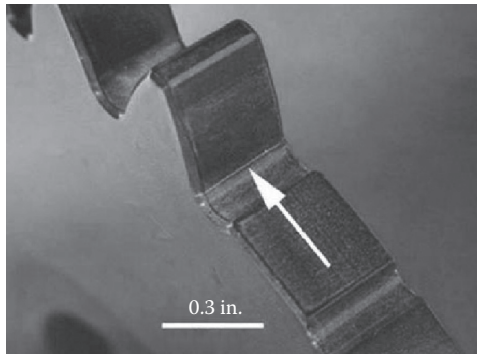


**FIGURE 10.7**

Cracked STBF test gear tooth showing MPI crack indication. (Courtesy of Boeing Co., Philadelphia, Pennsylvania. From Brown, F.W., et al., *Gear Technology*, June/July 2011, 46–55. With permission.)

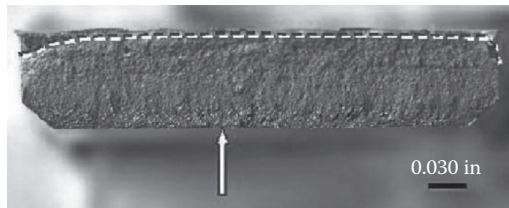


**FIGURE 10.8**

Fractograph of STBF test tooth. (Courtesy of Boeing Co., Philadelphia, Pennsylvania. From Brown, F.W., et al., *Gear Technology*, June/July 2011, 46–55. With permission.)

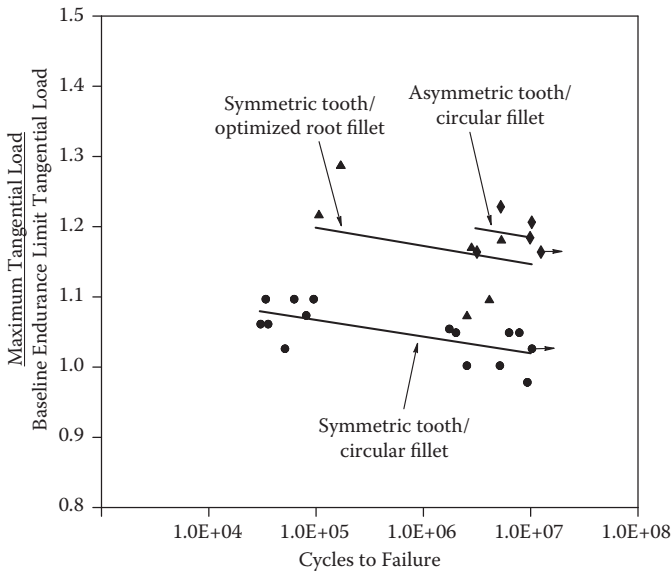


**FIGURE 10.9**

STBF data for asymmetric gears and optimized root fillet gears along with baseline symmetric tooth/circular fillet test data. (From Brown, F.W., et al., *Gear Technology*, June/July 2011, 46–55. With permission.)

Typical scuffing failures are shown in Figures 10.10 and 10.11. These figures show the vertical scratches indicative of a scuffing failure, associated with the breakdown of the separating lubricant film between the gears. Figure 10.12 shows the scuffing results for baseline and asymmetric gears. The 35° pressure angle asymmetric gears showed an improvement of approximately 25% in the mean scuffing load (torque) compared to the baseline symmetric tooth specimens. The mean 3-sigma levels are also shown, based on a population of eight baseline data points and six asymmetric data points.

### 10.2.5 Results Analysis

The STBF test results shown in Figure 10.9 indicate the asymmetric tooth gear design mean endurance limit was significantly higher, on the order of 16% higher, than the mean endurance limit of the baseline symmetric tooth design. It should be pointed out that there are relatively few data points, four failure points and one run-out (included as a failure point in the data analysis), for the asymmetric tooth specimens. Nonetheless, the results of this testing indicate that asymmetric teeth offer an improvement in bending fatigue strength, although additional testing would serve to refine the magnitude of the improvement. It is interesting to note that the FE analysis of the asymmetric tooth STBF design predicted a 5.5% reduction in maximum bending stress compared to the baseline symmetric design.



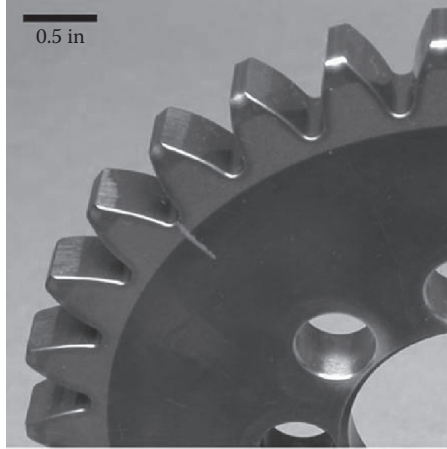


**FIGURE 10.10**

Scuffing failure of baseline test gear. (Courtesy of Boeing Co. Philadelphia, Pennsylvania. From Brown, F.W., et al., *Gear Technology*, June/July 2011, 46–55. With permission.)

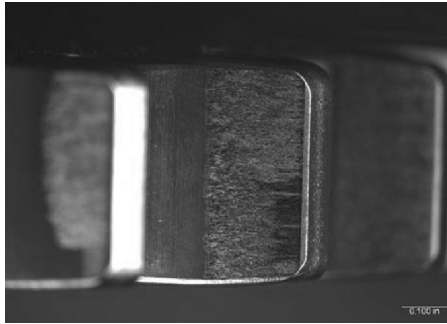


**FIGURE 10.11**

Close-up view of a representative scuffed tooth. (Courtesy of Boeing Co., Philadelphia, Pennsylvania. From Brown, F.W., et al., *Gear Technology*, June/July 2011, 46–55. With permission.)

The STBF results for the optimized fillet geometry design showed an improvement in mean gear tooth bending fatigue strength exceeding 10%, based on limited testing—six failure points. The data points for these tests display more variation (scatter) than either the baseline data or the asymmetric tooth data. Post-test evaluation of the test specimens and observations of the fracture surfaces did not indicate any anomalies that could explain the variation, such as variations in optimized fillet form/dimensions or specimen metallurgy. One theory is that the test fixture was damaged while testing at the higher load levels. The FEA of the optimized fillet design indicated a reduction in maximum bending stress (calculated) of 16.4% compared to the baseline circular fillet design. While not tested in this project, the combination of asymmetric teeth and optimized fillet geometry together, in the

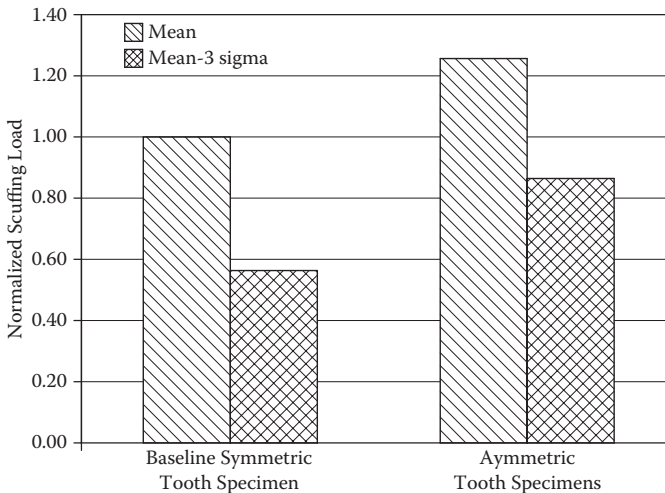


**FIGURE 10.12**

Results of baseline symmetric and asymmetric gear scuffing tests. (From Brown, F.W., et al., *Gear Technology*, June/July 2011, 46–55. With permission.)

same gear design, may offer improvements in tooth bending fatigue strength greater than either of the concepts taken individually. The decision was made early in this project to test each concept separately. The reasoning was that if one concept or the other proved to be impractical from a manufacturing standpoint, data of value would still be attained for the other concept. Since both concepts appear viable from a manufacturing standpoint, their combination in one gear design is worth further investigation.

The scuffing test results (Figure 10.12) indicated an improvement in mean scuffing load (torque) to failure of 25% for the asymmetric tooth gear specimens compared to the baseline symmetric tooth specimens. The improvement in calculated mean 3-sigma scuffing performance is even greater. Although based on limited testing, eight baseline points and six asymmetric tooth data points, this is a very significant improvement in scuffing resistance due to asymmetric gear tooth geometry. This improvement was in the primary drive direction of the asymmetric teeth. The opposite (coast) direction scuffing performance of the asymmetric teeth was not tested in this project. This improvement in scuffing resistance can be utilized to advantage in high-speed, scuffing-critical gear applications.

### 10.2.6 Testing Results Conclusion

Test results demonstrated higher bending fatigue strength for both the asymmetric tooth form and optimized fillet than for baseline designs. Scuffing resistance was significantly increased for the asymmetric tooth form compared to a traditional symmetric involute tooth design.

---

### 10.3 Design Method Selection

Analytical and experimental comparison of traditional and direct approaches to gear design indicates certain benefits of Direct Gear Design for custom gear drives. These benefits mainly include bending stress reduction that increases tooth strength, and contact stress reduction that increases the tooth surface endurance and wear resistance, reducing the pitting and scuffing probability. Stress reduction provided by advanced tooth geometry allows boosting of the gear drive power transmission density, increasing its load capacity or reducing its size and weight, prolong its life, and improve its reliability. Possible stress and gear size reduction leads to potential cost reduction by using a reduced amount or less expensive materials.

Application of the asymmetric tooth profile with a higher pressure angle, besides the stress reduction, provides lower specific sliding velocities and higher thickness of the elastohydrodynamic lubricant film (because of larger tooth contact curvature radii) on the drive flanks of the gear teeth. This leads to increased gear efficiency. Independent parameter selection of the drive and coast flanks, and the root fillet profile of asymmetric teeth, also makes it possible to reduce gear tooth stiffness, noise, and vibration.

Now the gear designer has a choice to make: which gear design approach is more suitable for a particular gear drive application. Table 10.5 summarizes the main characteristics of both traditional and Direct Gear Design methods.

Further development of the Direct Gear Design method, and testing database accumulation, should encourage its implementation in custom gear transmission.

**TABLE 10.5**

Summary of Traditional and Direct Gear Design

Traditional Gear Design	Direct Gear Design
<i>Basic Principle</i>	
Gear design is driven by standards and manufacturing convenience	Gear design is driven by application, and product technical and market performance requirements
<i>Advantages</i>	
<ul style="list-style-type: none"> <li>• Universal applicability</li> <li>• Availability of standard design manuals, software, and tooling</li> <li>• Gear interchangeability</li> <li>• Low tooling inventory</li> <li>• Vast accumulated experience and testing database</li> </ul>	<p>High gear drive performance provided by bending and contact stress reduction includes:</p> <ul style="list-style-type: none"> <li>• High power transmission density—high load capacity or reduced size and weight</li> <li>• Longer life</li> <li>• Lower cost</li> <li>• Lower noise and vibration</li> <li>• Higher efficiency and reliability</li> </ul>
<i>Drawbacks</i>	
Limited gear drive performance	Requires custom dedicated tooling for every gear; limited experience and testing database
<i>Typical Applications</i>	
<p>Standardized gears and gear drives:</p> <ul style="list-style-type: none"> <li>• Stock gears</li> <li>• Gearboxes with interchangeable gear sets</li> <li>• Low production volume machined gears</li> </ul>	<p>Custom gear drives:</p> <ul style="list-style-type: none"> <li>• Formed gears fabricated by plastic and metal injection molding, powder metal processing, die cast, net forging, etc.</li> <li>• High production volume machined gears</li> <li>• Gear drives with special requirements and extreme applications (aerospace, racing, automotive transmissions, etc.)</li> </ul>



# 11

---

## *Implementation Examples*

---

The Direct Gear Design® approach has been implemented in many custom gear drives. This chapter describes three such implementation examples presenting different applications, gear tooth geometries, materials, and fabrication technologies.

---

### 11.1 Speed Boat Gearbox

The Marine Technology, Inc. turbine race boat powered by twin Lycoming T55 turboshaft engines required light and compact gearboxes. The boat power train arrangement also necessitated a significant vertical offset between the turbine shaft and propeller shaft. This offset defined the gearbox envelope with two idler gears. Its schematic arrangement is shown in Figure 11.1.

#### 11.1.1 Gear Design

Gearbox data:

- Lycoming T55 turboshaft engine maximum power: 3000 HP
- Turbine shaft RPM: 16,000
- Gear ratio: 2:1
- Vertical input/output shaft offset: 21.20 in.
- Overall gearbox dimensions (length × height × width): 16 × 34 × 5 in.
- Gearbox weight: 270 lb

The gearbox was designed and manufactured by Three Sigma Manufacturing, Inc. (Kent, Washington) that subcontracted AKGears, LLC (Shoreview, Minnesota) for gear design and optimization. The high contact ratio (HCR) spur gear tooth geometry was chosen to provide high load capacity, low vibration level, and zero axial thrust load on the bearings. Symmetric gear tooth profiles were selected because of two idler gears that have both tooth flanks equally loaded. The tooth root fillets were optimized to minimize

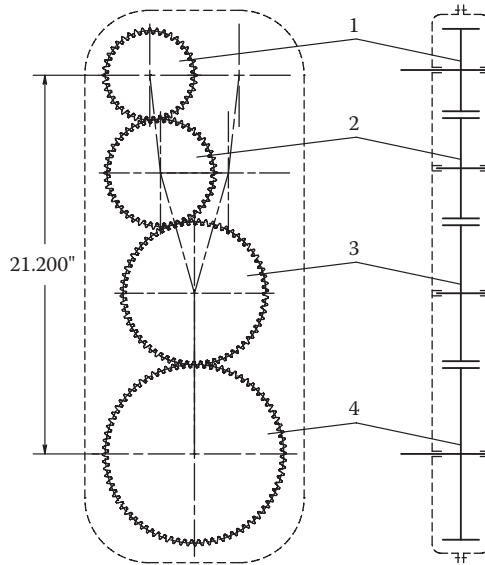


**FIGURE 11.1**

Gearbox arrangement. 1 - input gear; 2 - idler gear 1; 3 - idler gear 2; 4 - output gear.

bending stress concentration. Table 11.1 presents the gear design data and the stress analysis results, and gear tooth profiles are shown in Figure 11.2.

### 11.1.2 Gear Fabrication

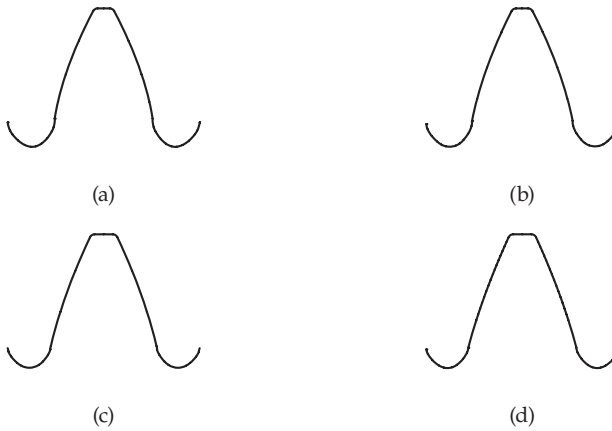
Considering low production volume (only two gearboxes required), a unique gear wire-cut EDM fabrication technology was applied. Unlike conventional gear cutting and grinding, it did not require special cutting tools. Gears were made out of the AISI 9310 steel, with a surface hardness of Rc 59-61, core hardness of about Rc 36, and final carburized depth of 0.020–0.030 in. The wire cutting process, although proprietary, can be summarized as follows: The gear blanks were roughly turned and heat treated to required core hardness. Final turning of the blanks was then performed and some preparatory machining carried out in order to begin the EDM wire cutting process. The tooth forms were preliminarily wire cut, leaving only 0.005 in. stock. Then gears were carburized and quenched. It should be noted that the tooth tips were not carburized. The final tooth geometry was then generated by the wire-cut EDM process, with special positioning techniques used to ensure uniform stock removal. A 10  $\mu\text{m}$  Ra surface finish was achieved. The internal spline is also produced in the same fixture, providing for extremely close concentricity to the gear teeth. The gears were then treated with the REM process [108], which also rounded all sharp edges and improved the surface finish on the tooth flanks to 4  $\mu\text{m}$  Ra.

TABLE 11.1

## Speedboat Gearbox Data

Gear	Input Gear	Idler Gear 1	Idler Gear 2	Output Gear
Number of teeth	40	48	64	80
Diametral pitch, in.	8.000	8.000	8.000	8.000
Pressure angle, °	21.0	21.0	21.0	21.0
Pitch diameter, in.	5.000	6.000	8.000	10.000
Base diameter, in.	4.6679	5.6015	7.4686	9.3358
Tooth tip diameter, in.	5.321/5.326	6.326/6.331	8.315/8.323	10.307/10.315
Maximum form diameter, in.	4.763	5.758	7.7385	9.7368
Root diameter, in.	4.623/4.629	5.629/5.635	7.632/7.638	9.633/9.641
Tooth thickness at pitch diameter, in.	0.1906/0.1931	0.1906/0.1931	0.1906/0.1931	0.1906/0.1931
Tooth tip radius, in.	0.010/0.013	0.010/0.013	0.010/0.013	0.010/0.013
Tooth tip land, in.	0.028/0.040	0.028/0.040	0.035/0.049	0.042/0.055
Face width, in.	1.650	1.650	1.550	1.550
Center distance, in.	5.5000 ± 0.0025	7.0000 ± 0.0025	9.0000 ± 0.0025	
<i>Accuracy and Inspection Parameters</i>				
Accuracy grade per AGMA 2000-A88 [105]	Q11B	Q11B	Q11B	Q11B
Run-out tolerance, in.	0.0012	0.0012	0.0013	0.0014
Pitch variation, in.	±0.0003	±0.0003	±0.0003	±0.0003
Profile tolerance, in.	0.0004	0.0004	0.0004	0.0004
Lead tolerance, in.	0.0004	0.0004	0.0004	0.0004
Pin diameter, in.	0.250	.250	.250	.250
Measurement over pins, in.	5.406/5.412	6.408/6.414	8.411/8.416	10.412/10.418
<i>Tolerance Analysis Results</i>				
Operating pressure angle, °	20.90/21.10	20.92/21.08	20.93/21.04	
Operating contact ratio	2.01/2.11	2.04/2.15	2.02/2.15	
Operating normal backlash, in.	0.003/0.013	0.003/0.013	0.003/0.014	
Radial clearance, in.	0.016/0.029	0.018/0.032	0.020/0.034	0.017/0.030
<i>Stress Analysis Results</i>				
Power, HP		3,000		
RPM	16,000	13,333	10,000	8,000
Torque, in.-lb	11,657	13,988	18,651	23,314
Bearing load, lb	4,995	4,995	4,995	4,995
Bending stress, psi	35,920	34,380	36,720	36,530
Contact stress, psi	142,200	133,470		115,423
Gear material	AISI 9310 (carburized, harden)			



**FIGURE 11.2**

Tooth profiles: (a) input gear, (b) idler gear 1, (c) idler gear 2, (d) output gear.

### 11.1.3 Gearbox Performance Testing

Performance testing was done with the gearbox installed in the race vehicle. Gearbox performance was judged by its temperature, vibration level, and overall vehicle performance. There were no major maintenance issues, temperature was in the range considered safe, and vibration was minimal. The vehicle ultimately exceeded 210 mph numerous times and the gearbox project was deemed a success. Photos of the input gear teeth, gears, mounted gearbox, and racing boat are shown in Figures 11.3 to 11.6.

---

## 11.2 Turboprop Engine Gearbox

The first known application of gears with asymmetric teeth in the aerospace industry was for the TV7-117S turboprop engine gearbox [109–111]. The engine and gearbox were developed by Klimov Corporation (St. Petersburg, Russia) with the assistance of Central Institute of Aviation Motors (CIAM, Moscow, Russia) for a commuter airplane Ilyushin Il-114 and produced by Chernyshev Enterprise (Moscow, Russia). The main characteristics of its gearbox are presented in Table 11.2.

The TV7-117S gearbox arrangement is shown in Figure 11.7. This arrangement was used in an older generation of Russian turboprop engines AI-20 and AI-24, and it has proved to provide high-power transmission density for required gear ratios. The first planetary differential stage has three planet gears. The second “star” type coaxial stage has five planet (idler) gears and a stationary planet carrier. The first-stage sun gear is connected to the engine

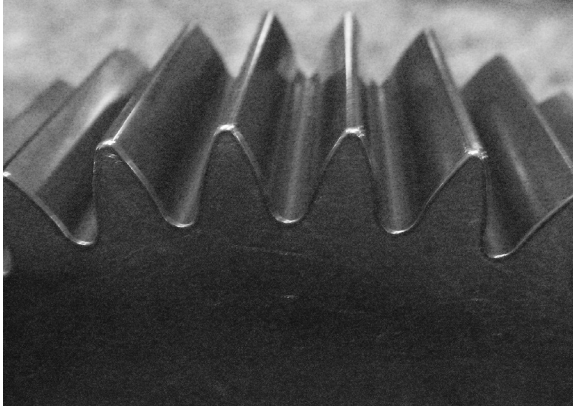


**FIGURE 11.3**  
(See color insert.) Input gear teeth. (Courtesy of Three Sigma Manufacturing, Inc., Kent, Washington.)

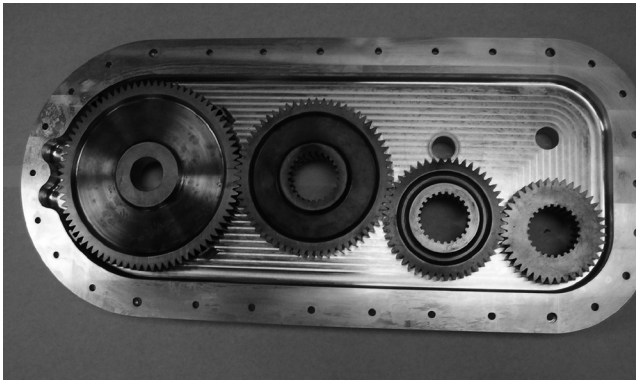


**FIGURE 11.4**  
(See color insert.) Gears in mesh. (Courtesy of Three Sigma Manufacturing, Inc., Kent, Washington.)

turbine shaft. Its ring gear is connected with the second-stage sun gear, and its planet carrier is connected to the second-stage ring gear and output propeller shaft. This arrangement makes it possible to transmit about 33% of the engine power through the first-stage carrier directly to the propeller shaft, bypassing the second stage. This allows the size and weight of the second stage to be reduced, transmitting only 67% of engine power from the first-stage ring gear to the second-stage sun gear, and then through the planets to the second-stage ring attached to the propeller shaft.

All gears have an asymmetric tooth profile. Gear geometry and accuracy parameters, and operating torques and stresses are presented in Table 11.3. All gears were made out of the forged blanks of the steel 20KH3MVF (EI-415). Its

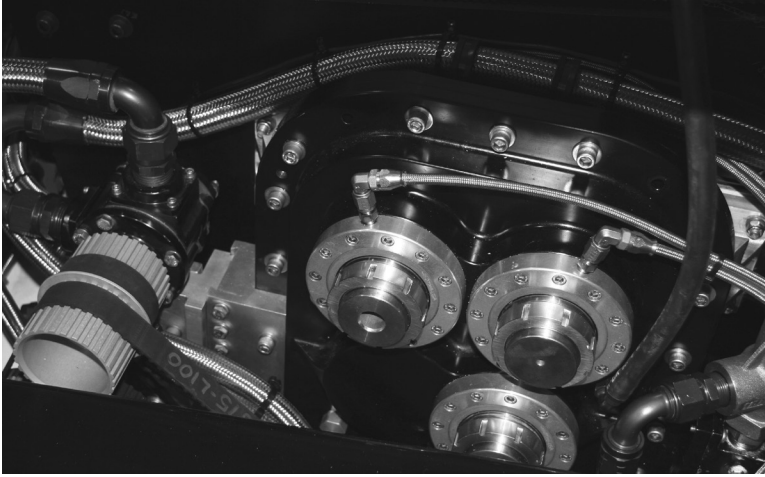


**FIGURE 11.5**  
(See color insert.) Mounted gearbox. (Three Sigma Manufacturing, Inc., Kent, Washington.)



**FIGURE 11.6**  
(See color insert.) Race boat. (Courtesy of Three Sigma Manufacturing, Inc., Kent, Washington.)

**TABLE 11.2**

TV7-117S Turboprop Engine Data

Input turbine RPM	17500
Output prop RPM	1200
Total gear ratio	14.6:1
Overall dimensions, mm:	
• Diameter	520
• Length	645
Gearbox weight, N	1050
Maximum output power, hp	2800
Extreme output power, hp	3500

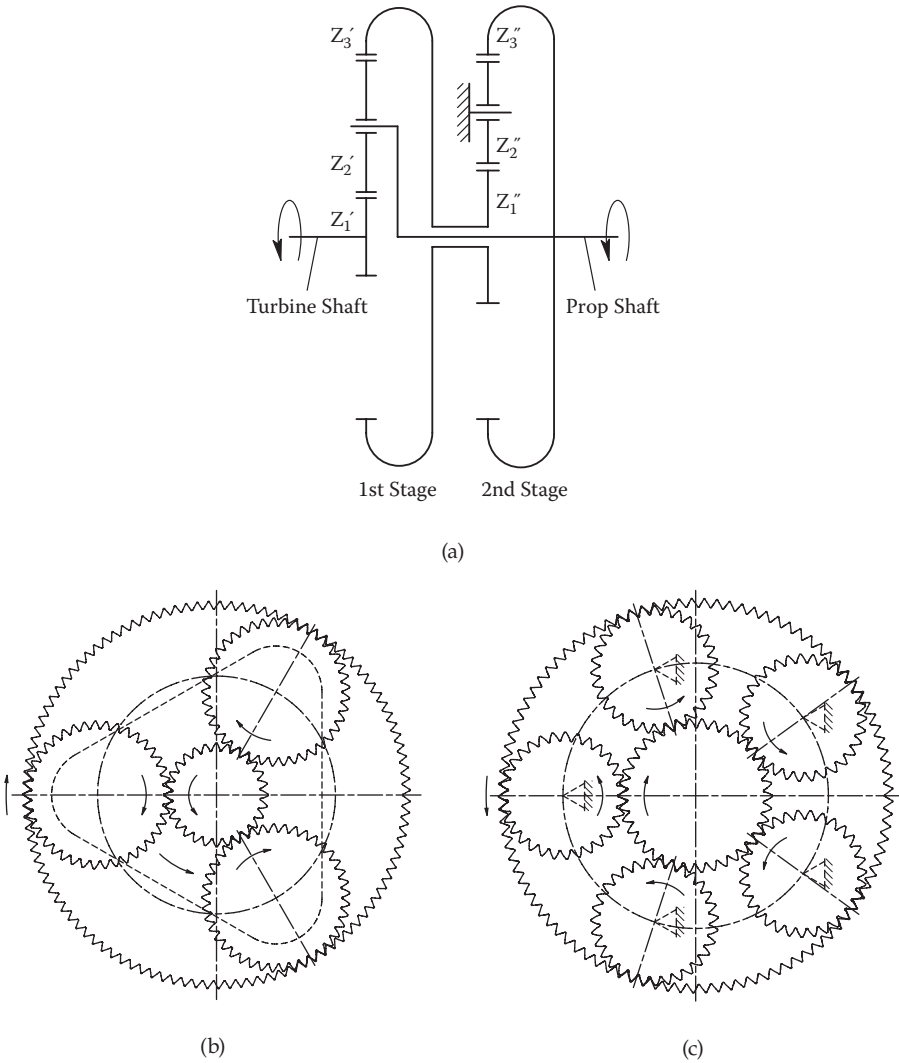


**FIGURE 11.7** Gearbox arrangement (a), first (b) and second (c) stages with rotation directions (view from input shaft). ((a) from Novikov, A.S., et al., *Gear Technology*, January/February 2008, 60–65. With permission.)

chemical composition includes: Fe, base material; C, 0.15–0.20%; S, <0.025%; P, <0.030%; Si, 0.17–0.37%; Mn, 0.25–0.50%; Cr, 2.8–3.3%; Mo, 0.35–0.55%; W, 0.30–0.50%; Co, 0.60–0.85%; and Ni, <0.5%.

Protuberance hobbing was applied for the sun and planet gear machining prior to carburizing and quenching. A custom protuberance hob (see Figure 11.8) was used to provide a final cutting of the gear tooth root fillet, leaving the grinding stock only on the tooth involute flanks. This allowed

**TABLE 11.3**  
Gear Geometry Data

Stage	First			Second		
	Sun	Planet	Ring	Sun	Planet	Ring
Number of gears	1	3	1	1	5	1
Nominal number of teeth	28	41	107	38	31	97
Module, mm	3.000	3.000	3.000	3.362	3.362	3.362
Nominal drive pressure angle, °	33	33 and 25	25	33	33 and 25	25
Nominal coast pressure angle, °	25	25 and 33	33	25	25 and 33	33
Nominal pitch diameter, mm	84.000	123.000	321.000	127.756	104.222	326.114
Drive base diameter, mm	70.448	103.156 and 111.476	290.925	107.145	87.408 and 94.457	295.560
Coast base diameter, mm	76.130	111.476 and 103.156	269.213	115.786	94.457 and 87.408	273.502
Tooth tip diameter, mm	90.02/90.16	128.44/128.60	323.88/324.11	134.07/134.23	110.93/111.07	329.67/329.90
Root diameter, mm	76.55/77.05	114.55/115.05	337.50/337.70	118.56/119.06	95.45/95.95	345.00/345.20
Tooth thickness at nominal pitch diameter, mm	4.773/4.814	4.325/4.365	-0.667/ -0.621	4.972/5.018	5.253/5.299	-1.104/ -1.059
Tooth tip radius, mm	0.20/0.40	0.20/0.40	0.30/0.50	0.20/0.40	0.20/0.40	0.30/0.50
Tooth tip land, mm	0.630/0.982	0.596/0.960	0.395/0.806	0.711/1.081	0.717/1.074	0.350/0.761
Face width, mm	34.75/35.00	31.75/32.00	25.48/26.00	37.75/38.00	34.75/35.00	27.48/28.00
Center distance, mm		103.50 ± 0.01			116.00 ± 0.01	

<i>Accuracy and Inspection Parameters</i>		5-5-4B	5-5-4B	5-5-4B	5-5-4B	5-5-4B	5-5-4B
Accuracy grade per GOST 1643-81[112]		5-5-4B	5-5-4B	5-5-4B	5-5-4B	5-5-4B	5-5-4B
Run-out tolerance, mm		0.016	0.022	0.022	0.022	0.016	0.022
Pitch variation, mm		±0.006	±0.007	±0.007	±0.007	±0.006	±0.007
Profile tolerance, mm		0.006	0.007	0.007	0.007	0.006	0.007
Lead tolerance, mm		0.0055	0.0055	0.0055	0.0055	0.0055	0.0055
Pin diameter, mm		6.000	6.000	6.000	6.000	7.000	7.000
Measurement over pins, mm		93.754/93.819	131.991/132.057	320.476/320.554	138.929/139.004	115.665/115.738	325.309/325.385
<i>Tolerance Analysis Results</i>							
Operating drive pressure angle, °		32.98/33.02	29.87/29.93			32.99/33.03	29.88/29.93
Operating coast pressure angle, °		24.97/25.03	36.64/36.68			24.98/25.04	36.65/36.68
Operating drive contact ratio		1.18/1.26	1.33/1.36			1.20/1.28	1.35/1.38
Operating coast contact ratio		1.33/1.42	1.18/1.21			1.36/1.44	1.21/1.24
Operating normal backlash, mm		0.196/0.322	0.197/406			0.189/0.320	0.206/0.414
Radial clearance, mm		0.651/1.033	0.936/1.308	0.953/1.376	0.921/1.159	0.978/1.356	0.948/1.336
<i>Stress Analysis Results</i>							
Maximum power, HP			2800				
RPM		17,500	-11,132	-3063	-3063	3755	1200
Torque per mesh, Nm		374	548	1430	858	700	2191
Bending stress, MPa	Tension	240	257	280	289	318	345
	Compression	-384	-403	-306	-470	-500	-385
Contact stress, MPa		960	604	604	1043	809	809

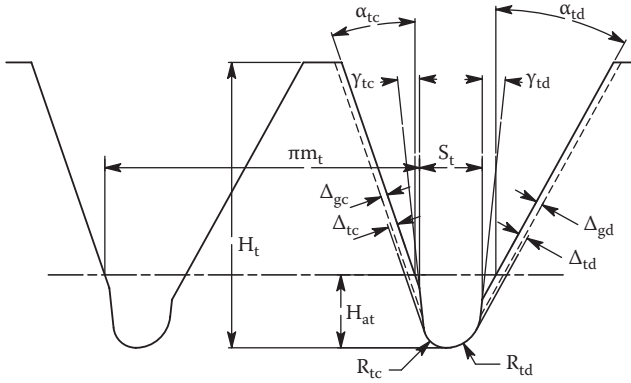


**FIGURE 11.8**  
Protuberance gear hob profile.

**TABLE 11.4**

Protuberance Gear Hob Profile Data

Stage	First		Second	
	Sun	Planet	Sun	Planet
Number of teeth	28	41	38	31
Hob module, mm	$m_t$ 2.876	2.905	3.224	3.224
Hob tooth thickness at pitch line, mm	$S_t$ 2.356	2.480	2.312	2.521
Hob tooth addendum, mm	$H_{at}$ 2.124	2.157	1.858	2.124
Minimal whole depth, mm	$H_t$ 7.80	7.80	8.20	8.20
Drive profile angle, °	$\alpha_{td}$ 29.0	30.0	29.0	29.0
Coast profile angle, °	$\alpha_{tc}$ 19.064	20.631	19.064	19.064
Drive protuberance angle, °	$\gamma_{td}$ 6.0	6.0	6.0	6.0
Coast protuberance angle, °	$\gamma_{tc}$ 6.0	6.0	6.0	6.0
Drive protuberance offset, mm	$\Delta_{td}$ 0.29	0.31	0.31	0.31
Coast protuberance offset, mm	$\Delta_{tc}$ 0.29	0.31	0.31	0.31
Drive grinding stock, mm	$\Delta_{gd}$ 0.17	0.20	0.20	0.20
Coast grinding stock, mm	$\Delta_{gc}$ 0.17	0.20	0.20	0.20
Drive side tip radius, mm	$R_{td}$ 1.00	1.00	1.20	1.10
Coast side tip radius, mm	$R_{tc}$ 0.65	0.70	0.80	0.80

avoiding possible grinding “hotspots” that propagate initial cracks in the root area. Nonground tooth root fillet remains residual compressive stress (about 300–600 MPa [113]) after heat treatment, which increases tooth bending strength. Protuberance gear hob profile parameters are shown in Table 11.4. The sun or ring gear tooth profile after protuberance hobbing is shown in Figure 11.9.

The ring gear involute flanks were preliminarily machined with a special asymmetric tooth shaper cutter. Then the form disk mill cutter was used to

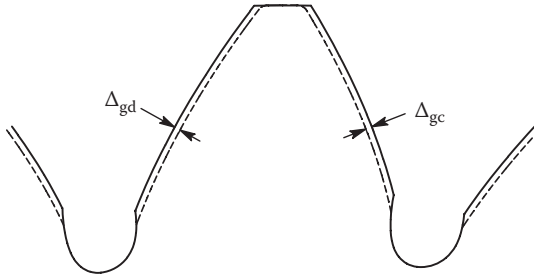


**FIGURE 11.9** Sun or planet tooth profile after protuberance hobbing.  $\Delta_{gd}$  and  $\Delta_{gc}$  - drive and coast flank grinding stocks.

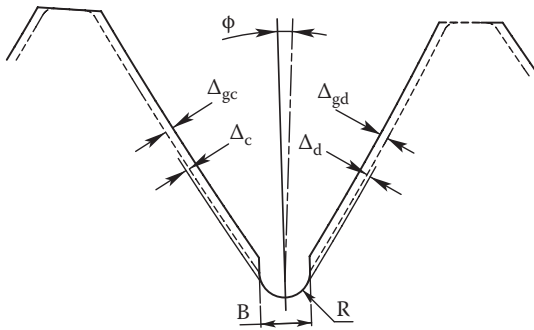


**FIGURE 11.10** Ring gear tooth space profile.  $\Delta_{gd}$  and  $\Delta_{gc}$  - drive and coast flank grinding stocks;  $\Delta_d$  and  $\Delta_c$  - drive and coast flank undercuts;  $R$  - root fillet radius;  $B$  - fillet cut width;  $\phi$  - fillet angle.

cut root fillets. The ring gear tooth profile after machining, and before heat treatment, is shown in Figure 11.10. Its parameters are presented in Table 11.5.

Unlike gears with symmetric teeth, the asymmetric gear blanks' position relative to the cutting tool is critical. Otherwise, the drive flank of one gear can be positioned in contact with the coast profile of the mating gear, which makes assembly impossible. After the tooth cutting the gears are carburized and heat treated to achieve a tooth surface hardness of >59 HRC with the case depth of 0.6–1.0 mm. The core tooth hardness is 33–45 HRC.

The MAAG generating gear grinding machines were used for final gear tooth grinding. Simultaneous processing of both flanks of asymmetric teeth required a special grinding machine setup. The tip/root relief profile modification was applied to the driving tooth flanks of the sun gears and both flanks of the planet gears (see Figure 11.11). Flank modification parameters are presented in Table 11.6.

Assembly of the gearbox includes selection of planet gears and their initial angular orientation based on transmission error function of every gear. All planet gears were classified by transmission error (TE) function in several



**TABLE 11.5**  
Ring Gear Root Fillet Data

Stage		First	Second
Gear		Ring	Ring
Number of teeth		107	97
Fillet radius, mm	$R$	0.60/0.70	0.65/0.75
Fillet cut width, mm	$B$	1.20/1.40	1.30/1.50
Fillet angle, °	$\varphi$	3.4	3.3
Drive flank fillet undercut, mm	$\Delta_d$	0.06/0.08	0.06/0.08
Coast flank fillet undercut, mm	$\Delta_c$	0.06/0.08	0.06/0.08
Drive grinding stock, mm	$\Delta_{gd}$	0.19/0.20	0.19/0.20
Coast grinding stock, mm	$\Delta_{gc}$	0.19/0.20	0.19/0.20

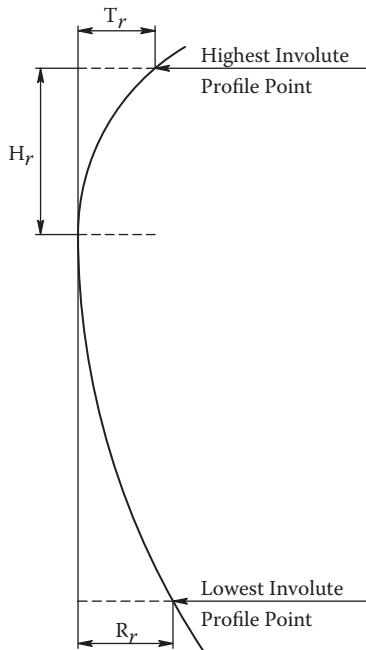


**FIGURE 11.11**

Tooth flank modification chart.  $H_r$  - tip relief height;  $T_r$  - tip relief depth;  $R_r$  - root relief depth.

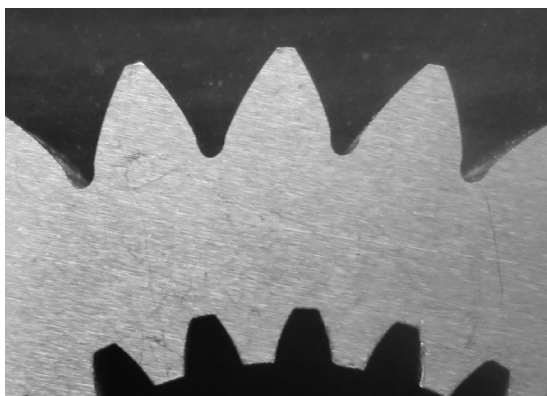
groups. Each group has planet gears with the similar TE function. Then during assembly position and orientation of each planet gear depend on its TE function profile, providing better engagement of the driving flanks and load distribution between planet gears [5].

Application of the asymmetric teeth helped to provide a very low weight-to-output torque ratio, a significantly reduced noise and vibration level, and cut down duration and expense of operational development [109]. A section

**TABLE 11.6**

Tooth Flank Modification Parameters

Stage	Gear	First		Second	
		Sun	Planet	Sun	Planet
	Number of teeth	28	41	38	31
	Tip relief height, mm	$H_r$ , 2.5/3.5	2.0/3.0	3.0/4.0	2.0/3.0
	Tip relief depth, mm	$T_r$ , 0.006/0.010	0.002/0.006	0.008/0.012	0.003/0.008
	Root relief depth, mm	$R_r$ , 0.008/0.014	0.002/0.006	0.010/0.017	0.002/0.008

**FIGURE 11.12**

(See color insert.) First-stage sun gear section. (Courtesy of Chernyshev Enterprise, Moscow, Russia.) (From Novikov, A.S., et al., *Gear Technology*, January/February 2008, 60–65. With permission.)

of the first-stage sun gear is shown in Figure 11.12. Photos of the gears and gear assemblies of the TV7-117S gearbox are shown in Figures 11.13 to 11.18. Figure 11.19 shows the Ilyushin Il-114 commuter airplane with the TV7-117S engines.

### 11.3 Seed Planter Gearboxes

Direct Gear Design was applied for helical crossed-axis plastic gears of the John Deere's Pro-Shaft cable drives. Their drives replace chain/sprocket drives in agricultural machinery to provide value-improved performance, operation safety, and a trouble-free way to power seed meters of the John Deere MaxEmerge 2<sup>TM</sup> and MaxEmergePlus<sup>TM</sup> Planters (Figure 11.20). The Pro-Shaft cable drive is shown in Figure 11.21. Figure 11.22 shows the Pro-Shaft cable drive gearboxes. Gear geometry and accuracy parameters, and operating torques and stresses are presented in Table 11.7.

**FIGURE 11.13**

(See color insert.) First-stage sun gear. (Courtesy of Chernyshev Enterprise, Moscow, Russia.) (From Novikov, A.S., et al., *Gear Technology*, January/February 2008, 60–65. With permission.)

**FIGURE 11.14**

(See color insert.) First-stage assembly. (Courtesy of Chernyshev Enterprise, Moscow, Russia.) (From Novikov, A.S., et al., *Gear Technology*, January/February 2008, 60–65. With permission.)

Gears are designed and made by Kleiss Gears, Inc. (Grantsburg, Wisconsin). The mold tool development had presented an intricate task and took significant effort, because of the thick wall sections and very high helix angle. An unscrewing mechanism was incorporated in the molding tool to minimize stress on the teeth during ejection of the helical gear. The thick wall sections

**FIGURE 11.15**

(See color insert.) Second-stage sun gear. (Courtesy of Chernyshev Enterprise, Moscow, Russia.) (From Novikov, A.S., et al., *Gear Technology*, January/February 2008, 60–65. With permission.)

**FIGURE 11.16**

(See color insert.) Second-stage planet gear carrier assembly. (Courtesy of Chernyshev Enterprise, Moscow, Russia.) (From Novikov, A.S., et al., *Gear Technology*, January/February 2008, 60–65. With permission.)

of these gears required the cycle time to be much longer than is usual in the industry, well over a minute. Figure 11.23 presents the seven-tooth pinion molding cavity.

The CMM scanning was employed for gear measuring to define exact dimensions and accuracy during tooling and molding process development. For continuing production quality control the roll test inspection was used.



**FIGURE 11.17**  
(See color insert.) Second-stage planet gear carrier assembly. (Courtesy of Chernyshev Enterprise, Moscow, Russia.)

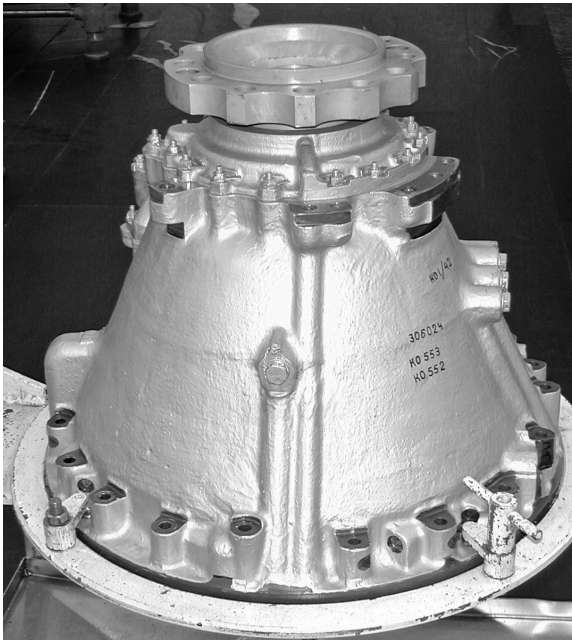


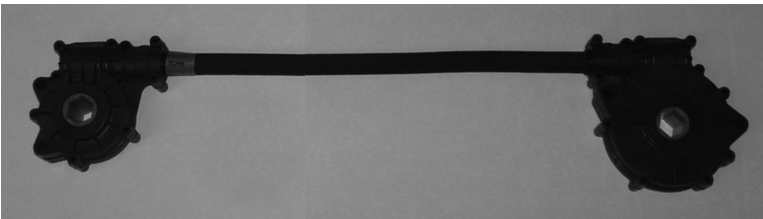
**FIGURE 11.18**  
(See color insert.) Assembled gearbox. (Courtesy of Chernyshev Enterprise, Moscow, Russia.)  
(From Novikov, A.S., et al., *Gear Technology*, January/February 2008, 60–65. With permission.)



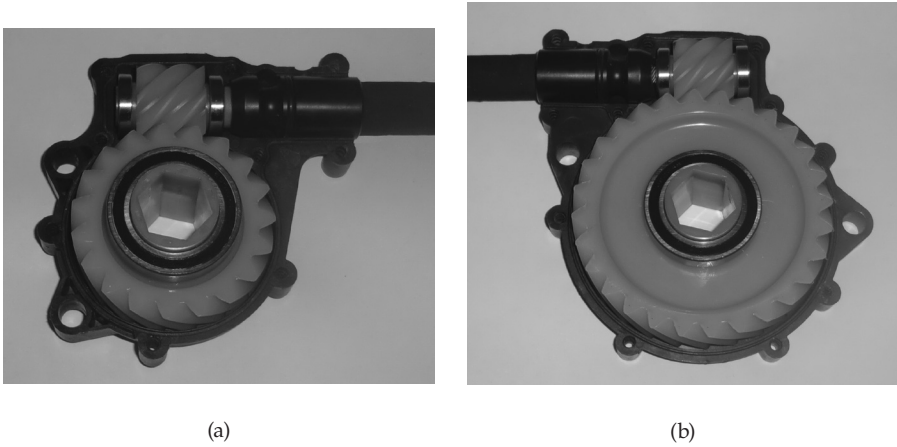
**FIGURE 11.19**  
(See color insert.) Ilyushin Il-114 commuter airplane.



**FIGURE 11.20**  
(See color insert.) Deere MaxEmergePlus planter. (Courtesy of John Deere Co., Moline, Illinois.)



**FIGURE 11.21**  
Pro-Shaft cable drive. (Courtesy of John Deere Co., Moline, Illinois.)

**FIGURE 11.22**

(See color insert.) Pro-Shaft cable drive gearboxes: (a) 19:7 gear ratio, (b) 7:28 gear ratio. (Courtesy of John Deere Co., Moline, Illinois.)

The Pro-Shaft cable drives present ultimate metal-to-plastic gear conversion, replacing the chain/sprocket drives in agricultural machinery. According to John Deere Company's website [114] the Pro-Shaft drive provides many advantages over a conventional chain drive, including:

- Durable, lubricated for life, and maintenance-free
- No more chain knock-offs in high-residue planting situations
- No more need for trash shields on your planter
- Skips in the field are eliminated due to the removal of chain knock-off and rusty chain links
- Chain and sprocket maintenance is eliminated, so you can stay in the field longer
- Completely safe

**TABLE 11.7**  
Gear Geometry Data

Gear Drive	19:7 Ratio		7:28 Ratio	
	Driving	Driven	Driving	Driven
Nominal number of teeth	19	7		28
Diametral pitch, 1/in.	10	10		10
Normal pressure angle, °	25	25		25
Helix angle, °	45	45		45
Hand of helix	Left	Left		Left
Helix lead, in.	8.4415	3.1100		12.4401
Shaft angle, °		90	90	
Pitch diameter, in.	2.6863	0.9899		3.9598
Base diameter, in.	2.2432	0.8264		3.3057
Tooth tip diameter, in.	2.802/2.812	1.239/1.245		4.077/4.087
Root diameter, in.	2.366/2.376	0.793/0.803		3.630/3.640
Normal tooth thickness at pitch diameter, in.	0.116/0.120	0.179/0.183		0.116/0.120
Tooth tip radius, in.	0.010	0.010		0.010
Normal tooth tip land, in.	0.017/0.019	0.012/0.014		0.018/0.020
Face width, in.	0.840	1.000		0.840
Center distance, in.		1.838 ± 0.007		2.475 ± 0.007
<i>Accuracy and Inspection Parameters</i>				
Accuracy grade per AGMA 2000-A88	Q7A	Q7A		Q7A
Run-out tolerance, in.	0.0034	0.0027		0.0037
Pitch variation, in.	±0.0011	±0.0009		±0.0011
Profile tolerance, in.	0.0013	0.0011		0.0014
Lead tolerance, in.	0.0006	0.0006		0.0006
Tooth-to-tooth composite error, in.	0.0021	0.0025		0.0020
Total composite error, in.	0.0054	0.0053		0.0058
Pin diameter, in.	0.1800	0.1800		0.1800
Measurement over balls, in.	2.859/2.867	1.264/1.271		4.141/4.149
<i>Tolerance Analysis Results</i>				
Normal operating drive pressure angle, °		24.66°/25.33°		24.74°/25.25°
Contact ratio		1.15/1.39		1.15/1.40
Operating normal backlash, in.		0.0021/0.0250		0.0015/0.0260
Operating radial clearance, in.		0.018/0.048		0.020/0.050

continued



**TABLE 11.7 (continued)**

Gear Geometry Data

Gear Drive	19:7 Ratio		7:28 Ratio	
	Driving	Driven	Driving	Driven
<i>Stress Analysis Results</i>				
RPM	88.4	240	60	240
Gear efficiency, %		80.1	80.1	
Torque, in.-lb	113.2	33.4	107	33.4
Bending stress, psi	1743	1685	1712	1685
Gear material	Zytel® 101L BKB080			
Gearbox housing gear material	30% glass fiber-reinforced Zytel 70G30HSLR BK099			

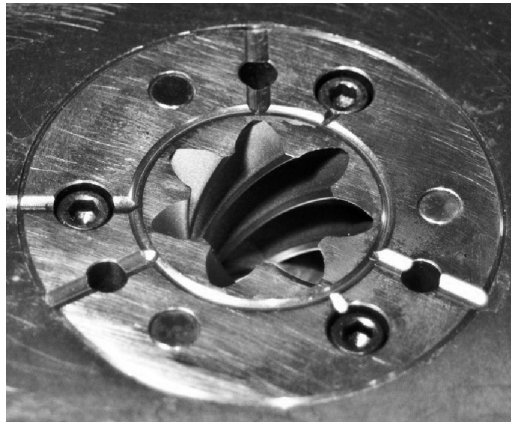


**FIGURE 11.23**

(See color insert.) Seven-tooth pinion molding cavity. (Copyright © Kleiss Gears, Inc., Grantsburg, Wisconsin.)

---

## References

---

1. Dudley, D.W. 1966. *The evolution of the gear art*. AGMA.
2. Litvin, F.L. 1998. *Development of gear technology and theory of gearing*. NASA.
3. McVittie, D. 1993. The European rack shift coefficient "X" for Americans. *Gear Technology*, July/August, 34–36.
4. Goldfarb, V.I., and A.A. Tkachev. 2005. New approach to computerized design of spur and helical gears. *Gear Technology*, January/February, 26–32.
5. Vulgakov E.B. (ed.). 1981. *Aviation gearboxes. Handbook*. Moscow: Mashinostroenie.
6. Vulgakov, E.B. 1974. *Gears with improved characteristics*. Moscow: Mashinostroenie.
7. Vulgakov, E.B., and L.M. Vasina. 1978. *Involute gears in generalized parameters*. Moscow: Mashinostroenie.
8. Vulgakov, E.B. 1995. *Theory of involute gears*. Moscow: Mashinostroenie.
9. Standard ANSI/AGMA1006-A97. 1997. Appendix F: Generating gear geometry without racks. In *Tooth proportion for plastic gears*. AGMA.
10. Kleiss, R.E., A.L. Kapelevich, and N.J. Kleiss Jr. 2001. New opportunities with molded gears. Paper presented at the annual technical meeting of the AGMA, Detroit.
11. Standard AGMA909-A06. 2006. *Specifications for molded plastic gears*. Appendix C: An alternative method for specifying molded plastic gears. AGMA.
12. Woodbury, R.S. 1958. The first epicyclic gear teeth. *ISIS*, 49(4): 375–377.
13. Willis, R. 1841. *Principles of mechanism*. London: John W. Parker.
14. Reuleaux, F. 1894. *The constructor. A hand-book of machine design*. Philadelphia: H.H. Suplee.
15. Thumb shaped gear teeth profiles. 1882. KMODDL. [http://kmoddl.library.cornell.edu/model\\_metadata.php?m=111](http://kmoddl.library.cornell.edu/model_metadata.php?m=111).
16. Leutwiler, O.A. 1917. *Element of machine design*. London: McGraw-Hill Book Company.
17. Bolotovskiy, I.A., O.F. Vasil'eva, and V.P. Kotelnikov. 1984. Involute gears with asymmetric teeth. *Vestnik Mashinostroeniya*, 4: 15–17.
18. DiFrancesco, G., and S. Marini. 1997. Structural analysis of asymmetrical teeth: Reduction of size and weight. *Gear Technology*, September/October, 47–51.
19. Gang, G., and T. Nakanishi. 2001. Enhancement of bending load carrying capacity of gears using an asymmetric involute tooth. Paper presented at the JSME International Conference on Motion and Transmissions (MPT2001-Fukuoka), Fukuoka, Japan.
20. Karpat, F., K. Cavdar, and F.C. Babalik. 2005. Computer aided analysis of involute spur gears with asymmetric teeth. *VDI Berichte*, 1904(I): 145–163.
21. Brecher, C., and J. Schafer. 2005. Potentials of asymmetric tooth geometries for the optimization of involute cylindrical gears. *VDI Berichte*, 1904(I): 705–720.
22. Yang, S.C. 2007. Study on an internal gear with asymmetric involute teeth. *Mechanism and Machine Theory*, 42: 977–994.
23. Pedersen, N.L. 2010. Improving bending stress in spur gears using asymmetric gears and shape optimization. *Mechanism and Machine Theory*, 45: 1707–1720.

24. Wang, S., G.R. Liu, G.Y. Zhang, and L. Chen. 2011. Design of asymmetric gear and accurate bending stress analysis using the ES-PIM with triangular mesh. *International Journal of Computational Methods*, 8(4): 759–772.
25. Yoerkie, C.A., and A.G. Chory. 1984. Acoustic vibration characteristics of high contact ratio planetary gears. *Journal of American Helicopter Society*, 40: 19–32.
26. Howe, D.C., C.V. Sundt, and A.H. McKibbin. 1988. *Advanced counter-rotating gearbox*. NASA Contractor Report 180883.
27. Vulgakov, E.B., and G.V. Rivkin. 1976. Design of gears with asymmetric tooth profile. *Mashinovedenie*, 5: 35–39.
28. Kapelevich, A.L. 1984. Research and development of geometry of modernized involute gears. PhD Dissertation, Moscow State Technical University.
29. Kapelevich, A.L. 1987. Synthesis of asymmetric involute gearing gears. *Mashinovedenie*, 1: 62–67.
30. Vulgakov, E.B., and A.L. Kapelevich. 1986. Asymmetric gear transmissions: Possible developments. *Vestnik Mashinostroeniya*, 4: 14–16.
31. Kapelevich, A.L. 2000. Geometry and design of involute spur gears with asymmetric teeth. *Mechanism and Machine Theory*, 35: 117–130.
32. Litvin, F.L. 1994. *Gear geometry and applied theory*. Upper Saddle River, NJ: Prentice Hall.
33. Sheveleva, G.I. 1999. *Theory of form and contact development of moving bodies*. Moscow: Stankin.
34. Litvin, F.L., Q. Lian, and A.L. Kapelevich. 2000. Asymmetric modified gear drives: Reduction of noise, localization of contact, simulation of meshing and stress analysis. *Computer Methods in Applied Mechanics and Engineering*, 188: 363–390.
35. Vulgakov, E.B., and A.L. Kapelevich. 1982. Helical gear mesh possibilities. *Vestnik Mashinostroeniya*, 3: 12–14.
36. Kapelevich, A.L., and R.E. Kleiss. 2002. Direct Gear Design for spur and helical gears. *Gear Technology*, September/October, 29–35.
37. Vulgakov, E.B., and A.L. Kapelevich. 1980. Area of existence of helical gearing. *Vestnik Mashinostroeniya*, 7: 9–11.
38. Townsend, D.P. 1967. *Dudley's gear handbook*. 2nd ed. New York: McGraw Hill.
39. Kapelevich, A.L., and Y.V. Shekhtman. 2010. Area of existence of involute gears. *Gear Technology*, January/February, 64–69.
40. Vulgakov, E.B., and A.L. Kapelevich. 1986. Asymmetric gear transmissions: Possible developments. *Vestnik Mashinostroeniya*, 4: 14–16.
41. Alipiev, O.L., and S.D. Antonov. 2010. Asymmetric involute—antenn meshing formed by identical spur gears with a small number of teeth. *VDI-Berichte*, 2018: 925–939.
42. NASA/SP-8100. 1974. *Liquid rocket engine turbopump gears*. NASA.
43. Wildhaber, E. 1926. Helical gearing. U.S. Patent 1,601,750.
44. Novikov, M.L. 1956. USSR Patent 109,750.
45. Henry Z.S. 1995. *Bell helicopter advanced rotorcraft transmission (ART) program*. Contract Report ARL-CR-238. NASA.
46. Anderson N.E., and S.H. Loewenthal. 1984. *Efficiency of nonstandard and high contact ratio involute spur gears*. AVSCOM Technical Report 84-C-9. NASA.
47. Kapelevich, A.L. 2012. Asymmetric gears: Parameter selection approach. *Gear Technology*, June/July, 48–51.
48. Standard ISO 6336. 2006. *Calculation of load capacity of spur and helical gears*.

49. Standard ANSI/AGMA 2001-D04. 2004. *Fundamental rating factors and calculation methods for involute spur and helical gear teeth*.
50. Lewis, W. 1892. Investigation of strength of gear teeth. In *Proceedings of Engineers Club*, Philadelphia, 16–23.
51. Inoue, K., and T. Masuyama. 2006. Possibilities of fatigue strength simulation in reliability design of carburized gears. Paper presented at the International Conference Power Transmissions '06, Novi Sad, Serbia.
52. Pedersen, N.L. 2009. Reducing bending stress in external spur gears by redesign of the standard cutting tool. *Structural and Multidisciplinary Optimization*, (3): 215–227.
53. Der Hovanesian, J., et al. 1989. Gear root stress optimization using photoelastic optimization techniques. *SAE Transactions*, 97(4): 748–755.
54. Pulley, F.T., et al. 2000. Method for producing and controlling a fillet on a gear. U.S. Patent 6164880.
55. Spitas, V., T. Costopoulos, and C. Spitas. 2005. Increasing the strength of standard involute gear teeth with novel circular root fillet design. *American Journal of Applied Sciences*, 2(6): 1058–1064.
56. Sanders, A.A., D.R. Houser, A. Kahraman, J. Harianto, and S. Shon. 2011. An experimental investigation of the effect of tooth asymmetry and tooth root shape on root stresses and single tooth bending fatigue life of gear teeth. Paper presented at the 11th International ASME Power Transmission and Gearing Conference, Washington, DC.
57. Kapelevich, A.L., and Y.V. Shekhtman. 2003. Direct Gear Design: Bending stress minimization. *Gear Technology*, September/October, 44–49.
58. Kapelevich, A.L., and Y.V. Shekhtman. 2009. Tooth fillet profile optimization for gears with symmetric and asymmetric teeth. *Gear Technology*, September/October, 73–79.
59. Hansong, X., J.W. Zu, and W. Zaton. 2005. Fillet shape optimization for gear teeth. ASME Power Transmission and Gearing Conference, Long Beach, CA, September 24–28.
60. Rastrigin, L.A. (ed.). 1969. *Random search theory and application*. Riga: Zinatne.
61. Kapelevich A.L., and V.M. Ananiev. 2011. Gear transmission density maximization. *Gear Technology*, November/December, 46–52.
62. Lynwander, P. 1983. *Gear drive systems. Design and application*. New York: Marcel Dekker.
63. *Gearbox weight minimization software*. UTS 580 System.
64. Henriot, G. 2001. *Gears and planetary gear trains*. Reggio nell'Emilia: Brevini.
65. Kudriavtsev, V.N. 1966. *Planetary gears*. Leningrad: Mashinostroenie.
66. Kudriavtsev, V.N., and Y.N. Kirdiashev (eds.). 1977. *Planetary gears. Handbook*. Leningrad: Mashinostroenie.
67. Kapelevich A.L. 2009. Planetary gear. U.S. Patent US2011/0009232 A1 (pending).
68. Popper J.B. 1961. Cooperating wedges including mating worms. U.S. Patent 2973660.
69. Munster N.S., and G.V. Tzarev. 1968. *Self-locking cylindrical gears, theory mechanisms and machines*. Publications of Tashkent Polytechnic Institute, 30A: 3–6.
70. Iskhakov, T.G. 1969. *Self-locking in gear mechanisms*. Publications of the Kazan Aviation Institute, 105: 3–15.
71. Timofeev, G.A., and V.V. Panukhin. 2003. Self-locking criteria analysis. *Vestnik Mashinostroenia*, 9: 3–8.

72. Kapelevich, A.L., and E. Taye. 2012. Self-locking gears: Design and potential applications. *Gear Solutions*, May, 53–58.
73. Kargin, P.A. 2006. Synthesis of new self-locking gear drive arrangement. *Izvestiya Vuzov, Severo-Kavkazskii Region, Technical Sciences*, 1: 96–97.
74. Taye, E. 2009. Actuator with self-locking helical gears for a continuously variable valve lift system. U.S. Patent US2009/0283062 A1 (pending).
75. Adams, C.E. 1986. *Plastic gearing*. New York: Marcel Dekker.
76. Starzhinsky, V.E., E.V. Shalobaev, et al. 1998. *Plastic gears in instrument mechanisms*. Saint-Petersburg–Gomel: MPRI NASB.
77. Standard ANSI/AGMA 1006-A97. 1997. *Tooth proportions for plastic gears*. AGMA.
78. Standard ANSI/AGMA 1106-A97. 1997. *Tooth proportions for plastic gears (metric addition)*. AGMA.
79. Standard ANSI/AGMA 920-A01. 2001. *Materials for plastic gears*. AGMA.
80. Mao, K., W. Liebig, C.J. Hooke, and D. Walton. 2010. Polymer gear surface thermal wear and its performance prediction. *Tribology International*, 43(1–2): 433–439.
81. Moya, J.L., A.S. Machado, J.A. Velásquez, R. Goytisolo, A.E. Hernández, J.E. Fernández, and J.M. Sierra. 2010. A study in asymmetric plastic spur gears. *Gear Solutions*, April, 32–41.
82. Starzhinsky, V.E., N.N. Ishin, and A.M. Goman. 2011. Perfection of quality parameters of plastic gears by using asymmetric tooth profile. *Machine Design*, 3(2), 109–114.
83. Kapelevich A.L., and T.M. McNamara. 2006. Plastic gearing for small engine applications. Paper presented at SAE International Conference, San Antonio.
84. Barone S. 2001. Gear geometric design by B-spline curve fitting and sweep surface modelling. *Engineering with Computers*, 17(1): 66–74.
85. Kleiss, N.J. Designing gears—The ideal geometry. <http://kleiss.mystarband.net/design.pdf>.
86. ANSI/ASME Y14.7. 1971. *Gear drawing standard. Part 1. For spur, spur, helical, double helical and rack*.
87. ANSI/ASME Y14.7. 1971. *Gear drawing standard. Part 2. For bevel and hypoid gears*.
88. American Standard ANSI/AGMA 2015-1-A01. 2002. *Accuracy classification system—Tangential measurements for cylindrical gears*. AGMA.
89. American Standard ANSI/AGMA 2015-2-A06. 2006. *Accuracy classification system—Radial measurements for cylindrical gears*. AGMA.
90. International Standard ISO 1328-1. 1995. *Cylindrical gears—ISO system of accuracy. Part 1. Definitions and allowable values of deviations relevant to corresponding flanks of gear teeth*. ISO.
91. International Standard ISO 1328-2. 1997. *Cylindrical gears—ISO system of accuracy. Part 2. Definitions and allowable values of deviations relevant to radial composite deviations and runout information*. ISO.
92. Zou, Z., and E. Morse. 2001. Statistical tolerance analysis using GapSpace. Paper presented at the 7th CIRP International Seminar on Computer Aided Tolerancing, ENS de Cachan. France.
93. Creveling, C.M. 1996. *Tolerance design: A handbook for developing optimal specifications*. Englewood Cliffs, NJ: Prentice Hall.
94. Cox, N.D. 1986. *How to perform statistical tolerance analysis*. Milwaukee: American Society for Quality Control.
95. Saari, O.E. 1954. How to calculate exact wheel profiles for form grinding helical gear teeth. *American Machinist*, September 13, 172–175.

96. Kapelevich, A.L., A.I. Tolchenov, and A.I. Eidinov. 1985. Application of the fly cutters in experimental production. *Aviatsionnaya Promyshlennost*, 3: 39–40.
97. Flodin, A., and M. Andersson. 2012. Tooth root optimization of powder metal gears—Reducing stress from bending and transient loads. Paper presented at the Powder Metal World Congress and Exhibition (PM2012), Yokohama, Japan.
98. Kleiss, R.E. How to achieve a successful molded gear transmission. [www.kleissgears.com/index.php/download\\_file/view/88/94/](http://www.kleissgears.com/index.php/download_file/view/88/94/).
99. Walsh, S.F. 1993. Shrinkage and warpage prediction for injection molded components. *Journal of Reinforced Plastics and Composites*, 12(7): 769–777.
100. Autodesk® Moldflow® plastic injection molding simulation software. <http://usa.autodesk.com/moldflow/>.
101. Kapelevich, A.L., Y.V. Shekhtman, and T.M. McNamara. 2005. Turning an art into science. *Motion System Design*. August, 26–31.
102. Kapelevich, A.L. 1986. Measurement over pins of the gears with asymmetric teeth. *Mashinovedenie*, 6: 109–110.
103. Kapelevich, A.L. 2011. Measurement of directly designed gears with symmetric and asymmetric teeth. *Gear Technology*, January/February, 60–65.
104. Nezhurin, I.P. 1961. Calculation of the measurement over pins of the helical gears with odd number of teeth. *Vestnik Mashinostroeniya*, 2:14–17.
105. Standard ANSI/AGMA 2000-A88. 1988. *Gear classification and inspection handbook*. AGMA.
106. Coy, J.J., D.P. Townsend, and E.V. Zaretsky. 1985. *Gearing*. NASA Reference Publication 1152, AVSCOM Technical Report 84-C-15. NASA.
107. Brown, F.W., S.R. Davidson, D.B. Hanes, D.J. Weires, and A.L. Kapelevich. 2011. Analysis and testing of gears with asymmetric involute tooth form and optimized fillet form for potential application in helicopter main drives. *Gear Technology*, June/July, 46–55.
108. Winkelmann, L.W., M.D. Michaud, G. Sroka, A.A. Swiglo, and D. Mahan. 2001. Chemically accelerated vibratory finishing for the virtual elimination of wear and pitting for steel gears. 01FTM7. AGMA Fall Technical Meeting, Detroit, MI.
109. Sarkisov, A.A., and E.B. Vulgakov. 2000. The new gearbox of Klimov Corporation. *Aerospace Courier*, 2: 32–33.
110. Vulgakov, E.B., and A.L. Kapelevich. 2000. The gearbox for the TV7-117S turbo-prop engine. *Vestnik Mashinostroeniya*, 11: 13–17.
111. Novikov, A.S., A.G. Paikin, V.L. Dorofeyev, V.M. Ananiev, and A.L. Kapelevich. 2008. Application of gears with asymmetric teeth in turboprop engine gearbox. *Gear Technology*, January/February, 60–65.
112. GOST 1643-81. 1981. *Tolerances for cylindrical gears*. Interstate standard. Moscow: IPK.
113. Yeliseev, Y.S., V.V. Krymov, I.P. Nezhurin, V.S. Novikov, and N.M. Ryzhov. 2001. *Fabrication of gas turbine engine gears*. Moscow: Vysshaya Shkola.
114. Pro-shaft drive enhancement kits for John Deere MaxEmerge 2™ and MaxEmergePlus™ planters. [https://jdparts.deere.com/partsmkt/document/english/16mac/9686\\_fb\\_ProShaftDriveEnhancementKit.htm](https://jdparts.deere.com/partsmkt/document/english/16mac/9686_fb_ProShaftDriveEnhancementKit.htm).



# DIRECT GEAR DESIGN

ALEXANDER L. KAPELEVICH

“Direct Gear Design by Alexander L. Kapelevich is exactly the book that established or new generation engineers should look for. The book is practical, informative, includes recommendations, useful charts, diagrams, and tables, provides valuable information on gear geometry limitations, and brings implementation examples of different gearbox applications. The book introduces a new vision of gear design while addressing the old gear design challenges of reducing the stress level and increasing reliability of the gear trains.”

—Mr. Yuriy Gmirya, Sikorsky Aircraft Corporation, USA

“A modern description of how gears should be designed today when we have computer tools that allow us to optimize our gear designs far beyond what the standards allow us.”

—Dr. Anders Flodin, Höganäs AB, Sweden

“... a useful tool for gear and transmission designers to come up with optimum gear design. Today we are forced to increase load carrying capacity, reduce transmission weight and fulfill noise requirements without increasing manufacturing costs. The described new method DGD and asymmetric gear design is helpful to reach this target.”

—Dr. Franz J. Joachim, ZF Friedrichshafen AG, Germany

**Direct Gear Design** introduces an alternate gear design approach to maximize gear drive performance in custom gear applications. Developed by the author, the Direct Gear Design® method has been successfully implemented in a wide variety of custom gear transmissions over the past 30 years. The results are maximized gear drive performance, increased transmission load capacity and efficiency, and reduced size and weight. This book explains the method clearly, making it easy to apply to actual gear design. Written by an engineer for engineers, it offers a wealth of practical advice and examples on using Direct Gear Design to improve gear transmission performance in demanding custom gear drive applications.



www.taylorandfrancisgroup.com

6000 Broken Sound Parkway, NW  
Suite 300, Boca Raton, FL 33487  
711 Third Avenue  
New York, NY 10017  
2 Park Square, Milton Park  
Abingdon, Oxon OX14 4RN, UK

K13536

ISBN: 978-1-4398-7618-3



9 781439 876183

www.crcpress.com